UNIVERSITÀ DEGLI STUDI DI TRIESTE

XXXVIII CICLO DEL DOTTORATO DI RICERCA IN

BIOMEDICINA MOLECOLARE

ICGEB

Impact of miR-30d on Cancer cell and Tumour Microenvironment Crosstalk

Settore scientifico-disciplinare: BIO/11

DOTTORANDA
SUVARNA CHATTERJEE

COORDINATORE
PROF. ALESSANDRO TOSSI

SUPERVISORE DI TESI
PROF. GIANNINO DELSAL

CO-SUPERVISORE DI TESI
PROF. FIAMMA MANTOVANI

ANNO ACCADEMICO 2024/2025

Abstract

Cancer progression is driven not only by genetic and epigenetic alterations within tumour cells but also by their reciprocal interactions with the tumour microenvironment (TME). In healthy tissues, the extracellular matrix (ECM), nutrient limitations, and immune surveillance maintain homeostasis and suppress malignant transformation. As cancer evolves, however, tumour cells progressively corrupt this protective environment. With time, as oncogenic programs are induced, crosstalk between tumour cell and stromal components residing in the tissue environment promotes activation of cancer-associated fibroblasts (CAFs), ECM remodelling, abnormal angiogenesis, and immune suppression, collectively establishing a tumour permissive niche. Key oncogenic drivers such as mutant p53 (mutp53), HIF1α, and YAP/TAZ respond to stromal cues such as hypoxia, ECM stiffening, nutrient deprivation, and inflammation to reinforce these pro-tumourigenic changes. Understanding how these pathways contribute to poorly immune-infiltrated tumours, associated with limited response to immune checkpoint blockade (ICB), is essential for improving the efficacy of anticancer therapies. Notably, mutp53, HIF1α and YAP/TAZ can promote immune evasion by dampening the cGAS/STING/IFN-I pathway, a central innate immune axis required for effective anti-tumour immunity.

We have previously demonstrated that mutp53-induced overexpression of the onco-miRNA miR-30d in invasive breast cancer (IBC) cells promotes the release of a pro-malignant secretome, that profoundly modifies both the local and distant TME, ultimately promoting tumour growth and accelerating metastasis onset (Capaci et al., 2020). miR-30d level is frequently found elevated in BC and other solid tumours and its role in late-stage disease is established, but its contribution to the earliest phases of tumourigenesis remains largely unexplored.

Through my phD project, I am investigating how miR-30d influences the regulation of the TME using a cellular model of pre-invasive breast ductal carcinoma in situ (DCIS). The findings revealed that miR-30d level is already high in this early BC model, where it can actively suppress innate immune signalling by attenuating the cGAS/STING/IFN-I cascade. Notably, inhibition of miR-30d by specific Locked nucleic acid (LNA) or Decoy inhibitors both triggers upstream induction and favors the execution of the cGAS/STING/IFN-I pathway in BC cells, while not in normal breast epithelial cells.

Mechanistically, miR-30d preserves nuclear envelope (NE) integrity, thus controlling cytosolic release of cGAS-inducing dsDNA, and preventing TREX1 nuclear entry and genomic DNA damage. This effect was largely attributed to the ability of miR-30d to sustain Lamin B expression through the LATS2/YAP axis. Specifically, miR-30d was found to inhibit LATS2, thus activating YAP and driving expression of Lamin B and other NE components. In parallel, miR-30d inhibition restores the ER–Golgi trafficking of STING, by normalizing secretory pathway function. Across BC cell lines, patient-derived organoids (PDO) and in cell lines derived from different tumour types, miR-30d inhibition leads to robust activation of the cGAS/STING pathway, causing secretion of type-I IFN and cGAMP. In turn, cGAS/STING activation consequent to miR-30d blockade also suppresses proliferation and induces STING-dependent apoptosis of cancer cells, synergizing with DNA-damaging agents such as doxorubicin and with CDK4/6 inhibitors. In immunocompetent mouse models of BC, miR-30d inhibition enhances NK and $CD8^+$ T cells infiltration, suppresses tumour growth, and sensitizes resistant tumours to ICB therapy. Consistently, analysis of publicly available tumour gene expression datasets revealed a strong inverse correlation between miR-30d activity and anti-tumour immunity in BC patients' samples, suggesting that elevated miR-30d levels are associated with an immune-cold, poorly infiltrated TME, and with limited immunotherapy response.

Collectively, these findings identify miR-30d as a key regulator of immune escape in BC and potentially other tumour types. Targeting miR-30d may restore a more immunogenic microenvironment, thereby enhancing the efficacy of immune-based therapies.

Keywords: Tumour microenvironment (TME), cGAS/STING/IFN-I pathway, Hippo pathway, miR-30d, nuclear envelope (NE), golgi apparatus (GA), anticancer immune therapies.

Dedicated to my parents,

Mr. Surjit and Mrs. Shanta,

for their enduring blessings, guidance and constant support

Table of Contents

List of Figures

List of Tables

List of Abbreviations

A1AT	alpha-1 antitrypsin
ACT	adoptive cell therapies
APC	antigen-presenting cell
ATCC	American Type Culture Collection
ATP	adenosine triphosphate
ADAMs	A Disintegrin And Metalloproteinase
BC	breast cancer
BMDC	bone marrow-derived cells
BMSCs	bone marrow-derived mesenchymal stem cells
BrdU	Bromodeoxyuridine
CAF	cancer-associated fibroblast
CAR-T	chimeric antigen receptors T cells
cDNA	Complementary DNA
cGAMP	cyclic GMP-AMP
cGAS	cyclic GMP-AMP synthase
CIN	chromosomal instability
circRNAs	circular RNAs
CLEM	correlative light-electron microscopy
CTL	Cytotoxic T lymphocytes
CTLA-4	Cytotoxic T-Lymphocyte Antigen 4
CXCL	CXC-chemokine ligand
Cyto-DR	cytosolic DNA response
DAMP	danger-associated molecular patterns
DC	dendritic cell
DCIS	ductal carcinoma in situ
Decoy-30d	Decoy construct for miR-30d
DEGS	differentially expressed genes
DGKZ	diacylglycerol kinase zeta
DNMTi	DNA methyltransferase inhibitors
dsDNA	double-strand DNA
DTC	dormant tumour cells
ECM	extracellular matrix

ECDF	empirical cumulative distribution function
EGA	european genome-phenome archive
EGF	epidermal growth factor
ELISA	Enzyme-linked immunosorbent assay
EndMT	endothelial-to-mesenchymal transition
EM	electron microscopy
EMT	epithelial-to-mesenchymal transition
ER	endoplasmic reticulum
EV	extracellular vesicles
EZH2	Enhancer of Zeste Homolog 2
FACS	Flow cytometry
GA	golgi apparatus
GAGs	glycosaminoglycans
GAPDH	glyceraldehyde 3-phosphate dehydrogenase
GCA	Golgicide A
GDCA	genomic data Commons
GFs	Growth factors
GFP	green fluorescent protein
GM130	Golgi matrix protein 130
GO	Gene ontology
GoF	Gain-of-function
GSEA	gene set enrichment analysis
GTP	guanosine triphosphate
HIF	hypoxia-inducible factor
HLA	human leukocyte antigen
hpt	hours post-transfection
IBC	invasive breast cancer
iCAFs	inflammatory CAFs
ICB	immune checkpoint blockade
ICI	immune checkpoint inhibitors
IF	immunofluorescence
IFN	Interferon
IgG	Immunoglobulin G
IHC	immunohistochemical

IL	interleukin
IP	intraperitoneal
IKK	IκB kinase
IRF	Interferon response factor
ISGs	interferon stimulated genes
JAK1	Janus kinase 1
KD	knockdown
KI	knock-in
KO	knockout
K/S	Kolmogorov-Smirnov
LATS1/2	Large Tumour suppressor 1/2
LNA	Locked nucleic acid
lncRNAs	Long non-coding RNAs
LNP	lipid nanoparticles
LoF	Loss-of-function
LOX	lysyl oxidase
mAb	monoclonal antibody
MAPKs	mitogen-activated protein kinases
mBC	metastatic breast cancer
MDSC	myeloid-derived suppressor cell
MHC	major histocompatibility complex
miRNA	microRNA
MMP	matrix metalloproteinase
MEM-NEAA	Minimum Essential Medium- Non-Essential Amino Acids
MN	micronuclei
mRNA	messenger RNA
MST1/2	mammalian STE20-like kinase 1/2
mtDNA	mitochondrial DNA
mutp53	mutant p53
myCAFs	myofibroblastic CAFs
ncRNAs	non-coding RNAs
NES	Normalized Enrichment Scores
NF-κB	Nuclear Factor kappa-light-chain-enhancer of activated B cells

NK	natural killer
NLS	nuclear localization signal
NE	nuclear envelope
OVT	oncolytic virus therapy
PAMPs	pathogen- associated molecular patterns
pCR	pathological complete response
PD-1	Programmed cell death 1
PDGF	platelet-derived growth factor
PD-L1	programmed-death ligand
PDO	patient derived organoids
PI3K	phosphoinositide 3-kinase
PLB	Passive Lysis Buffer
PLOD	procollagen- lysine, 2-oxoglutarate 5-dioxygenase
PMN	pre-metastatic niche
pre-miRNA	precursor-miRNA
pri-miRNA	primary miRNA
P/S	Penicillin-Streptomycin
qRT-PCR	quantitative real-time PCR
RD	residual disease
RIG-I	retinoic acid- inducible gene I
RISC	RNA-induced silencing complex
RLU	relative Luciferase Units
RNAi	RNA interference
ROS	reactive oxygen species
RT	room temperature
SASP	senescence associated secretory phenotype
SAV1	Salvador homologue 1
s.d	standard deviation
siRNA	small interfering RNA
STAT	signal transducer and activator of transcription
STING	Stimulator of interferon genes
TAM	tumour-associated macrophage
TAZ	transcriptional coactivator with a PDZ-binding domain
TBK1	TANK-binding kinase 1

TCGA	The Cancer Genome Atlas
TCGA-BRCA	TCGA breast cancer dataset
TEAD	transcriptional enhanced associated domain
TECs	tumour endothelial cells
TGF	transforming growth factor
TIME	tumour immune microenvironment
TMB	tumour mutational burden
TME	tumour microenvironment
TNBC	triple-negative breast cancer
TNF	tumour necrosis factor
TREX1	Three Prime Repair Exonuclease 1
Treg	T regulatory cells
T-VEC	talimogene laherparepvec
uPA	urokinase plasminogen activator
uniSTING	universal STING
UTR	untranslated region
VEGF	vascular endothelial growth factor
WB	Western Blot
WT	wild type
YAP	yes-associated protein

1 Introduction

1.1 The Tumour Ecosystem

Tumours are best understood as complex ecosystem rather than masses of cancer cells. Tumour behaviour does not arise only from cancer cell intrinsic programs but emerges from dynamic, reciprocal interactions between cancer cells and their surrounding microenvironment. Within this ecosystem, the tumour microenvironment (TME) acts as a central regulatory hub. It consists of extracellular matrix (ECM) components, stromal cells, vascular networks, and diverse immune populations that collectively shape tumour progression. Far from being a passive scaffold, the TME governs how cancer cells adapt to stress (e.g. nutrient availability) and evade immune surveillance and stromal resistance. In early stages, the native tissue microenvironment can impose tumour-suppressive constraints through limited nutrient and oxygen availability and physical confinement by the ECM. Over time, however, tumour cell-driven remodelling progressively converts this environment into a permissive and supportive niche (de Visser & Joyce, 2023; Quail & Joyce, 2013; S. Zhang et al., 2023). This reprogramming alters ECM architecture and stromal composition, establishing feed-forward interactions that promote tumour growth, metastatic dissemination, and resistance to conventional and immune-based therapies. This evidence underscores the importance of understanding how oncogenic events regulate tumour cells–TME interactions and, in turn, how these reciprocal dynamics influence cancer progression. Deciphering how the tumour landscape evolves over time will be critical for developing strategies that reshape the TME to sustain durable anti-tumour responses (Miao et al., 2025; Quail & Joyce, 2013). Ultimately, disrupting the tumour cells- TME axes that support malignancy, metastasis, and therapy resistance remains a central goal in the pursuit of transformative cancer therapies.

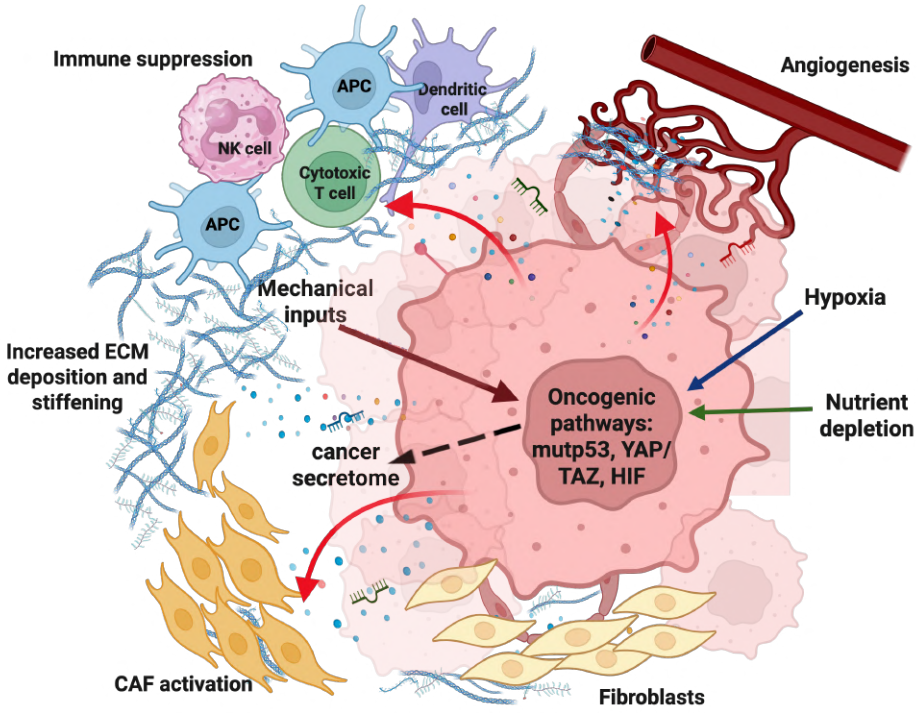

Figure 1. **The Tumour Ecosystem.** Schematic overview of the tumour mass illustrating the complex crosstalk between cellular components- such as cancer cells, immune cells, fibroblasts and non-cellular elements including the- extracellular matrix, cytokines, and growth factors of the TME. Alterations in intercellular communication within the TME profoundly influence tumour behaviour, promoting cancer progression, immune evasion, and contributing to therapy resistance. (Created with BioRender.com).

1.2 Stromal Components within the Tumour Microenvironment (TME)

1.2.1 Cancer-associated fibroblasts (CAFs)

Cancer-associated fibroblasts (CAFs) are among the most abundant and functionally diverse stromal cell types within the TME. While they are commonly derived from tissue-resident fibroblasts, they can also originate from a variety of other cell types, including bone marrow-derived mesenchymal stem cells (BMSCs), hematopoietic stem cells, pericytes, stellate cells, epithelial cells undergoing epithelial-to-mesenchymal transition (EMT), and endothelial cells undergoing endothelial-to-mesenchymal transition (EndMT) (Dzobo & Dandara, 2020; C. Fan et al., 2025). In the TME, fibroblasts are typically quiescent under normal physiological conditions but become activated in response to tumour-associated stress signals such as hypoxia, matrix remodeling and chronic inflammation. The tumour cell has the potential to secrete a wide range of molecules including growth factors (GFs) such as TGF-β, cytokines like IL-6, matrix-remodeling enzymes, and extracellular vesicles (EVs) that

collectively reshape the biochemical and biomechanical properties of the surrounding tissue. These signals induce the activation of resident fibroblasts, transforming them into myofibroblast-like cells known as cancer-associated fibroblasts (CAFs) (Kalluri, 2016; Lan et al., 2025). CAF activation is a result of extensive transcriptional reprogramming, often downstream of disrupted Notch and p53 signalling pathways (Sahai et al., 2020). This process is further regulated by the transcriptional cofactors Yes-associated protein (YAP) and transcriptional coactivator with PDZ-binding domain (TAZ), which are crucial for CAF-mediated ECM remodeling and the promotion of cancer cell invasion and angiogenesis (J. Luo et al., 2023; Sahai et al., 2020). Once activated, CAFs undergo distinct morphological changes, typically acquiring an elongated, spindle-shaped appearance. They also exhibit enhanced migratory and proliferative capabilities, and increased ability to synthesize and remodel ECM components. This activity leads to abnormal stiffening of the ECM, which alters the mechanical properties of the TME. CAFs further support tumour progression by promoting angiogenesis, altering tumour vasculature through the secretion of pro-angiogenic factors, and by modulating immune responses to create an immunosuppressive environment that favors cancer cell survival (Jia et al., 2025; Sahai et al., 2020). Recent studies have revealed that multiple CAF subtypes coexist within the TME, each exerting distinct effects on tumour biology (Biffi & Tuveson, 2021). For example, single-cell transcriptomic analysis in a mouse model of BC identified the transformation of normal mammary fibroblasts into two major CAF populations: inflammatory CAFs (iCAFs) and myofibroblastic CAFs (myCAFs). iCAFs are characterized by their secretion of inflammatory cytokines and their ability to enhance tumour cell invasion through matrix metalloproteinase (MMP) activity, particularly MMP1 and MMP3. myCAFs, on the other hand, display strong contractile features and are heavily involved in ECM remodeling, although their full functional profile is still being elucidated (Houthuijzen et al., 2023). In addition to MMPs, CAFs produce large quantities of lysyl oxidase (LOX) family proteins, which degrade basement membranes and reorganize collagen fibers activities that contribute to both structural breakdown and matrix stiffening. Beyond their structural roles, CAFs also secrete a wide array of pro-oncogenic factors, including VEGF-A, cytokines, chemokines, and GFs, all of which support tumour growth and survival. In addition, CAFs release metabolites such as amino acids, lipids, and lactate, which fuel tumour metabolism and enhance malignancy (C. Fan et al., 2025; Jia et al., 2025). Importantly,

as will be described below, many CAFs also influence the immune landscape of the TME. Their secreted molecules affect immune cell recruitment and activation, often promoting immunosuppressive conditions. For instance, dense collagen networks produced by CAFs can act as physical barriers that inhibit T cell infiltration into the tumour core, thereby limiting effective immune surveillance (Sahai et al., 2020; X. Wang et al., 2025). CAF-mediated immunosuppression is further reinforced by their crosstalk with immune inflammatory cells, particularly tumour-associated macrophages (TAMs). These macrophages, often polarized toward an M2-like phenotype within the TME, secrete cytokines such as IL-10 and TGF-β that support CAF activation. In turn, CAFs produce chemokines like CCL2 and CXCL12 that recruit and sustain TAM populations, creating a feedback loop that amplifies immunosuppressive signalling. This cooperative interaction between CAFs and TAMs contributes to the exclusion of cytotoxic immune cells, dampens anti-tumour immunity, and facilitates tumour progression. Collectively, these multifaceted roles position CAFs alongside their immune cell partners as central player of the TME, making them critical targets for therapeutic strategies aimed at disrupting tumour-stroma interactions and restoring effective anti-tumour immune responses.

1.2.2 The Extracellular Matrix (ECM) and mechanotransduction

The extracellular matrix is a dynamic, non-cellular three-dimensional network that provides structural integrity and mechanical support to tissues. Beyond its architectural role, the ECM serves as a bioactive scaffold that regulates cell behavior, modulates biochemical signalling, facilitates tissue repair, and delivers biomechanical cues essential for maintaining homeostasis (Bonnans et al., 2014; Frantz et al., 2010). Its composition is primarily made up of fibrous proteins such as collagen, elastin, fibronectin and laminin, alongside proteoglycans and glycosaminoglycans (GAGs) (Frantz et al., 2010). Collagen, the most abundant ECM protein, provides tensile strength and structural support, while elastin contributes elasticity, allowing tissues to recover their shape after deformation (Frantz et al., 2010). Fibronectin and laminin are key regulators of cell adhesion, migration and differentiation (Frantz et al., 2010). Additionally, the extracellular milieu is also enriched with soluble signalling molecules like GFs, including epidermal growth factor (EGF), transforming growth factors α and β (TGF- α/β), fibroblast growth factors (FGFs), platelet-derived growth factor (PDGF),

and vascular endothelial growth factor A (VEGF-A) which collectively orchestrate cellular responses and angiogenesis (Radisky, 2024). Complementing these signals, several proteases such as matrix metalloproteinases (MMPs), ADAMs (A Disintegrin And Metalloproteinase), cathepsins, and urokinase plasminogen activator (uPA) are also secreted into the extracellular space, where they degrade ECM components, releasing sequestered GFs and cytokines, and cleave adhesion molecules (Radisky, 2024). This pericellular proteolysis not only facilitates tumour cell progression but also modulates angiogenesis and immune responses, further reinforcing the evolving complexity of the TME.

Beyond its molecular composition, the physical properties of the ECM such as stiffness and viscoelasticity are critical determinants of tumour cell behavior and fate (Courbot & Elosegui-Artola, 2025; M. Zhang & Zhang, 2025). For instance, ECM stiffness is influenced by collagen deposition, crosslinking, and enzymatic remodeling. Enzymes like lysyl oxidase (LOX) and Procollagen-Lysine,2-Oxoglutarate 5-Dioxygenase (PLOD) catalyze crosslinking of collagen fibers, enhancing the rigidity and tensile strength of the matrix (M. Zhang & Zhang, 2025). This stiffened ECM acts as a barrier to immune cell infiltration, thereby impairing antitumour surveillance.

ECM stiffness and ECM-derived mechanical cues also directly support tumour expansion and aggressive phenotypes by their ability to direct cell behavior, as these cues are converted into biochemical signals within receiving cells through the process of mechanotransduction (Stowers, 2019). This begins with the activation of integrins at the cell membrane, which engage focal adhesion kinase (FAK) and Src family kinases, initiating downstream signalling cascades. In epithelial cancer cells, these pathways activate Rho GTPases and mitogen-activated protein kinases (MAPKs), leading to cytoskeletal reorganization, increased contractility, and enhanced migratory capacity (Katoh, 2025). The pro-oncogenic outcomes of mechanotransduction are executed by mechanosensitive oncogenic drivers—including MYC (Croci et al., 2017), YAP/TAZ (Piccolo et al., 2023), mutant p53 (Ingallina et al., 2018), HIF1α and others that reinforce the mechanical and immunosuppressive properties of the TME (Bertolio et al., 2023; Chang et al., 2023; Ghosh et al., 2021) (discussed in detail in the next sections).

1.2.3 Tumour-associated vasculature modified by hypoxic TME

The tumour-associated vasculature comprises blood and lymphatic vessels that are essential for transporting oxygen, nutrients, and immune cells throughout the tissue. Under normal physiological conditions, this vascular network is well-organized, with stable endothelial cell junctions, intact basement membranes, and regulated blood flow. However, in the context of tumour progression, this architecture becomes profoundly altered. As tumours grow, their metabolic demands increase, often exceeding the capacity of the existing vasculature to supply adequate oxygen and nutrients. This imbalance leads to the development of hypoxic regions within the tumour mass (Matuszewska et al., 2021). Hypoxia is a potent driver of vascular remodeling and is primarily mediated by hypoxia-inducible factors (HIFs), particularly HIF-1α. In response to low oxygen tension, HIF-1α becomes stabilized and activates the transcription of numerous pro-angiogenic genes, including vascular endothelial growth factor (VEGF), interleukin-8 (IL-8), and angiopoietins (Liu et al., 2025). These factors are secreted not only by cancer cells but also by stromal and immune components of the TME, collectively triggering an “angiogenic switch” (Baeriswyl & Christofori, 2009; Weis & Cheresh, 2011). This switch converts quiescent endothelial cells into tumour endothelial cells (TECs), which exhibit enhanced proliferation, migration, and tube formation. Activated TECs detach from their junctional adhesions, proliferate, and form immature vascular structures. They recruit pericytes for stabilization and undergo remodeling to establish a new, albeit abnormal, vascular network (Hida et al., 2016). Unlike normal vessels, tumour-associated vasculature is characterized by chaotic branching, irregular and fragmented basement membranes, and highly variable blood flow. These structural abnormalities result in leaky vessels that facilitate both intravasation and extravasation of cancer cells, thereby promoting local invasion and distant metastasis. Vascular leakiness also elevates interstitial fluid pressure, disrupting the distribution of oxygen, nutrients, and therapeutic agents within the TME. This contributes to the formation of edema and exacerbates hypoxia in localized regions, further impairing immune cell infiltration and promoting immune evasion (Ribatti, 2024). In addition to structural changes, TECs can engage mechanosensitive signalling pathways such as YAP/TAZ and Nuclear Factor kappa-light-chain-enhancer of activated B cells (NF-κB), which amplify inflammatory responses. Activation of these pathways leads to the secretion of pro-inflammatory

cytokines (e.g., TNFα, IL-6) and chemokines (e.g., IL-8, MCP-1), fostering a tumour-permissive and immune-suppressive milieu (Cao et al., 2024; Hooglugt et al., 2021). Thus, tumour-induced vascular changes not only support cancer progression but also foster an immunosuppressive microenvironment, highlighting the therapeutic potential of targeting abnormal vasculature to improve treatment outcome.

1.3 The Tumour immune microenvironment (TIME)

The tumour immune microenvironment (TIME) is a defined component of the complex TME. It refers to the immune cell populations (discussed in detail below) present within the tumour milieu. This landscape is highly context dependent as it can either exert anti-tumour effects through surveillance and cytotoxicity, or promote progression via immune evasion and chronic inflammation, with this balance shaping tumour's fate and therapeutic response (Racacho et al., 2025). It is well known that immune system's fundamental role is to act like a guardian protecting the host against pathogens and abnormal cells. This function is executed through two cooperating arms: first a rapid, non-specific innate response and later a slower, antigen-specific adaptive response that establishes immunological memory (Chi et al., 2024; Suresh, 2013; R. Wang et al., 2024). In cancer, this surveillance function is initially tumour-suppressive, but becomes reshaped over time by a process termed cancer immunoediting, which comprises three sequential phases. During elimination state, nascent malignant cells are detected and removed by innate and adaptive effectors. Then, during the equilibrium phase, a subset of tumour cells survives immune pressure but is kept in check. Finally, during the escape state, immune-resistant variants expand and the microenvironment becomes progressively immunosuppressive (Lasek, 2022; Vesely & Schreiber, 2013). This evolving balance between immune-mediated tumour control and immune-driven selection of resistant clones explains why immunity can both suppress and unintentionally enable tumour progression. The TIME as described above is pooled with both innate immune populations that provide immediate responses and adaptive populations that provide specificity and memory. Innate effectors include macrophages, neutrophils, natural killer cells (NK), dendritic cells (DC) and monocytes. These cells detect danger signals through pattern recognition and other receptors, mount inflammation, phagocytose

abnormal cells, and secrete cytokines and chemokines that shape downstream adaptive responses (R. Wang et al., 2024). Adaptive effectors principally include $CD8^+$ cytotoxic T lymphocytes, which mediate antigen-specific killing; B cells, which produce antibodies and establish long-term immune memory; and $CD4^+$ helper T cells, which coordinate immune responses by providing essential cytokine signals, supporting cytotoxic T cell activation, and promoting B cell differentiation (R. Wang et al., 2024). Antigen-presenting cells (APC), especially DC and macrophages, bridge innate and adaptive immunity by processing tumour antigens and presenting them to T cells in lymphoid organs, thereby initiating and tailoring the adaptive response. Among innate populations, macrophages exemplify functional plasticity and play a central role in TIME dynamics (Chaplin, 2010; Huang et al., 2024). In early anti-tumour responses macrophages can adopt pro-inflammatory, tumouricidal phenotypes that produce cytokines, present antigen and stimulate cytotoxic lymphocytes. However, with the evolving TME, macrophages are often reprogrammed toward immunosuppressive, tissue-remodelling states that resemble M2-like functions. These tumour-associated macrophages (TAMs) support angiogenesis, ECM crosslinking and stiffening, metabolic adaptation, and suppression of cytotoxic lymphocytes, and high TAM abundance frequently correlates with poorer prognosis (Huang et al., 2024). Neutrophils also exhibit stage-dependent duality like early N1-like neutrophils can produce reactive oxygen species (ROS) and cytokines that limit tumour initiation, whereas later N2-like neutrophils promote matrix remodelling, angiogenesis and immunosuppression (H. Xu et al., 2025). Natural killer (NK) cells provide rapid cytotoxicity against cells lacking normal MHC expression and can enhance antigen cross-presentation, but their infiltration and activity are often impaired in established tumours (Vojdani et al., 2024). Dendritic cells (DC) are essential initiators of antitumour T cell responses, yet in the TME they may become functionally tolerogenic or ineffective at antigen presentation, undermining T cell priming. T lymphocytes are the principal mediators of adaptive antitumour immunity and their function is tightly regulated by antigen recognition and co-stimulatory or inhibitory signals. $CD8^+$ cytotoxic T cells recognize tumour-derived peptides presented on MHC I and execute targeted killing, while $CD4^+$ helper subsets direct immune orchestration through cytokine production and help for $CD8^+$ responses and B cell antibody production. Conversely, regulatory T cells and other suppressive lymphocyte subsets can blunt

effective immunity by secreting cytokines IL-10, TGF-β and other immunosuppressive mediators (R. Wang et al., 2024). Chronic antigen exposure, inhibitory checkpoint signalling and a hostile metabolic and stromal environment progressively exhaust effector T cells, reduce their proliferation and cytotoxicity, and favour tumour-tolerant states. Interestingly, interactions between immune subsets and stromal elements create reinforcing feedback loops that promote immune suppression. For instance, TAMs and CAFs mutually recruit and activate each other via TGF-β, VEGF, PDGF, EGF, and FGF, generating stiff ECM and chemokine gradients that physically and biochemically exclude cytotoxic lymphocytes. In parallel, metabolic competition and CAF-derived metabolites also rewire immune cell metabolism and function. Protease-mediated ECM remodelling and aberrant vasculature further limit immune cell trafficking and antigen delivery. Collectively, these mechanisms reduce antigen visibility, impair effector function, and enable immune escape (J. Luo et al., 2025).

To address the complex landscape of the TME, immune-based therapies have been developed to harness the TIME and elicit antitumour responses. Their efficacy, however, is often constrained by the immunosuppressive nature of the TIME, where stromal barriers, regulatory immune cells, aberrant vasculature, and metabolic competition hinder effector infiltration and promote immune evasion. While immune checkpoint inhibitors (ICI), adoptive cell therapies (ACT), and tumour vaccines have shown sustained benefit in some patients (Cole et al., 2023), many tumours remain intrinsically resistant or develop adaptive mechanisms such as antigen loss, upregulation of inhibitory ligands, and recruitment of suppressive populations. Some tumours also become immunologically cold, by silencing pathways required to activate effector cells- such as interferon (IFN) signalling. Recently, restoring these pathways, with STING agonists, has been shown to enhance immune infiltration, boost IFN responses, and improve immunotherapy efficacy (discussed in detail under section 1.5). Overcoming these barriers requires integrated strategies that reprogram the TIME with rational combinations of checkpoint blockade with agents capable of targeting the tumour landscape offer a promising route to convert non-responsive tumours into immunologically active and treatable ones to improve patients outcome.

1.4 Induction of the interferon response

Cytosolic sensing of aberrant nucleic acids is crucial to activate defence mechanisms that detect cellular distress and links innate immune activation to adaptive responses. Within the cytosol, specialized receptors are present acting as molecular guard, constantly checking for unusual RNA or DNA species. Upon ligand recognition, these receptors trigger signalling cascades that culminate in robust production of type I interferons (IFN-I) and proinflammatory cytokines. These nucleic-acid sensing pathways are engaged not only by viral or bacterial genomes but also by endogenous danger signals derived from damaged mitochondria, nuclear DNA leakage, retroelements, micronuclei or tumour-derived nucleic acids, and their activation can profoundly reshape the microenvironment by recruiting and activating APC cells, stimulating cytotoxic lymphocytes, and enhancing antigen cross-presentation (Bonjardim, 2005; Hopfner & Hornung, 2020; K. N. Miller et al., 2021; H. Wang & Petrini, 2025).

The two major pathways involved in IFN-I signalling are- i) cytosolic RNA sensing by retinoic acid- inducible gene I (RIG-I)-MAVS pathway and ii) cytosolic DNA sensing by the cyclic GMP-AMP synthase-stimulator of interferon genes (cGAS-STING) pathway (Iurescia et al., 2018). The RIG-I recognizes short double-stranded or 5′-triphosphate-containing RNAs and, upon RNA engagement, undergoes conformational changes that expose its CARD domains and permit interaction with the mitochondrial antiviral-signalling protein MAVS. MAVS then nucleates downstream activation of TBK1/IKKε and transcription factors that drive IFNβ and proinflammatory gene expression (Thoresen et al., 2021). On the other hand, the cGAS-STING pathway is triggered when cGAS detects cytosolic dsDNA and synthesizes cGAMP, which activates STING on the endoplasmic reticulum. STING then translocates to the Golgi, recruits TBK1, and activates IRF3 and NF-κB, leading to the production of type I interferons and proinflammatory cytokines (discussed under section 1.5 in detail) (Samson & Ablasser, 2022). Both the above mentioned pathways converge on IFN production in spite of their different ligand specificity and subcellular localization. Remarkably, within tumours, activation of RIG-I–MAVS or cGAS-STING can convert an immune-suppressed microenvironment into an immune-hot one by enhancing DC maturation, increasing type I IFN-dependent cross-priming of $CD8^+$ T cells, and promoting chemokine-driven recruitment of effector immune cells, which raises

considerable interest in therapeutically harnessing these pathways to potentiate immunotherapies. Importantly, however, nucleic acid sensing in cancer displays context-dependent, sometimes paradoxical effects as its chronic or dysregulated activation can induce immunosuppressive feedback loops, upregulate immune checkpoint molecules such as PD-L1, or engage autophagy and other cell-intrinsic adaptations that blunt antitumour immunity (Won & Bakhoum, 2020). Thus, while targeted activation of RIG-I or cGAS-STING holds promise for reprogramming the TIME and improving responses to immunotherapy, their impact might be maximized when combined with broader strategies that overcome the suppressive features of the tumour milieu.

1.5 Overview of the cGAS/STING/IFN-I pathway

The cytosolic DNA sensing pathway governed by cyclic GMP–AMP synthase (cGAS) and stimulator of interferon genes (STING) is a backbone of the innate immune system, enabling cells to detect aberrant cytosolic double-stranded DNA (dsDNA) and mount protective responses. STING was first identified in 2008 by Glen Barber's group as an adaptor protein that senses cyclic dinucleotides, while in 2013 Zhijian James Chen and colleagues introduced cGAS as the primary DNA sensor that synthesizes cGAMP upon detection of foreign or self-DNA (Ishikawa et al., 2009; Ishikawa & Barber, 2008; Racacho et al., 2025; L. Sun et al., 2013). Activation of this cascade induces interferon-stimulated genes and drives the release of inflammatory cytokines and chemokines, thereby recruiting immune cells and enhancing antitumour immunity (Fig. 3), including responses to immunotherapies such as immune checkpoint blockade (ICB). Beyond its cytotoxic effects, this evolutionarily conserved pathway serves as a key regulator of host defence, exerting critical control over cancer and other diseases (Hopfner & Hornung, 2020). Importantly, the cGAS–STING axis functions as a double-edged sword: while acute activation promotes interferon production and immune cell recruitment, chronic or dysregulated signalling can foster immune suppression, inflammation-driven tumour progression, and therapy resistance (J. min Du et al., 2022). Tumours frequently exploit evasion strategies such as DNA degradation, cGAMP hydrolysis, or epigenetic silencing of pathway components to attenuate interferon signalling and escape immune surveillance. Thus, maintaining the balance between activation and evasion of the cGAS–STING pathway is critical for

harnessing its full therapeutic potential in cancer (detailed description in the following subsection).

1.5.1 Acute activation of cGAS/STING pathway in cancer

In the context of cancer, the cGAS–STING pathway is frequently activated by the accumulation of aberrant cytosolic dsDNA, which typically originates from endogenous sources. Structural disruptions such as nuclear envelope (NE) rupture and micronuclei (MN) breakdown are key contributors. During tumour progression, mechanical stress arising from altered cytoskeletal dynamics, elevated actomyosin contractility, and spatial confinement compromises NE integrity, allowing genomic DNA to leak into the cytoplasm. To mitigate this, tumour cells engage mechano-protective responses that preserve NE architecture and limit cGAS–STING activation (Frittoli et al., 2023; Nader et al., 2021). MN represent another source of cytosolic dsDNA. These small extranuclear bodies form during mitosis due to chromosome missegregation or defective DNA repair, and often contain whole chromosomes or fragments. Their fragile NE is prone to rupture, releasing DNA into the cytoplasm. (Bakhoum et al., 2018; Bona & Bakhoum, 2024; Hosea et al., 2024).

Once in the cytosol, dsDNA is sensed by cGAS, which binds DNA via a dedicated surface and undergoes a conformational change that enables the enzymatic synthesis of 2′3′-cyclic GMP–AMP (cGAMP) from adenosine triphosphate (ATP) and guanosine triphosphate (GTP) (Ablasser et al., 2013; Civril et al., 2013; Samson & Ablasser, 2022; L. Sun et al., 2013). Notably, upon binding to cytosolic dsDNA, cGAS undergoes liquid–liquid phase separation, forming dynamic droplets where both cGAS and DNA are spatially concentrated to facilitate efficient cGAMP synthesis (M. Du & Chen, 2018). cGAMP further binds to STING, a transmembrane adaptor protein on the endoplasmic reticulum (ER), inducing a conformational rearrangement of STING dimers. This structural change enables side-by-side packing into tetramers and higher-order oligomers (Shang et al., 2019). Activated STING then undergoes COPII-dependent trafficking from the ER to the Golgi apparatus (GA), a critical step for downstream signalling (Dobbs et al., 2015; P. Gao et al., 2013; Ishikawa et al., 2009). At the Golgi, STING recruits and activates TANK-binding kinase 1 (TBK1), which phosphorylates STING at the critical serine residues S366 and S358 allowing recruitment of the interferon regulatory factor 3 (IRF3) and its subsequent

phosphorylation by TBK1 (Tanaka & Chen, 2012; Y. Yan et al., 2025; C. Zhang et al., 2019). Phosphorylated IRF3 dimerizes and dissociates from STING. This conformational change exposes a previously masked nuclear localization signal (NLS), allowing IRF3 to translocate into the nucleus. Once inside, IRF3 partners with transcriptional co-activators CBP/p300 to initiate transcription of type I interferons (IFNα and IFNβ) and a broad array of interferon-stimulated genes (ISGs) that orchestrate antitumour responses (Y. Yan et al., 2025). In parallel, STING might also activate the IκB kinase (IKK) complex, leading to nuclear translocation of nuclear factor-κB (NF-κB) and the induction of proinflammatory cytokines such as tumour necrosis factor (TNF), interleukin-1b (IL-1b), and interleukin-6 (IL-6) (de Oliveira Mann et al., 2019; Yum, 2021). Secreted type I interferons signal through the IFNAR1/IFNAR2 receptor complex to activate the Janus kinase–signal transducer and activator of transcription (JAK–STAT) pathway, amplifying ISG expression and promoting antigen presentation, and immune cell recruitment (Gan et al., 2022; Ruiz-Iglesias et al., 2025). Following activation, STING is trafficked to endolysosomes for degradation (Won & Bakhoum, 2020).

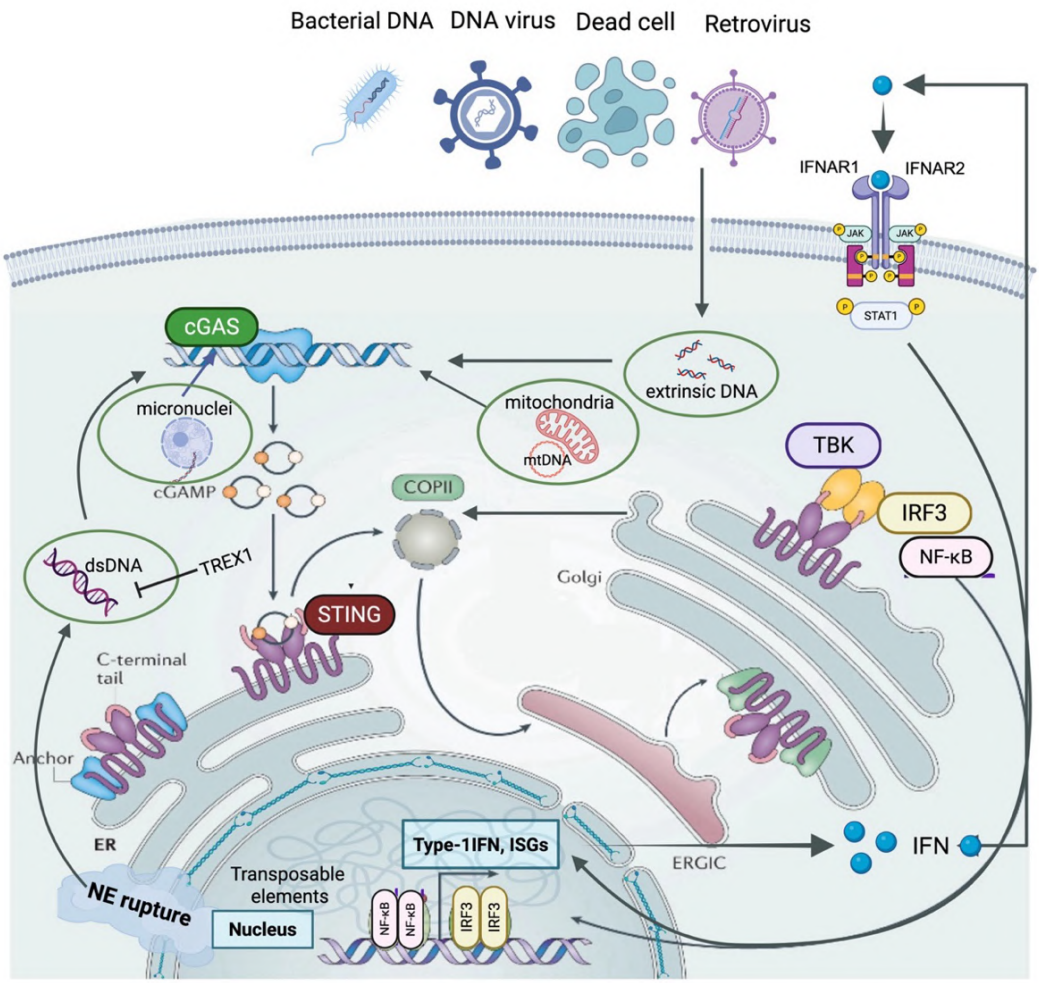

Figure 2. **Schematic representation of cGAS/STING signalling in tumour cell.**

The recognition of cytosolic DNA by cGAS leads to its activation and consequent production of cGAMP, that stimulates STING. Once activated, STING translocates from ER to the Golgi, where it forms a signalling complex that recruits TBK1 to phosphorylate IRF3. Phosphorylated IRF3 enters the nucleus and triggers the expression of type-I interferon and other immune mediators. At the same time, STING also binds and stimulates IKK, triggering the transcriptional activation of NF-κB leading to the expression and secretion of pro-inflammatory cytokines. (Adapted from *(Hopfner & Hornung, 2020)* and modified with BioRender.com)

1.5.2 Role of cGAS/STING pathway in cancer immune surveillance

There is ample evidence that cGAS-STING activation promotes antitumour immunity through both tumour-intrinsic effects and immune-cell-mediated mechanisms. In tumour cells, STING signalling activates IRF3-driven transcription of type I interferons and ISGs, which recruit and activate NK cells and cytotoxic $CD8^+$ T cells to mediate direct tumour cell killing (Samson & Ablasser, 2022; Won & Bakhoum, 2020). Tumour-intrinsic STING activity can also reduce cancer cell fitness by promoting apoptosis and driving cellular senescence. Notably, activated IRF3, downstream of STING–TBK1 signalling, can bind and activate the pro-apoptotic Bax protein, promoting mitochondrial apoptosis and thereby contributing to tumour-cell elimination (Chattopadhyay et al., 2010). Senescent tumour cells adopt a senescence-associated secretory phenotype (SASP) that releases chemokines and proinflammatory cytokines and these factors act both cell-autonomously to reinforce growth arrest and non-cell-autonomously to recruit and activate immune effectors for tumour clearance (Shen et al., 2025; Takasugi et al., 2023). Together, these linked programs bridge intrinsic stress responses with extrinsic immune surveillance to limit malignant progression.

Interestingly, cGAS-STING pathway activation occurs not only within tumour cells but also in APCs, particularly DCs, where cGAS-derived cGAMP activates STING and triggers interferon release that promotes DC maturation, enhances antigen presentation and cross-priming, and strengthens $CD8^+$ T-cell cytotoxic responses (Diamond et al., 2011; Duong et al., 2022; Shen et al., 2025). In addition paracrine transfer of cGAMP and tumour-derived DNA to stromal DCs and macrophages further amplifies the effect of professional APCs to prime naïve T cells and sustain effector function within the TME (Marcus et al., 2018). Thus, activated cGAS-STING signalling has the potential to convert tolerogenic into immunogenic cell death by promoting danger-associated molecular patterns (DAMP) release (e.g., HMGB1, ATP, calreticulin) through membrane perturbation, ER-stress and pore-mediated export, and by inducing type I interferons and amplifying inflammasome-linked cytokines. Together these events enhance antigen uptake, cross-presentation and durable $CD8^+$ T-cell responses for tumour clearance.

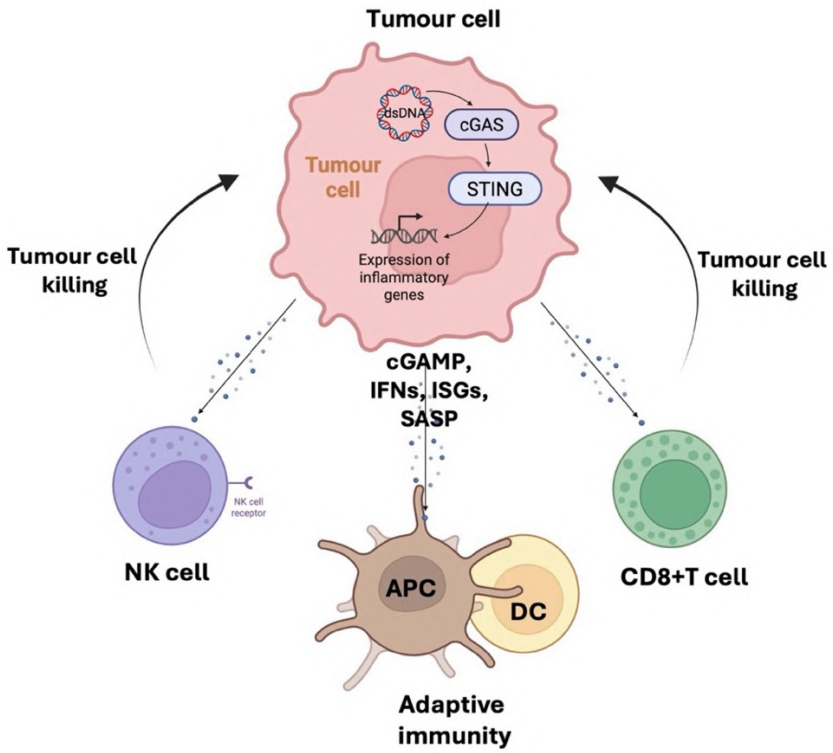

Figure 3. **Schematic representation of cGAS/STING signalling in tumour cell and its impact on the immune TME.**

The cGAS-STING pathway is activated by cytosolic dsDNA in tumour cells and culminates in the release of type-I IFNs and immune-stimulatory cytokines, which trigger tumour cell killing by immune cell populations like NK cell and $CD8^{+}$T cells. In addition, tumour-derived DNA and cGAMP produced by tumour cells represent signals that activate the cGAS-STING pathway also in APC, further amplifying both the interferon production and antitumour immune responses. (Created with BioRender.com)

1.5.3 Pro-Tumourigenic roles of the cGAS/STING pathway

As evident till now, the acute activation of the cGAS-STING pathway is critical for tumour suppression. This occurs by triggering type I interferon-driven immune surveillance which helps preserve tissue integrity and prevent malignant transformation (Samson & Ablasser, 2022). However, emerging evidence highlights the context-dependent nature of this pathway, revealing its potential to promote tumour progression under certain conditions (Won & Bakhoum, 2020). For example, STING-deficient mice exhibit resistance to chemically induced skin carcinogenesis, suggesting that persistent STING-driven inflammation may contribute to tumour development (Ahn et al., 2014). In tumours with high chromosomal instability (CIN), chronic activation can rewire the signalling from type I interferons and canonical NF-κB toward non-canonical NF-κB pathway, a shift that promotes invasive behaviour and

metastatic progression (Bakhoum et al., 2018; J. Li et al., 2023). Moreover, in chromosomally unstable tumour cells, STING signalling is often diverted toward an ER stress response. This altered signalling may explain the intrinsic resistance of such tumours to STING agonists (see section 1.5.4), limiting the efficacy of therapies aimed at activating this pathway (J. Li et al., 2023). Additionally, non-canonical NF-κB signalling has been implicated in promoting tumour progression following radiotherapy, partly by suppressing DC function and mobilizing myeloid-derived suppressor cells (MDSCs), which dampen antitumour immunity (Hou et al., 2018). Notably, chronic cGAS-STING signalling also drives persistent SASP factor accumulation that promotes epithelial invasiveness, malignant transformation, and metastatic progression (J. min Du et al., 2022). These factors underscores the importance of precise regulation of cGAS-STING signalling to harness its therapeutic potential without triggering pro-tumourigenic effects.

1.5.4 Anti-cancer therapy: relevance of the cGAS/STING/IFN-I pathway

Over the past decades, cancer treatment has largely relied on two complementary strategies that directly attack tumour cells. Chemotherapy uses cytotoxic drugs that preferentially kill rapidly dividing cells and remains effective across many cancer types, but its lack of specificity often causes significant off-target toxicity to normal tissues (Anand et al., 2023). For example, in BC, anthracycline-based doxorubicin and other drugs like- the antimetabolite 5-fluorouracil and paclitaxel all are being used to treat triple-negative (TN), high-risk early and neoadjuvant settings due to their potent cytotoxicity, but their use is limited by dose-dependent toxicities, prompting careful patient selection (Obidiro et al., 2023).

As opposed to conventional chemotherapies, targeted therapies are a newer, more selective approach that inhibits specific molecular drivers responsible for tumour growth, offering improved precision and reduced systemic toxicity (Min & Lee, 2022). Among many clinically approved ones are Trastuzumab and Pertuzumab monoclonal antibodies targeting HER2-positive BC (Jagosky & Tan, 2021), PARP inhibitors like Olaparib and Talazoparib for patients with BRCA1/2-mutated tumours (Piha-Paul et al., 2024) and CDK4/6 inhibitors like palbociclib, ribociclib and others that selectively block cell-cycle drivers and have become standard partners to endocrine therapy in HR+/HER2− advanced BC, substantially improving disease control (Braal et al., 2021).

Despite these advances, tumours frequently develop resistance by rewiring signalling and metabolic pathways or by altering the structure and function of the targeted molecules, which limits long-term efficacy of targeted therapies.

The idea of deploying the immune system as a tool to treat cancer originated in the 19th century (Waldman et al., 2020) and the advent of KO mouse models provided the necessary technology to experimentally demonstrate a link between immunodeficiency and cancer (Chow et al., 2012). Unlike the previously described treatments that target cancer cells, immunotherapy aims to boost the body's natural ability to fight cancer while disrupting the signals that help tumours evade immunity. Moreover, it exhibits lesser off-target effects and has led to markedly improved outcomes in multiple cancer types (M. Zhang et al., 2025). Effective immunotherapeutic approaches include virus- or cell-based strategies- notably oncolytic virus therapy (OVT), uses natural or engineered viruses that selectively lyse tumour cells and stimulate local antitumour immunity (Chowaniec et al., 2024); adoptive cell therapies (ACT), which reprogram effector lymphocytes such as chimeric antigen receptors T cells (CAR-T cells) often combined with DC vaccines to target malignancies (Qian & Liu, 2025) and antibody-based interventions, like immune-checkpoint inhibitors (ICIs), which release inhibitory brakes on T cells to restore antitumour responses (Mc Neil & Lee, 2025).

Immune-checkpoint inhibitors are the most clinically established and widely adopted form of cancer immunotherapy to date. Immune checkpoints are surface ligands that regulate T cell responses by modulating TCR signalling and preventing autoimmunity. Tumours exploit checkpoints such as PD-1 (Programmed Death-1)/ PD-L1 (Programmed Death-Ligand 1) and CTLA-4 (Cytotoxic T-Lymphocyte Antigen 4) to evade immune detection. ICIs, designed as monoclonal antibodies, block these inhibitory receptors or ligands, thereby unleashing T cells to destroy cancer cells. The most common ICIs include anti-PD-1, anti-PD-L1, and anti-CTLA-4. In particular, the US Food and Drug Administration (FDA) has approved a human monoclonal antibody (mAb) blocking CTLA-4 inhibitor Ipilimumab for the treatment of metastatic melanoma, the PD-1 inhibitor Nivolumab for treatment of melanoma, lung cancer, kidney cancer and Hodgkin’s lymphoma and the PD-1 inhibitor Pembrolizumab for the treatment of lung cancer, and head-and-neck cancer (Wei et al., 2018). This therapy can produce durable antitumour response as they reactivate T cells and form a long lasting memory

against cancer cells, potentially maintaining benefit after therapy stops. This property makes ICIs especially valuable for hard-to-treat cancers, including selected BC subtypes (Mc Neil & Lee, 2025).

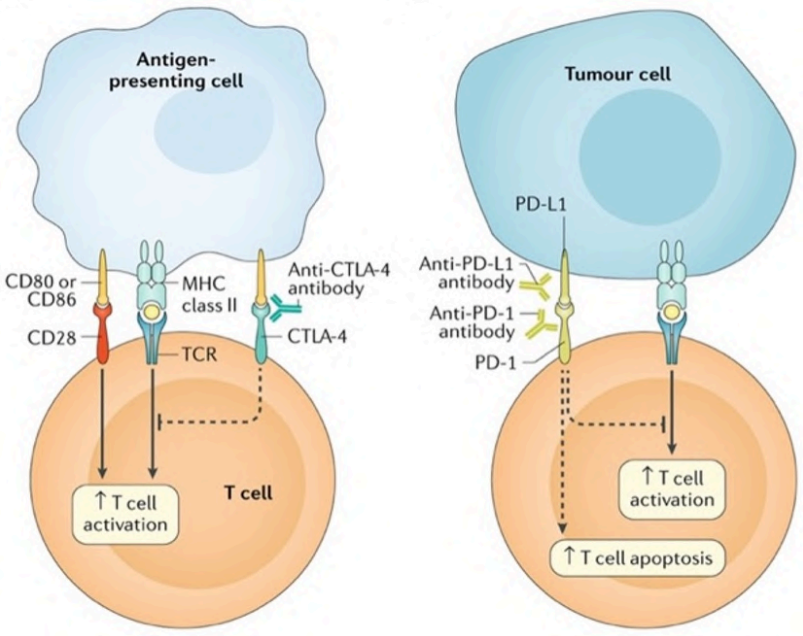

Figure 4. **Schematic representation showing of how IC therapy promotes T-cell activitation.**

Left. T cell activation requires two signals: first, antigen recognition by the T cell receptor (TCR) following antigen presentation by MHC class II molecules on the surface of antigen-presenting cells. CTLA-4 is located on the T-cell surface and involved in blocking T cell activation. Hence, CTLA-4 inhibitors facilitate T cell activation. **Right.** PD-1 is a surface receptor that is expressed by T-cells and promotes apoptosis of antigen-specific T-cells and reduces apoptosis of regulatory T-cells through its interaction with its ligand PD-L1, which is expressed by tumour cells and myeloid cells. PD-1 and PD-L1 inhibitors block the PD-1–PD-L1 interaction, facilitating T cell activation and survival. (Adapted from (Ramos-Casals et al., 2020))

However, a significant proportion of patients still fail to respond to these therapies and the underlying causes of this heterogeneity remain poorly understood. Resistance to ICI might arise from tumour-intrinsic factors including ECM stiffness, tumour mutational burden (TMB), and high PD-L1 expression and many others (Shiravand et al., 2022). As explained before stiff ECM hinders immune infiltration and alters checkpoint expression, undermining therapy (Shiravand et al., 2022). High TMB cancers like melanoma and NSCLC respond better due to abundant neoantigens enhancing T cell recognition, making TMB a predictive biomarker (Shiravand et al., 2022). Tumours with PD-L1 overexpression has led to approval of anti-PD-1/PD-L1

therapies contributing to tumour regression in certain cancers, as blocking these pathways restores T cell cytotoxicity (Shiravand et al., 2022). Yet, responses remain inconsistent as less than 40% of cancer patients benefit from anti-PD-1 therapy, and ~25% relapse within 21 months due to mechanisms such as JAK1/2 loss of function mutations impairing interferon signalling or compensatory upregulation of TIM-3 (Zielińska et al., 2025). To overcome these hurdles, combination therapy, such as anti-PD-1 with anti-CTLA-4, is rigorously being tested.

A more promising strategy is to combine ICIs with agents that reactivate the interferon pathway especially cGAS-STING, which is often suppressed in immune-desert tumours. In this vein, cyclic dinucleotides, small-molecule and STING agonists are being developed. A STING agonist basically is a drug that activates the STING protein to kick-start the immune system. They act like immunotherapy boosters, when injected directly into tumours, trigger rapid innate activation, drive DC maturation and recruit T cells, often causing local tumour shrinkage and inducing systemic, long-lived antitumour immunity (B. Wang et al., 2024). These promising effects have motivated early-phase clinical testing of STING agonists administered alone or in combination with systemic therapies. For example, STING agonists like ADU-S100, MK-1454, and DMXAA are accepted for research and are in clinical trials (Hines et al., 2023). Combination approaches are particularly attractive because the cGAS-STING axis synergizes mechanistically with established modalities like ionizing radiation and many genotoxic chemotherapies like cisplatin, doxorubicin which increase the presence of dsDNA burden in tumour cells and thereby potentiate endogenous STING activation, while immune checkpoint inhibitors can relieve T-cell suppression and exploit improved antigenicity and DC priming driven by STING-induced interferons (Colangelo et al., 2024; Pantelidou et al., 2019). Despite encouraging rationale, STING agonists face key hurdles like systemic toxicity from widespread inflammation, tumour resistance due to pathway component silencing or cGAMP degradation, and the risk that chronic activation can trigger immunosuppressive, pro-tumour programs. In order to tackle these hurdles, a novel immunotherapeutic strategy has emerged through the development of a universal STING mimic (uniSTING), which enhances antitumour immunity. Unlike conventional STING agonists that often face limitations due to poor delivery and downregulated endogenous STING expression in the TME, uniSTING is engineered to trigger robust STING signalling independent of endogenous STING

levels. It was shown that, when delivered by lipid nanoparticles (LNP), uniSTING-mRNA treatment produces a STING mimic in both tumour and DC cells, further activating IRF3 and triggering IFN-I release. Tumour cells treated with uniSTING also release EVs carrying miRNAs that showed the potential to reactivate the immune components of TME. Thus, this platform represents a significant advancement in innate immune modulation, offering positive results in mouse models of liver, lung and TNBC difficult-to-treat tumours (Y. Wang et al., 2024).

1.5.5 Modulation of the cGAS/STING pathway in cancer

Remarkably, the cellular context of the cGAS/STING pathway is subject to multilayered regulation in tumour cells, ranging from rapid post-translational controls to longer-term genetic and epigenetic adaptations that collectively determine whether cytosolic DNA sensing elicits productive antitumour immunity or is attenuated to permit immune escape. Several positive and negative regulators of the pathway have been identified, among the positive regulators, TRIM32 and TRIM56 mediate ubiquitination of STING, enhancing its interaction with TBK1 and facilitating downstream signalling (Tsuchida et al., 2010; J. Zhang et al., 2012). Additionally, palmitoylation of Golgi-localized STING at residues C88 and C91 has also been shown essential for the induction of type I interferons, further amplifying the immune response (Mukai et al., 2016). Conversely, pathway activity is constrained by nucleic acid modifying enzymes and competitive inhibitors that limit ligand availability or second-messenger stability. Cytosolic exonucleases may degrade DNA before it engages cGAS, while phosphodiesterases hydrolyse cGAMP, thereby restricting STING activation. Beyond these examples, cGAS and STING are also modulated by other set of post-translational modifications (PTM) like phosphorylation and SUMOylation which influence protein stability, trafficking and assembly into signalling complexes. Moreover, caspase-mediated cleavage during apoptosis actively inactivates components of the pathway to prevent inappropriate inflammatory signalling (Z. D. Zhang & Zhong, 2022).

Multiple mechanisms may allow transformed cells to acquire tumour-specific suppression of the pathway like epigenetic silencing of cGAS or STING expression, or somatic mutations that impair sensor or adaptor function, are frequently observed in cancer. Moreover, cancer cells exploit and amplify endogenous brakes, for instance,

increased expression of TREX1 nucleases may blunt accumulation of cytosolic DNA, and upregulation of extracellular cGAMP hydrolases prevents paracrine activation of neighbouring immune cells. Excessive CIN and DNA damage, MN formation and NE rupture, which are hallmarks of many malignancies, generate the ligands that can activate cGAS, but the frequency, size and repair competence of these events influence whether signalling is acute and immunogenic or chronic and tolerogenic (Beernaert & Parkes, 2023). Similarly, events leading to mitochondrial DNA (mtDNA) release differ in immunological consequence depending on whether release occurs in the context of apoptosis, which couples DNA release to caspase-mediated pathway suppression, or in viable cells, where mitochondrial permeability events permit cGAS engagement (White et al., 2014). The TME further modulates pathway output through nutrient and metabolic stress, hypoxia, and stromal interactions that alter both DNA availability and immune responsiveness. Collectively, these layers of regulation create a spectrum of cGAS-STING activity across cancers, where some tumours retain intact, inducible signalling that can be therapeutically harnessed, whereas others select for durable suppression of the pathway to evade immune surveillance. Understanding these regulatory mechanisms is essential for designing interventions that restore productive innate sensing while avoiding chronic inflammation.

1.6 Regulation of cGAS/STING pathway by cellular processes

1.6.1 Effect of wild-type and mutant p53 on cGAS/STING pathway

The p53 protein, often referred to as guardian of the genome, in its native wild type (wt) form acts as a potent tumour suppressor. It monitors a broad spectrum of cellular stresses and activates appropriate tumour preventing responses to maintain genomic integrity. p53 belongs to a protein family with its siblings p63 and p73, which share structural homology and both contribute to tumour suppression and development. In unstressed cells, wtp53 levels are generally low through ubiquitin-mediated degradation driven primarily by the E3 ligase MDM2 in cooperation with MDM4, but cellular stresses disrupt this interaction, leading to p53 stabilization and activation (Hernández Borrero & El-Deiry, 2021). Once activated, wtp53 functions as a tetrameric transcription factor that orchestrates a stress response by regulating gene programs like cell-cycle arrest e.g., induction of CDKN1A/p21 to enforce G1/S and G2/M checkpoints, DNA repair -to promote nucleotide- and base-excision repair and damage

recognition, apoptosis by inducing pro-apoptotic genes like BAX, PUMA, and NOXA in damaged cells, and senescence for sustained growth arrest accompanied by SASP (Hernández Borrero & El-Deiry, 2021; Stracker, 2024). Beyond these canonical outputs, p53 also modulates metabolic homeostasis and autophagy (B. Xu et al., 2025). Through the above mentioned mechanisms, p53 maintains overall cellular homeostasis and genomic stability. In addition to coding genes, p53 also regulates several miRNA families, like the miR-34, miR-192 and miR-215 which behave as tumour-suppressors by promoting apoptosis, cell cycle arrest, and senescence (Feng et al., 2011). Beyond its cell-intrinsic tumour-suppressive roles, p53 also shapes the TME by promoting immune surveillance. During senescence in hepatic stellate cells, p53 regulates the SASP, promotes an anti-tumour M1 macrophage state, and activates NK cells (Lujambio et al., 2013), and p53 reactivation within liver cancer induces tumour-cell senescence, alters the tumour secretome, and provokes innate immune-mediated tumour regression (Xue et al., 2007). Interestingly, wtp53 helps the immune system spot emerging tumours by activating the cGAS-STING cascade. By limiting DNA clearance mediated by TREX1, wtp53 increases cytosolic dsDNA that activates the pathway, stimulating IFN-I production and enhanced recruitment of effector immune cells. Thus, wtp53 not only preserves genome integrity but also amplifies innate and adaptive antitumour immunity (Ghosh et al., 2023).

Not surprisingly, it is clearly evident that mutations in the TP53 gene are frequently observed in human malignancies, result in the loss of tumour-suppressive functions and are associated with poor prognosis in multiple cancer types (Baliakas & Soussi, 2025). Remarkably, between 60-70% of TP53 mutations are missense point mutations (Lozano et al., 2025). This means that cancer cells express a full-length mutant version of p53 that differs from the wt form by just a single amino acid change. The great majority of missense mutations, including hotspots (R175H, G245S, R248Q, R249S, R273H and R289W) occur within the DNA-binding domain of p53 (Freed-Pastor & Prives, 2012). Missense mutant forms of p53 (mutp53 hereafter) not only lose tumour-suppressive functions, failing to activate canonical target genes, but also exert dominant-negative effects over the wt protein. Additionally, many mutp53 variants acquire novel oncogenic properties, known as gain-of-function (GOF), by interacting with various intracellular effectors that reprogram the transcriptome and proteome of tumour cells (Alvarado-Ortiz et al., 2021; Mantovani et al., 2019). Stabilization of

mutp53 is essential for its oncogenic activity and is largely dependent on interactions with heat-shock proteins like Hsp90. Environmental factors such as ECM stiffness and hypoxia strongly influence mutp53 behaviour (Mantovani et al., 2019). Said that, a stiff matrix activates mechanotransduction pathways that increase cytoskeletal tension and trigger RhoA activation, enhancing actomyosin contractility. This mechanically induced stress disrupts the normal degradation of mutp53 particularly its interaction with MDM2, leading to its stabilization and nuclear accumulation (Ingallina et al., 2018; Mantovani et al., 2019). Once stabilized, mutp53 does not act alone, rather it cooperates with other mechanosensitive oncoproteins, like YAP/TAZ, to drive pro-tumourigenic transcriptional programs that fuel proliferation, invasion, and metastatic dissemination (Di Agostino et al., 2016). In parallel, hypoxic stress promotes oncogenic cooperation between mutp53 and HIF1α enhancing its recruitment to chromatin at hypoxia-responsive loci, moreover mutp53 represses the HIF inhibitor SHARP1, thereby stabilizing HIF-1α and amplifying HIF-driven pro-malignant transcriptional programs (Amelio et al., 2018; Montagner et al., 2012). mutp53 drives cancer progression not only through cell-intrinsic mechanisms but also by influencing the TME. In particular, mutp53 promotes the release of a pro-malignant secretome rich in GFs, angiogenic signals, onco-miRNAs, and inflammatory cytokines. For example, mutp53 enhances angiogenesis by inducing VEGF and stabilizing IL8 and GRO1 via ID4 upregulation (Fontemaggi et al., 2009). It also facilitates invasion and EMT by increasing expression of alpha-1 antitrypsin (A1AT) (Shakya et al., 2017). Furthermore, mutp53 alters intercellular communication through exosome secretion. For example in colon cancer, mutp53-induced exosomes containing miR-1246 reprogram macrophages toward a tumour-supportive M2 phenotype. These exosomes can also transfer mutp53 to stromal fibroblasts, activating Nrf2 pathways and converting them into CAFs (Cooks et al., 2018; Ma et al., 2021). mutp53 has been shown to stoke and benefit from cancer-related inflammation, often through sustained activation of NF-κB under TNFα stimulation, leading to chronic expression of chemokines like CXCL5, CCL2, and CXCL1 that enhance tumour cell migration and invasion in multiple cancer type (Di Minin et al., 2014; Mahat et al., 2025). It also influences inflammation through NF-κB-independent routes, by directly upregulating inflammatory CXCL1 (W. Yan & Chen, 2009). This

reprogramming supports cancer progression by enhancing proliferation and immune evasion.

Recent studies indicate that oncogenic mutp53 promotes immune evasion by sculpting a poorly infiltrated, immunosuppressive tumour landscape. In particular, mutp53 can impair the cGAS-STING signalling cascade by sequestering and inhibiting TBK1, thereby preventing IRF3 activation and nuclear translocation and silencing IFN-I responses that are critical for innate immune activation (Ghosh et al., 2021). mutp53 also reduces tumour cell immunogenicity by downregulating antigen-processing components such as TAP1 and ERAP1 (Zhu et al., 1999) and by promoting expression of immune-checkpoint ligands including PD-L1 (Dong et al., 2017), which together impair peptide presentation and foster T-cell dysfunction and exhaustion. Through these complementary mechanisms mutp53 expressing tumours suppress antitumour immune responses and establish an immune-cold niche that limits effective antitumour immunity.

1.6.2 Effect of hypoxia and HIF on cGAS/STING/IFN-I pathway

Having a hypoxic microenvironment is a common and salient feature of most solid tumours and drives extensive phenotypic reprogramming in cancer cells. Hypoxia triggers a complex cascade of cellular adaptations that broadly impacts tumour progression and immune evasion. Hypoxia-inducible factors (HIFs) play a central role in orchestrating these changes, influencing both cancer cell behaviour and reshaping the TME. The HIF family has two distinct subunits: α (HIF-1α, HIF-2α, and HIF-3α) and β (HIF-1β) (Z. Luo et al., 2022). Under hypoxic conditions, the a subunits are stabilized by its N-terminal transactivation domain and translocated into the nucleus, where it forms dimers with HIF-1β to initiate transcriptional programs that leads to metabolic shifts, enhanced invasiveness, and increased metastatic potential in cancer cells (Z. Luo et al., 2022). Additionally, HIF-mediated changes extend beyond the cell autonomous effect, altering the behaviour and intercellular communication between stromal cells and immune components within the TME. For example, HIF activation reshapes the TME through enhanced secretion of angiogenic factors such as VEGF-A, which stimulate endothelial cells, pericytes, and bone marrow-derived cells (BMDC) to support neovascularization. Additionally, secretion of signalling molecules, like TGF-β, bFGF, and PDGF-B contributes to transform normal fibroblast to CAFs (Petrova et

al., 2018). The hypoxic microenvironment in solid tumours also induces ECM remodelling by inducing collagen gene expression and regulating collagen-modifying enzymes predominantly by CAFs (Petrova et al., 2018). HIF can be activated not only by hypoxia but also by mechanotransduction as well as by mutations in other oncogenic pathways, and remarkably by cooperation with mutp53 (Acuña-Pilarte & Koh, 2025; Capaci et al., 2020). Hypoxia also influences intercellular communication by modulating the cargo and release of EVs. For instance, BC cells under hypoxic stress increase exosome production through HIF-dependent expression of the small GTPase RAB22A, which facilitates endosomal trafficking and vesicle formation. This process also reshapes the miRNA profile within EVs, promoting the release of immunomodulatory miRNAs such as miR-210, a well-established hypoxamiR involved in angiogenesis and immune modulation (Lowry & O'Driscoll, 2018; T. Wang et al., 2014).

Importantly, recent studies indicate that Hypoxia impairs anti-tumour immunity by modifying the immune cells of the TME. Under hypoxic conditions, cancers are infiltrated with several immunosuppressive cells, such as Tregs and MDSCs, which restrict access of cytotoxic cells like NK cells and $CD8^+$ T lymphocytes (McGettrick & O'Neill, 2020). HIFs also lead to secretion of chemoattractants such as Sema3A and EMAPII, ET-1,2 that facilitate the recruitment of macrophages from the bloodstream to the TME, enhancing immunosuppression (Petrova et al., 2018). HIFs can also upregulate the expression of immune checkpoint ligands like PD-L1 on tumour cells. This upregulation interferes with T-cell receptor signalling, thereby suppressing the activation and cytotoxic function of effector T cells and contributing to a more immunosuppressive niche (Bandopadhyay & Patranabis, 2023). The complex interplay between hypoxia and immune surveillance involves several molecular mechanisms. HIF acts as a networking hub coordinating activities of multiple signalling pathways like JAK-STAT3, NF-κB, and MAPK pathway (Acuña-Pilarte & Koh, 2025). Through these pathways, HIFs regulate a wide array of genes involved in metabolism, angiogenesis, ECM remodelling and immune evasion. Hypoxia has also been shown to suppress the cGAS–STING pathway through both HIF-linked transcriptional/post-transcriptional programs and HIF-independent processes. In HIF-associated routes, stabilized HIF proteins reprogram transcriptional networks and induce hypoxia-induced miRNAs like miR-25 and miR-93, which have been shown to

reduce cGAS expression by targeting NCOA3 transcription, thereby lowering basal DNA sensing and downstream type I interferon output. Parallel, HIF-independent mechanisms further blunt pathway activity by decreasing STING protein levels, enhancing nucleic-acid clearance via upregulated nucleases and altering cellular metabolism in ways that limit the availability or immunostimulatory potency of cytosolic DNA ligands (Gareev et al., 2023; Wu et al., 2017).

The immunosuppressive effects of hypoxia extend much beyond molecular signalling by altering the functional landscape of immune cells within the TME. For example, $CD8^+$ T cells and APCs show poor functionality under hypoxic conditions. This dysfunction is further enhanced due to the accumulation of metabolic byproducts such as adenosine and lactate, which inhibit key signalling pathways and promote immune tolerance. Additionally, hypoxia also drives structural remodelling of stromal and endothelial compartments, leading to physical barriers that restrict leukocyte and cytokine infiltration, thereby reinforcing immune exclusion (Fu et al., 2021). These multifaceted adaptations collectively establish a resilient immunosuppressive niche, enabling tumour cells to evade immune detection. Thus, therapeutic strategies aimed at targeting hypoxia-regulated miRNAs and modifying physical barriers within the TME hold promise for restoring immune activation.

1.6.3 Hippo-YAP/TAZ mediated cGAS/STING pathway regulation

The Hippo pathway is a central regulator of tissue homeostasis, enabling cells to sense and respond to their microenvironment through cues such as ECM stiffness, GFs, cytoskeletal tension, and cell polarity. Its core components include mammalian STE20-like kinase 1/2 (MST1/2), protein Salvador homologue 1 (SAV1), large tumour suppressor kinase 1/2 (LATS1/2), the transcriptional co-activators Yes-associated protein (YAP) and WW-domain-containing transcription regulator 1 (TAZ), and the transcriptional enhanced associated domain (TEAD) family. Under physiological conditions, MST1/2 activate LATS1/2, which phosphorylate YAP/TAZ, leading to their cytoplasmic retention and degradation, thereby preventing nuclear activity (Moya & Halder, 2019; Piccolo et al., 2023; J. Zhang et al., 2025). This dynamic regulation is essential to keep YAP/TAZ turned off so cells don’t divide unnecessarily. As tissues shift toward pathological states like during tumour proliferation, mechanical and biochemical cues like ECM stiffening, enhanced integrin–FAK/Src and RhoA–ROCK

contractility, and robust actin stress fibers suppress LATS1/2 and permit YAP/TAZ nuclear translocation (Panciera et al., 2017). Concurrently, aberrant extracellular signalling like GPCR, Wnt, TGFβ and hypoxia-driven pathways further converge to sustain YAP/TAZ activation (Piccolo et al., 2023; J. Zhang et al., 2025). Once inside the nucleus, YAP/TAZ bind TEADs to activate enhancer-driven transcription programs that fuel aggressive tumour phenotypes. They upregulate mitogenic and survival factors like CTGF, CYR61, BCL2 family, induce EMT regulators and matrix remodelers (SNAI1/2, TWIST1, MMPs), and reinforce stemness and lineage plasticity (SOX2, LGR5). YAP/TAZ also cooperate with AP-1 (FOS/JUN) at enhancers to drive oncogenic growth (Zanconato et al., 2015), and recruit co-activators such as BRD4 and p300/CBP at super-enhancers to amplify transcriptional output, sustaining proliferation, invasion, and metabolic adaptation (Zanconato et al., 2018). Beyond TEADs and AP-1, YAP/TAZ interact with SMADs, linking Hippo to TGFβ signalling, b-catenin/TCF integrating Wnt signalling and HIF-1α promoting hypoxia adaptation, thereby broadening their transcriptional reach. This integrated output underpins therapy resistance by enhancing anti-apoptotic signalling, adaptive transcriptional states, and immune evasion (Piccolo et al., 2023; Zanconato et al., 2018; J. Zhang et al., 2025). For example, in pancreatic cancer, hypoxia-driven stiff ECM promotes YAP/TAZ nuclear localization and activation. In several solid tumours, increased YAP/TAZ activity have also been shown to correspond with high grade tumours that generally lack effective therapeutics (Zanconato et al., 2016). For example, advanced BC patients exhibit high nuclear YAP/TAZ levels, and rely on them for driving BC cell growth and aggressiveness (M. Kim et al., 2015; Zhao et al., 2007). In BC, HIF-1α subunit was shown to directly activate YAP leading to increased expression of YAP target genes such as CTGF and CYR61, which support tumour growth and resistance to apoptosis (Yang et al., 2024).

Despite extensive research on Hippo-YAP/TAZ in cell fate and cancer, its role in shaping tumour immunity remains poorly explored. Emerging evidence indicates that dysregulated YAP activity drives immunosuppression across multiple malignancies by reprogramming tumour cells to secrete factors that modulate immune cell recruitment, differentiation, and function within the TME. For instance, in prostate cancer, YAP-driven CXCL5 expression attracts immunosuppressive MDSCs, facilitating tumour immune escape and correlating with poor prognosis (G. Wang et al., 2016).

Evidence in BC further supports this paradigm. TAZ activity has been shown to foster an immune-suppressive microenvironment by enhancing Treg recruitment and myeloid infiltration (Gershoni et al., 2023). In TNBC, YAP activity has been linked to ECM remodeling and immunosuppressive TME, where inhibition of upstream regulators such as NEDD4 reprograms the TME and enhances immune responses via the β-TrCP/YAP/ECM axis (Su et al., 2025). Further, YAP/TAZ activation in BC and stromal compartments contributes to immune evasion, poor infiltration of effector T cells, and resistance to immunotherapy (H. S. Kim & Nam, 2025).

Beyond the above-described effects on immune cell recruitment, YAP/TAZ have recently emerged as critical modulators of innate immunity by suppressing the cGAS-STING axis. In several cancer models, YAP has been implicated in suppressing STING signalling, either through direct transcriptional repression of pathway components or by interfering with downstream signalling. LATS2, functions as a positive regulator of cGAS-STING signalling through YAP-dependent fashion (Uppala et al., 2024). Notably, during HIV-1 infection, LATS2 phosphorylates PQBP1, a key cofactor required for effective cGAS activation, thereby enabling the cGAS–STING–TBK1 cascade and robust interferon responses also in a YAP independent fashion (He et al., 2022). Loss of LATS2 disrupts PQBP1 function and impairs antiviral signalling, underscoring its role in supporting DNA sensing. On the other hand, YAP has been identified as a negative regulator of the cGAS–STING axis, dampening interferon production. Mechanistically, YAP/TAZ suppress innate immune signalling by blocking TBK1 activation, which prevents IRF3 phosphorylation and downstream type I interferon induction (Q. Zhang et al., 2017). Complementary studies proved that YAP activation downregulates expression of the core components STING and IRF3, dampening anti-tumour immunity (Hao, 2022). Together, these findings highlight a Hippo–DNA sensing axis in which LATS2 enhances, while YAP suppresses, cGAS–STING signalling, with broad implications for disease progression and treatment. Thus, targeting YAP activation or activity may offer novel therapeutic opportunities to reprogram the TME, restore immune surveillance, and enhance the efficacy of immunotherapies across multiple malignancies.

1.6.4 Modulation of the cGAS/STING pathway in cancer by non-coding RNAs (ncRNAS)

Noncoding RNAs constitute a large fraction of the human transcriptome. These functional RNA transcripts lack protein-coding potential, but still regulate gene expression, chromatin state and cell signalling, and thereby contribute to a far more diverse RNA landscape than previously assumed in performing multiple cellular functions. They can be divided into various categories, majorly including Long non-coding RNAs (lncRNAs), circular RNAs (circRNAs) and microRNAs (miRNAs) depending on the structure and length of RNA strands (Diamantopoulos et al., 2018, 2025). lncRNAs comprise molecules more than 200 nucleotides in length, associated with several biological processes like chromatin structure, transcription control, and post-transcriptional events (Nandwani et al., 2021). circRNAs are highly stable, covalently closed loop structures that act as molecular sponges for microRNAs, influencing gene regulation and playing a significant role in pathogenesis of cancer (J. Li et al., 2022). microRNAs (miRNAs), first discovered by Ambros and Ruvkun in 1993 in *Caenorhabditis elegans* (Lee et al., 1993) are very short (19-22 nucleotides) single-stranded non-coding RNAs that bind to target mRNAs to suppress their translation or promote degradation, playing key roles in regulating cell growth, apoptosis, and immune responses (Martino et al., 2025).

In the canonical miRNA processing pathway, miRNAs are initially transcribed as a long, capped and polyadenylated primary miRNA (pri-miRNA) by RNA polymerases II and III. The Drosha complex crops the pri-miRNA into a hairpin-shaped precursor-miRNA (pre-miRNA). Then, Exportin-5 promotes the nuclear translocation of the pre-miRNA which is further processed by the Dicer complex. Following Dicing, the resulting miRNA duplex is dissociated, and the mature miRNA is incorporated into the RNA-induced silencing complex (RISC) where it functions to mediate gene silencing either by translational inhibition or by promoting the degradation of target mRNAs with complementary regions in the 3′-UTR of target genes. A key determinant of miRNA target recognition is the seed sequence, a highly conserved 6–8 nucleotide region at the 5′ end of the miRNA. This short motif plays a central role in directing the RISC complex to its mRNA targets. Then there is, partial complementarity between the seed region and the 3′-UTR of target transcripts, leading primarily to translational repression and mRNA destabilization mechanisms that allow a single miRNA to fine-tune the

expression of numerous genes. In contrast, there could also be perfect complementarity, which resembles siRNA-mediated interactions, triggers direct endonucleolytic cleavage of the target mRNA. Through these modes of interaction, miRNAs act as molecular guides that base-pair with specific target mRNAs to negatively regulate gene expression (S. Lin & Gregory, 2015).

Notably, dysregulation of all the above mentioned ncRNAs, especially miRNAs, is increasingly implicated in the onset, progression and therapeutic resistance of multiple cancer types (J. Li et al., 2022; Martino et al., 2025; Zhou et al., 2022). For instance, miRNAs have been shown to promote oncogenesis by repressing tumour-suppressive networks and by subverting innate immune sensing. In this vein, several miRNAs directly target components of the cGAS-STING and RIG-I pathways, thereby blunting type-I interferon responses and facilitating immune evasion (Gareev et al., 2023) . For example, miR-181a has been reported to inhibit RB1 and to suppress STING mRNA via its 3′UTR in TNBC and ovarian cancer, enhancing genomic instability and weakening IFN-driven surveillance (Knarr et al., 2020) . EYA2-driven upregulation of miR-93 reduces STING translation in BC, similarly diminishing antitumour immunity (L. Ren et al., 2022). Global surveys further highlighted that ncRNAs regulate innate immune sensing by targeting multiple nodes of the cGAS–STING and RIG-I pathways (Gareev et al., 2023). Several miRNAs directly repress downstream interferon sensors, for example, miR-23b and miR-146a bind IRF transcripts, miR-217 targets NOD1, and miR-15a acts on TRIF. Suppression of DNA sensing is also reported- miR-23a/b target cGAS mRNA, while miR-24, miR-210 and miR-24-3p reduce STING expression. Other miRNAs modulate RNA sensing, for example, miR-202 and miR-218 inhibit RIG-I/DDX58 and TRIM25 (Gareev et al., 2023). Thus, targeting miRNAs has unique advantages because each miRNA can regulate multiple genes at once, allowing broad and coordinated effects that aren’t possible by altering a single coding gene. Their small size and stability also make them easier to deliver or inhibit. Since many diseases show distinct miRNA patterns, they serve as precise therapeutic targets and biomarkers. By modulating ncRNA levels, it’s possible to influence immune responses, pathogen recognition, and the TME. Altogether, targeting specific miRNAs offers a powerful strategy to enhance immunotherapy and improve cancer treatment outcomes.

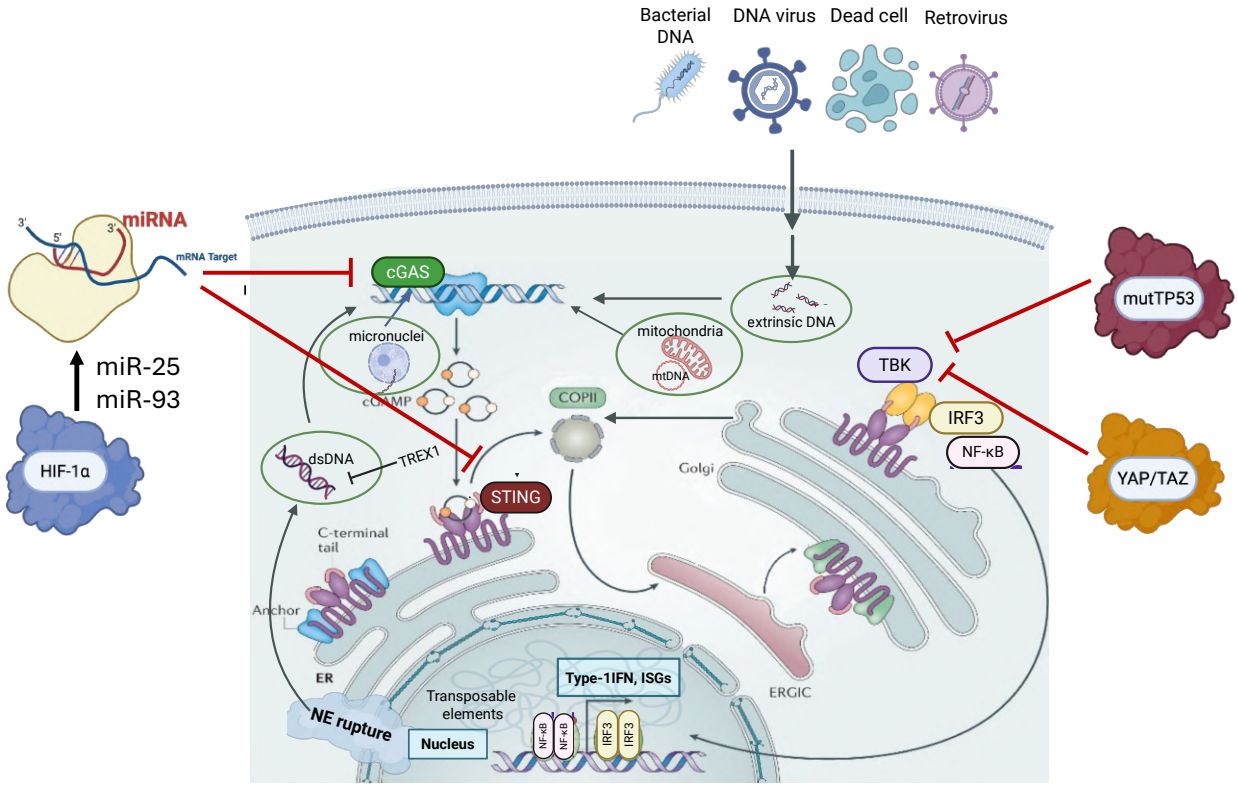

Figure 5. **Schematic representation of cellular pathways modulating cGAS/STING/IFN-I signalling in cancer.** (Adapted from (Hopfner & Hornung, 2020) and modified with BioRender.com)

1.7 miRNA modulation strategies

As highlighted above, miRNA dysregulation has emerged as a hallmark of various cancers underscoring the importance of developing targeted strategies that either inhibit oncogenic miRNAs or restore the function of tumour-suppressive ones. These approaches include antisense inhibitors to miRNA mimics.

One of the traditionally used techniques for oncogenic miRNA knockdown (KD) is use of small interfering RNAs (siRNAs). These are short dsRNAs that guide the RISC to degrade complementary RNA sequences. They are designed to target primary or precursor miRNA transcripts, thereby silencing mature miRNA expression at the transcriptional level. For example, in BC, the onco-miR-221/miR-222 are often upregulated, driving tumour cell proliferation, invasion, and resistance to endocrine therapies. Targeted KD of these miRNAs using siRNAs was shown to restore the expression of tumour-suppressive regulators such as $p27^{Kip1}$ and drug sensitivity, reversing endocrine resistance in experimental models (Rao et al., 2011). However, a

key limitation of siRNA-based strategies is the risk of off-target effects, as siRNAs may unintentionally silence other transcripts due to partial sequence complementarity.

Another biologically inspired strategy for miRNA inhibition involves the use of miRNA sponges, also referred to as Decoy, that act as inhibitors by presenting multiple binding sites for endogenous miRNAs, thereby blocking their interaction with target mRNAs. These sponges can be engineered with complementary heptameric seed sequences, enabling a single construct to neutralize. For example, our group highlighted that a Decoy-30d construct was able to efficiently neutralize oncogenic miR-30d effect in xenograft BC model (Capaci et al., 2020).

Going beyond conventional inhibitors, synthetic circular RNA (circRNA) Decoys represent a promising class of miRNA antagonists. Their covalently closed structure resists exonuclease degradation, prolonging intracellular stability, and they can be engineered with multiple high-affinity binding sites to selectively sequester oncogenic miRNAs. For instance, a synthetic circRNA Decoy was designed to target onco-miR-21 in both invitro and invivo model. Delivery of this circRNA reduced the availability of miR-21 to repress tumour-suppressor genes such as PTEN and PDCD4. This led to reactivation of tumour-suppressive pathways, decreased proliferation and impaired tumour growth in mice (Müller et al., 2020).

Among the latest emerging strategies for oncogenic miRNA inhibition, Locked Nucleic Acid (LNA) antisense oligonucleotides have gained particular attention as one of the most robust and clinically relevant approaches. LNAs are short chemically modified oligonucleotides in which the ribose ring is locked by a methylene bridge, conferring exceptional binding affinity to target miRNAs and strong resistance to nuclease degradation. This configuration allows LNAs to persist longer inside cells, maintaining their inhibitory activity over extended periods. Importantly, several studies have demonstrated that LNAs can selectively silence oncogenic miRNAs such as miR-21 and miR-221, leading to significant reductions in tumour growth in vivo (Martino et al., 2025). Another important example of the therapeutic potential of LNA was shown by targeting miR-205-5p. This microRNA is frequently found upregulated in aggressive BC, where it drives EMT and enhances metastatic spread. By designing an LNA perfectly complementary to miR-205-5p, the researchers were able to selectively silence its activity. Mechanistically, the LNA sequestered miR-205-5p, thereby disrupting EMT programs. As a result, tumour-suppressor proteins were re-expressed,

leading to reduced migration and invasion in vitro and a marked impairment of tumour growth and metastasis in xenograft models (De Cola et al., 2018). Compared to above mentioned miRNA inhibition strategies, effects of LNAs efficiency stay longer, thereby reducing the need for frequent dosing and avoiding additional side effects. Taken together, these properties position LNA as a promising and durable platform for cancer therapy.

In contrast to tumour-promoting miRNAs, many tumour-suppressive miRNAs are significantly downregulated in cancer, and their loss contributes to uncontrolled proliferation, EMT, and metastatic progression. To counteract this, miRNA mimic strategies have been developed to restore protective networks in cancer cells. These mimics are synthetic dsRNA molecules designed to functionally replace endogenous tumour-suppressive miRNAs that cancer cells have silenced. Once delivered into tumour cells, miRNA mimics are incorporated into the RISC complex, where they bind complementary sequences on target mRNAs and suppress oncogenic signalling through mRNA degradation or translational inhibition (Chen et al., 2015; Martino et al., 2025). In BC, several preclinical studies have demonstrated the therapeutic potential of this approach. For instance, re-expression of miR-200c has been shown to reverse EMT and markedly limit metastatic colonization in TNBC models (Rogers et al., 2019). Likewise, the miR-34a mimic MRX34, a synthetic p53-regulated tumour suppressor frequently lost in aggressive breast tumours, significantly reduces tumour growth and promotes apoptosis in vivo. Notably, MRX34 also progressed into early-phase clinical trials, highlighting the translational promise of miRNA replacement therapy (Martino et al., 2025).

However, targeted delivery of the above mentioned RNA-based therapeutics remains a major challenge, limiting their clinical translation. Naked oligonucleotides or mimics are often unstable in circulation, prone to rapid degradation, and might face poor cellular uptake to tumour site. To overcome these barriers and enhance both delivery and bioavailability, nanoparticle-based systems have emerged as versatile carriers for anti-miRNAs and Decoys. Among this lipid nanoparticles (LNPs) formulated with ionizable lipids, cholesterol, and stabilizing components, encapsulate and protect miRNAs from degradation while ensuring efficient uptake by tumour cells (Silva-Cazares et al., 2020). Then, polymeric micelles, built from amphiphilic block copolymers, create a hydrophobic core that traps therapeutic RNAs and prolongs

circulation, and can be functionalized for tumour targeting (Junnuthula et al., 2022). These designs are used to protect therapeutic cargo and enable precise delivery to tumour tissues. An interesting case study in BC highlighted the use of fluorescent nanodiamonds to deliver miR-34a mimics, which is a tumour-suppressive miRNA often suppressed in cancer. These nanodiamonds protected and transported the mimics efficiently into tumour cells, where restored miR-34a activity repressed oncogenic pathways and slowed tumour growth (Abate et al., 2023). Beyond direct tumour suppression, treated cells released EVs that reprogrammed the TME, enhancing DC function and antitumour immune responses. This dual action highlights the potential of nanoparticle-mediated miRNA therapy in solid tumours like BC. Another study showed that LNPs were engineered with ionizable lipids, cholesterol, and PEG-lipids to encapsulate anti-miR-21 oligonucleotides, protecting them from degradation and ensuring tumour-targeted delivery. In Lung cancer model, this approach effectively suppressed onco-miR-21, restored PTEN signalling, reduced tumour growth, and enhanced chemosensitivity, demonstrating the therapeutic potential of LNP-mediated anti-miR delivery in solid tumours (Z. Zhang, Huang, et al., 2023). In parallel, exosome-mediated delivery leverages the natural intercellular communication pathways of EVs. For instance, engineered exosomes can be loaded with miRNA inhibitors or mimic and directed toward specific cell types, offering an efficient delivery system (Abate et al., 2023; Volpini et al., 2023).

In recent years, aptamers have attracted growing attention as precision delivery vehicles in cancer therapy. These are short, ssDNA or RNA molecules that fold into unique 3D structures, allowing them to bind with high specificity and affinity to target proteins, often cell-surface receptors. These are synthetically generated through rigorous selection processes, making them highly tunable and less immunogenic. In cancer therapy, aptamers can be engineered to recognize receptors that are overexpressed on tumour cells, such as HER2 or EGFR, thereby serving as molecular guides to deliver therapeutic cargo directly to malignant tissues (Driscoll et al., 2025). When combined with miRNA inhibitors such as LNAs, circRNA decoys and others, aptamers act as precision delivery vehicles, limiting off-target effects (Driscoll et al., 2025). A case study highlighted that in TNBC and in melanoma, a chimeric AXL–miR-214 sponge aptamer showed therapeutic efficacy by exerting a dual function- first binding to the oncogenic tyrosine kinase receptor AXL to block pro-metastatic

signalling, and second simultaneously sequestering pro-metastatic miR-214 to restore tumour-suppressive gene expression. This integrated mechanism reduced tumour dissemination and enhanced antitumour immune responses (Quirico et al., 2025).
Collectively, these strategies reflect the growing sophistication of miRNA inhibition technologies, integrating molecular precision with advanced delivery systems to overcome biological barriers and achieve durable therapeutic outcomes.

1.8 miR-30d and its impact on tumour-stroma crosstalk

In our laboratory, miR-30d was previously identified as a potent oncogenic microRNA with multifaceted roles in tumour progression, impacting cancer secretome and affecting tumour-stroma crosstalk (Capaci et al., 2020).
miR-30d is an 22-nucleotide microRNA belonging to the miR-30 family, which in humans comprises six members: miR-30a, miR-30b, miR-30c-1, miR-30c-2, miR-30d, and miR-30e. The miR-30d gene is located on chromosome 8q24.22, spanning base pairs 134,804,876 to 134,804,945 on the antisense DNA strand (GRCh38). This genomic locus encodes the precursor hairpin i.e pre-miR-30d, which gives rise to two mature strands, namely miR-30d-5p and miR-30d-3p, depending on which arm of the hairpin is processed and incorporated into the RISC, the mature miR-30d-5p sequences typically being the dominant and functionally active (Mao et al., 2018); (miRBase v22.1). miR-30 family members share a conserved seed sequence near the 5′ end but possess distinct regulatory flanking sequences near the 3′ end. These variations account for the ability of miR-30 family miRNAs to target different mRNA transcripts, thereby conferring unique biological roles. Accordingly, unlike many other miRNAs, members of the miR-30 family have been reported to function as either oncogenes or tumour suppressors, also depending on the specific type of cancer. In particular, there is ample evidence supporting miR-30d's role as tumour promoting. miR-30d has been previously reported to be aberrantly expressed in BC and several other solid tumours due to genomic amplification. For instance, Li et al. 2012 identified miR-30d as an onco-miRNA through a combined genomic and functional screening approach. This study highlighted that miR-30d was overexpressed in more than 30% of 1,283 human solid tumours across multiple tissue types including breast, ovarian, colon, liver, and prostate cancers. miR-30d expression correlated with increased

proliferation, migration, and suppressed CASP-3 apoptotic pathway, thus acting as a tumour enhancer associated with poor clinical outcomes (N. Li et al., 2012).

Another interesting research found that high miR-30d expression is part of a 16-miRNA signature linked to increased recurrence and poor survival in colon cancer (Jacob et al., 2017). Another study reported that bile-derived extracellular miR-30d-5p is significantly elevated in patients with cholangiocarcinoma and proposed miR-30d-5p as a potential diagnostic biomarker. Here, pathway enrichment of predicted targets highlighted putative associations with key signalling pathways, including p53, Hippo and EGFR (H. S. Han et al., 2020). Elevated expression of oncogenic miR-30d in prostate cancer patients was shown to promote aggressive tumour behavior, including enhanced proliferation, migration, invasion, and angiogenesis. Mechanistically, miR-30d directly targets MYPT1, a negative regulator of angiogenesis, whose suppression leads to increased phosphorylation of c-JUN and activation of VEGFA signalling. This axis contributes to endothelial tube formation and tumour vascularization, underscoring the oncogenic role of miR-30d in prostate cancer progression (Z. yuan Lin et al., 2017). Similarly, in BC, Han et al. (2018) reported that miR-30d directly targets KLF11, leading to activation of STAT3 signalling, which in turn promotes EMT, and other tumour-promoting behaviors (M. Han et al., 2018). In contrast to its oncogenic functions, miR-30d has also been reported to exert tumour-suppressive effects in specific tumour types, underscoring its context-dependent role in cancer. For instance, in colon cancer, miR-30d suppresses autophagy by directly targeting the 3' untranslated region (UTR) region of mRNAs encoding the pro-autophagy-related genes, including ATG5 and Beclin 1. Disrupting the autophagic machinery led to increased cellular stress and induced apoptosis, contributing to tumour suppression (R. Zhang et al., 2017). Similarly, miR-30d has also been shown to suppress tumour growth and block the proliferative and invasive behaviour of pancreatic cancer cells by targeting the transcription factor SOX4 and modulating the PI3K-AKT signalling pathway (X. Xu et al., 2021). In esophageal squamous cell carcinoma, miR-30d functioned as a tumour-suppressor to inhibit the migratory and invasive capabilities of human cells by regulating the expression of enhancer of zeste homolog 2 (EZH2) at the post-transcriptional level (Xie et al., 2017). Furthermore, a case study showed that in BC patients cancerous tissues exhibited lower levels of miR-30d and higher levels of SERPINE1 whereas overexpression of miR-30d resulted in promoting fatty acid b-oxidation, reducing SERPINE1 expression and thereby suppressing BC cell

progression (L., R. S., & L. Y. Zhang, 2024). Collectively, these opposing effects highlight that the role of miR-30d highly depends on the specific targets available in each cancer type.

An important question that currently remains poorly explored regards our current understanding of non cell-autonomous functions of miR-30d in modulating the TME.

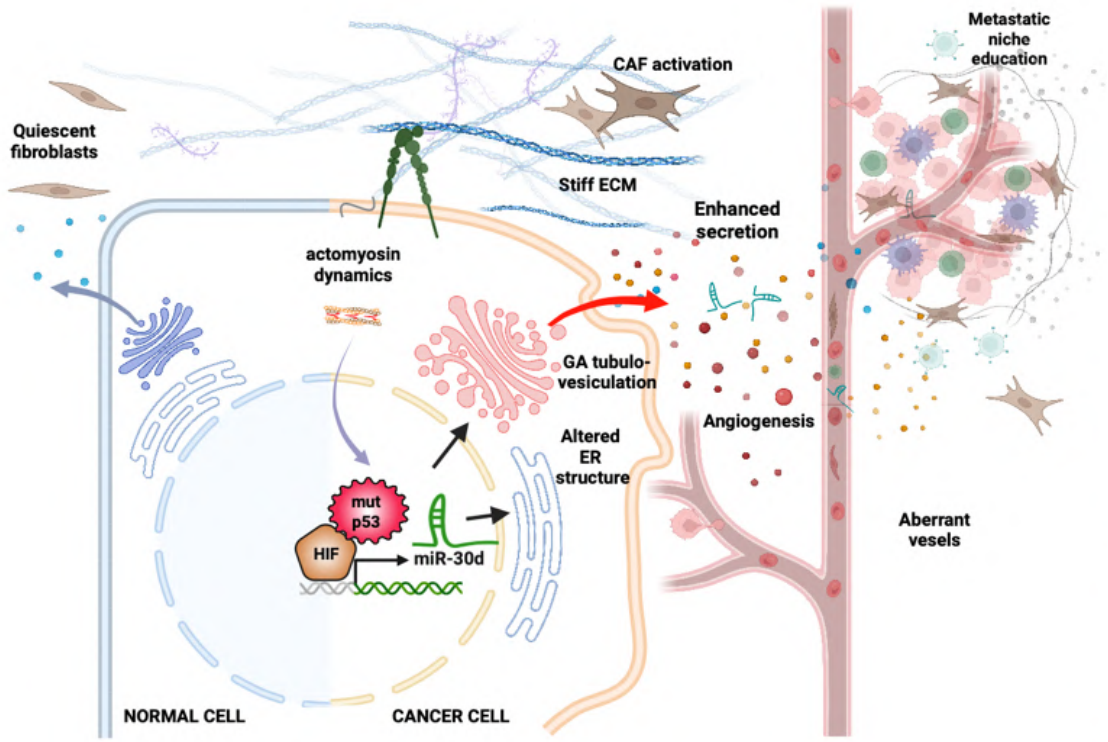

Figure 6. **miR-30d reprograms the secretory pathway and promotes tumour progression.**

Schematic overview illustrating how miR-30d alters the architecture of the ER–Golgi network, enhancing pro-tumourigenic secretion at both primary tumour and distant metastatic sites. (Adapted from (Capaci et al., 2020)).

In this vein, previous findings from our laboratory uncovered that in invasive BC cells miR-30d expression is upregulated through a transcriptional complex formed between HIF1α and missense mutp53 proteins (specifically R175H, R273H, R280K), which binds to the MIR30D promoter region, enhancing its expression in a manner responsive to both hypoxia and mechanical stress, which activate HIF and mutp53, respectively. This leads to repression of mRNA targets including DGKZ and VPS26B, thereby significantly altering the endoplasmic reticulum (ER) and Golgi apparatus (GA) architecture. Our research group proved that miR-30d overexpression in normal-like

breast epithelial cells leads to Golgi tubulo-vesiculation characterized by increased number of COPI vesicles. Notably, GA tubulo-vesiculation has previously been associated with enhanced secretory activity (Beznoussenko et al., 2014). Consistent with this, our findings highlighted that miR-30d overexpression indeed facilitated rapid cargo diffusion and accelerated secretory trafficking. This enhanced secretion of a malignant secretome, which promotes ECM stiffening, CAF activation, and angiogenesis, accelerating BC progression and metastasis in preclinical models. The tumour-promoting effects of miR-30d were shown to depend on the secretome's paracrine influence on both primary and distant sites. Importantly, inhibition of miR-30d using a Decoy inhibitor was shown to restore normal Golgi structure and to reduce stromal activation and ECM remodelling, and delayed tumour progression and metastatic spread in invasive BC xenograft model (Capaci et al., 2020).

Interestingly, recent studies have highlighted an emerging role of miR-30d in immune modulation. Aberrant expression of miR-30d along with miR-30b has been associated with metastasis enhancement and poor clinical outcomes in melanoma. In this study, miR-30d was found to target GALNT7, a Golgi-resident enzyme, thereby increasing immunosuppressive IL-10 secretion and promoting invasion, dampening immune cell recruitment and fostering an immunosuppressive TME (Gaziel-Sovran et al., 2011). Beyond its intracellular functions, miR-30d has also been identified as a secreted microRNA, detectable within exosomes or bound to proteins, across both healthy and disease contexts (J. Li et al., 2021; Melman et al., 2015; Vilella et al., 2015). In reproductive biology, EV-associated miR-30d has been shown to mediate maternal embryo communication (Vilella et al., 2015), while in cardiac remodeling it regulates stress responses through a combination of intracellular and paracrine signalling (J. Li et al., 2021). Importantly, cancer studies provide direct evidence of miR-30d's secretion in cholangiocarcinoma. Bile-derived extracellular miR-30d-5p was significantly elevated and proposed as a diagnostic biomarker (H. S. Han et al., 2020), and in cervical cancer, exosomal miR-30d has been reported as a non-invasive biomarker (Zheng et al., 2019). Taken together, these findings demonstrate that miR-30d operates not only within cells but also as a secreted factor capable of shaping the behaviour of recipient cells in the TME, reinforcing its potential as a diagnostic and prognostic biomarker in cancer.

2 Preliminary results

The available knowledge highlights that miR-30d expression is elevated in breast cancer and other solid tumours characterized by low immune infiltration, including cholangiocarcinoma, colon cancer, ovarian cancer, prostate cancer, and hepatocellular carcinoma (Capaci et al., 2020; Han et al., 2020; Jacob et al., 2017; Li et al., 2012; Lin et al., 2017; Yao et al., 2010) and has been implicated in IL-10 mediated immune evasion in melanoma (Gaziel-Sovran et al., 2011). Additionally, miR-30d is transcriptionally regulated by oncogenic and stromal cues including hypoxia, HIF1α, mutp53, and ECM stiffness, all known contributors of immune escape (Arnaiz & Harris, 2022; Capaci et al., 2020; Ghosh et al., 2021; Prakash & Shaked, 2024; Wu et al., 2017). We were intrigued by the possibility that miR-30d may act as a broader regulator of immune evasion, opening avenues to identify targets and mechanisms that could be leveraged to enhance the effectiveness of anticancer immunotherapies in BC and other poorly immune-infiltrated tumours. For this purpose, we set out to study the impact of miR-30d during early stages of BC, using a model of ductal carcinoma in situ (DCIS). This is a pre-invasive BC stage characterized by partial immune surveillance (Risom et al., 2022), contrasting with the strongly immunosuppressive TME typical of invasive breast cancer (IBC) (Gil Del Alcazar et al., 2017). This immune landscape makes DCIS an ideal model to study early stage immune-modulatory mechanisms.

For this study, I chose a human DCIS-derived cell line previously employed in our laboratory, namely MCF10.DCIS.com (hereafter DCIS). DCIS cells retain wtp53 and H-Ras expression and bear a functional cGAS/STING DNA-sensing machinery (Behbod et al., 2009; Frittoli et al., 2023; Hu et al., 2008; Miller et al., 2000). I initially verified miR-30d expression levels by qRT-PCR in non-transformed MCF10A epithelial cells, in MCF10.DCIS.com cells, and in the engineered DCIS-KI^{mutp53R175H} variant (kindly provided by Luca L. Fava, University of Trento, Trento, Italy). Quantitative analysis revealed that miR-30d expression was markedly elevated in MCF10.DCIS.com cells compared to MCF10A cells and further increased upon KI of the mutp53 allele (R175H) (Fig. 7a), consistent with our previous findings that mutp53 can transcriptionally regulate miR-30d expression (Capaci et al., 2020). These results collectively suggest that miR-30d upregulation may represent an early event in BC

development, preceding TP53 mutation, and is further reinforced by mutp53 during progression from DCIS to a more aggressive tumour stage (Morrissey et al., 2022).

To investigate the signalling pathways regulated by miR-30d, RNA sequencing was performed on DCIS cell model. To this aim, miR-30d was inhibited in DCIS cells by transfection with a specific locked nucleic acid (LNA) inhibitor (hereafter referred to as LNA-30d), an antisense oligonucleotide designed to bind miR-30d with perfect sequence complementarity, forming highly stable heteroduplexes that prevent its interaction with target mRNAs (Fig. 7b). As a control, LNA-control inhibitor (hereafter referred to as Ctrl) was used, which matches LNA-30d in sequence length but lacks homology to any known mRNA. The obtained transcriptomic data were used to perform an overrepresentation analysis of differentially expressed genes (DEGs) through Gene Set Enrichment Analysis (GSEA), using the MSigDB Hallmark and Reactome databases (performed by Dr L. Triboli in the lab). This analysis revealed robust activation of innate immune signalling upon miR-30d inhibition in DCIS cells, with significant upregulation of type-I interferon (IFN-I) and Nuclear Factor kappa-light-chain-enhancer of activated B cells (NF-κB) signalling pathways (Fig. 7c,d,e). Further analysis showed that miR-30d inhibition triggered induction of a cytosolic DNA response signature (Cyto-DR) (detailed description in section 4.2 and further listed in methods), marked by increased expression of type I and III interferons, interferon-stimulated genes (ISGs), and immune-activating cytokines, along with their upstream regulators (Fig. 7f).

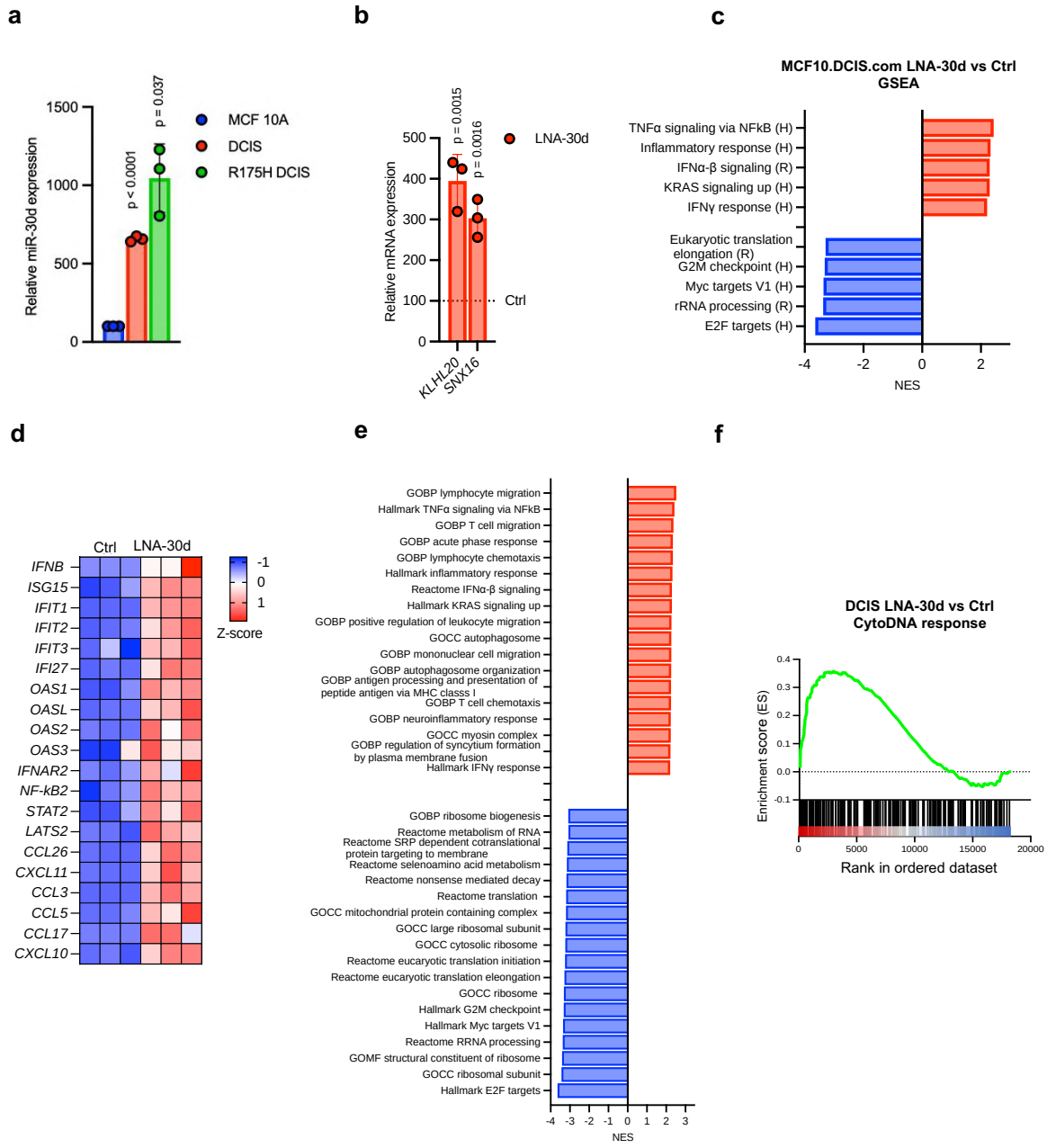

Figure 7. **miR-30d activity inhibits IFN-I response in BC cells.**

a. qRT-PCR analysis of miR-30d expression in MCF10A, DCIS-wt and DCIS-KI^{mutp53R175H} cells. *RNU5G* was used as a reference gene. **b** mRNA expression of the indicated miR-30d targets was analyzed by qRT-PCR in DCIS cells transfected with either LNA-30d or control LNA (Ctrl), to verify efficient miR-30d inhibition by LNA-30d, relative to next Fig.7c,d,e. **a-b.** Bar graphs represent the mean ± standard deviation (s.d.) from n ≥ 3 independent experiments. Statistical significance was determined using Two-tailed unpaired Student's t-test. **c,e.** Bar plot showing Gene Set Enrichment Analysis (GSEA) of Differentially Expressed Genes (DEGs) from RNA-seq of DCIS cells transfected with either 50 nM of LNA-30d or control LNA (Ctrl) for 48hr. The y-axis ranks differentially regulated gene sets from the MSigDB Human Molecular Signatures Database (H=Hallmark, R=Reactome) based on Normalized Enrichment Scores (NES). Positively (NES > 0) and negatively (NES < 0) enriched gene sets are shown in red and blue, respectively. All pathways are statistically significant (FDR.q.val<0.05; Two-tailed

Student's t-test adjusted for multiple testing using GSEA default method). **d.** Heatmap displaying the differential expression of genes related to Interferon/inflammatory response, related to RNA-seq data analyzed in c. Expression levels were normalized using Z-scores for gene-wise comparison, with higher expression in red and lower expression in blue. The three columns correspond to biological replicates for each condition. All displayed genes are differentially expressed with statistical significance (DESeq2 Two-tailed modified t-test adjusted for multiple testing using Benjamini-Hochberg method). **f.** GSEA plot of Cyto-DR signature score in DCIS cells, relative to c. The green line represents gene enrichment within the pathway, while black bars indicate gene rankings. The pathway shown is statistically significant (FDR.q.val<0.05; Two-tailed Student's t-test adjusted for multiple testing using GSEA default method).

Collectively, these results suggest that miR-30d might suppress innate immune responses during the early stages of breast cancer development.

3 Aim of the thesis

Our preliminary data lead us to hypothesize that miR-30d suppresses cytosolic DNA response and IFN-I innate immune signalling in DCIS breast cancer cells. This suppression may contribute to immune evasion and foster a permissive tumour microenvironment that supports tumour progression. Conversely, inhibition of miR-30d in cancer cells may restore innate immune signalling, enhance antitumour immunity, and improve the efficacy of immunotherapies.

To verify this hypothesis, my PhD project aims to:

i) investigate the impact of miR-30d inhibition on the regulation of IFN-I signalling in BC and other tumours;
ii) dissect the molecular mechanisms by which miR-30d attenuates the cGAS/STING/IFN-I pathway in BC cells;
iii) evaluate the cell-autonomous effects of miR-30d inhibition alone and in combination with chemotherapeutic agents as a consequence of the activation of cGAS/STING/IFN-I signalling in BC cells;
iv) assess the antitumour effects of miR-30d inhibition in preclinical models of BC, including its potential synergy with immune-based therapies.

4 Results

4.1 miR-30d attenuates the expression of IFN-I response genes in BC and other tumour types by suppressing the cGAS/STING pathway

I first aimed to validate the transcriptional activation of a panel of type I interferons (IFN-I) and interferon-stimulated genes (ISGs) in DCIS cells following miR-30d depletion. To achieve this, I inhibited miR-30d expression either with LNA-30d or with a Decoy-30d. The Decoy-30d construct has been previously described in (Capaci et al., 2020) and has been obtained by cloning two copies of a miR-30d Decoy sequence, which acts as a molecular sponge binding the mature miRNA, in the lentiviral vector pTWEEN 3′UTR EGFP (Bonci et al., 2008). The anti-miR-30d sequences are embedded within the EGFP 3'UTR sequence, so that binding of endogenous miR-30d to Decoy sequences both sequesters the miRNA and prevents EGFP expression. As a control, the empty vector pTWEEN 3′UTR EGFP was used.

As shown in Fig. 8a, qRT-PCR quantitative analysis highlighted that LNA-30d treatment led to a ~10-fold increase in the expression of *IFNA1*, *IFNB*, and several ISGs including *ISG15*, *IFIT1*, *IFI44*, and *OAS1* compared to control-treated cells. Similar results were obtained when cells were treated with Decoy-30d (Fig. 8b), confirming the specificity of the effect. Notably, the effect of miR-30d blockade in DCIS cells mirrored the transcriptional response to dsDNA (Fig. 8c), a known activator of the cGAS/STING pathway. Based on these findings, I then sought to verify whether this transcriptional activation is translated into increased cytokine secretion. For this purpose, I performed a Human Interferon Beta ELISA assay to measure IFN-β1 levels in the culture supernatant. As shown in Fig. 8d, increased IFN-β1 secretion was observed upon miR-30d inhibition in DCIS cells as compared to control.

Based on reports that show that miR-30d levels are upregulated in BC (N. Li et al., 2012), I was interested in understanding whether its overexpression could further dampen interferon response. To explore this, I ectopically transfected miR-30d mimic construct in DCIS cells and observed that this suppressed *IFNB* mRNA expression while miR-30d level was elevated as compared to control-transfected cells, as assessed by qRT-PCR analysis (Fig. 8e,f). The results below suggest that indeed miR-30d acts as a suppressor of interferon response, as its inhibition enhances IFN-I and ISG expression and cytokine secretion, while its overexpression dampens interferon responses in BC.

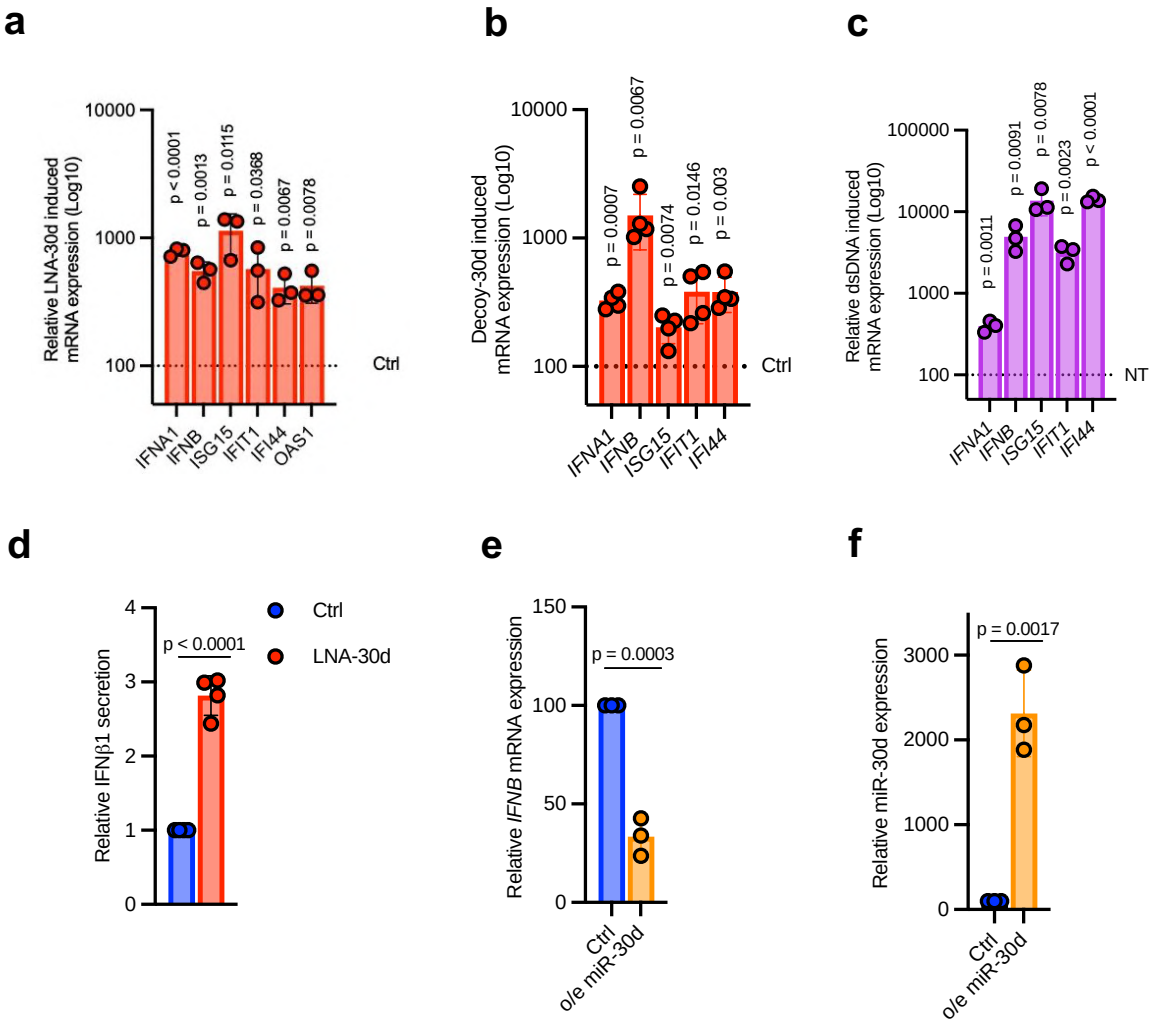

Figure 8. **miR-30d activity suppresses IFN-I response in BC cells.**

a,b. qRT-PCR analysis of indicated IFN-response genes in DCIS cells at 48 hours post-transfection (hpt) with LNA-30d/ control LNA (Ctrl) or Decoy-30d/control construct. mRNA levels in LNA-30d or Decoy-30d transfected cells (red bars) relative to Ctrl (dotted line) are shown in a) and b), respectively. **c.** qRT-PCR analysis of indicated IFN-response genes in DCIS cells transfected with 1 μg/ml dsDNA as compared to control-transfected cells (NT, dotted line). **d.** ELISA quantification of secreted IFNβ1 in DCIS cells at 48hpt with LNA-30d or Ctrl. Absolute values (pg/ml) were normalized for cell numbers in each condition, and the relative increase compared to Ctrl is shown. **e.** qRT-PCR analysis of *IFNB* mRNA expression in DCIS cells transfected with 3 nM miR-30d mimic (o/e miR-30d) or control. **f.** miR-30d expression levels are shown relative to e. *RNU5G* was used as a reference gene. **a-f.** Bar graphs represent the mean ± standard deviation (s.d.) from n ≥ 3 independent experiments. Statistical significance was determined using Two-tailed unpaired Student's t-test.

To determine whether the induction of interferon response genes following miR-30d depletion is mediated through the cGAS pathway, DCIS cells were transfected with LNA-30d and subsequently treated with either the cGAS inhibitor RU.521 or vehicle

control (DMSO). As shown in Fig. 9a, pharmacological inhibition of cGAS effectively blocked the upregulation of *IFNA1* and *IFNB* induced by miR-30d suppression, indicating that cGAS activation is required for this response. To further assess the involvement of downstream signalling components, I co-transfected DCIS cells with LNA-30d (or control oligonucleotides) alongside RNA interference constructs targeting STING, IRF3, or NF-κB p65. Knockdown (KD) of each factor markedly reduced *IFNB* mRNA expression upon miR-30d inhibition (Fig. 9b), demonstrating that STING, IRF3, and NF-κB are essential mediators of this pathway.

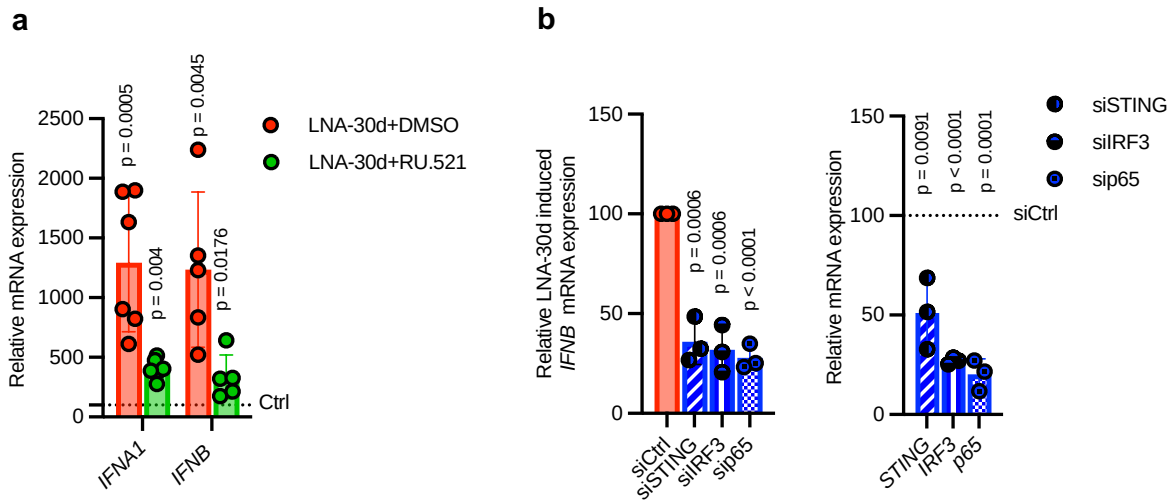

Figure 9. **Inhibition of miR-30d induces IFN-I response in BC cells in a cGAS/STING/IRF3/NF-κB dependent manner.**

a. qRT-PCR analysis of *IFNA1* and *IFNB* mRNA expression in DCIS cells transfected with LNA-30d (red bars) and treated or not with 10μM cGAS inhibitor RU.521 (green bars) for 48hr. mRNA levels relative to cells transfected with control LNA (Ctrl, dotted line) are shown. **b.** Left: qRT-PCR analysis of *IFNB* mRNA expression in DCIS cells co-transfected with LNA-30d and either control siRNA (red bar) or indicated gene-specific siRNAs (blue bars). Right: the relative expression of each gene upon KD is shown as compared to that in control-RNAi transfected cells (siCtrl, dotted line). **a-b.** Bar graphs represent the mean ± standard deviation (s.d.) from n ≥ 3 independent experiments. Statistical significance was determined using Two-tailed unpaired Student's t-test.

These data indicate that miR-30d inhibition activates cGAS/STING/IFN-I signalling in DCIS cells, suggesting that miR-30d may act as an inhibitor of this pathway during early BC development.

To strengthen the mechanistic interpretation of our findings and establish a functional range of miR-30d expression associated with IFN-I pathway modulation, we assessed basal miR-30d expression levels across a panel of tumour cell lines, including metastatic BC cell lines (MCF-7, MDA-MB-231, and SK-BR-3), as well as cell lines derived from different tumour origin: colon (HCT 116), liver (Hep G2, Mahlavu), cholangiocarcinoma (SNU-245), prostate (PC-3), and melanoma (WM-115). Notably, this upholds varying TP53 mutational status, allowing us to assess the broad applicability of miR-30d's immunomodulatory effects across distinct tumour contexts. As shown in Fig. 10a, basal miR-30d expression proved consistently elevated across all tested cancer cell lines as compared to non-transformed MCF10A cells. This panel of cancer-derived cell lines provided us an opportunity to evaluate whether the suppressive effect of miR-30d on IFN-I response may broadly extend across multiple cancer types. As shown in Fig. 10b, upon miR-30d inhibition using LNA-30d, a robust transcriptional activation of IFN-I response genes including *IFNA1*, *IFNB*, and *IFIT1*—was consistently observed across all tested cell lines regardless of tissue origin. Remarkably, this analysis did not highlight a clear correlation between miR-30d levels and expression of IFN response genes upon miR-30d inhibition in different cells lines, suggesting that the variability in expression of other pathway component as well as TP53 status, both known to impact IFN response is likely relevant (Qin et al., 2023; Sood, 2025; Z. Zhang & Zhang, 2025).

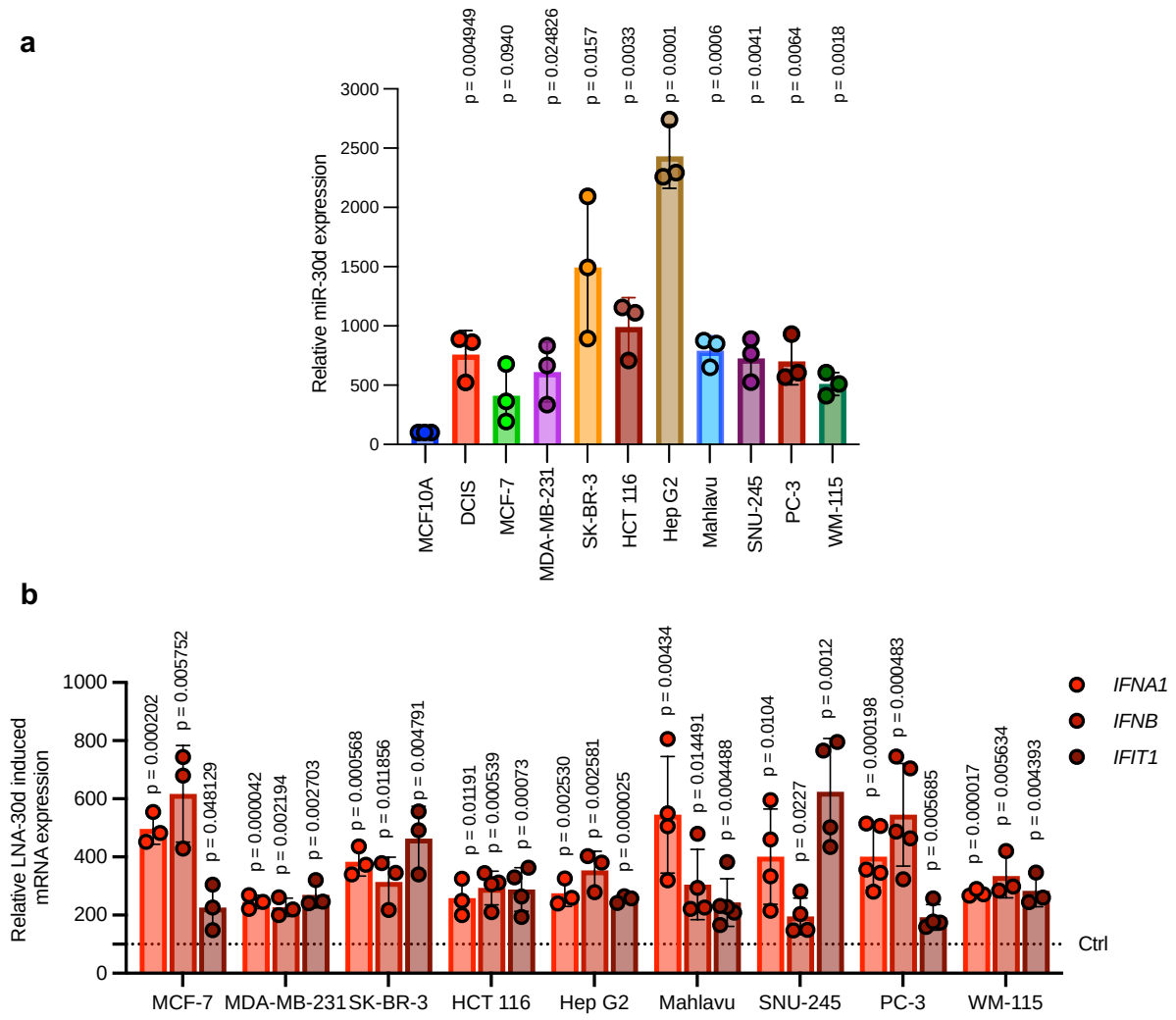

Figure 10. **miR-30d activity inhibits IFN-I response in cells of different cancer types.**

a. qRT-PCR analysis of miR-30d expression in the indicated cell lines. *RNU5G* was used as a reference gene**. b.** qRT-PCR analysis of *IFNA1*, *IFNB* and *IFIT1* mRNA expression in the indicated cancer-derived cell lines upon transfection with control LNA (Ctrl) or LNA-30d. mRNA levels in LNA-30d transfected cells (red bars) relative to Ctrl (dotted line) are shown. Bar graphs represent the mean ± standard deviation (s.d.) from n ≥ 3 independent experiments. Statistical significance was determined using Two-tailed unpaired Student's t-test.

These findings suggest that miR-30d acts as a broad suppressor of innate immune signalling and that its inhibition may putatively restore anti-tumour immunity in multiple malignancies, irrespective of tissue origin or TP53 status.

4.2 miR-30d expression inversely correlates with type I interferon response in patient datasets

To further investigate whether high miR-30d expression is associated with suppression of cytosolic DNA response in human tumours, we analyzed the transcriptomic data of the BC cohort from The Cancer Genome Atlas (TCGA). Gene expression correlation analysis revealed a significant inverse correlation between miR-30d expression levels and the cytosolic DNA response (Cyto-DR) signature (Fig. 11a), implicating miR-30d in the attenuation of innate immune activation. The Cyto-DR signature represents a composite gene set capturing cytosolic DNA response pathway activity, comprising established type I interferon-related genes from MSigDB collections (GOBP_INTERFERON_ALPHA_PRODUCTION,HALLMARK_INTERFERON_ALPHA_RESPONSE,GOBP_INTERFERON_BETA_PRODUCTION,GOBP_TYPE_I_INTERFERON_PRODUCTION) plus 9 curated genes (*CGAS*, *STING1*, *TBK1*, *IRF3*, *IFNB1*, *ISG15*, *IFIT1*, *OAS1*, *CXCL10*) from prior dsDNA-response studies.

To validate these findings in an independent cohort, we analyzed the METABRIC BC dataset. Since direct measurements of miR-30d expression were unavailable in this dataset, Dr. L. Triboli generated a miR-30d activity signature based on differentially expressed genes from our DCIS RNA-seq dataset (see Method section, Fig. 34 and related details). This signature correlated strongly with miR-30d expression in the TCGA cohort, thereby providing a robust proxy for miR-30d activity. Using this signature, we confirmed a significant inverse correlation between miR-30d activity and the Cyto-DR signature in both the TCGA and METABRIC BC datasets (Fig. 11a,11b). Interestingly, this inverse correlation was also observed across different TCGA tumour cohorts including colon, liver, cholangiocarcinoma, prostate, and melanoma (Fig. 11c), further highlighting the potential role of miR-30d as a broad suppressor of innate immune signalling across tumours.

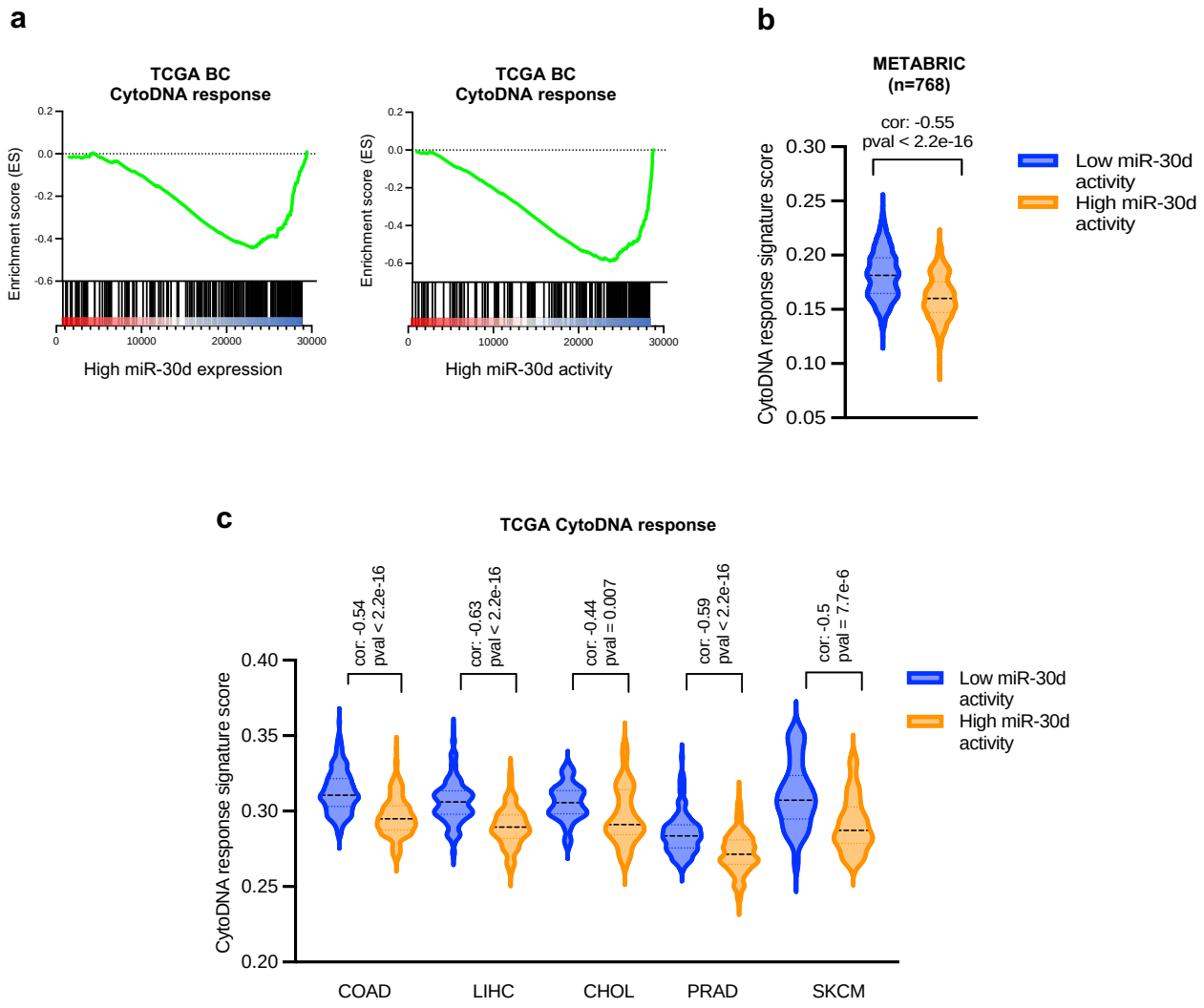

Figure 11. **miR-30d inhibits type I interferon response in patient datasets.**

a. GSEA plots of Cyto-DNA response signature score in human BC samples from the TCGA dataset (n=921 patient samples), classified based on miR-30d expression (left) or activity (right), using the median of the distribution. The green line represents gene enrichment within the pathway, while black bars indicate gene rankings. The pathway shown is statistically significant (FDR.q.val<0.05; Two-tailed Student's t-test adjusted for multiple testing using GSEA default method). **b,c.** Violin plot illustrating the Cyto-DNA response signature score in human samples of the METABRIC cancer dataset (n=768), and of the indicated TCGA cancer datasets, classified based on miR-30d activity. Violin colors represent low (blue) and high (orange) miR-30d activity. All displayed comparisons are statistically significant (Two-tailed Student's t-test), and the correlation was calculated using the cor.test function from the R package stats. Signature value cutoff is -0.2 and p cutoff is 0.05.

To evaluate the transcriptome-wide consequences of miR-30 inhibition, we examined how predicted miR-30 targets were distributed among the differentially expressed genes. Using TargetScan to define the miR-30 seed-family target set (miR-30a/b/c/d/e-5p with 1,304 transcripts), we compared their log2 fold-change values with those of all other expressed genes (n = 16,888). Upon treatment with the LNA-30d, predicted targets showed a clear shift toward higher expression relative to non-target genes, indicating that they are preferentially upregulated. This enrichment is consistent with the expected derepression of direct miR-30 targets following loss of miR-30 activity. Although individual transcript may be affected indirectly, the Empirical Cumulative Distribution Function (ECDF) based right shift of the target set provides a robust, unbiased readout demonstrating that miR-30 inhibition produces a coherent transcriptional signature characteristic of overall reduced microRNA activity (Fig. 12a).

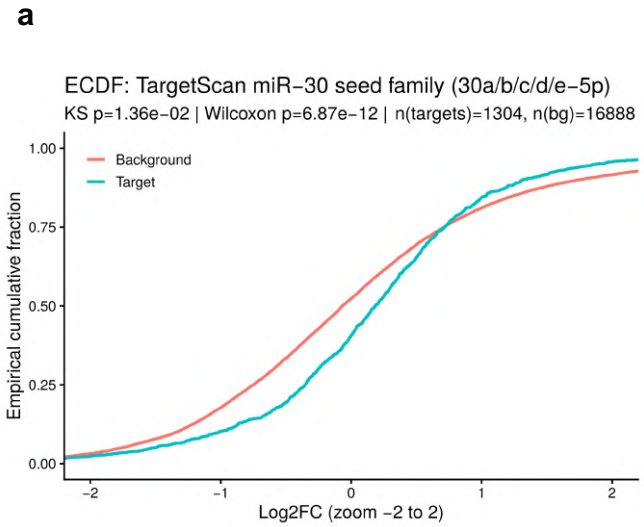

Figure 12. **ECDF analysis of transcriptome-wide changes upon miR-30 inhibition.**

a. Empirical cumulative distribution functions (ECDFs) of gene-level log2 fold-changes (log2FC) from the comparison of LNA anti-miR-30d vs LNA ctrl are shown for predicted miR-30 seed-family targets (TargetScan; miR-30a/b/c/d/e-5p; n = 1304) and for the corresponding background gene set (n = 16888, all non-target genes). A right-shift of the target ECDF around log2FC = 0 indicates that miR-30 targets are enriched among transcripts upregulated upon miR-30 inhibition, consistent with de-repression of direct targets. The difference between distributions was quantified using one-sided Kolmogorov–Smirnov and Wilcoxon rank-sum tests, and effect size was estimated by Cliff's delta (targets vs background: Δmedian = 0.254, %log2FC>0 = 0.594 vs 0.477, KS p = 0.014, Wilcoxon p = 6.9×10^{-12}).

4.3 mutant p53 attenuates cGAS/STING cytosolic DNA sensing pathway in BC cells via miR-30d

It has been previously shown that missense mutant p53 oncoproteins (mutp53) dampen the STING/IFN-I cascade in cancer cells, by blocking TBK activation (Ghosh et al., 2021). Given that our research group previously demonstrated that miR-30d is transcriptionally induced by mutp53 in BC cells (Capaci et al., 2020), we aimed to verify whether the inhibitory effect of mutp53 on the IFN-I response may in part rely on miR-30d induction. To this aim, we overexpressed missense mutp53^{R280K} transiently in wtp53 expressing DCIS cells and analyzed the expression of miR-30d and type-I interferon genes by qRT-PCR. As expected, introduction of mutp53 (Fig. 13a) led to fourfold increase of miR-30d expression (Fig. 13b). mutp53 overexpression concurrently caused a significant decrease in IFN-I gene expression (Fig. 13c), consistent with published evidence (Ghosh et al., 2021). Remarkably, this suppression was reversed upon miR-30d inhibition (Fig. 13c), indicating that miR-30d contributes to mutp53-mediated suppression of IFN-I pathway. Further, to better mimic the genetic landscape of human breast tumours, we employed the above-described DCIS-KI^{mutp53R175H} cell line. qRT-PCR analysis showed that when DCIS-KI^{mutp53R175H} cells were transfected with dsDNA they failed to induce *IFNA1* and *IFNB* mRNA expression, consistent with impaired activation of the cGAS/STING pathway in the presence of mutp53 (Fig. 13d). However, this effect was rescued by treatment with LNA-30d, which significantly restored IFN-I gene expression (Fig. 13d).

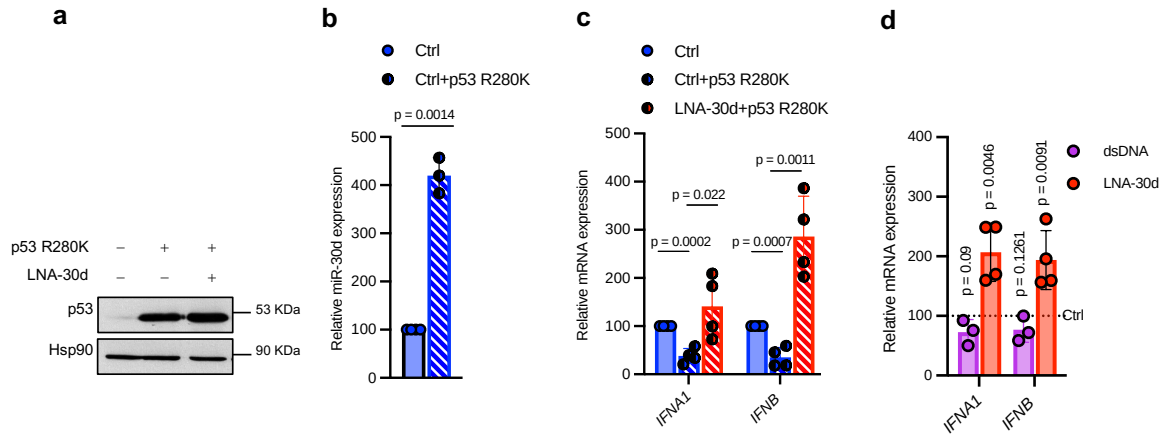

Figure 13. **mutant p53 inhibits IFN-I response in BC cells via miR-30d.**

a. WB analysis of p53 protein in the experiment shown in b,c, using Hsp90 as loading control. **b.** qRT-PCR analysis of miR-30d expression in DCIS-wt and ectopically expressed mutp53^{R280K} in DCIS cells. *RNU5G* was used as a reference gene. **c.** qRT-PCR analysis *IFNA1* and *IFNB* expression in DCIS cells

co-transfected with indicated combinations of mutp53^{R280K} expression construct and either LNA-30d or control LNA (Ctrl). mRNA levels relative to cells transfected with empty plasmid (Ctrl) are shown. **d.** qRT-PCR analysis of *IFNA1* and *IFNB* mRNA expression in gene-edited DCIS-KI^{mutp53R175H} cells. Magenta bars: cells transfected with 1 μg/ml dsDNA; red bars: cells transfected with LNA-30d. mRNA expression relative to control-transfected cells (dotted line: no DNA or control LNA, respectively) is shown. **a-d.** Bar graphs represent the mean ± standard deviation (s.d.) from n ≥ 3 independent experiments. Statistical significance was determined using Two-tailed unpaired Student's t-test.

Collectively, these results demonstrate that mutp53 impairs IFN-I response in BC cells at least in part by increasing miR-30d expression.

4.4 miR-30d suppresses STING/TBK1/IRF3 pathway activation by altering the ER-Golgi trafficking in BC cells

Having demonstrated that inhibition of miR-30d leads to increased expression of immune stimulatory genes in cancer cells by engaging the STING/IRF3/NF-κB cascade, I wished to understand the mechanisms leading to activation of these factors as a consequence of miR-30d blockade. Upon binding to cGAMP, the ER-resident STING protein is translocated to Golgi membranes and forms a clustered platform on which TBK1 kinase phosphorylates the transcription factor IRF3. Remarkably, our group has previously demonstrated that miR-30d overexpression in normal breast epithelial cells leads to structural and functional reprogramming of the ER and Golgi apparatus (Capaci et al., 2020). I thus hypothesized that in cancer cells high levels of miR-30d might interfere with STING/TBK/IRF3 activation by altering the architecture and function of these organelles, that are essential for cGAS–STING signalling activation (Samson & Ablasser, 2022). Vice versa, miR-30d inhibition in cancer cells would be expected to normalize the secretory pathway, thereby favouring execution of downstream steps of the STING/TBK/IRF3 cascade. I first checked the Golgi apparatus (GA) morphology in DCIS cells by immunofluorescence (IF) analysis with the Golgi marker GM130, which indicated that dispersed Golgi morphology was prevalent in these cells, in contrast to the compact, polarized GA observed in non-transformed MCF10A cells, which express much lower miR-30d levels. Remarkably, inhibition of miR-30d using a Decoy construct restored GA compaction in DCIS cells (Fig. 14a), similarly to what previously observed (Capaci et al., 2020) while not affecting the compact GA morphology of MCF10A cells (shown later).

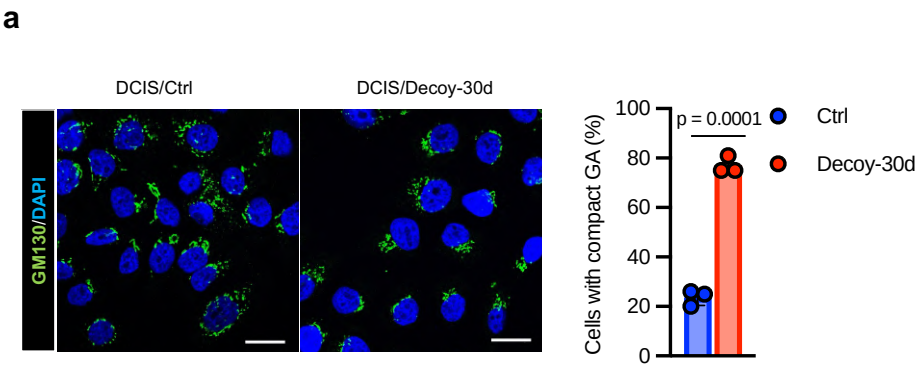

Figure 14. **miR-30d alters Golgi structure in BC cells.**

a. Representative IF analysis of Golgi Apparatus (GA) stained with anti-GM130 Ab (green) in DCIS cells transfected with either miR-30d Decoy (Decoy-30d) or control construct. Nuclei were counterstained with DAPI; scale bar: 20 μm. Quantifications of cells with compact GA are shown on the right. Bar graphs represent the mean ± standard deviation (s.d.) from n ≥ 3 independent experiments. Statistical significance was determined using Two-tailed unpaired Student's t-test.

Next I monitored changes in STING protein localization dependent on miR-30d in DCIS cells. To this aim, I downregulated miR-30d expression with the Decoy construct and then transfected with a construct expressing the RFP-STING protein. I then stained RFP-STING expressing cells with antibodies against markers for Endoplasmic reticulum (PDI) or Golgi apparatus (GM130). As shown in Fig. 15a, RFP-STING protein was mainly localized on ER in control-treated cells, whereas upon miR-30d inhibition it was found co-localized with the GA (Fig. 15b), suggesting that inhibition of miR-30d in cancer cells may promote the translocation of STING protein from ER to GA. To determine whether miR-30d mediated remodelling of the secretory pathway can indeed affect STING translocation, I sought to test whether inhibition of miR-30d activates STING when Golgi compaction is prevented. This was obtained by forcing GA dispersal with the drug Golgicide A (GCA), which disrupts COPI vesicle association with Golgi membranes and subsequently disassembles the trans-Golgi network (Sáenz et al., 2009; Uhlorn et al., 2020). I thus performed an experiment where DCIS cells were transfected with Decoy-30d and RFP-STING construct, and either treated with GCA (1μM) or DMSO as control. As evident from Fig. 15b, GCA treatment efficiently prevented GA compaction in DCIS cells transfected with miR-30d inhibitor. Concomitantly, in the same experimental setting, GCA also abolished the translocation of RFP-STING protein from ER to GA. Consistently with this result, preventing GA compaction with GCA also reduced the induction of IFN-I genes upon miR-30d

inhibition as measured by qRT-PCR (Fig. 15c). In line with the notion that miR-30d impacts GA organization by downregulating its direct target diacylglycerol kinase zeta (DGKZ) (Capaci et al., 2020), RNAi-mediated KD of DGKZ dispersed the GA in DCIS cells transfected with Decoy-30d (Fig. 15d). As shown in Fig. 15e,f I further observed that in this experimental setting KD of DGKZ reduced induction of IFN-I response caused by miR-30d inhibition.

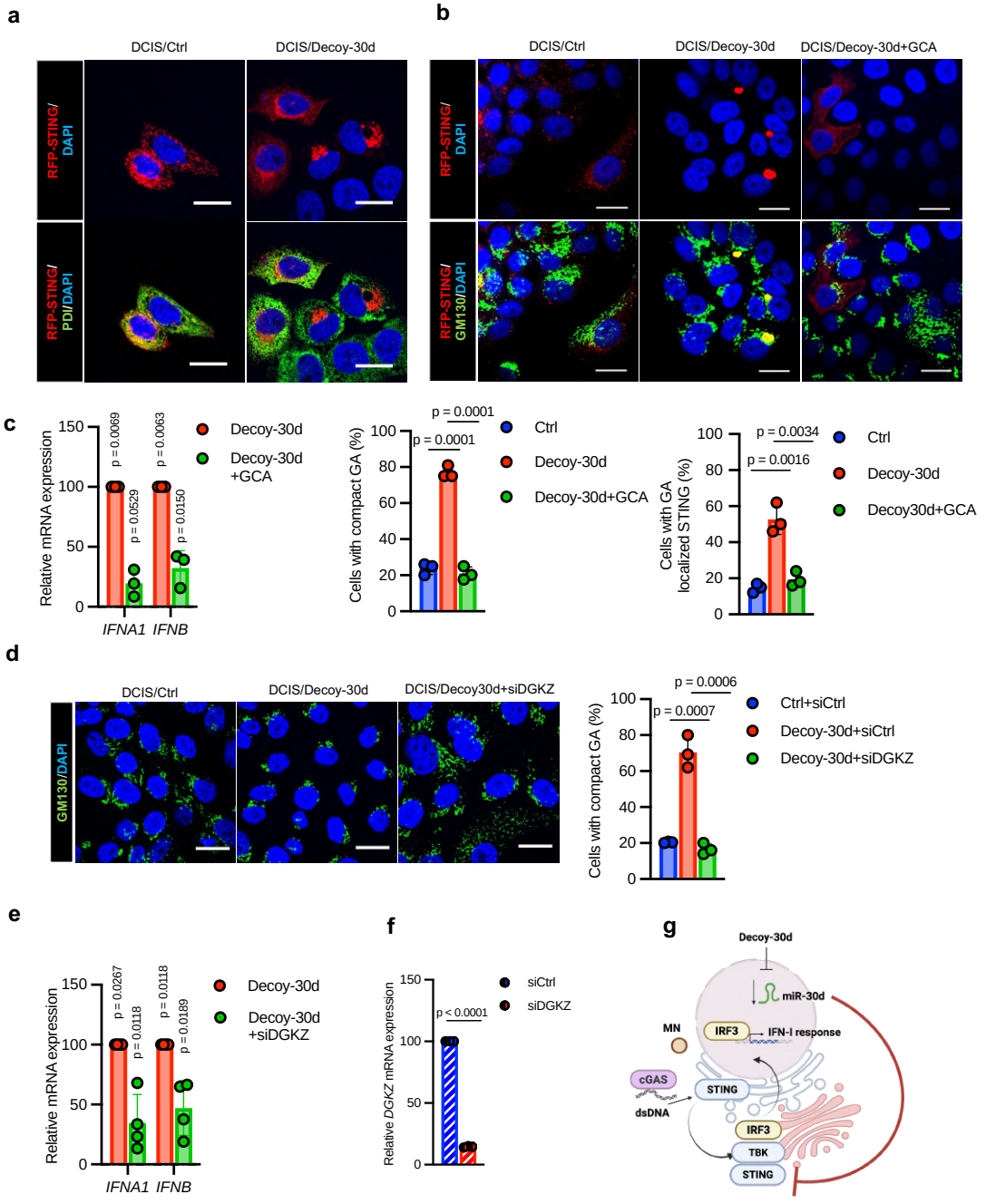

Figure 15. **miR-30d suppresses STING/IFN-I signalling in BC cells by altering Golgi structure.**

a. Representative IF analysis of ectopically expressed RFP-STING with anti-RFP Ab (red) and of Endoplasmic Reticulum (ER) with anti-PDI Ab (green) in DCIS cells transfected with either control or miR-30d Decoy construct. Nuclei were counterstained with DAPI. Scale bar: 20 μm. **b.** Top: representative images showing IF analysis of ectopically expressed RFP-STING (red) in DCIS cells transfected with either miR-30d Decoy construct or control and either treated or not with 1 μM Golgicide A (GCA) for 48hr. RFP was detected using anti-RFP Ab, Golgi Apparatus (GA) was stained with anti-GM130 Ab (green) and nuclei were counterstained with DAPI. Scale bar: 20 μm. Below: quantification of DCIS cells with compact GA (left) and of GA-localized RFP-STING (right) in the different conditions. **c.** qRT-PCR analysis of *IFNA1* and *IFNB* mRNA expression in the experiment shown in b. **d.** Representative IF analysis (left) and quantification (right) of GA using GM130 Ab in DCIS cells transfected with miR-30d Decoy construct and DGKZ siRNA in the indicated combinations. Scale bar: 20 μm. **e.** qRT-PCR analysis of *IFNA1* and *IFNB* mRNA expression in the experiment shown in d. **f.** qRT-PCR analysis of *DGKZ* mRNA in the experiment shown in d. **a-f.** Bar graphs represent the mean ± standard deviation (s.d.) from n ≥ 3 independent experiments. Statistical significance was determined using a Two-tailed unpaired Student's t-test. **g.** Schematic representation of the effects of miR-30d on STING trafficking by altering the GA structure (Created with Biorender.com).

Altogether, these results suggest that high levels of miR-30d may block STING translocation and subsequent IFN-I induction by altering the structural organization of the secretory pathway in cancer cells. Conversely, inhibition of miR-30d might restore normal GA structure, thereby facilitating STING activation and enhancing IFN-I response in DCIS cells.

Notably, these results are in agreement with the previous observation, by F. Di Camillo, that inhibiting miR-30d in DCIS cells led to robust activating phosphorylation of both TBK and STING, which occurs upon their interaction at GA membranes (not shown). Following this, with IF analysis, I also confirmed that miR-30d inhibition was accompanied by enhanced TBK1 phosphorylation on compact GA membranes (Fig. 16a) and RNAi-mediated KD of DGKZ dispersed the GA in DCIS cells transfected with Decoy-30d and reduced TBK1 phosphorylation (Fig. 16b) . As per literature, STING translocation and TBK activation further leads to IRF3 nuclear translocation, and also triggers the activation of NF-κB transcription factor which eventually regulate the expression of IFN signature genes (Samson & Ablasser, 2022). Given that miR-30d inhibition leads to IFN-I induction in a IRF3- and NF-κB-dependent manner (shown in section 4.1), I sought to verify whether these events are also induced as a consequence of miR-30d inhibition in BC cells. To this aim, I transiently transfected DCIS cells with a IRF3-GFP reporter construct (kindly provided by A. Marcello, ICGEB, Trieste, Italy) together with either LNA-30d or control. As shown in Fig. 16c, in control-transfected cells IRF3 was mainly localized in the cytoplasm, whereas inhibition of miR-30d resulted in a significant increase of its nuclear localization. Next, to verify whether

NF-κB activation is similarly triggered upon miR-30d inhibition, I used the same experimental setting, and analyzed phosphorylation of the endogenous p65 subunit of NF-κB by WB. As a positive control for NF-κB activation, I treated cells with TNFα. As a result, I observed robust phosphorylation of endogenous p65 subunit when DCIS cells were treated with LNA-30d (Fig. 16d).

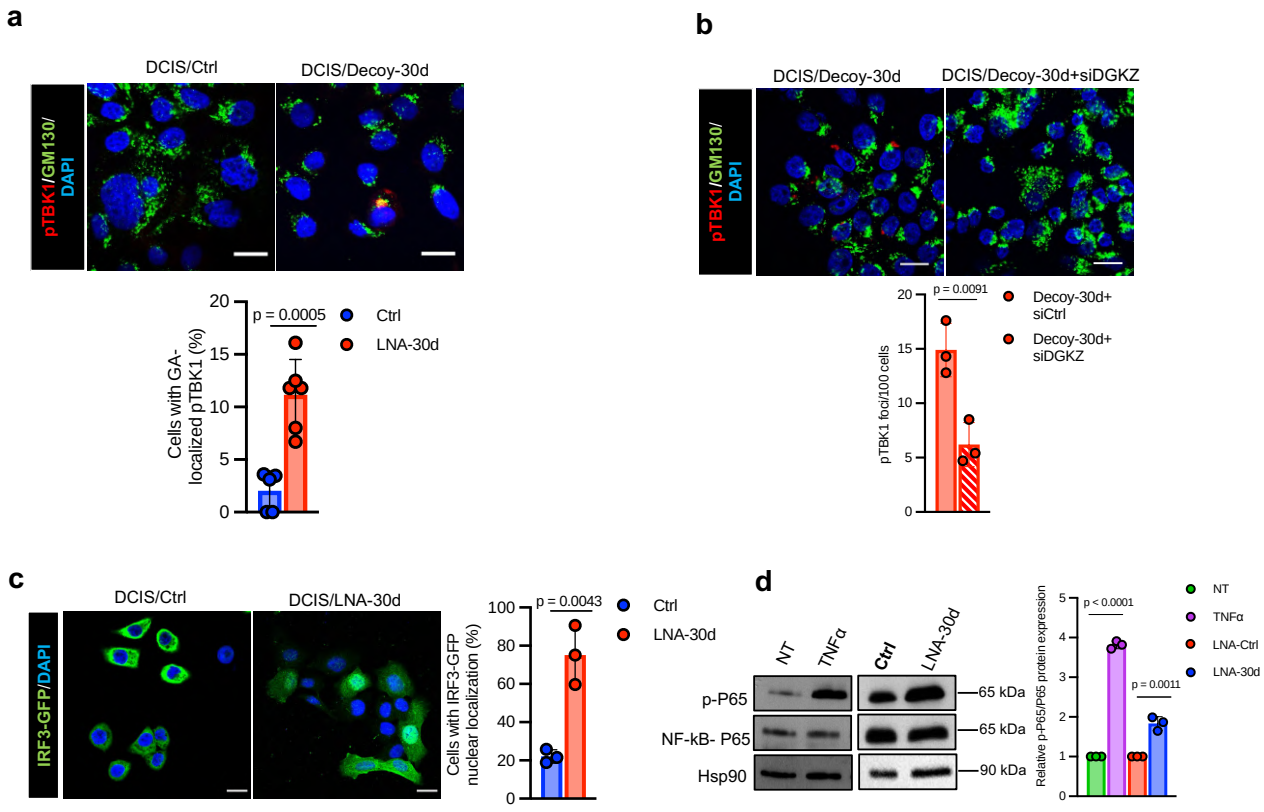

Figure 16. **miR-30d suppresses TBK1/IRF3/NF-κB signalling in BC cells by altering Golgi structure.**

a,b. Representative image showing IF analysis of phospho-(S172) TBK1 (red) and GM130 (green) in cells treated as in Fig. 14a, and Fig. 15d. Scale bar: 20 μm. The bar plot (down) shows the quantification of cells with GA-localized pTBK1. **c.** Left: Representative images showing IF analysis of IRF3-GFP with anti-GFP antibody (Ab) in DCIS cells transfected either with LNA-30d or control LNA. Scale bar: 20 μm. Right: quantification of cells displaying nuclear localization of IRF3-GFP. **d** WB analysis of the indicated proteins in DCIS cells transiently transfected with LNA-30d or control LNA for 48hr. NF-κB activation was measured as the ratio of P-p65 vs total p65 protein. Hsp90 levels were used as loading control. As a positive control, TNFα (10ng/ml) was administered to DCIS cells. **a-d.** Bar graphs represent the mean ± standard deviation (s.d.) from n ≥ 3 independent experiments. Statistical significance was determined using a Two-tailed unpaired Student's t-test.

I then wished to compare the effect of miR-30d inhibition on the secretory machinery in non-transformed human breast epithelial cell line MCF10A, where miR-30d level is very low (see section 4.1). When miR-30d was downregulated in MCF10A cells either

with LNA-30d or Decoy-30d construct, it did not change the architecture of GA, nor did it activate key components of the cGAS/STING signalling cascade, such as TBK kinase or interferon gene expression (Fig. 17a,b,c), although as evidenced by WB and qRT-PCR, these responses were readily triggered by dsDNA transfection (Fig. 17b,d).

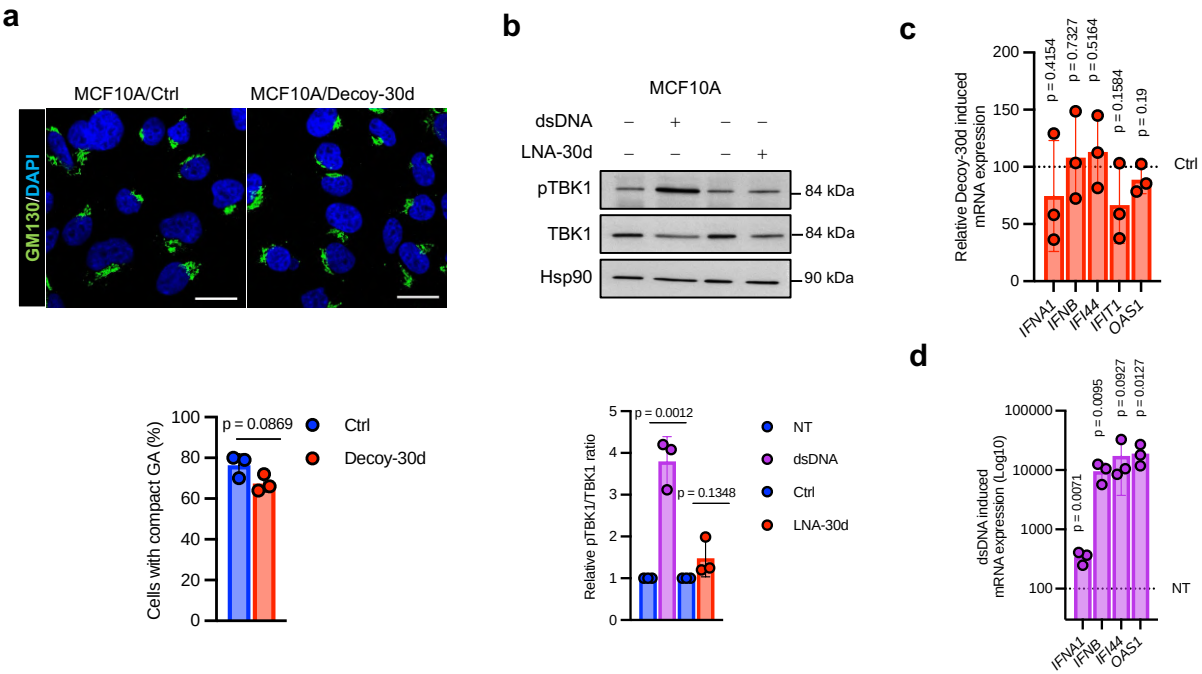

Figure 17. **miR-30d inhibition fails to activate the cGAS/STING pathway in non-transformed breast epithelial cells.**

a. Representative IF analysis of GA stained with anti-GM130 Ab (green) MCF10A cells transfected with either miR-30d Decoy-30d or control construct. Nuclei were counterstained with DAPI; scale bar: 20 μm. Quantifications of cells with compact GA are shown below. **b.** WB analysis (Top) and its quantification (below) of phospho-(S172) TBK1 in MCF10A cells transfected with either 1 μg/ml dsDNA or LNA-30d. Hsp90 was used as a loading control. **c.** qRT-PCR analysis of indicated IFN-response genes in MCF10A cells transfected with Decoy-30d (red bars) as compared to cells transfected with control construct (Ctrl, dotted line). **d.** qRT-PCR analysis of indicated genes in MCF10A cells transfected with 2.5 μg/ml of dsDNA for 24hr (magenta bars) as compared to control-transfected cells (NT, dotted line). **a-d.** Bar graphs represent the mean ± standard deviation (s.d.) from n ≥ 3 independent experiments. Statistical significance was determined using a Two-tailed unpaired Student's t-test.

These results indicate that high levels of miR-30d suppress STING/TBK1 activation in BC cells by disrupting GA architecture, and when miR-30d is depleted from these cells, the resulting structural modifications of the secretory pathway may sustain robust activation of the cascade, leading to engagement of IRF3 and NF-κB and to IFN-I induction. In contrast, in normal cells bearing low miR-30d expression and normal secretory pathway, administration of miR-30d inhibitors does not lead to alterations of either ER or GA and fails to induce activation of the pathway.

4.5 miR-30d inhibition induces nuclear envelope ruptures, DNA leakage, and cGAS activation

GA compaction induced by miR-30d inhibition would however not be sufficient to cause STING activation in the absence of cGAS-inducing stimuli, i.e. cytoplasmic double-stranded DNA (dsDNA). Previous observations by F. Di Camillo and our results highlighted that IF analysis of DCIS and other BC cell lines revealed minimal cytoplasmic dsDNA under basal conditions (Fig. 18a,c), in agreement with the notion that transformed cells may release nuclear and/or mitochondrial DNA, that is largely degraded by cytoplasmic nucleases to prevent excessive cGAS activation (Lim et al., 2024; Samson & Ablasser, 2022). Interestingly, when DCIS cells were depleted for miR-30d, I observed a time-dependent accumulation of perinuclear dsDNA, detectable by anti-dsDNA antibody staining as early as 12 hours post LNA-30d transfection, with levels increasing up to 48 hours (Fig.18a,b). Parallel IF analysis using anti-cGAS antibody showed a corresponding increase in cGAS foci colocalizing with these cytoplasmic DNA aggregates, beginning at 12 hours and intensifying over time (Fig.18a,b). Based on these findings, and as per the literature I then sought to verify whether the increased dsDNA and cGAS colocalization observed upon miR-30d inhibition further promotes the synthesis of 2’3’- cyclic GMP-AMP (cGAMP) an essential secondary messenger needed to execute the downstream cGAS/STING cascade. To this aim, I performed a 2’3’-cGAMP ELISA assay to measure both extracellular and intracellular cGAMP production. As shown in Fig. 18d, cGAS enzymatic activity increased significantly, as evidenced by elevated intracellular and secreted 2′-3′ cGAMP levels, comparable to the response induced by transfecting exogenous dsDNA (Fig. 18e,f).

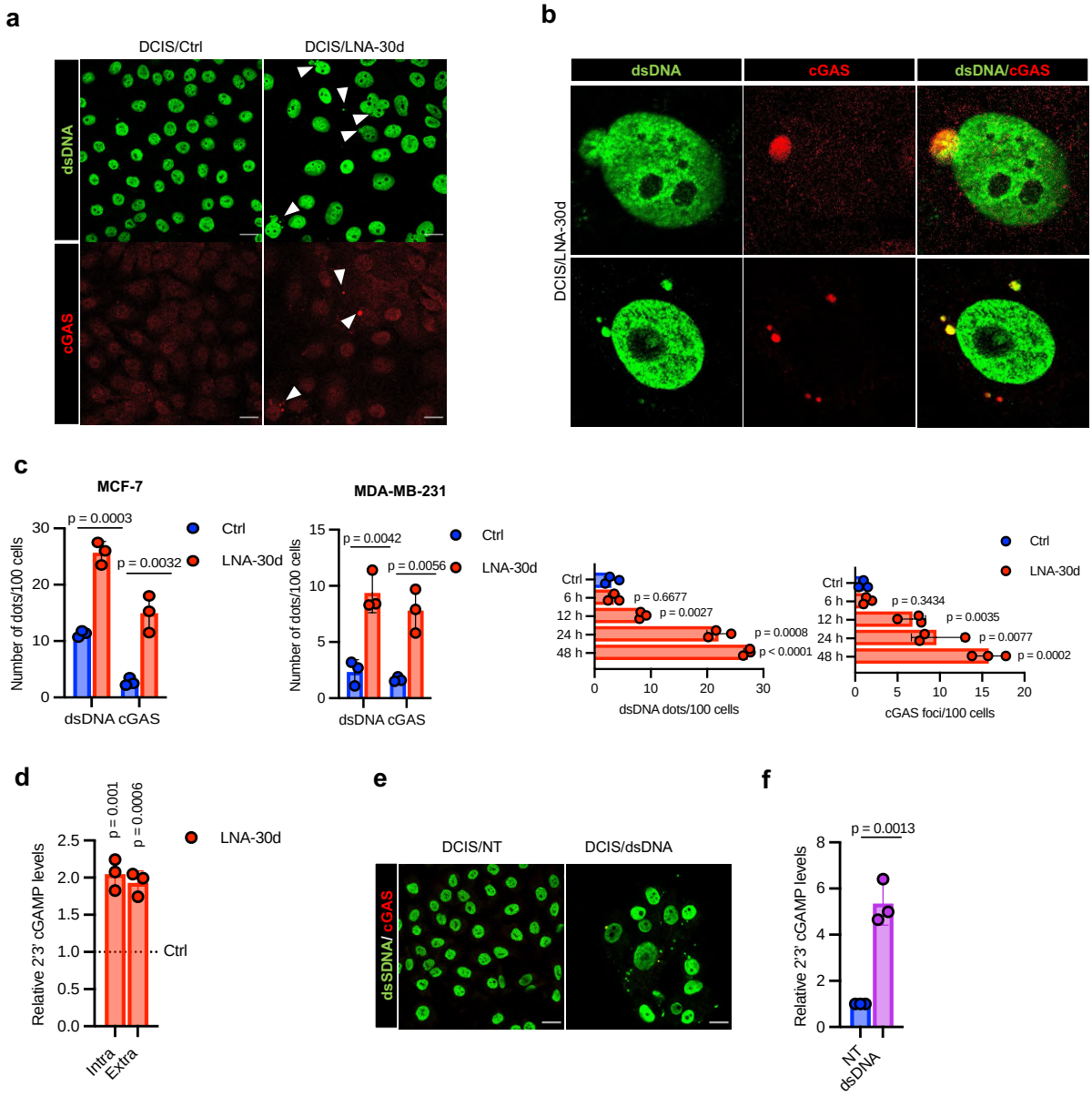

Figure 18. **miR-30d inhibition promotes cytosolic DNA release and cGAS activation in BC cells.**

a. Full-size image (related to b) showing IF analysis of dsDNA (green) and cGAS (red) in DCIS cells transfected with either LNA-30d or control LNA (Ctrl). White arrows highlight cytoplasmic dsDNA and cGAS foci. Scale bar: 20 μm. **b.** Top: representative images showing IF analysis of dsDNA and cGAS in DCIS cells at 48hpt with LNA-30d. Comparison with LNA-control transfected cells is shown in a. Below: Quantification of cytosolic dsDNA and cGAS foci per 100 cells at indicated conditions and timepoints. **c.** Quantification of dsDNA and cGAS cytoplasmic foci per 100 cells in MCF-7 and MDA-MB-231 cell lines, transfected as in a. **d.** ELISA analysis of intracellular and secreted (extra) 2'3'-cGAMP in DCIS cells transfected as in a at 48hpt. Absolute values (pg/ml) were normalized for cell numbers in each condition. Relative increase compared to transfection with control LNA (dotted line) is shown. **e.** Representative images showing IF analysis of dsDNA and cGAS in DCIS cells transfected with 1 μg/ml dsDNA or control (NT). Scale bar: 20 μm. **f.** ELISA analysis of intracellular 2'3'-cGAMP in DCIS cells transfected as in e. Absolute values (pg/ml) were normalized for cell numbers in each condition, and the relative increase compared to control is shown. **a-f.** Bar graphs represent the mean ± standard deviation (s.d.) from n ≥ 3 independent experiments. Statistical significance was determined using a Two-tailed unpaired Student's t-test.

Next, I was curious to determine the source of cytosolic dsDNA in cancer cells, which could be either nuclear or mitochondrial in origin (Fig. 19a). Determining the origin is critical because nuclear envelope (NE) ruptures implicate distinct upstream mechanisms compared with mitochondrial rupture to cGAS activation after miR-30d inhibition. To address this question, we generated a mitochondrial DNA (mtDNA) depleted derivative of the DCIS cell line, designated DCIS/ρ^0, to test the contribution of mtDNA (Fig. 19b). By IF analysis we observed that inhibition of miR-30d with LNA-30d still resulted in cytosolic dsDNA accumulation and cGAS activation to a similar extent in both wt DCIS cells and DCIS/ρ^0 cells (Fig.19c,b), indicating that mitochondrial DNA is not the main cGAS trigger upon miR-30d inhibition.

We next examined whether miR-30d inhibition affects NE integrity and leakage of genomic DNA. To this aim, in order to critically observe the NE structure and position of cGAS dots upon miR-30d inhibition, correlative light-electron microscopy (CLEM) and electron tomography was performed in collaboration with Galina Beznoussenko, at IFOM, Milan, Italy. For this, DCIS cells were transduced with EGFP-cGAS plasmid and LNA-30d in our laboratory and subjected to ultrastructural analysis by CLEM and electron tomography (for detailed information regarding staining and imaging see methods). As shown in Fig. 19d, the results confirmed the accumulation of cytoplasmic EGFP-cGAS aggregates at sites of condensed chromatin immediately adjacent to ruptures in both the inner and outer NE membranes of DCIS cells treated with LNA-30d.

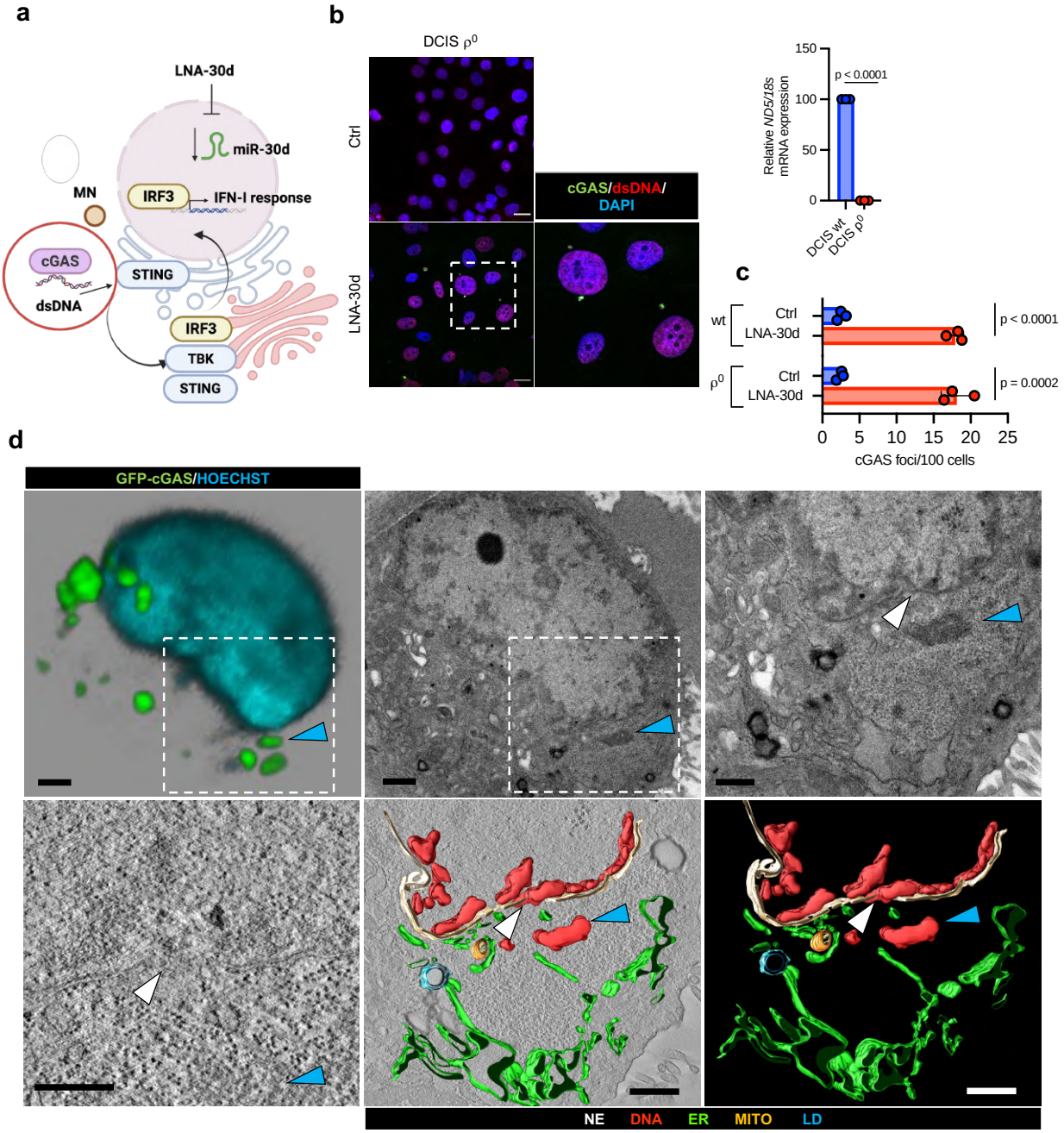

Figure 19. **miR-30d inhibition promotes NE ruptures, cytosolic DNA release and cGAS activation in BC cells.**

a. Schematic representation to identify the source of dsDNA triggering cGAS activation upon miR-30d inhibition (Created with Biorender.com). **b.** Left: representative images showing IF analysis of dsDNA and cGAS in DCIS/ρ0 cells, with magnification. Scale bar: 20 μm. Right: qRT-PCR analysis of *ND5* mRNA expression in DCIS-wt and DCIS/ρ0 cells. *18S* gene was used as reference gene. **c.** Quantification of cGAS cytoplasmic foci per 100 cells in wt-DCIS and DCIS/ρ^0 cells (see main text) transfected with LNA-30d or control LNA (Ctrl). Representative IF images are shown in b. **b-c.** Bar graphs represent the mean ± standard deviation (s.d.) from n ≥ 3 independent experiments. Statistical significance was determined using a Two-tailed unpaired Student's t-test. **d.** Correlative Light Electron Microscopy (CLEM) and electron tomography analysis of NE structure and cGAS perinuclear foci on DCIS cells transduced with EGFP-cGAS and LNA-30d. Upper panels: EGFP-positive cell identified by confocal microscopy (left) was processed for electron microscopy (EM). Dashed boxes indicate regions

that were progressively magnified in EM: a cGAS aggregate is marked by a blue arrowhead, and a site of NE rupture is indicated by a white arrowhead. Bottom images show a higher magnification image from EM 3D tomographic reconstruction (left) and 3D model (middle and right) of the NE rupture site. Scale bars: 400 nm. NE: Nuclear Envelope. ER: Endoplasmic Reticulum. MITO: mitochondria. LD: Lipid Droplet.

To functionally verify whether inhibition of miR-30d may disrupt NE integrity, I transfected DCIS cells with EGFP-NLS reporter construct, which is imported in the nucleus upon translation, and with either control LNA or LNA-30d (Frittoli et al., 2023). As shown in Fig. 20a, the fraction of cells displaying cytoplasmic leakage of EGFP-NLS increased upon miR-30d inhibition, suggesting that NE ruptures may occur under these conditions. Based on prior evidence that ER-resident TREX1 can translocate into the nucleus during NE rupture (Nader et al., 2021), we supposed that miR-30d downregulation may facilitate nuclear entry of TREX1. Consistent with this model, NE rupture would not only allow cytosolic leakage of nuclear DNA as a causal mechanism, rather, it would enable TREX1 access to the nuclear compartment, where it may induce genomic DNA damage. Consistently, by confocal Z-stack imaging, I observed that when DCIS cells were transfected with LNA-30d and GFP-TREX1 plasmid, intranuclear localization of GFP-TREX1 was observed after 48 hours (Fig. 20b), whereas in control cells TREX1 dots were mostly found in the cytoplasm. As shown in Fig. 20c and 20d, inhibition of miR-30d in DCIS and other BC cell lines (MCF-7 and MDA-MB-231) led to a pronounced increase in phosphorylated histone H2AX (γ-H2AX) nuclear foci, a well-established marker of dsDNA breaks (Kuo, 2008). In parallel, we observed a strong rise in nuclear foci of 53BP1 (Fig. 20e), a DNA damage response protein that accumulates at sites of dsDNA breaks and promotes non-homologous end joining repair (Z. Zhang, Samsa, et al., 2023). Together, the increase in γ-H2AX and 53BP1 foci upon miR-30d depletion suggests that loss of miR-30d leads to accumulation of genomic damage across multiple BC cell types. To confirm if the observed DNA damage is indeed mediated by TREX1 nuclear entry, we repeated the same experiment on DCIS cells together with silencing TREX1 by RNAi and LNA-30d treatment and observed a decrease in γ-H2AX foci as compared to control LNA-30d treated cells. This result confirms that TREX1 is involved at least in part in increased DNA damage upon miR-30d inhibition in DCIS cells (Fig. 20f).

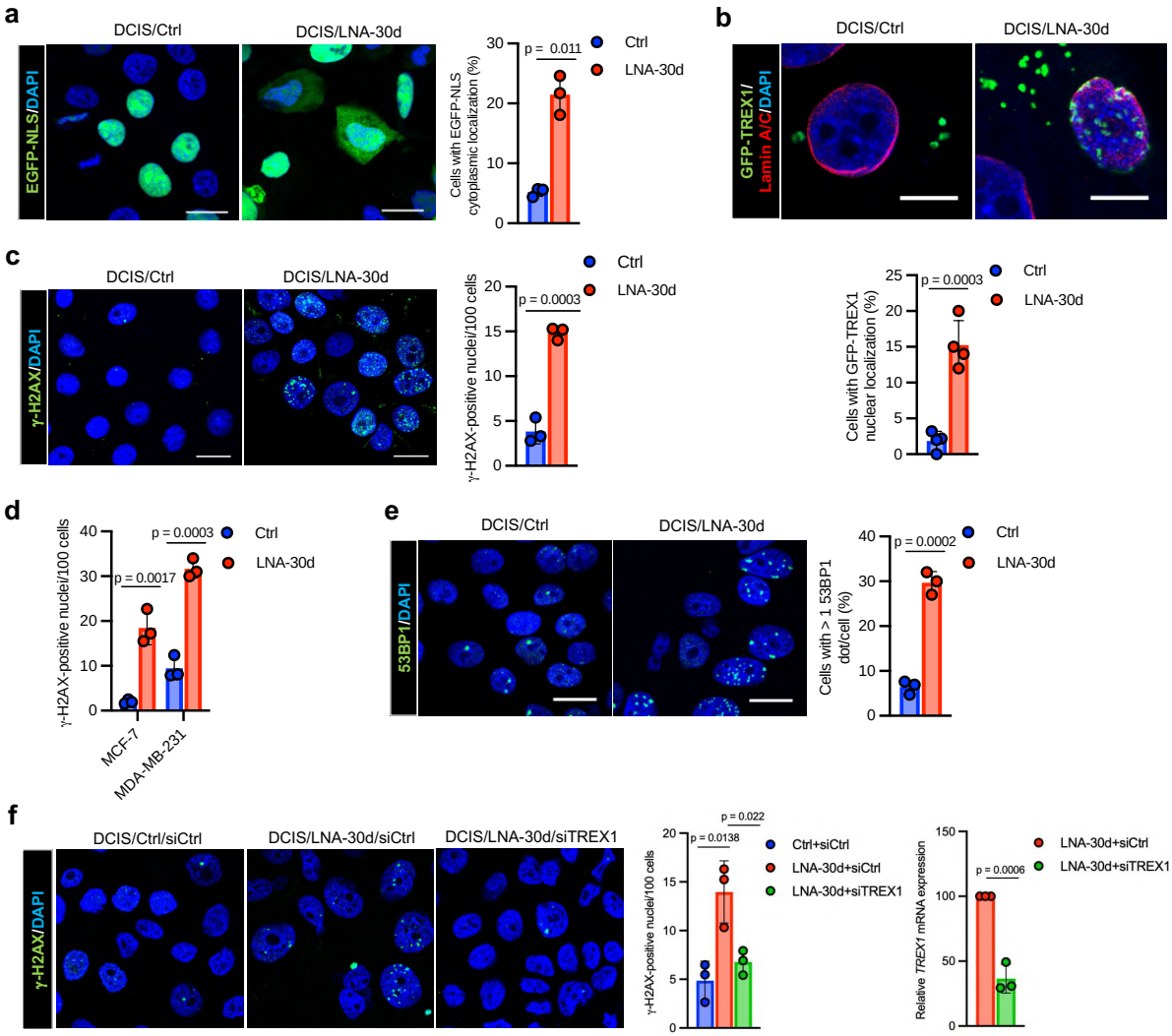

Figure 20. **miR-30d inhibition promotes NE ruptures and TREX1 mediated DNA damage.**

a. Left: analysis of cellular localization of EGFP-NLS reporter in DCIS cells transfected with either LNA-30d or control LNA (Ctrl) with EGFP-NLS reporter and stained with DAPI. Scale bar: 20 μm. Right: The graph shows quantification of EGFP-NLS cytoplasmic localization. **b.** Analysis of the cellular localization of ectopically expressed GFP-TREX1 by confocal scanning laser microscopy on DCIS cells transfected as in a). NE was stained with anti-Lamin A/C Ab (red) and nuclei were counterstained with DAPI; representative images show sections corresponding to the center of the nucleus. Scale bar: 10 μm. The graph (below) shows quantification of cells displaying nuclear localization of GFP-TREX1. **c,d.** IF analysis of γ-H2AX nuclear foci in DCIS, MCF-7 and MDA-MB-231 cells transfected with either LNA-30d or control LNA (Ctrl) and relative quantification. Scale bar: 20 μm. **e.** IF analysis of nuclear DNA damage foci using anti-53BP1 antibody in DCIS cells transfected as in c and relative quantification. Scale bar: 20 μm. **f.** IF analysis of γ-H2AX nuclear foci in DCIS cells co-transfected with LNA-30d or control LNA (Ctrl) and either control siRNA (blue and red bar) or siTREX1 (green bars) with quantification on the right. **a-f.** Bar graphs represent the mean ± standard deviation (s.d.) from n ≥ 3 independent experiments. Statistical significance was determined using a Two-tailed unpaired Student's t-test.

We then sought to verify whether NE fragility in miR-30d-depleted cancer cells directly contributes to cGAS activation and induction of the cGAS–STING–IFN-I pathway. To this aim, I transfected DCIS cells with LNA-30d and its control counterpart and then treated with Remodelin, a small-molecule inhibitor of NAT10 acetyltransferase previously shown to restore nuclear shape in progeroid mice & in cells with reduced laminB through normalization of NE–cytoskeletal interactions (Larrieu et al., 2014; Sladitschek-Martens et al., 2022). Remarkably, Remodelin has been reported to decrease DNA damage in progeroid cells and to suppress cGAS activation in aging fibroblasts (Sladitschek-Martens et al., 2022). IF analysis confirmed that treatment of DCIS cells with Remodelin effectively rescued NE shape abnormalities (Fig. 21a) and reduced both cytoplasmic leakage of NLS-GFP and GFP-TREX1 nuclear entry induced by miR-30d depletion (Fig. 21b,c). Following this, I also observed a significant reduction in DNA damage, dsDNA and cGAS foci formation (Fig. 21d,e). These findings confirm that miR-30d contributes to maintain NE integrity in cancer cells, and that its loss promotes cGAS activation via nuclear rupture and DNA leakage.

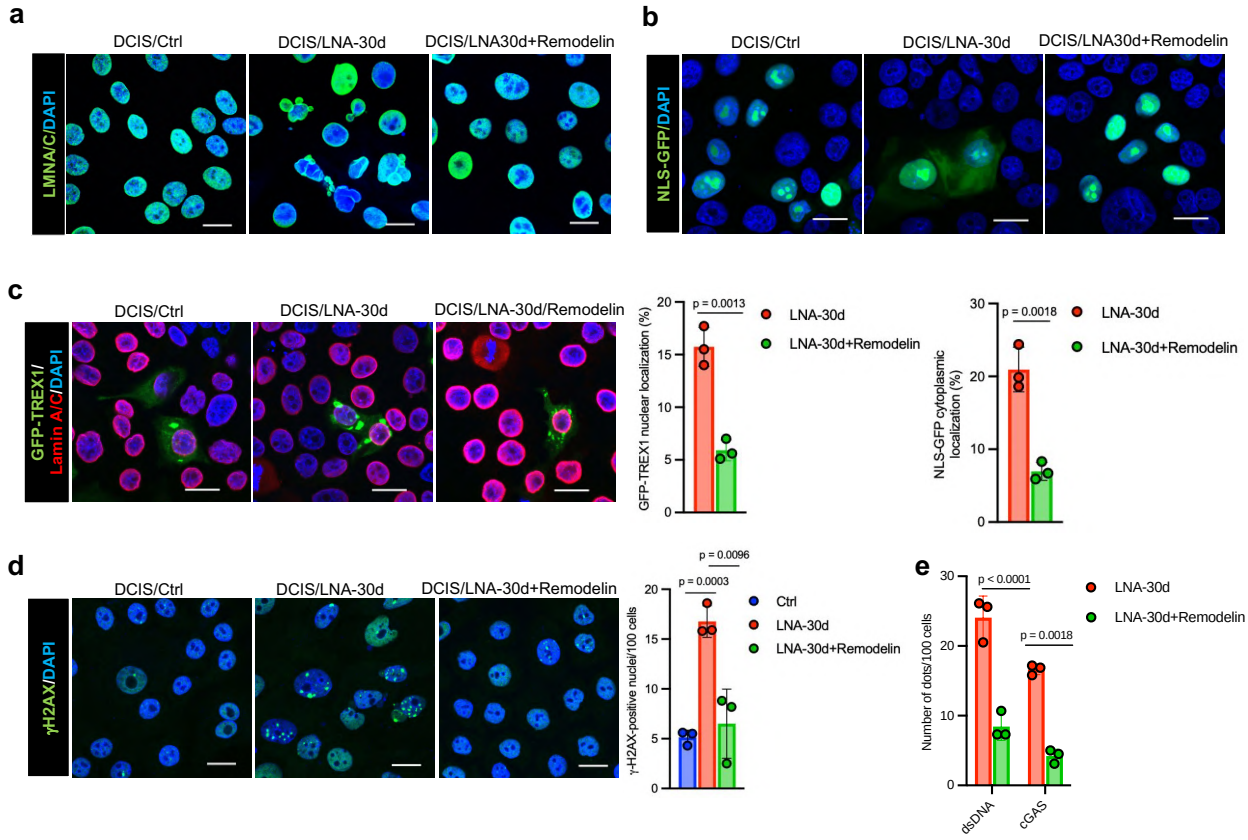

Figure 21. **miR-30d maintains NE integrity thereby inhibiting TREX1 mediated DNA damage and cGAS activation.**

a. Representative IF image of the NE stained with Lamin A/C Ab (green) in DCIS cells transfected with either LNA-30d or control LNA (Ctrl) and either treated or not with 20 μM Remodelin for 48hr. Scale bar: 20 μm. **b.** Top: IF analysis of cellular localization of NLS-GFP reporter in DCIS cells transfected with either LNA-30d or control LNA (Ctrl) with NLS-GFP reporter and either treated or not with 20 μM Remodelin for 48hr and stained with DAPI. Scale bar: 20 μm. Bottom: The graph shows quantification of NLS-GFP cytoplasmic localization. **c.** Analysis of the cellular localization of ectopically expressed GFP-TREX1 by confocal scanning laser microscopy on DCIS cells transfected as in a). NE was stained with anti-Lamin A/C Ab (red) and nuclei were counterstained with DAPI. The graph (right) shows quantification of cells displaying nuclear localization of GFP-TREX1. Scale bar: 20 μm. **d.** IF analysis of γ-H2AX nuclear foci in DCIS cells, transfected as in a and relative quantification right. **e** Quantification of dsDNA and cGAS cytoplasmic foci per 100 cells in DCIS cell line, transfected as in a. **b-e.** Bar graphs represent the mean ± standard deviation (s.d.) from n ≥ 3 independent experiments. Statistical significance was determined using a Two-tailed unpaired Student's t-test.

We then sought to obtain hints on the process(es) induced by miR-30d that may lead to NE fragility and consequent accumulation of genomic damage, cytosolic DNA and cGAS induction. To this aim, we took advantage of the transcriptomic analysis performed on DCIS cells upon inhibiting miR-30d with LNA-30d, which highlighted downregulation of several genes encoding structural components of the NE (Fig. 22a) including Lamin-B1, which has been shown to act as a key NE protein to preserve NE integrity (Lammerding et al., 2006; Vergnes et al., 2004) and suppress cGAS activation (Sladitschek-Martens et al., 2022). As shown in Fig. 22b and Fig. 23e, WB and qRT-PCR analysis confirmed a significant decrease of both *LMNB1* and *LMNB2* at mRNA and protein levels upon miR-30d inhibition with LNA-30d, whereas *Lamin A/C* levels remained unaffected. Conversely, when miR-30d was overexpressed with mimic-30d construct in DCIS cells, the protein levels of both Lamin-B1 and Lamin-B2 increased (Fig. 22c). In agreement with reduced expression of NE components, staining DCIS cells transfected with LNA-30d with anti-LMNA/C antibody highlighted multiple NE abnormalities including wrinkles, blebs, indentations, and lobulations (Fig. 22d)—starting as early as 12 hours post-transfection and progressing over time (Fig. 22e) and were quantified by a significant decrease in NE circularity (Fig. 22f). These defects were not only observed in DCIS cells but also in MCF-7 and MDA-MB-231 BC cell lines (Fig. 22g), suggesting a conserved role for miR-30d in preserving NE architecture in BC. Interestingly, inhibition of miR-30d with LNA-30d also resulted in a marked increase in the formation of Lamin A/C-enclosed micronuclei. Micronuclei (MN) are small, membrane-bound extranuclear structures that form when chromosome fragments or whole chromosomes fail to be incorporated into the daughter nuclei

during cell division. Due to their fragile envelope lacking key nuclear components like Lamin B and nucleoporins, MN are prone to rupture, releasing DNA to the cytosol and can potentially activate immune responses like the cGAS-STING pathway (Bona & Bakhoum, 2024; Hosea et al., 2024; Maiato & Silva, 2023) (Fig. 22d,h). Additionally, LMNB1 silencing in DCIS cells also recapitulated NE dysmorphia (Fig. 22i) and cGAS accumulation (Fig. 22j), phenocopying miR-30d inhibition.

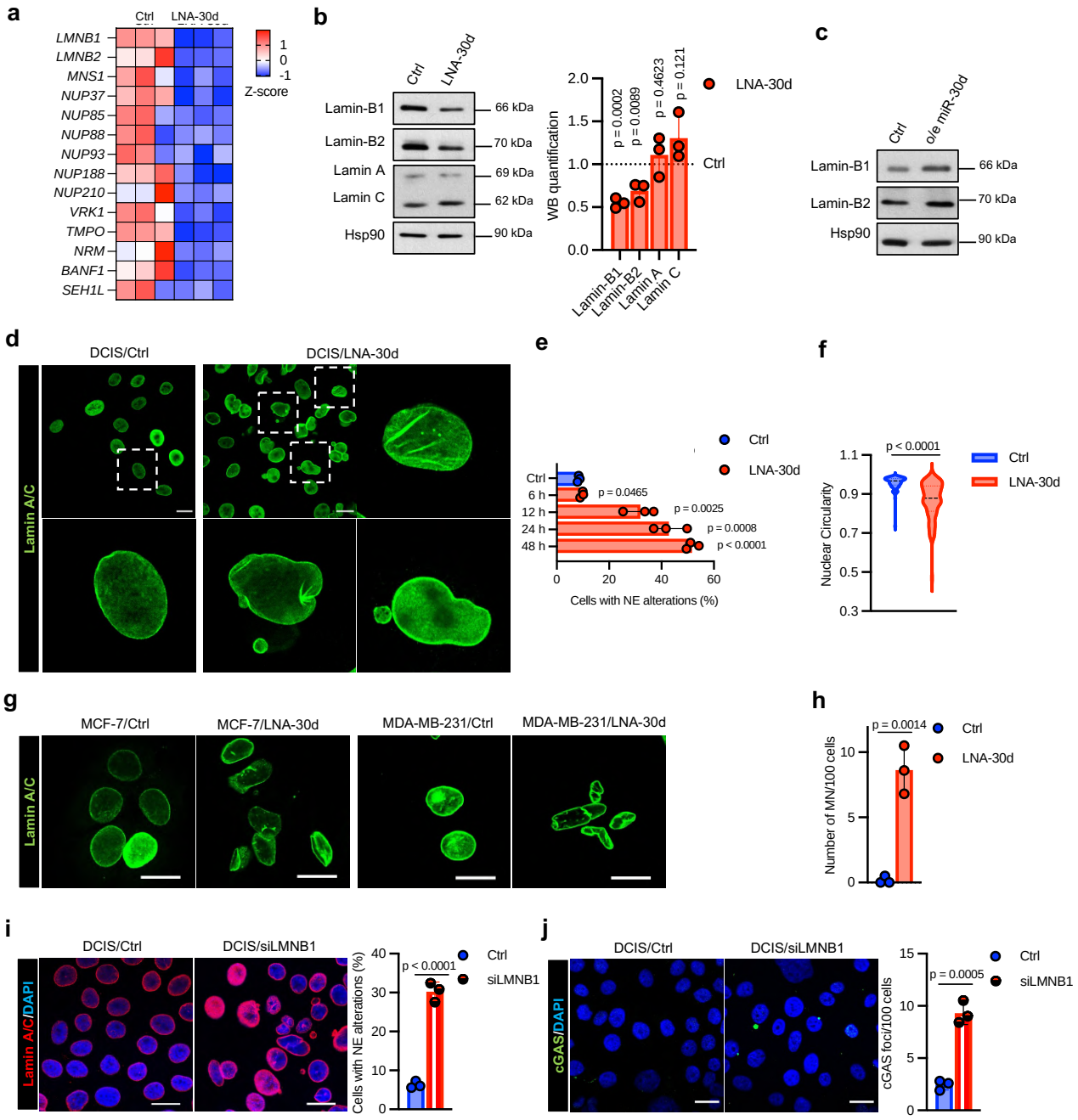

Figure 22. **miR-30d inhibition promotes NE ruptures, cytosolic DNA release and cGAS activation in BC cells.**

a. Heatmap of RNA-seq data (related to Fig. 7c) displaying the differential expression of genes related to NE processes in DCIS cells transfected with either LNA-30d or control LNA (Ctrl). Expression levels were normalized using Z-scores for gene-wise comparison, with high expression shown in red and low expression in blue. Each condition includes three biological replicates. All displayed genes are differentially expressed with statistical significance (DESeq2 Two-tailed modified t-test adjusted for multiple testing using Benjamini-Hochberg method). **b.** Representative WB analysis (Left) of Lamin-B1, Lamin-B2 and Lamin A/C proteins in DCIS cells transfected as in Fig. 17a. Hsp90 was used as loading control. Quantification is shown in Right. **c.** WB analysis of the indicated proteins in DCIS cells transfected with either miR-30d mimic (o/e miR-30d) or control. Hsp90 was used as loading control. **d.** IF analysis of the nuclear lamina stained with Lamin A/C Ab in DCIS cells transfected as in Fig. 18a. Dashed boxes indicate regions magnified in the lower panels. **e.** Quantification of NE alterations in DCIS cells (see main text), based on nuclear lamina staining at indicated time points upon transfection as in Fig. 18a**. f.** Violin plots showing nuclear circularity values calculated based on DAPI staining (see Methods) in DCIS cells transfected as in Fig. 18a. Quantification includes 100 cells per sample from n=3 independent experiments. **g.** Representative images of IF analysis with anti-Lamin A/C Ab in MCF-7 and MDA-MB-231 cells transfected as in Fig. 20d**.** Scale bar: 20 μm. **h.** Quantification of micronuclei (MN) in DCIS cells transfected as in Fig. 18a and subjected to IF analysis with anti-Lamin A/C antibody. **i.** IF analysis with Lamin A/C Ab (red) in DCIS cells transfected with either LMNB1 siRNA or Ctrl siRNA, with quantification of NE alterations on the right. Scale bar: 20 μm. **j.** IF analysis of cGAS in DCIS cells transfected as in i and quantification of cytoplasmic cGAS dots. Scale bar: 20 μm. **b-j.** Bar graphs represent the mean ± standard deviation (s.d.) from n ≥ 3 independent experiments. Statistical significance was determined using a Two-tailed unpaired Student's t-test.

Together, these findings suggest that inhibition of miR-30d may disrupt NE structure through decreasing the expression of laminB and possibly other NE components, supporting the hypothesis that miR-30d functions as a key regulator of NE integrity in BC cells. By maintaining nuclear lamina components, miR-30d may help prevent NE rupture and subsequent genomic DNA damage and leakage into the cytosol, thereby suppressing activation of cGAS–STING–IFN-I signalling.

4.6 miR-30d safeguards the integrity of nuclear envelope via a LATS2/YAP axis

To elucidate the molecular pathways underlying Lamin-B downregulation and NE destabilization upon miR-30d inhibition, we took advantage of the transcriptomic analysis performed on DCIS cells upon inhibiting miR-30d (Fig.7 and Fig. 22a). We observed that a substantial fraction of the genes downregulated upon miR-30d inhibition overlapped with known direct transcriptional targets of YAP/TAZ transcriptional regulators (Zanconato et al., 2015, 2018; H. Zhang et al., 2009), that were recently found to contribute to NE integrity and to restrain cGAS activation in normal fibroblasts, partly through the transcriptional regulation of Lamin-B1 (Sladitschek-Martens et al., 2022). GSEA analysis on our RNA-seq data revealed

significant suppression of YAP/TAZ transcriptional activity upon miR-30d inhibition in DCIS cells (Fig. 23a), whereas IF analysis revealed that miR-30d overexpression in normal MCF10A breast epithelial cells, achieved by transfecting mimic-30d construct, enhanced YAP nuclear localization (Fig. 23b) and transcriptional activity, while not affecting *YAP* mRNA levels (Fig. 23c). This suggests that miR-30d may sustain YAP/TAZ signalling, thereby promoting NE stability. Indeed, inhibition of miR-30d with LNA-30d closely mirrored the effect of YAP depletion achieved by RNAi (Fig. 23d), as for reduced mRNA expression of *LMNB1* and *LMNB2*, while not *LMNA/C*, increased NE abnormalities, and cGAS activation (Fig. 23d,e,f). Notably, the phenotypic consequences observed upon miR-30d inhibition were more pronounced than those observed following silencing of either YAP (Fig. 23f) or Lamin-B1 alone (Fig.22i,j), indicating that miR-30d likely controls additional effectors that contribute to maintain NE integrity.

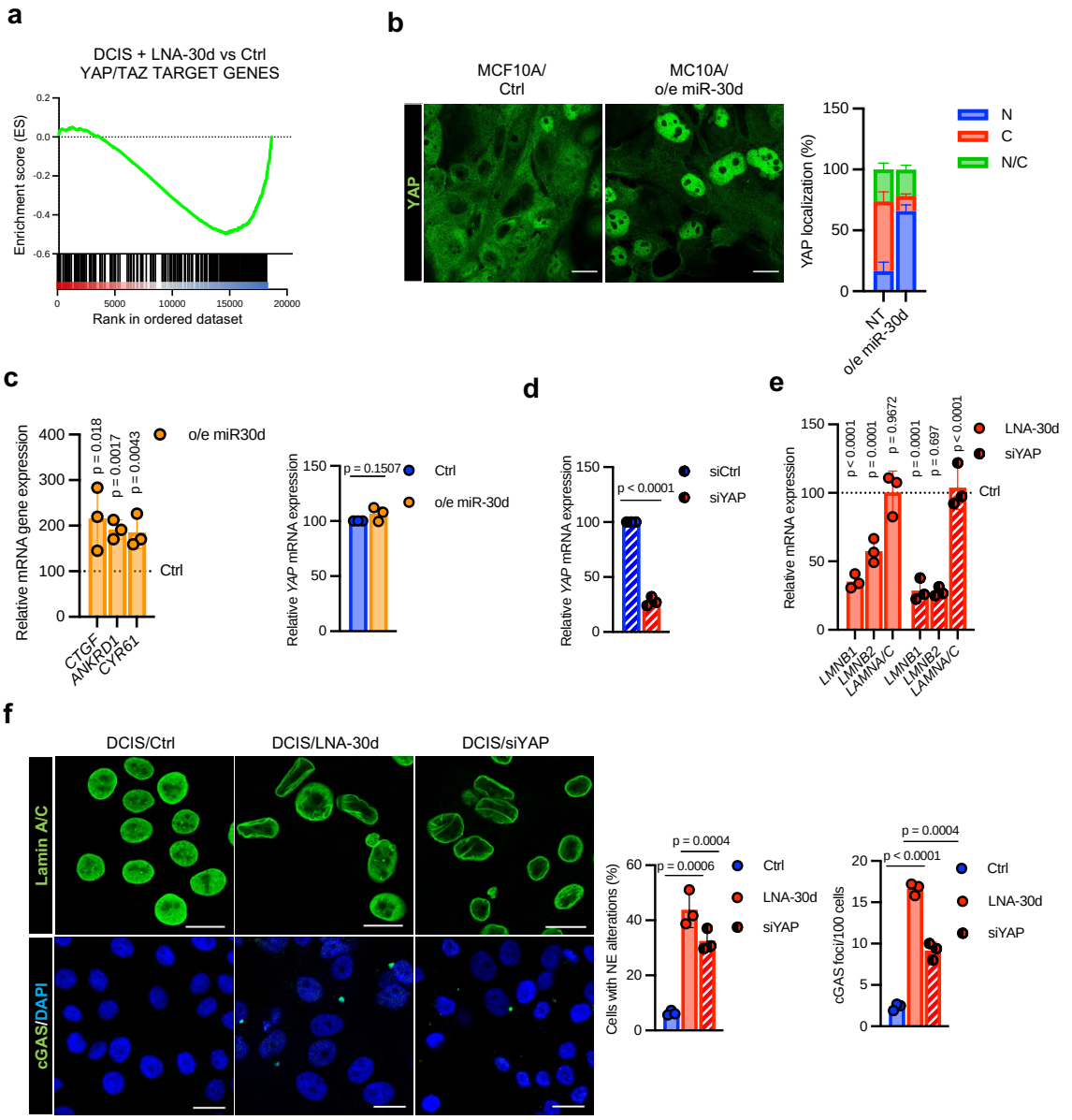

Figure 23. **miR-30d safeguards NE integrity via a LATS2/YAP/Lamin-B axis.**

a. GSEA plot of YAP/TAZ activity signature in DCIS cells transfected with either LNA-30d or control LNA. The green line indicates the enrichment of each gene in the pathway, while the black bars represent gene ranking. The displayed pathway is statistically significant (FDR.q.val<0.05; Two-tailed Student's t-test adjusted for multiple testing using GSEA default method). **b.** IF analysis of YAP subcellular localization in MCF10A cells transfected with either miR-30d mimic (o/e miR-30d) or control. Scale bar: 20 μm. Relative quantification for each condition is shown on the right. N = nuclear localization, C = cytoplasmic localization, N/C = nuclear and cytoplasmic localization. **c.** Left: qRT-PCR analysis of mRNA expression of indicated YAP target genes in MCF10A cells transfected with either miR-30d mimic (o/e miR-30d) or control construct (related to b). Right: qRT-PCR analysis of *YAP* mRNA expression in the same experiment. **d.** qRT-PCR analysis of *YAP* mRNA expression in DCIS cells transfected with either YAP siRNA or control siRNA related to e. **e.** qRT-PCR analysis of indicated mRNAs in DCIS cells at 48hpt with LNA-30d (solid bars) or YAP siRNA (striped bars) as compared to Ctrl (dotted line). **f.** Left: Representative IF analysis of the nuclear lamina stained with anti-Lamin A/C Ab (upper panels) and of cGAS (lower panels) in DCIS cells transfected as in e. Scale bar: 20 μm. Right: Quantification of NE defects and of cGAS foci is shown respectively. **a-f.** Bar graphs represent

the mean ± standard deviation (s.d.) from n ≥ 3 independent experiments. Statistical significance was determined using a Two-tailed unpaired Student's t-test.

To obtain mechanistic insight into the effect of miR-30d on YAP/TAZ, we sought to identify genes repressed by miR-30d that may inhibit YAP. To this aim, Dr. L. Triboli intersected three datasets (Fig. 24a): (i) the YAP interactome (BioGRID), (ii) transcripts upregulated upon miR-30d inhibition in DCIS cells (RNA-seq), and (iii) predicted direct targets of miR-30 (TargetScan v8). This approach led to the identification of several candidate mediators that may contribute to the downstream effects of miR-30d inhibition. Among these we found some negative regulators of YAP/TAZ signalling, including LATS2, AMOTL2, WWP1, and PTPN21 (Hwang et al., 2021; X. Li et al., 2016; Yu et al., 2015; Zhao et al., 2011). Notably, at mRNA level all of these genes were found to be upregulated following treatment with LNA-30d (Fig. 24b and detailed in Table 6). Given its central role in the Hippo signalling pathway, we chose to focus our analysis on LATS2. LATS2 encodes a serine/threonine kinase that directly phosphorylates YAP at serine127, a modification that promotes YAP inactivation by facilitating its retention in the cytoplasm and preventing its transcriptional activity in the nucleus (Zhao et al., 2007). This regulatory mechanism is critical for maintaining cellular homeostasis and controlling proliferation, and its modulation by miR-30d suggests a broader impact on tumour cell signalling networks. To investigate whether miR-30d directly regulates *LATS2* expression, we examined its interaction with the 3′ untranslated region (3′UTR) of *LATS2* mRNA. Bioinformatic analysis predicted a miR-30d binding site within the *LATS2* 3′UTR, suggesting potential post-transcriptional regulation. To validate this, a luciferase reporter assay was performed using a construct containing the wt *LATS2* 3′UTR. Co-transfection with miR-30d resulted in dose-dependent repression of luciferase activity (Fig. 24c). Importantly, mutation of the predicted miR-30d binding site abolished this repression (Fig. 24d), confirming direct repression by miR-30d. Conversely, inhibition of miR-30d led to increased reporter activity (Fig. 24e), further supporting its role as a negative regulator of LATS2. Remarkably, at the protein level, overexpression of miR-30d in DCIS cells with mimic-30d construct significantly reduced LATS2 expression, while LATS1 levels remained unaffected (Fig. 24f), consistent with the absence of a miR-30d target site in the LATS1 transcript. These findings collectively establish LATS2 as a direct target of miR-30d,

implicating miR-30d in the modulation of Hippo pathway activity through post-transcriptional repression of LATS2. Functionally, inhibition of miR-30d led to a marked increase in LATS2 protein levels, which in turn promoted phosphorylation of YAP/TAZ at serine 127 and their subsequent sequestration in the cytoplasm in a LATS2-dependent manner (Fig. 24g,h,i). This post-translational modification is known to inhibit YAP/TAZ transcriptional activity, and accordingly we observed a significant downregulation of canonical YAP target genes (Zanconato et al., 2015) following miR-30d inhibition (Fig. 24j). To further investigate the functional relevance of LATS2 in this regulatory axis, we performed LATS2 KD experiments in DCIS cells treated with LNA-30d. Remarkably, silencing LATS2 restored Lamin-B1 expression (Fig. 24k) and significantly reduced NE abnormalities (Fig. 24l,m), as well as downstream activation of the cGAS pathway and *IFNB* production (Fig. 24n,o). These results underscore the central role of LATS2 as a mediator of miR-30d, linking its regulatory activity to YAP signalling, NE integrity, and innate immune activation.

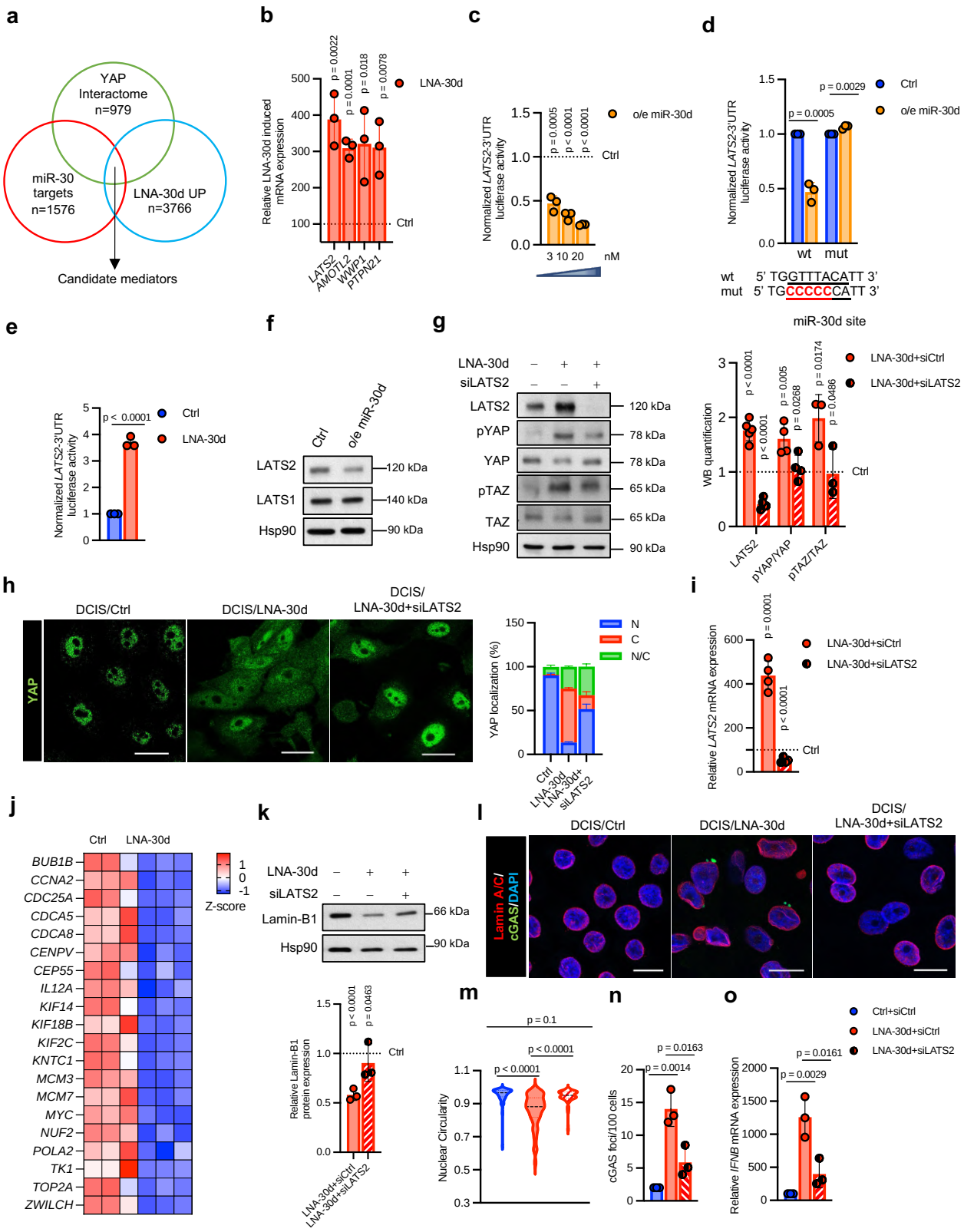

Figure 24. **miR-30d safeguards NE integrity via a LATS2/YAP/Lamin-B axis.**

a. Venn diagram representing the intersection between genes upregulated (p-value < 0.05) in DCIS RNA-seq upon LNA-30d transfection (LNA-30d UP, n=3766), predicted miR-30 target genes from TargetScan v8 (miR-30 targets, n=1576) and genes from the YAP interactome obtained from BioGRID

(n=979). **b.** qRT-PCR analysis of mRNA expression for indicated genes in DCIS cells transfected with either LNA-30d or control LNA (Ctrl, dotted line). Genes analyzed were selected from the intersection in a**. c.** Luciferase assay in DCIS cells transfected with wild-type (wt) *LATS2*-3'UTR-luciferase reporter constructs and miR-30d mimic (o/e miR-30d) or control, with dosage indicated on the x-axis. **d.** Luciferase assay in DCIS cells transfected with either wt or mutagenized (mut) *LATS2*-3'UTR-luciferase reporter constructs and miR-30d mimic (miR-30d o/e). The sequence from the 3'UTR of *LATS2* mRNA containing a putative miR-30d target site (underlined) is shown. The mutagenized sequence is shown in red. **e.** Luciferase assay performed as in d on DCIS cells transfected with LNA-30d or control LNA (Ctrl). **f.** WB analysis of the indicated proteins in DCIS cells transfected with either miR-30d mimic or control. Hsp90 was used as loading control. **g-i, k-o** All panels refer to DCIS cells co-transfected with LNA-30d and LATS2 siRNA in the indicated combinations. **g.** WB analysis of the indicated proteins in DCIS cells transfected with LNA-30d and either Ctrl or LATS2 siRNA. Hsp90 was used as loading control. Quantification of protein levels relative to those measured in cells transfected with control LNA (Ctrl, dotted line) is shown on the right. **h.** IF analysis of YAP subcellular localization, with relative quantification shown on the right. Scale bar: 20 μm. N = nuclear localization, C = cytoplasmic localization, N/C = nuclear and cytoplasmic localization. **i.** qRT-PCR analysis of *LATS2* mRNA expression in DCIS cells transfected with either LATS2 siRNA or control siRNA. **j.** Heatmap of RNA-seq data in DCIS cells transfected with LNA-30d or control LNA (Ctrl) (related to Fig. 7c) displaying the expression of YAP/TAZ direct target genes. The expression levels were normalized using Z-score to allow gene-wise comparison, with high expression in red and low expression in blue. The three columns correspond to biological replicates for each condition. All displayed genes are statistically differentially expressed (DESeq2 Two-tailed modified t-test adjusted for multiple testing using Benjamini-Hochberg method). **k.** WB analysis (upper panel) and relative quantification (lower panel) of Lamin-B1 protein levels. Hsp90 was used as loading control. **l.** Representative images of IF analysis of Lamin A/C and cGAS for each condition. **m.** Violin plot showing nuclear circularity calculations based on DAPI staining. Quantification includes 100 cells per sample from n=3 independent experiments. **n.** Quantification of cGAS foci per 100 cells in each condition. **o.** qRT-PCR analysis of *IFNB* mRNA expression in each condition. **b-o.** Bar graphs represent the mean ± standard deviation (s.d.) from n ≥ 3 independent experiments. Statistical significance was determined using a Two-tailed unpaired Student's t-test.

Interestingly, the regulatory relationship between miR-30d and LATS2 appears to be conserved across multiple cancer types. Experimental data demonstrated that inhibition of miR-30d consistently led to upregulation of *LATS2* mRNA levels in a range of cell lines derived not only from BC but also from other tumour origin (Fig. 25a), with a clear correlation between miR-30d levels (see section 4.1) and expression of *LATS2* mRNA upon miR-30d inhibition in different cells lines (Fig. 25a).

To further explore the clinical relevance of this axis, we analyzed transcriptomic data from TCGA. This analysis revealed a robust inverse correlation between *LATS2* expression and a miR-30d activity signature across several malignancies, including breast, colon, liver, cholangiocarcinoma, and prostate cancers (Fig. 25b).

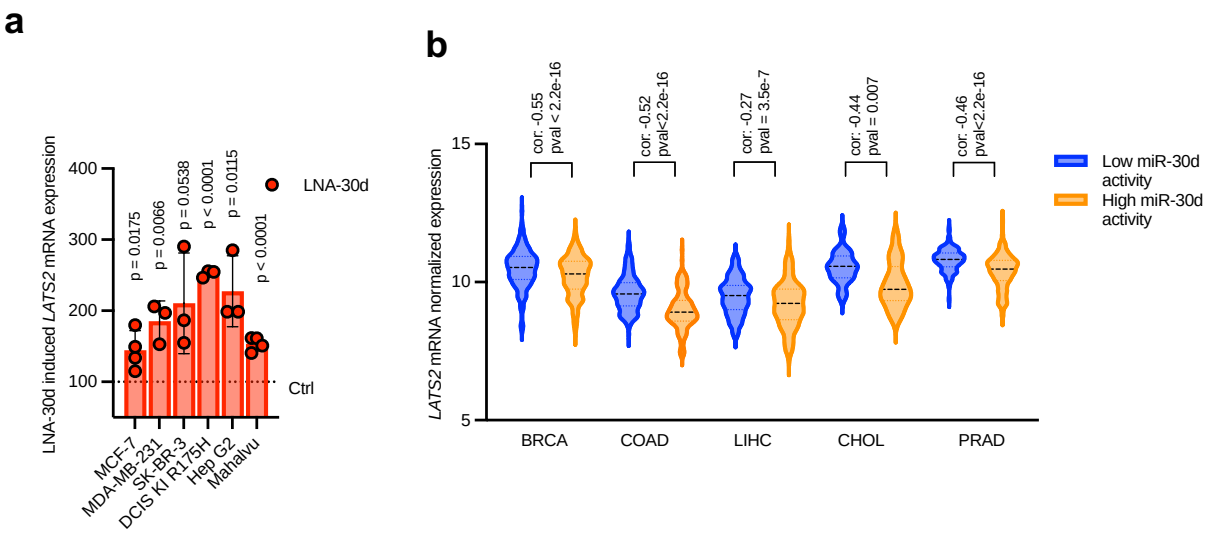

Figure 25. **miR-30d targets LATS2 in multiple cell lines and tumour types.**

a. qRT-PCR analysis of *LATS2* mRNA expression in the indicated cancer-derived cell lines, transfected with either LNA-30d or control LNA (Ctrl, dotted line). Histone *H3* was used as a reference gene. Bar graphs represent the mean ± standard deviation (s.d.) from n ≥ 3 independent experiments. Statistical significance was determined using a Two-tailed unpaired Student's t-test. **b.** Violin plot showing Z-score normalized *LATS2* mRNA expression in human samples of the indicated TCGA cancer datasets, classified based on miR-30d activity. Violin colors (blue and orange) correspond to low and high miR-30d activity, respectively. All comparisons are statistically significant (Two-tailed Student's t-test) and correlation was calculated using the cor.test function of the stats package in R. Correlation value cutoff is -0.2 and p-value cutoff is 0.05.

These findings suggest that miR-30d-mediated repression of LATS2 and the resulting modulation of YAP signalling is a broadly conserved mechanism contributing to tumour progression in multiple cancer types.

4.7 miR-30d downregulation impairs Breast Cancer cell viability

The cGAS/STING pathway is known to exert various cell-intrinsic effects that limit tumour growth, including antiproliferative responses like activation of cell-cycle checkpoints, senescence and apoptosis and maintenance of chromosomal stability (Ranoa et al., 2019; Samson & Ablasser, 2022; F. Sun et al., 2019). This suggests that by repressing this cascade, miR-30d may enhance tumour cell fitness, a cell-intrinsic effect that would complement its role in fostering an immune-suppressive TME. Consistent with this notion, analysis of our RNA-seq data highlighted that when miR-30d was depleted with LNA-30d in DCIS cells, it led to upregulation of several

antiproliferative genes like CDKN1A, GADD45A, GADD45B, BCL10 and CASP7 (Fig. 26a). As shown in Fig. 26b, this was accompanied with marked reduction of cell proliferation as judged by BrdU incorporation assays. Several mechanisms may explain this reduction in cell proliferation. First, the observed induction of DNA damage following miR-30d inhibition could evoke a p53-mediated response, culminating in transcriptional activation of CDKN1A (p21), a canonical effector of cell cycle arrest (Sullivan et al., 2018). Consistent with this, WB analyses revealed a marked upregulation of both p53 and p21 protein levels in LNA-30d treated DCIS cells (Fig. 26c), supporting the notion that miR-30d depletion triggers a p53–p21 axis that enforces G1/S checkpoint control and suppresses proliferation. To further probe the contribution of nuclear stress to this phenotype, I used remodelin, as described in section 4.5 and observed that remodelin treatment reversed accumulation of both p53 and p21 proteins in cells treated with LNA-30d (Fig. 26c), suggesting that loss of nuclear integrity and consequent DNA damage modulate the extent of p53 pathway activation in this context. In addition to p53-dependent cell cycle arrest, the activation of cGAS–STING pathway observed upon miR-30d depletion may also directly suppress BC cell growth by inducing apoptosis (Chattopadhyay et al., 2010; Lohard et al., 2020). To explore this, I co-transfected DCIS cells with LNA-30d or control, alongside RNAi constructs targeting STING1 and IRF3. Apoptotic activation, measured using a Caspase-3/7 activity assay, showed a significant increase upon miR-30d depletion, and this effect was strongly reduced upon KD of either STING or IRF3, indicating that the induction of apoptosis is mainly mediated through a STING-IRF3-dependent pathway in DCIS BC cells (Fig. 26d). Notably, this result was consistently observed across other BC cell lines like MCF-7 and MDA-MB-231 (Fig. 26e). This said, it is conceivable that p53 activation may also contribute to induce apoptosis, as we observed increased expression of pro-apoptotic p53 target genes like BAX, PUMA and NOXA upon miR-30d inhibition in DCIS cells (not shown).

Based on the above evidence, I further hypothesized that miR-30d inhibition may sensitize BC cells to DNA-damaging agents by triggering a STING- and IRF3-dependent apoptotic response, and that combining low doses of DNA damaging drugs with miR-30d inhibitors as a cGAS–STING–activating strategy could limit toxicity while overcoming chemoresistance. To validate this, genotoxic drugs were tested that are in clinical practice to treat BC patients, such as doxorubicin and Palbociclib, in combination with miR-30d inhibition. I transfected DCIS cells with control

oligonucleotide together with low-dose doxorubicin. As shown by IF in Fig. 26f, this treatment effectively caused DNA damage, as evidenced by nuclear γ-H2AX accumulation, however it resulted in only minimal apoptotic cell death (Fig. 26g, blue curve). In contrast, co-treatment with LNA-30d and doxorubicin led to a marked increase in apoptosis, with a ~7–10-fold enhancement in Caspase-3/7 activity (Fig. 26g, red curve), indicating the possibility that miR-30d inhibition sensitizes BC cells to genotoxic drugs through a STING-mediated apoptotic mechanism. To determine whether this effect extends to more aggressive BC subtypes, I performed the same combination treatment in MDA-MB-231 cells, a metastatic BC cell line which harbors *TP53*^{R280K} missense mutation and has intrinsic resistance to doxorubicin as compared to DCIS cells. Notably, a similar synergistic increase in cell death was observed in this model (Fig. 26h,i), suggesting that miR-30d targeting may overcome resistance mechanisms associated with p53 mutations. Furthermore, I evaluated whether miR-30d inhibition could enhance the cytotoxic effects of Palbociclib, a CDK4/6 inhibitor approved for ER-positive, HER2-negative advanced BC (Beaver et al., 2015). Palbociclib has also been shown to cause DNA damage, impact DNA repair machinery, and activate cGAS/STING signalling, leading to senescence and apoptosis (H. Fan et al., 2023; T. H. Wang et al., 2021). Caspase 3/7 activity revealed that when DCIS cells were co-transfected with LNA-30d and low-dose of Palbociclib, it resulted in a synergistic apoptotic response (Fig. 26j,k), further supporting the idea that miR-30d inhibition enhances both the immunogenic and apoptotic consequences of therapeutically induced DNA damage.

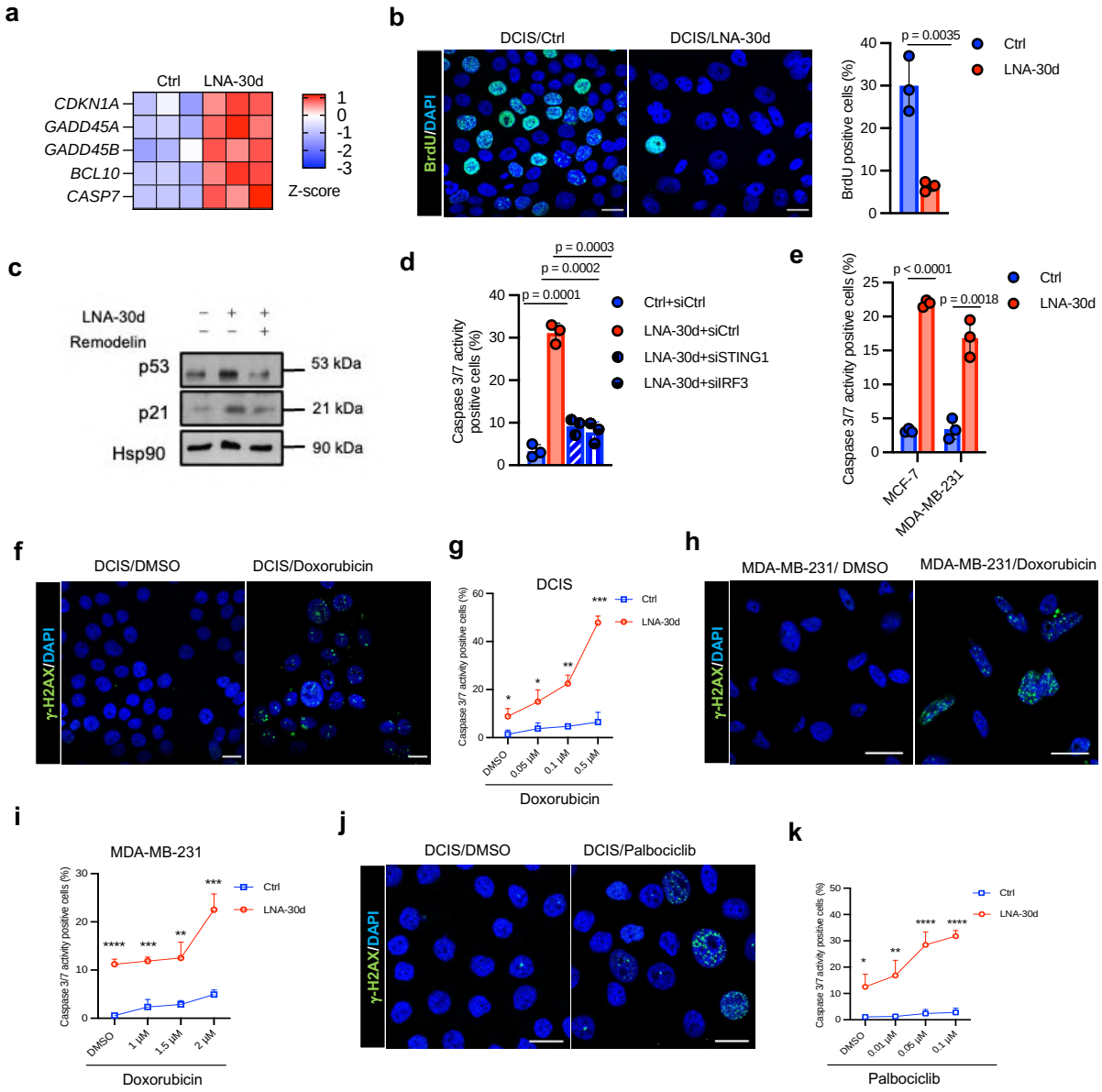

Figure 26. **Inhibition of miR-30d impairs viability of BC cells and synergizes with DNA-damaging agents.**

a. Heatmap of RNA-seq data (related to Fig. 7c) displaying the expression of genes related to DNA damage response in DCIS cells transfected with either LNA-30d or control LNA (Ctrl). Expression levels were normalized using Z-scores for gene-wise comparison, with high expression in red and low expression in blue. The three columns represent biological replicates for each condition. Displayed genes are significantly differentially expressed (DESeq2, two-tailed modified t-test with Benjamini-Hochberg correction). **b.** Representative images of BrdU incorporation assay by anti-BrdU IF (green) in DCIS cells transfected as in a, and relative quantification (right). Nuclei were counterstained with DAPI. Scale bar: 20 μm. **c.** WB analysis of indicated protein levels transfected as in Fig. 21a. Hsp90 was used as loading control. **d.** Apoptotic rate (percentage of cells with activated caspase 3/7) of DCIS cells transfected with control LNA (solid blue bar) or LNA-30d (red bar) and co-transfected with either STING or IRF3 siRNA (striped, blue bars). **e.** Apoptotic rate (% cells with activated caspase 3/7) of MCF-7 and MDA-MB-231 BC cells transfected with LNA-30d (red bars) or with control LNA (Ctrl, blue bars). **f.** Representative IF analysis of γ-H2AX DNA damage foci in DCIS cells treated with 0.05 μM doxorubicin for 48hr. Scale bar: 20 μm. **g.** Apoptotic rate of DCIS cells transfected with LNA-control (Ctrl, blue curve) or LNA-30d (red curve) and treated with increasing doses of doxorubicin (indicated on x-axis). p value:

p < 0.05 [*], p < 0.01 [**], p < 0.001 [***] by Two-tailed Student's t-test. **h.** Representative IF analysis of γ-H2AX DNA damage foci in MDA-MB-231 cells treated with 0.05 μM doxorubicin for 48hr. **i.** Apoptotic rate of MDA-MB-231 cells transfected with LNA-control (Ctrl, blue curve) or LNA-30d (red curve) and treated with increasing doses of doxorubicin (indicated on x-axis). p value: p < 0.05 [*], p < 0.01 [**], p < 0.001 [***] by Two-tailed Student's t-test. **j.** Representative IF analysis of γ-H2AX DNA damage foci in DCIS cells treated with 0.5 μM Palbociclib for 48hr. **k.** Apoptotic rate of DCIS cells transfected with LNA-control (Ctrl, blue curve) or LNA-30d (red curve) and treated with increasing doses of Palbociclib (indicated on x-axis). p value: p < 0.05 [*], p < 0.01 [**], p < 0.001 [***] by Two-tailed Student's t-test. **a-k.** Bar graphs represent the mean ± standard deviation (s.d.) from n ≥ 3 independent experiments. Statistical significance was determined using a Two-tailed unpaired Student's t-test.

Given the role of miR-30d in cancer cells, I sought to determine whether its inhibition would similarly impact normal breast epithelial cells. To this end, I assessed the effects of miR-30d inhibition on cell proliferation and apoptosis in MCF10A cells using BrdU incorporation and Caspase 3/7 activity assays. The result highlighted that miR-30d inhibition attained by LNA-30d treatment did not affect the proliferation and viability of these normal cells (Fig. 27a,b). This lack of effect is consistent with the intrinsically low expression of miR-30d in MCF10A cells and the absence of functional STING/TBK1/IFN-I pathway activation upon miR-30d inhibition (Fig. 17), further supporting the notion that miR-30d plays a limited role in maintaining homeostasis in normal cells. Also, upon miR-30d inhibition NE architecture remained intact in MCF10A cells, as evidenced by the absence of morphological abnormalities/circularity and preserved nuclear localization of EGFP-NLS signal (Fig. 27c,d). Consistently, IF analysis confirmed that there was no detectable accumulation of cytosolic dsDNA, nor cGAS activation (Fig. 27e) or DNA damage observed upon LNA-30d treatment in MCF10A cells (not shown). These findings prove a cancer-specific dependency on miR-30d for preserving nuclear integrity and restraining innate immune signalling, showing that tumour cells depend on miR-30d to prevent aberrant DNA damage accumulation, suppress cytosolic DNA sensing and STING pathway activation, and thereby evade apoptotic programs and immune responses that would otherwise compromise their survival.

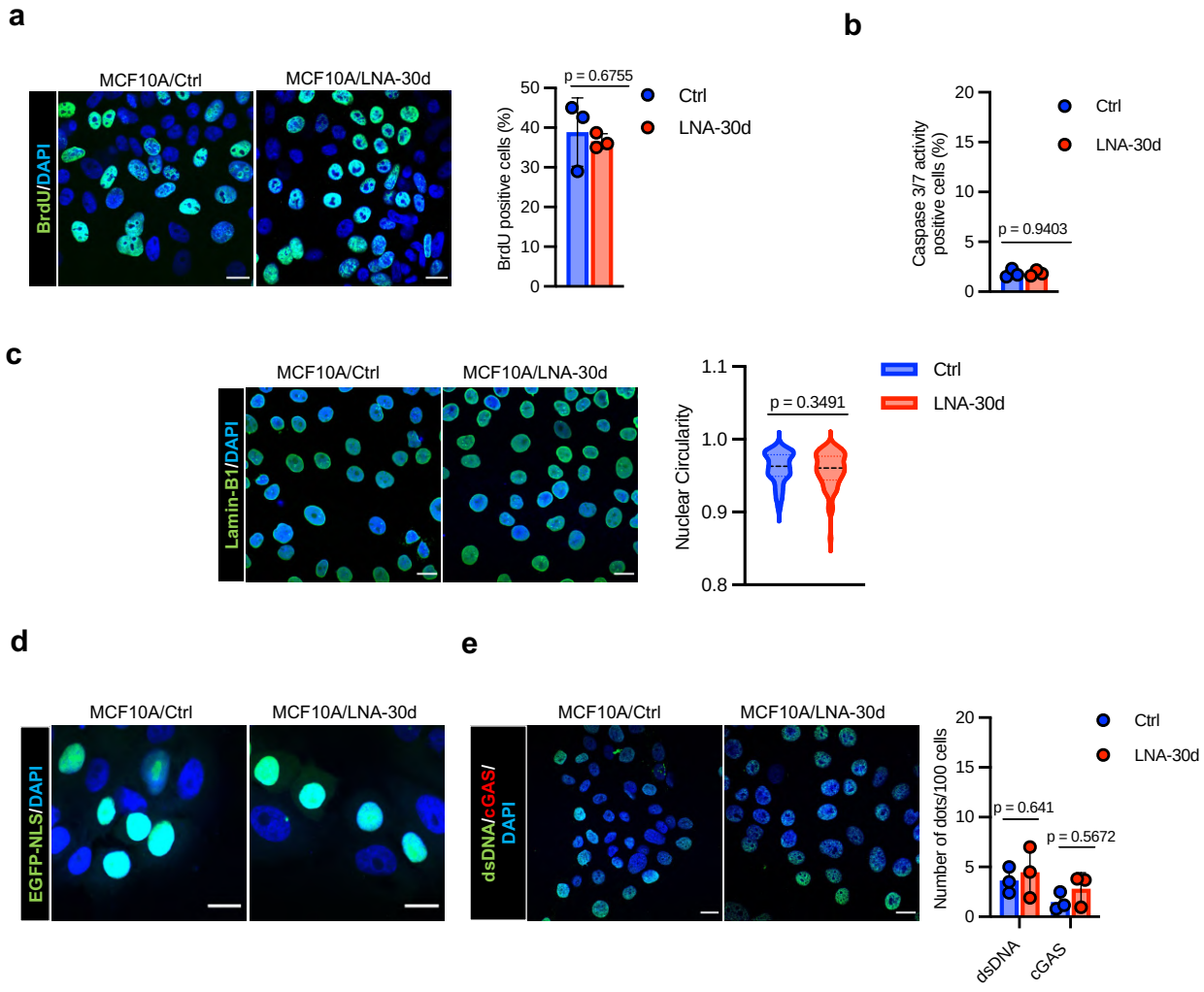

Figure 27. **Inhibition of miR-30d does not impair viability of non-transformed breast epithelial cells and fails to trigger cGAS activation.**

a-e Experiments performed in MCF10A cells transfected with either LNA-30d or control LNA (Ctrl). IF images have a: 20 μm scale bar. Bar graphs represent the mean ± standard deviation (s.d.) from n ≥ 3 independent experiments. Statistical significance was determined using a Two-tailed unpaired Student's t-test. **a** Representative images and quantification of BrdU incorporation assays in MCF10A cells transfected with either LNA-30d or control LNA (Ctrl). **b** apoptotic rate analysis in MCF10A cells, transfected as in a and performed as in 26d. **c** Left panel: representative images of nuclear lamina IF analysis with anti-Lamin-B1 antibody. Right panel: Violin plot showing the calculation of nuclear circularity based on DAPI staining. **d** Representative images showing EGFP-NLS subcellular localization transfected as in a. **e** Representative images and quantification of dsDNA and cGAS IF transfected as in a.

Next, to evaluate the therapeutic potential of miR-30d inhibition in stimulating IFN-I responses within tumours, I conducted experiments using patient-derived breast cancer organoids (PDOs). PDOs serve as robust and physiologically relevant preclinical models, recapitulating the genetic, phenotypic, and morphological characteristics of the original tumour tissues. PDOs can be grown in 3D matrices,

where both the chemical and physical stiffness of the environment can closely mimic the native TME (Qu et al., 2024). In this study, BC-PDOs were cultured and once they reached the desired confluency, they were transiently transfected for 48 hrs with a fluorescently labeled LNA-30d for better monitoring, or with control oligonucleotide. As represented in Fig. 28a,b,c, imaging with digital inverted fluorescence microscope highlighted that transfection of one BC-PDO with LNA-30d-FAM led to a marked reduction in both the number and size of organoids as compared to control. Following the expression levels of IFN-I response genes were quantified via qRT-PCR, which showed a robust induction of these genes upon miR-30d inhibition (Fig. 28d).

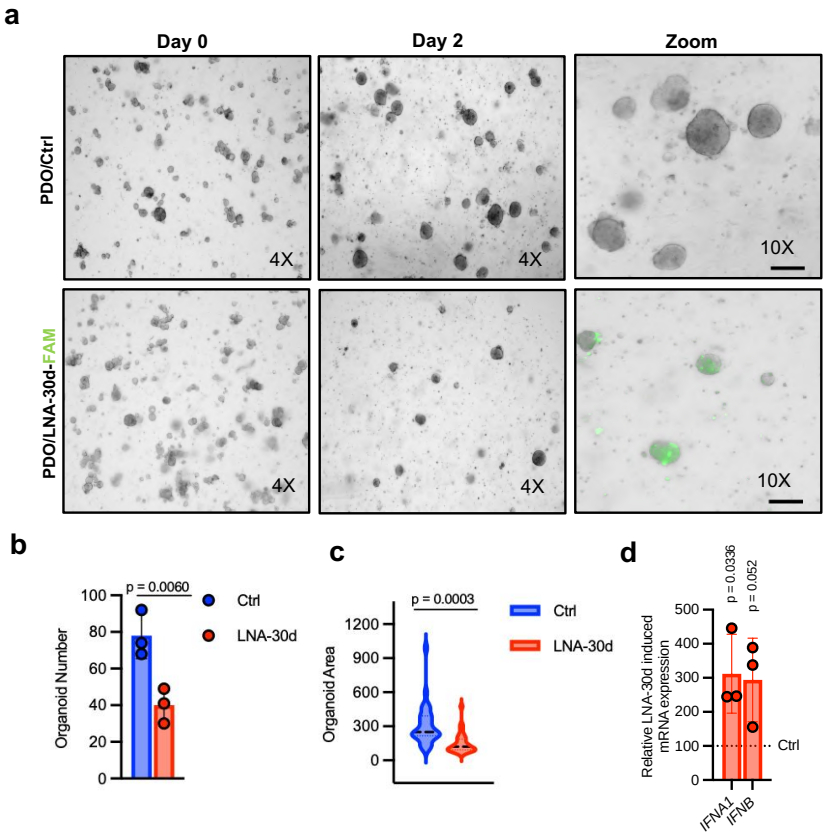

Figure 28. **miR-30d activity suppresses IFN-I response in patient-derived breast cancer organoids.**

a. Representative brightfield images of a BC-PDO at 0 and 48hpt with indicated LNA reagents. Scale bar: 100 μm. **b.** Quantification of organoid number from three independent biological replicates derived from a single BC-PDO transfected as shown in panel a. **c.** Violin plots illustrating the distribution of organoid area measurement, calculated based on individual organoid sizes from the same transfection condition as a. Quantification includes 100 cells per sample from n=3 independent experiments. **d.** qRT-PCR analysis of indicated genes in three different BC-PDOs transfected with either LNA-30d-FAM or control LNA (Ctrl) for 48hr. Bar graphs represent the mean ± standard deviation (s.d.) from n ≥ 3 independent experiments. Statistical significance was determined using Two-tailed unpaired Student's t-test.

The effects on IFN response were consistently observed across three independent PDO lines derived from breast carcinomas, suggesting activation of the cGAS/STING/IFN-I pathway not only in 2D cell cultures but also in tumour tissues embedded in a solid ECM (Fig. 28d).

4.8 miR-30d inhibition enhances IFN-I signalling and immune infiltration and sensitizes tumours to anti-PD-1 checkpoint inhibition

Previous research demonstrated that activation of the cGAS/STING/IFN-I cascade within cancer cells can favor antitumour immunity (J. Hu et al., 2023; Samson & Ablasser, 2022). Based on this evidence, I sought to investigate the effect of miR-30d in modulating this pathway using an immunocompetent murine BC model. To this aim, I first generated a 4T1 mouse metastatic BC cell line in which miR-30d expression was stably inhibited. This was achieved by transducing 4T1 cells with the TWEEN-EGFP-Decoy-miR-30d construct. As a control, 4T1 cells were transduced with the TWEEN-3'UTR-EGFP construct, which lacks the miR-30d Decoy sequence (Fig. 29a). I asked whether stable inhibition of miR-30d in these cells effectively activates the cGAS/STING/IFN-I pathway to a similar extent observed in human BC cells. As shown in Fig. 29a–f, miR-30d inhibition indeed led to increased NE fragility, evidenced by cytoplasmic leakage of the EGFP-NLS reporter, and accumulation of cytoplasmic cGAS foci. These upstream nuclear alterations were accompanied by downstream signalling events, including Golgi compaction, enhanced phosphorylation of TBK1, and robust induction of IFN-I and ISGs in 4T1/Decoy-30d cells.

To assess the relevance of these findings *in vivo*, the engineered 4T1 cell lines were orthotopically injected into the mammary fat pad of immunocompetent syngeneic Balb/c mice by Dr. F. Di Camillo and Dr. A. Rustighi. Tumour volume was evaluated at a regular interval in a physiologically intact host. After 25 days post-injection, primary tumours were harvested and analyzed. Remarkably, immunohistochemical (IHC) analysis of primary BC tissues highlighted a significant increase in perinuclear cGAS signal and elevated *Ifnb* expression in tumours derived from 4T1-Decoy-30d cells, as confirmed by qRT-PCR (Fig. 29g). These results indicate that miR-30d inhibition has the potential to activate the cGAS/STING/IFN-I pathway not only in cellular 2D models but also within breast tumours *in vivo*. Given the immunostimulatory potential of this

pathway (Shen et al., 2025) we asked whether its activation in tumour cells could influence the recruitment of immune cells within the TME. To test this, IHC analysis was performed by Dr. V. Cancila (Univ Palermo, Italy) on primary tumours from the same experiment as before to assess immune cell infiltration. Notably, tumours derived from 4T1-Decoy-30d cells exhibited increased infiltration of cytotoxic $CD8^+$ T cells and NK cells, suggesting effective recruitment of effector immune components (Fig. 29h). Notably, this enhanced immune infiltration was associated with reduced primary tumour growth (Fig. 29i), suggesting that the recruited immune cells may contribute to the suppression of BC progression. Collectively, these findings demonstrate that miR-30d inhibition reprograms the TME toward an immune active state, thereby restricting tumour growth.

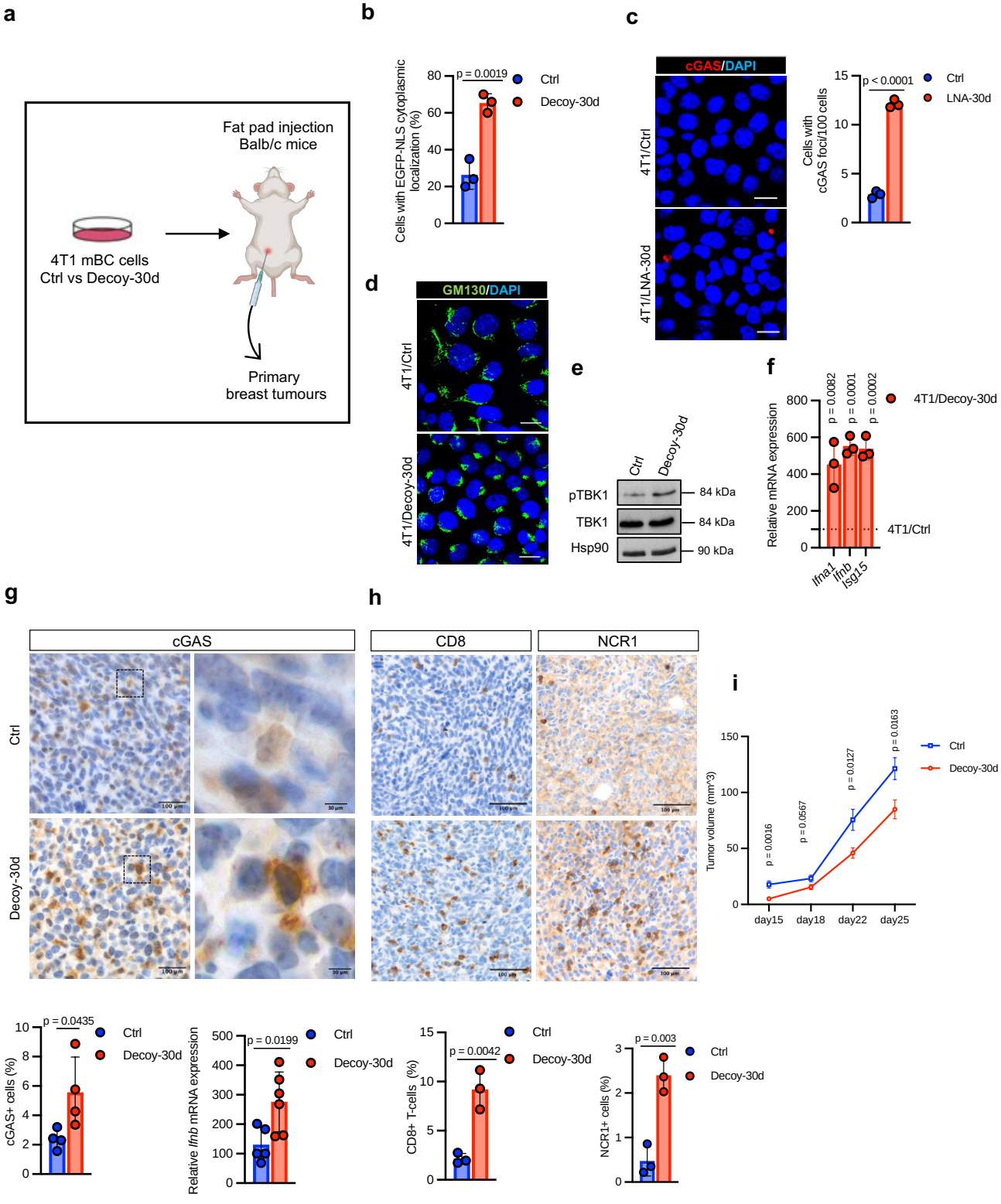

Figure 29. **Inhibition of miR-30d enhances IFN-I signalling and immune infiltration of primary BC *in vivo*.**

a. Schematic representation of immunocompetent *in vivo* experiment, where 4T1/Ctrl and 4T1/Decoy-30d cells were orthotopically transplanted in Balb/C mice (4T1/Ctrl group: n=6, 4T1/Decoy-30d group n=7), and primary BC tumours analyzed after 25 days. **b-f.** Bar graphs represent the mean ± standard deviation (s.d.) from n ≥ 3 independent experiments. Statistical significance was determined using a Two-tailed unpaired Student's t-test. **b.** Quantification of cytoplasmic localization of ectopically

expressed EGFP-NLS reporter per 100 cells in the indicated conditions. **c.** Representative images showing IF analysis of cGAS cytoplasmic foci, and relative quantification (right). Scale bar: 20 μm. **d.** Representative image of GA IF analysis performed with anti-GM130 antibody. Scale bar: 20 μm. **e.** WB analysis of TBK1 phosphorylation, using Hsp90 as loading control. **f.** qRT-PCR analysis of indicated genes in mouse 4T1 cells stably expressing miR-30d Decoy (Decoy-30d, red bars) as compared to 4T1 cells expressing control construct (4T1/Ctrl, dotted line), at the time of orthotopic transplantation (Fig. 28a). **g.** Representative images of immunohistochemical (IHC) analyses of cGAS in primary BC tumours from a; dashed boxes indicate regions magnified in the right panels. The bar plots below show the quantification of cells with perinuclear cGAS staining (left, n ≥ 3 samples per group), and qRT-PCR analysis of *Ifnb* mRNA expression in tumour tissues (n≥5 samples per group). **h.** Representative images of IHC analyses of $CD8^+$ T and NCR1 cells in primary BC tumours from a and relative quantification below, as in g. **i.** Measurement of primary tumour volume (mm^3) from a at indicated time points following orthotopic transplant.

An immune cold TME, characterized by the absence of infiltrating T cells and a lack of inflammatory signalling, is widely recognized as a major barrier to the efficacy of immune checkpoint blockade (ICB) therapies (Bagaev et al., 2021; Khosravi et al., 2024; Samson & Ablasser, 2022). Our experiments demonstrated that pharmacological inhibition of miR-30d in tumour cells activates the cGAS/STING pathway, leading to the recruitment of immune effector cell populations and a shift towards a more immunogenic TME. These observations prompted us to investigate whether miR-30d inhibition could sensitize tumours to ICB therapy. Notably, miR-30d inhibition resulted in a significant upregulation of *Pd-l1* expression, as measured by both flow cytometry (not shown) and qRT-PCR in 4T1-Decoy-30d cells and in corresponding tumour tissues (Fig. 30a), giving a hint of potential synergy of miR-30d inhibition with PD-1-targeting therapy (Harris et al., 2024). To evaluate this hypothesis, I employed the 4T1 murine BC model, widely recognized for its aggressive nature. The 4T1 cell line, derived from a spontaneous mammary tumour in BALB/c mice, closely mimics human triple-negative breast cancer (TNBC) and is characterized by poor immunogenicity, low T-cell infiltration, and a highly immunosuppressive TME (Katuwal et al., 2023; Kau et al., 2012; Park et al., 2025). These features make 4T1 tumours largely unresponsive to ICB such as anti-PD-1 or anti-PD-L1 antibodies. To test the impact of miR-30d inhibition on ICB responsiveness, 4T1 cells stably expressing miR-30d decoy construct (4T1/Decoy-30d) or control cells (4T1/Ctrl) were orthotopically transplanted into the mammary fat pad of syngeneic BALB/c mice as before. Once tumours reached a volume of approximately 25 mm^3, mice were treated with five intraperitoneal (IP) injections of anti-PD-1 antibody or IgG control, administered every two days. Tumour volume was monitored using the formula (d × d × D)/2, where "d" represents the smaller diameter and "D" the larger diameter. Consistent with the

known resistance of the 4T1 model, anti-PD-1 therapy alone had minimal impact on tumour growth in mice bearing 4T1/Ctrl tumours. In contrast, mice injected with 4T1/Decoy-30d cells exhibited a marked reduction in tumour growth following anti-PD-1 treatment (Fig. 30b,c), confirming that miR-30d inhibition effectively enhances ICB responsiveness.

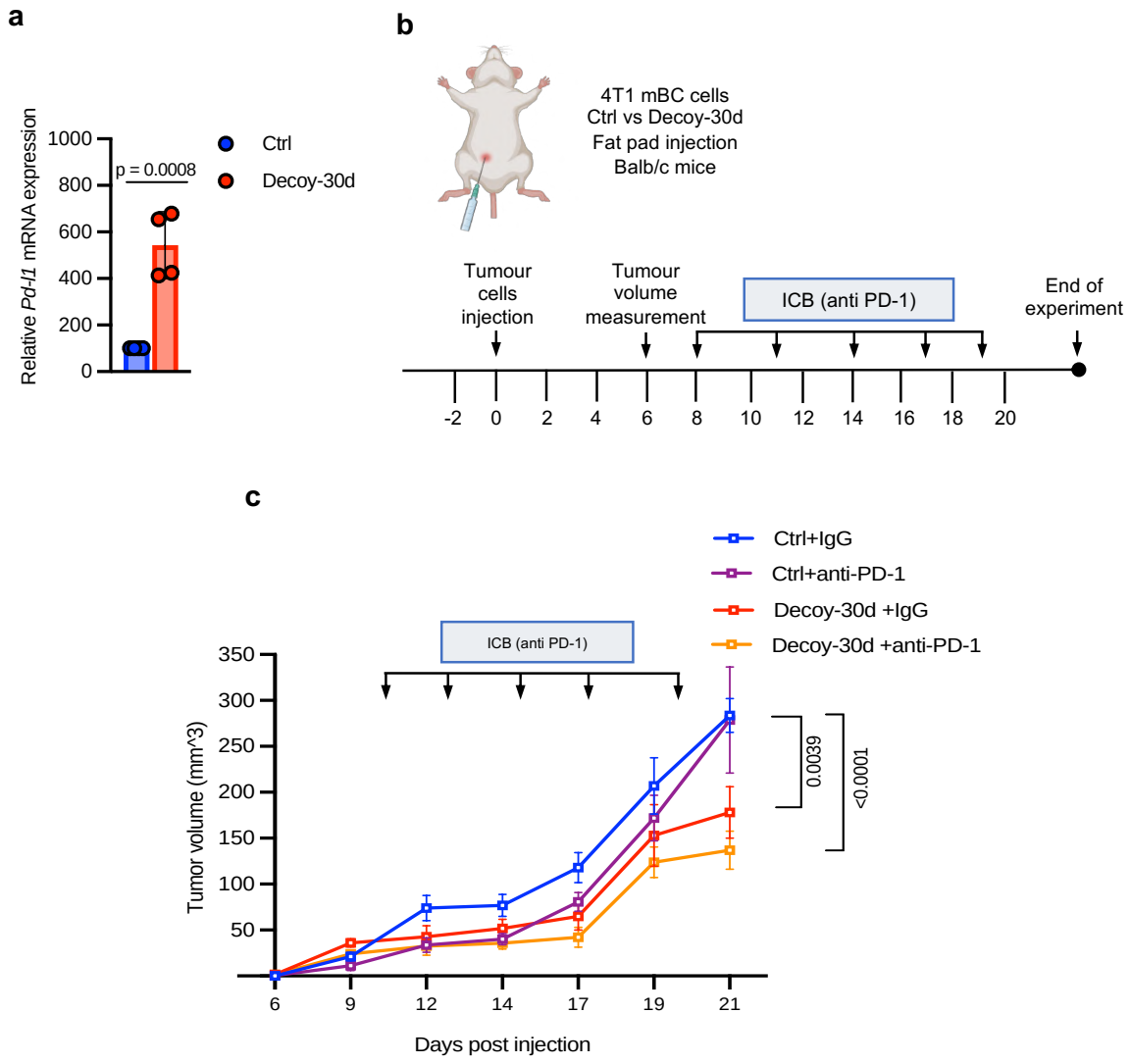

Figure 30. **Inhibition of miR-30d enhances *Pd-l1* expression and sensitizes BC tumours to anti-PD-1 checkpoint inhibition.**

a. qRT-PCR analysis of *Pd-l1* mRNA expression in 4T1 cells stably expressing miR-30d Decoy (Decoy-30d, red bars) as compared to 4T1 cells expressing control construct (Ctrl, blue bars). **b.** Schematic representation of ICB experiment. Balb/c mice were orthotopically transplanted as in 28a and, as the tumour reached 25 mm^3, were injected i.p. with 5 doses (2 days interval) of anti-PD-1 Ab or IgG as control, and tumour growth was monitored as indicated. **c.** Growth curves of primary tumour volume (mm^3) of mice with 4T1/Ctrl IgG group (n=3), 4T1/Ctrl anti-PD-1 group (n=5), 4T1/Decoy-30d IgG group (n=5) and 4T1/Decoy-30d anti-PD-1 group (n=4). Statistics by Two-way ANOVA, data are presented as means ± SEMs.

These findings support the concept that miR-30d functions as a negative regulator of innate immune activation in BC and that its inhibition can reprogram the TME to favor antitumour immunity. Furthermore, the data suggest that combining miR-30d inhibitors with anti-PD-1 treatment may represent a promising therapeutic strategy to overcome resistance in poorly immunogenic tumours and might effectively sensitize resistant tumours to ICB.

To evaluate the clinical relevance of these findings, we analyzed transcriptomic data from the TCGA BC cohort. As shown in Fig. 31a, high miR-30d activity signature inversely correlated with multiple immune activation signatures (including IFN-γ response, tumour-infiltrating lymphocytes TILs, activated $CD8^+$ T cells, and MHC class II expression), all of which positively correlated with Cyto-DR signature. Similar associations were observed in the METABRIC BC dataset (Fig. 31b), reinforcing the link between elevated miR-30d activity and suppression of cGAS/STING-mediated immune signalling in human BC. To further test whether miR-30d activity predicts response to ICB, we examined transcriptomic data from the I-SPY2 clinical trial (n=71), in which TN and ER^+ BC patients were treated with standard neoadjuvant chemotherapy (paclitaxel) in combination with the PARP inhibitor Olaparib and the anti–PD-L1 antibody Durvalumab (Pusztai et al., 2021). Patients who achieved a pathological complete response (pCR) showed significantly lower miR-30d activity signature (Fig. 31c), along with higher expression of TILs, $CD8^+$ cytotoxic T lymphocytes, and cytosolic DNA sensing pathway signatures (Fig. 31d). In contrast, non-responders (RD, residual disease) displayed higher miR-30d activity signature and reduced expression of immune activation markers.

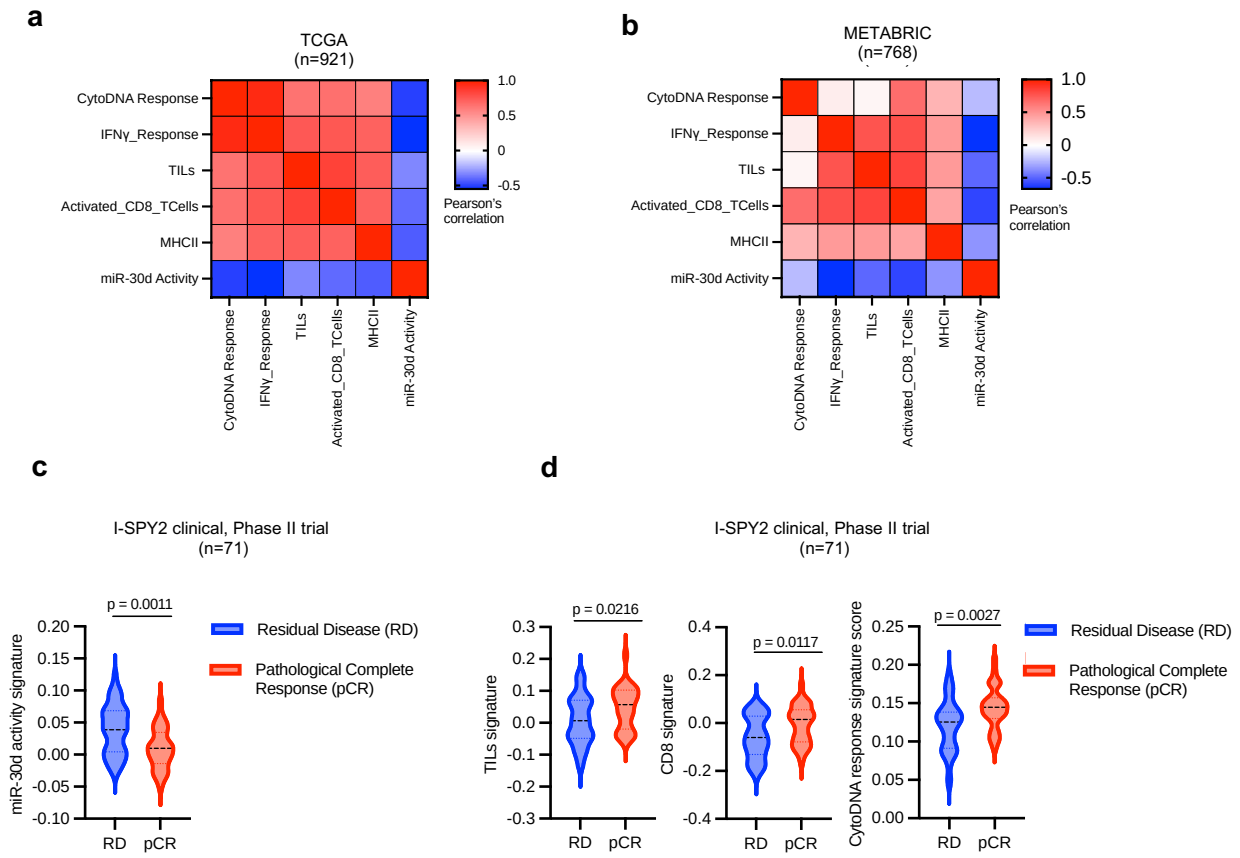

Figure 31. **High miR-30d activity correlates with attenuated immune response and reduced response to IC therapy in human breast tumours.**

a,b. Correlation heatmap of miR-30d activity signature with indicated immune-related signatures in RNA-seq data from TCGA-BRCA dataset (n=921) and METABRIC BC dataset. Each square represents the Pearson correlation between the respective row and column signatures, calculated using the rcorr function in R. The color scale indicates correlation strength, and all displayed correlations are statistically significant (p-value calculated using an approximation to the true distribution). **c.** Violin plot illustrating miR-30d activity signature score across human BC samples from the I-SPY2 study (n = 71; GSE173839), classified by response to IC therapy (pCR= pathological complete response; RD= residual disease). Difference between groups is statistically significant (Two-tailed Student's t-test). **d.** Average expression levels of TILs signature, CD8 signature and Cytosolic DNA sensing pathway in human BC samples of the I-SPY2 study (n = 71; GSE173839) classified according to response to IC therapy. Statistical significance was determined using a Two-tailed unpaired Student's t-test.

5 Discussion

Tumour progression is not driven solely by mutations within cancer cells, but it also depends on the constant bidirectional interactions between cancer cells and the surrounding TME, which can either fuel or restrain tumour growth. During tumour evolution, oncogenic drivers such as mutp53, HIF1α, and YAP/TAZ respond to external stimuli such as hypoxia, nutrient limitation, and ECM stiffening, and further orchestrate TME remodeling to favour tumour progression, immune exclusion and suppression. This contributes to the emergence of poorly infiltrated TME, associated with limited response to ICB (Bagaev et al., 2021). Research aimed at uncovering mechanisms that promote this immunosuppressive transition is crucial for designing efficient anticancer immune therapies. In this context, one promising strategy is the activation of the cGAS-STING pathway to reprogram tumour-immune interactions and initiate both innate and adaptive antitumour immunity (Samson & Ablasser, 2022). Yet, in many solid tumours this pathway is frequently attenuated by multifaceted mechanisms, enabling immune evasion.

The data presented in this thesis, together with prior research, have identified the onco-miRNA miR-30d, broadly upregulated across multiple cancer types, as a mechanistic driver of immune evasion, while also serving as a putative prognostic and predictive biomarker whose high expression correlates with decreased survival risk and poor immunotherapy outcomes.

Work from our laboratory and others has shown that in invasive BC, miR-30d acts downstream of oncogenic pathways to facilitate the remodeling of the TME, thus driving metastatic progression (Capaci et al., 2020; Gaziel-Sovran et al., 2011; Han et al., 2020; Jacob et al., 2017; Li et al., 2012; Lin et al., 2017; Yao et al., 2010). I found that miR-30d expression is higher in a cellular model of breast ductal carcinoma in situ (DCIS) cells compared to non-transformed breast epithelial cells. These findings suggest that miR-30d activation is initiated already at pre-invasive tumour stages, which still retain partial immune surveillance, unlike the immunosuppressive environment of the invasive state. Therefore, I focused on identifying the molecular mechanisms regulated by miR-30d during the early stages of BC: results reveal a central role of miR-30d in dampening innate immunity by inhibiting the cGAS/STING/IFN-I pathway.

In contrast to other miRNAs that directly inhibit specific component of this pathway (Gareev et al., 2023; Knarr et al., 2020; Ren et al., 2022), this work suggests that miR-30d impairs immune signalling by coordinating a dual mechanism that disrupts both upstream and downstream components of the cGAS/STING/IFN-I pathway (Fig. 32). On one side, miR-30d preserves NE integrity by modulating the LATS2/YAP/Lamin-B1 axis, thereby limiting DNA leakage into the cytosol. On the other side, it alters STING trafficking at the Golgi, preventing TBK1 activation, a critical step for signal propagation (Samson & Ablasser, 2022).

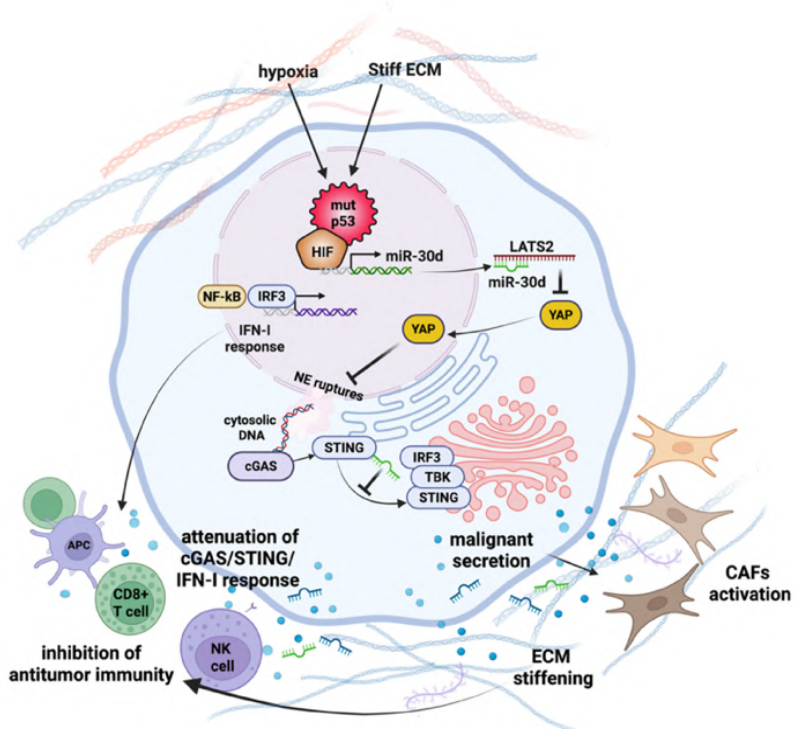

Figure 32. **Schematic model showing how miR-30d attenuates the cGAS/STING/IFN-I pathway through a dual mechanism.** miR-30d maintains NE integrity via the LATS2/YAP/Lamin-B1 axis to limit cytosolic DNA leakage, and blocks STING trafficking to prevent TBK1 activation in tumour cells. (Created with BioRender.com)

The findings from this thesis build on emerging evidence that organelle dynamics such as GA dispersal and NE integrity can serve as rheostat for cGAS-STING activity (Nader et al., 2021; Tao et al., 2020). The results demonstrate that miR-30d inhibition enhances the expression of immune-stimulating genes by activating the STING/IRF3/NF-κB cascade. This effect is dependent on miR-30d's ability to influence both Golgi and nuclear dynamics, offering a plausible mechanism by which a single

miRNA coordinates organelle states to fine-tune innate immunity in tumour cells (Nader et al., 2021; Tao et al., 2020).

Mechanistically, cGAMP binding facilitates STING translocation from the ER to the Golgi, where TBK1-mediated IRF3 phosphorylation occurs. Our previous work demonstrated that miR-30d overexpression induces structural and functional alterations of ER and Golgi compartments through direct downregulation of DGKZ kinase, a regulator of DAG metabolism (Capaci et al., 2020). This suggested us that high expression of miR-30d may disrupt the organelle architecture necessary for efficient cGAS-STING signalling (Samson & Ablasser, 2022). In fact, miR-30d inhibition both restored Golgi architecture in DCIS cells and promoted STING trafficking, thus enhancing IFN-I induction, while pharmacological disruption of Golgi integrity with GCA abolished these effects. Furthermore, silencing the miR-30d target DGKZ counteracted the immune activation induced by miR-30d inhibition, confirming its role in this pathway. Consistent with these findings, I observed that miR-30d depletion enhanced TBK1 phosphorylation at compact GA, driving IRF3 nuclear translocation and IFN-I gene expression, alongside NF-κB activation (Yum, 2021). These results align with studies showing that Golgi fragmentation impairs cGAS-STING signalling (Uhlorn et al., 2020).

Beyond STING regulation, Golgi organization may also influence immune responses by modulating the glycosylation patterns of ligands (Petrosyan et al., 2014; X. Ren et al., 2024) and the secretion of immunosuppressive factors (Gaziel-Sovran et al., 2011), which together impact immune recognition and signalling. Altered glycosylation can change how immune receptors recognize targets, shifting immune cells toward tolerance or suppression in the TME. This glycosylation-driven modulation creates a biochemical landscape that can hinder effective immune surveillance. Moreover, miR-30d secretion via EVs (Han et al., 2020; Vilella et al., 2015) suggests that its immunosuppressive effects might extend from tumour cells to stromal and immune cells in the TME. By transferring miR-30d to these neighbouring cells, the tumour could reshape their behavior, further enhancing immune evasion through suppression of antitumour immunity and remodeling of the local microenvironment. As a next step, it will be important to explore whether and how tumour-secreted miR-30d affects different stromal populations. For instance, whether it suppresses the cGAS-STING pathway in immune cells through paracrine transfer, using conditioned media, miRNA

mimics, or LNA inhibitors, as well as tumour-immune co-cultures. It would also be interesting to investigate its impact on fibroblasts, based on the evidence that miR-30d activates YAP/TAZ signalling and this may drive the transition of quiescent fibroblasts into CAFs. These future studies will help clarify how miR-30d shapes the tumour landscape.

Remarkably, missense mutp53 has been found to attenuate innate immunity by blunting STING-mediated IFN-I activation via directly interfering with TBK1 activation (Ghosh et al., 2021). Building on our prior observation that mutp53 transcriptionally induces miR-30d (Capaci et al., 2020), we found that mutp53 exerts its inhibitory effect on the pathway also indirectly, via induction of miR-30d. It would also be interesting to explore whether miR-30d, by altering Golgi architecture, enhances the ability of mutp53 to directly inhibit TBK. To address this, as a next step, I plan to use a proximity ligation assay to assess mutp53–TBK interactions and their subcellular localization in BC cells following miR-30d inhibition.

It is interesting to note that targeting miR-30d in mutp53-expressing DCIS cells not only rescued mutp53-induced suppression of IFN-I expression, but it further induced the pathway at a higher extent. In fact, Golgi compaction induced upon miR-30d inhibition would be insufficient per se to activate STING in the absence of upstream cGAS stimuli, i.e. cytosolic release of dsDNA. In cancer cells, exposure of self-DNA to the cytosol, which leads to cGAS engagement and triggering the IFN-I responses (Nader et al., 2021), may derive from multiple events. Most notably, mechanical perturbations or altered nuclear composition may cause NE rupture, thereby leading to leakage of genomic DNA into the cytosol. In this vein, an important novel finding of this thesis is the identification of miR-30d as a regulator of NE integrity. I demonstrated that by repressing the LATS2 kinase, miR-30d sustains YAP/TAZ activity and promotes Lamin-B expression, protecting against NE rupture and DNA leakage. While YAP's role in maintaining NE integrity has been described in fibroblasts (Sladitschek-Martens et al., 2022), this work extends this paradigm to epithelial cancer cells, positioning miR-30d as an upstream coordinator of NE integrity and immune evasion in tumourigenesis. The underlying regulatory network appears multifaceted, as the data in this thesis suggest that miR-30d may also target other YAP inhibitors such as AMOTL2, WWP1, and PTPN21 (Hwang et al., 2021; X. Li et al., 2016; Zhao et al., 2011), thereby reinforcing YAP activity. An important point that requires clarification is

the relevance of the miR-30d/LATS2/YAP axis in normal versus cancer cells. Results in this thesis suggest a cell-context-dependent effect. In normal epithelial cells, where miR-30d is expressed at lower levels, inhibition of miR-30d can increase *LATS2* mRNA and protein expression, however this fails to trigger the phenotypic consequences observed in cancer cells. This is likely because YAP/TAZ activity remains low in normal cells, and consequently increased LATS2 levels do not substantially alter YAP/TAZ signalling in these cells. In contrast, cancer cells suffer from persistent mechanical challenge impinging on NE integrity, and exhibit constitutively elevated YAP/TAZ activity, which is essential for their fitness, including proliferation and survival. In these cancer cells, miR-30d-mediated repression of LATS2 becomes critically important for sustaining YAP/TAZ-dependent oncogenic signalling and protecting NE integrity from rupture-induced immune activation. Therefore, upon miR-30d inhibition in cancer cells, the restoration of LATS2 activity unleashes a cascade of phenotypic changes like NE ruptures, cytosolic DNA leakage, cGAS activation, and IFN-I induction. This demonstrates that cancer cells are highly dependent on miR-30d-mediated adaptation of the LATS2/YAP axis for maintaining their fitness and allowing immune evasion. These observations favor the therapeutic window for targeting miR-30d in cancer cells. It is worth emphasizing however, that the severity of NE defects induced upon miR-30d inhibition exceeds the effect observed upon YAP or Lamin-B1 depletion alone, indicating that miR-30d may orchestrate multiple pathways critical for maintaining nuclear homeostasis. It is also conceivable that miR-30d contributes to NE repair through regulation of vesicular trafficking, a possibility that warrants further investigation.

Importantly, LATS2 itself has been shown to enhance cGAS-STING signalling through both YAP-dependent (Uppala et al., 2024) and independent routes (He et al., 2022), however it is often inactivated in aggressive tumours via copy number loss, methylation, or miRNA silencing (Y. Gao et al., 2017; N. Li et al., 2017). In addition, LATS2 stabilizes wtp53 (Aylon et al., 2006), suggesting that miR-30d mediated repression of both LATS2 and p53 (Kumar et al., 2011) may further weaken p53-dependent activation of the cGAS-STING pathway (Ghosh et al., 2023). In fact, our data clearly show that activation of the wt-p53/p21 axis and consequent induction of antiproliferative responses is a crucial event observed upon inhibition of miR-30d in DCIS cells. I observed that an important consequence of NE integrity loss upon

miR-30d depletion in BC cells is the accumulation of dsDNA breaks. This phenotype provides hint on a mechanistic link to TREX1 exonuclease, which is normally restricted to the cytosol, where it degrades aberrant DNA to prevent unwarranted cGAS activation. However, NE rupture may allow cytosolic TREX1 to enter the nucleus and cause genomic DNA damage (Nader et al., 2021). We indeed proved a role of TREX1 in the induction of DNA dsbreaks consequent to miR-30d inhibition. On one hand, this effect may be expected to increase the availability of fragmented or unchromatinized DNA for cytosolic cGAS activation. On the other hand, DNA damage represents an important trigger of p53 stabilization and activation. In fact, data revealed strong induction of p53, antiproliferative target genes and reduced cell proliferation in response to miR-30d inhibition, accompanied by induction of STING–IRF3 dependent apoptosis. Importantly, this apoptotic response synergized with genotoxic drugs and CDK4/6 inhibitors, suggesting that miR-30d inhibition can sensitize resistant tumours, including p53-mutant subtypes, to conventional therapies. Notably, these effects were observed only in tumour cells with no effect in normal cells, highlighting a favorable therapeutic target.

In this scenario, it still remains to be clarified what are the factors responsible for driving miR-30d induction at early tumour stages. Among those, hypoxia and HIF1α can transcriptionally induce miR-30d independently of mutp53 (Camps et al., 2014; Capaci et al., 2020), linking hypoxic signalling to suppression of innate immunity. Other HIF1α -responsive miRNAs, such as miR-25 and miR-93, have been shown to downregulate cGAS and impair STING activation (Wu et al., 2017), suggesting that HIF1α -driven miR-30d upregulation may represent a broader mechanism by which hypoxia attenuates IFN-I responses. As a further validation to these findings, I aim to prove that elevating miR-30d through hypoxic exposure may blunt cGAS-STING signalling and reduce IFN-I induction, highlighting a further connection of the hypoxic TME with impaired immune surveillance.

Our findings suggest that miR-30d might act as a mechanically modulated miRNA. Since it is induced by ECM stiffening (Capaci et al., 2020), it is crucial to investigate whether miR-30d levels continue to increase in proportion to rising rigidity, especially in late-stage tumours where matrix stiffening is significant. In fact, protection of NE integrity becomes increasingly critical as tumours progress, given that transient NE ruptures are more frequent during cancer cell migration and invasion (Kalukula et al.,

2022). Notably, increased ECM stiffness is a defining feature of immune-excluded tumours (Prakash & Shaked, 2024), underscoring the relevance of this mechanoprotective axis in late-stage disease. This opens up several questions for future research, e.g. to what extent do the protective effects on NE and cGAS activity rely on substrate stiffness, analyzing 3D cultures in matrices that mimic the biophysical properties of the mammary tumours. Addressing these questions is important to determine if the mutp53–miR-30d axis may represent a broader mechanoprotective program or one that depends on specific mechanical contexts.

In sum, the results identify miR-30d as a key regulator of cancer cell fitness and immune evasion, acting through both cell-intrinsic mechanisms and TME reprogramming. In immunocompetent murine models, stable inhibition of miR-30d in mouse metastatic BC cells triggered robust induction of IFN-I signalling, which translated into increased infiltration of cytotoxic $CD8^+$ T cells and NK cells and reduced tumour growth. Thus, miR-30d inhibition not only restores innate immune signalling within tumour cells but also promotes effective recruitment of immune effector populations. A particularly important finding in this work is that miR-30d inhibition also enhances responsiveness to ICB. Using the 4T1 murine model, which closely recapitulates the aggressive and treatment-refractory nature of human TNBC and is typically resistant to PD-1/PD-L1 blockade (Monjazeb et al., 2021), I observed marked tumour regression when miR-30d inhibition was combined with anti-PD-1 therapy, a strategy frequently employed also across other cancer types (E. H. Kim et al., 2022; Zabeti Touchaei & Vahidi, 2024). In fact, I observed upregulation of PD-L1 expression following miR-30d depletion, which may create a therapeutic vulnerability to PD-1 blockade. Together, these results suggest that miR-30d inhibition can convert poorly immune infiltrated tumours referred as “cold” into “hot” ones, thereby overcoming a major barrier to immunotherapy efficacy. While the current work demonstrates that miR-30d inhibition activates innate immune signalling and promotes $CD8^+$ T cell and NK cell infiltration, also leading to reduced tumour growth and enhanced ICB responsiveness, a more comprehensive mechanistic dissection of the immune contribution to tumour clearance is warranted. To establish whether the cGAS/STING pathway activation is causally required for the anti-tumour immune response, loss-of-function (LoF) experiments using STING knockout (STING KO) mice will be essential. Specifically, I plan to perform orthotopic transplant of 4T1/Decoy-30d cells into both

immunocompetent WT and STING-KO syngeneic BALB/c mice to directly assess whether STING ablation abrogates the tumour growth suppression and immune infiltration phenotypes observed upon miR-30d inhibition. Parallel experiments using immunocompromised mice such as NSG mice will determine whether the anti-tumour effects of miR-30d inhibition are exclusively immune-dependent, thereby distinguishing tumour-cell-intrinsic effects from immune-mediated tumour clearance. To comprehensively characterize the immune landscape reprogrammed by miR-30d inhibition, flow cytometry (FACS) analysis can be performed on tumour tissues, tumour-draining lymph nodes, and peripheral blood at multiple timepoints to quantify infiltration and activation status of $CD8^+$ T cells, NK cells, other lymphocyte subsets and intracellular IFNγ production, as well as PD-L1 expression on tumour cells and immune infiltrates before and after anti-PD-1 immunotherapy. These experiments will provide quantitative evidence of whether immune cell recruitment is sustained and whether cytotoxic effector function is enhanced. Additionally, IHC analysis of tumour tissues using multiplex staining approaches will spatially map the distribution of $CD8^+$ T cells, NK cells, and immune checkpoint molecules relative to tumour regions with high cGAS/STING activation, establishing whether immune infiltration is functionally linked to the STING pathway activation in miR-30d-inhibited tumours. These proposed experiments would establish the causal role of the cGAS/STING/IFN-I axis in orchestrating immune activation and would validate miR-30d as a therapeutic target by demonstrating that its inhibition converts immune-cold tumours to immune-hot ones through a mechanism fundamentally dependent on innate immune pathway activation. To further highlight the translational relevance of this study, we analyzed transcriptomic datasets from TCGA and METABRIC as well as clinical data from the I-SPY2 Phase II trial, in which TN and ER^+ BC patients received neoadjuvant paclitaxel combined with Olaparib and the PD-L1 inhibitor Durvalumab (Pusztai et al., 2021). This analysis revealed that tumours with high miR-30d activity show immune exclusion and resistance to ICB, while low miR-30d activity correlates with greater immune infiltration and improved therapeutic response. Taken together, miR-30d emerges as both a key regulator of innate immune suppression and a predictive biomarker for immunotherapy response. In perspective, measuring miR-30d levels in cancer patients could help guide treatment decisions, especially given that miR-30d is secreted into the bloodstream and can be readily detected through liquid biopsies as a non-invasive

diagnostic and prognostic biomarker. I plan to extend these analyses to BC patients by monitoring blood miR-30d levels and assessing their association with therapy response. In future work, I will also examine patient tumour samples using IHC and RNAscope to determine whether elevated miR-30d expression corresponds with poor immune infiltration.

In summary, the results of this thesis demonstrate miR-30d as a pivotal hub linking cellular architecture and transcriptional control to innate immune suppression. By uncovering its dual role in modulating the cGAS/STING/IFN-I axis, this work not only advances the mechanistic understanding of tumour-intrinsic immune evasion but also highlights miR-30d as a potent target for therapeutic intervention and potential biomarker.

6 Conclusion

The results shown in this thesis allow to conclude that elevated levels of oncogenic miR-30d in cancer cells play a critical role in dampening innate immune responses by suppressing the cGAS/STING/IFN-I signalling at multiple levels. Through the miR-30d/LATS2/YAP/Lamin-B axis, it maintains NE and genome integrity and prevents the activation of cytosolic DNA response, a key trigger of immune activation. Additionally, miR-30d alters architecture and function of the secretory pathway, impairing STING trafficking, which further attenuates IFN-I production and contributes to the development of an immune-suppressed TME. In contrast, inhibition of miR-30d leads to NE instability, DNA damage, and activation of cytosolic DNA response, resulting in antiproliferative effects and the release of IFN-I response and chemotactic signals that can altogether stimulate antitumour immunity. This further sensitizes cancer cells to DNA-damaging agents which are clinically accepted to treat BC patients and enhances their responsiveness to immune therapies. Moreover, circulating miR-30d might serve as a non-invasive biomarker for early detection and predicting patient response to immunotherapeutic interventions.

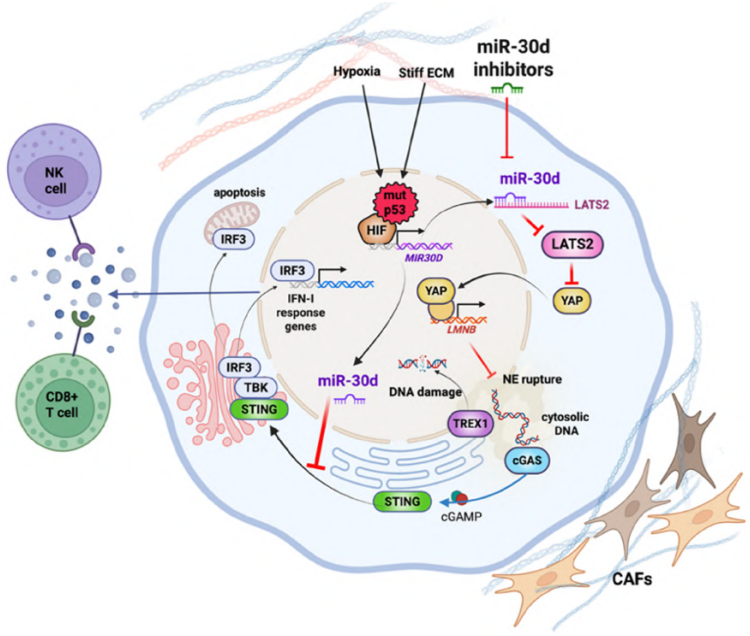

Figure 33. **Schematic Model.** miR-30d inhibits the cytosolic DNA-sensing cGAS/STING pathway. By repressing the LATS2/YAP/Lamin-B1 axis, miR-30d preserves NE integrity to prevent cytosolic DNA leakage and cGAS activation. Concurrently, it disrupts STING trafficking at the Golgi, blunting signal propagation. Use of miR-30d inhibitors like Decoy or LNA approach is capable to reactivate cGAS/STING/IFN-I signalling and enhancing immune infiltration. (Created with BioRender.com)

7 Materials and methods

7.1 Cell culture

MCF10A is an immortalized, normal human mammary epithelial cell line, MCF10.DCIS.com human cancer cell line derived from H-Ras mutated MCF10A cells expressing wtp53 and MCF10.DCIS-KI cell lines bearing mutp53^{R175H} were maintained in 1:1 DMEM/Ham's F12 (Euroclone), supplemented with insulin (10 μg/ml), epidermal growth factor (EGF, 20 μg/ml), hydrocortisone (0.5 μg/ml) and 5% Horse Serum. For generation of DCIS/ Rho0 (ρ^0) cells depleted for mitochondrial DNA, 2x10^5 cells were plated on 100 mm dish in their culture medium supplemented with 1mM Sodium Pyruvate (Gibco), 50 μg/ml uridine and 100 ng/ml EtBr. After four passages, depletion of mitochondrial DNA was tested by analyzing the expression of *ND5* mitochondrial gene by qRT-PCR, using ribosomal *18S* gene as reference. MDA-MB-231 (metastatic BC bearing mutant p53^{R280K}), SK-BR-3 (wtp53 metastatic BC) and HCT 116 (human colorectal carcinoma with wtp53 status) cells were cultured in DMEM supplemented with 10% Fetal Bovine Serum (FBS- Euroclone). MCF-7 (metastatic BC bearing wtp53), Mahlavu and Hep G2 (both liver cancer cell lines) were cultured in Minimum Essential Medium (MEM- Euroclone) supplemented with 10% FBS, 1% Minimum Essential Medium- Non-Essential Amino Acids (MEM- NEAA). WM-115 (melanoma cell line expressing wtp53), and SNU-245 (cholangiocarcinoma) cells were cultured in RPMI 1640 (Euroclone) supplemented with 10% FBS. PC-3 (p53-null metastatic prostate cancer cell line) were grown in 1:1 DMEM/Ham's F12, supplemented with 10% FBS, 1mM sodium pyruvate, 1% MEM- NEAA. HEK-293T (human embryonic kidney cell lines) cells were cultured in DMEM supplemented with 10% FBS (Euroclone). 4T1 is a p53-null mouse metastatic BC cells cultured in RPMI 1640 (Euroclone) supplemented with 10% FBS. Media were supplemented with 1% Penicillin-Streptomycin (P/S-Euroclone). All cell lines were maintained in a 37 °C, 5% CO_2 incubator, and regularly tested for mycoplasma contamination with negative results. They were received from American Type Culture Collection (ATCC) and collaborators of the project.

7.2 Chemical reagents for Cell treatments

The following compounds employed for cell treatments in this thesis: RU.521 (Invivogen, cat. #inh-ru521-2) was added at the working concentration of 10 μM. NU-7441 (Selleck Chemical cat. #S2638) and Nutlin-3 (Cayman Chemical, cat. #10004372) were used at the working concentration of 1 μM and 10 μM respectively. Golgicide A (GCA- Santa Cruz cat. #215103) was added at the working concentration of 1 μM. Remodelin (SIGMA, cat. #SML112) was added at the working concentration of 20 μM. Two chemo-drugs used in this study were Doxorubicin (Sigma-Aldrich-D1515) and Palbociclib (Selleck Chem, cat. #S1116). Doxorubicin was used at the working concentration 0.05-0.1-0.5 μM in DCIS cells and 1-1.5-2 μM in MDA-MB-231 cells. Palbociclib was used at the working concentration 0.01-0.05-0.1 μM in DCIS. DMSO was used as a negative control for all the above listed compounds, and cells were further processed after 48hr. Etoposide (Sigma-Aldrich cat. #E1383) treatment was used at the final concentration of 1 μM for 24hr.

7.3 Breast Cancer patient-derived organoids (BC-PDOs)

HCM-CSHL-0151-C50 and HCM-CSHL-0261-C50 BC-PDOs were obtained from ATCC. Both PDOs are derived from Infiltrating Ductal Carcinomas, were HCM-CSHL-0151-C50 resembles stage IA and HCM-CSHL-0261-C50 is stage IIA. BCRO-227 BC-PDO was obtained from B. Belletti and G. Baldassarre (CRO, Aviano). Once thawed, organoids were resuspended in 30 μL/well of growth factor (GF) reduced solubilized basement membrane (Matrigel®, Corning, cat. #CLS356231). The 24-well plate was inverted and placed in the 37 °C incubator with 5% CO_2 for 30 min, then placed upright and 500 μL growth media per well was added. The media used to maintain the above-mentioned BC-PDOs was Advanced DMEM:F12 (Gibco) supplemented with 1X Glutamax (ATCC, 30-2214), 10 mM Hepes (Thermo Fisher cat. #15630080), 50 ng/mL Primocin, 1X P/S, 5 mM Nicotinamide, 1.25 mM N-Acetylcystein, 1X B27 (Thermo Fisher cat. #17504-044) supplement, 250 ng/mL rhR-Spondin 3, 5 nM Heregulin b-1, 100 ng/mL Noggin, 20 ng/mL FGF-10, 5 ng/mL FGF-7, 5 ng/mL EGF, 500 nM A83-01, and 500 nM SB202190. 5 μM Y-27632 was added to culture media for the first three days of culture. Organoids were passaged at confluency, and medium was changed every 2-3 days. For organoids' passaging, Matrigel was displaced from the wells,

organoids collected and incubated for 1hr at 4°C with Cell Recovery solution (Corning; cat. #CLS354270). Organoids were then digested with TrypLE solution (Gibco; cat. #12-605-010) for 5 mins at 37°C. After enzyme neutralization and washing twice with 1XPBS, organoids were resuspended in Matrigel and reseeded as above in 24-well plate. BC-PDOs of size ≥ 25μm were considered for number and size quantification and images were acquired using EVOS M5000 (Invitrogen) at different magnification and processed with FiJi software.

7.4 DNA constructs

The following DNA constructs used in this thesis: The TWEEN 3' UTR EGFP-Decoy-30d lentiviral construct (Decoy-30d) was generated by Vector Builder (VB220727-1384vby) as previously described (Capaci et al., 2020). pTRIP-CMV-TagRFP-flag-hSTING1 was generated from pTRIP-CMV-TagRFP-flag-cGAS plasmid (Addgene #86676). pGL3-spacer-3'UTR-LATS2 vector was generated by cloning the LATS2 3′UTR into pGL3-spacer (Promega) downstream of firefly luciferase gene. The same plasmid was further engineered by mutagenizing miR-30d seed sequence GTTTACA to CCCCCCA through cross-over PCR. All oligonucleotides used for cloning are listed in Table 2. Other plasmids employed in this thesis were: Lentiviral vector encoding IRF3-GFP was kindly provided by A. Marcello, ICGEB Trieste collaborator. EGFP-3X-NLS (Addgene #58468), pcDNA3-p53^{R280K} (Walerych et al., 2016), GFP-TREX1 retroviral vector (Addgene #164245), and two virus packaging plasmids psPAX2 (Addgene #12260) and pMD2.G (Addgene #12259) were used in this study.

7.5 Cellular and Organoid Transfection

Cells were transfected at 70-80% confluence. For DNA transfections, LTX reagents (Thermo Fisher) or Lipofectamine 2000 were used following manufacturer's instructions. miR-30d Decoy and control vectors were transfected with Lipofectamine LTX Reagent and PLUS Reagent. For miR-30d overexpression, pre-miR hsa-miR30-d-5p (Ambion Life technologies Cat. AM17100) was used at the working concentration of 3 nM, exogenous dsDNA-EC (InvivoGen Cat. Tlrl-ecdna) was transfected at the final concentration of 1 μg/ml and salmon sperm dsDNA at 2.5 μg/ml for 24hr (Life technologies- 15632-011).

Locked Nucleic Acid (LNA) molecules, in detail miRNA Custom Power inhibitors (Qiagen Cat. 339146), which include the Negative Control A Custom miRC (YCI020254-DDA) and the mmu-miR-30d-5p Custom miRCURY (YCI0201748-DDA) were transfected with Lipofectamine RNAi-MAX (Thermo Fisher) at the final concentration of 50 nM.

For BC-PDO transfection, organoids were enzymatically dissociated into single cells with TrypLE solution and subsequently transfected in suspension for 6hr with 50nM LNA-miRNA inhibitor in the presence of Lipofectamine RNAiMax in antibiotic-free medium. Following transfection, cells were resuspended in 30 μL/well Matrigel and seeded into 24-well plates. After 30 min of incubation, 500 μL media was dispensed to each well.

7.6 Viral transduction

For lentiviral production, 293T packaging cells were transfected using 1 μg/μl PEI (Sigma-Aldrich) per μg DNA of the construct of interest in combination with packaging plasmids. 48hpt the viral supernatant was centrifuged 5 min at 500 rcf and filtered with 0.45 μM filter to remove cellular debris. Then, virus-containing media were added to recipient cells for 24-48hr. Infected cells were selected with puromycin.

DCIS cells expressing GFP-cGAS were obtained by transduction with lentiviral pTRIP-CMV-GFP-flag-cGAS vector. Lentiviral pTRIP-CMV-TagRFP-flag-hSTING1 and IRF3-GFP plasmid were transfected at 2 μg/ml for 24hr. Retroviral EGFP-3X-NLS and GFP-TREX1 plasmids were transfected at 2.5 μg/ml for 24hr.

$TP53^{R175H}$ mutation was introduced in MCF10.DCIS.com cells via electroporation: mix included RNPs (combining 120 pmol of recombinant Cas9 protein with 150 pmol of gRNA), 4 μM Alt-R Cas9 Electroporation Enhancer (IDT), and 4 μM single-stranded DNA donor templates (Ultramer DNA Oligonucleotide, IDT). Electroporated cells were treated with NU-7441 and enriched with Nutlin-3. Editing efficiency was assessed analyzing Sanger sequencing traces of PCR on genomic DNA using the ICE analysis tool (Synthego).

For *in vivo* experiments, mouse metastatic 4T1 BC cells were transduced with TWEEN-EGFP-Decoy-miR-30d or TWEEN-EGFP-3'UTR (control) lentiviral plasmids

and selected with puromycin (Sigma-Aldrich) with increasing concentration from 1.5 to 3 μg/ml for stable inhibition of miR-30d.

7.7 RNA Interference (RNAi)

For siRNA transfections, cells with 70% confluency were transfected with 40nM siRNA oligonucleotides using Lipofectamine RNAi-MAX. All siRNAs were purchased from Eurofins. As negative control, AllStars Negative Control (Qiagen Cat. #1027281) was used. Detailed list of siRNAs employed is in Table 1.

7.8 Enzyme-Linked Immunosorbent assay (ELISA)

In this study, a total of 1.5x10^5 DCIS cells were seeded in 6-well plates, and at 48hpt the cells were subjected to lysis, or alternatively, the culture medium was collected. The samples were then analyzed using Human Interferon Beta ELISA kit (Abcam cat. #278127) or 2'3'-cGAMP ELISA kit (Cayman Chemical cat. #501700) in accordance with the manufacturers' protocols and read with a spectrophotometer at wavelength 450 nm.

7.9 Luciferase assay

In this work, 1x10^5 DCIS cells were seeded in 12-well plates and transfected with mimic miR-30d at the final concentration of 3 nM or Ctrl. After 24hr cells were subsequently co-transfected with 1 μg of pGL3-spacer-*LATS2* 3'UTR reporter plasmid and 100 ng of pCMV-Renilla vector. For the titration experiment, mimic miR-30d was used at the final concentrations of 3 nM, 10 nM and 20 nM. At 48hpt, cells were lysed using 1X Passive Lysis Buffer (PLB) and treated according to the manufacturer's protocol (Dual-Luciferase® Reporter Assay System Promega cat. #E1910). Luciferase activity was measured using a luminometer and relative Luciferase Units (RLU) were calculated by normalizing the luciferase units measured for the firefly (*Photinus phyralis)* luciferase on the renilla (*Renilla reniformis)* luciferase units in each sample.

7.10 BrdU incorporation assay

For the BrdU incorporation assay, a total of 1.5x10^5 DCIS cells were seeded on coverslips in 6-well plates. Four hours prior to cell harvesting, the Cell proliferation Labelling Reagent, Bromodeoxyuridine BrdU (Amersham) was added to the culture media at a dilution of 1:1000 v/v. Following this incubation, the cells were blocked and IF staining was performed according to the protocol outlined below.

7.11 Apoptosis assay

For measuring apoptotic activity, 1.5x10^4 cells were seeded in 24-well plates. At 48hpt the cells were washed twice with 1XPBS and incubated for 1hr at 37°C and 5% CO_2 in culture medium containing the CellEvent Caspase 3/7 Detection Reagent (Thermo Fisher cat. #C10432). Following incubation, cells were examined using the EVOS M5000 fluorescence inverted microscope (Invitrogen).

7.12 Protein extraction and western blot (WB) analysis

Cell extracts were lysed with 1XRIPA buffer (50mM Tris-HCl pH 8, 150mM NaCl, 1% NP-40 10%, 1mM EDTA, supplemented with protease inhibitors: 10 μg/ml CLAP, 1 mM Na_3VO_4, 1 mM PMSF, 5mM NaF (all from Sigma-Aldrich) and sonicated. Protein concentration was measured with Bio-Rad Protein Assay Reagent (Bio-Rad cat. #500-0006) using Perkin Elmer EnSpire MultiMode Microplate Reader and lysates were denatured in Laemmli Sample Buffer 6X by heating for 5 min at 95 °C. Protein lysates were run through SDS/PAGE and transferred to nitrocellulose membranes (Cytiva). Blocking was performed in Blotto-tween (PBS, 0.2% Tween-20, not fat dry milk 5%) or with TBST (0.2% Tween-20, Tris/HCl 25 mM pH 7.5) plus 5% not fat dry milk or 5% BSA (PanReac Applichem) according to the antibody datasheet. Membranes were incubated with primary antibody diluted in blocking solution, whereas Hsp90 was used as a loading control. Anti-mouse and anti-rabbit HRP-conjugated (Sigma-Aldrich) were used as secondary antibodies in the same buffer. Membranes were analyzed by chemiluminescence using Pierce ECLTM or Pierce ECLTM Plus WB Substrate. Protein bands were quantified by densitometry of autoradiographic films using ImageJ software. Detailed list of antibodies employed is in Table 7.

7.13 Imaging and data analysis

7.13.1 Immunofluorescence staining (IF)

For IF analysis, cells on coverslips were washed in 1XPBS and fixed with 4% paraformaldehyde PFA (Sigma-Aldrich) for 20 min at room temperature (RT) and washed twice with 1XPBS. Cells were permeabilized with 0.1% Triton X-100 for 10 min and blocked in 3% FBS/PBS for 30 min. For BrdU incorporation, permeabilization was followed by 10 sec treatment with NaOH 50 mM and washed in 1XPBS. Cells were then incubated with primary antibodies, diluted in the same buffer at 37°C or at 4°C. The entire list of primary antibodies employed is provided in Table 7. After three washes with 1XPBS, coverslips were incubated with secondary antibody (goat anti-mouse, and donkey anti-rabbit Alexa Fluor 488, 568 Life Technologies) at 37°C for 45 min. Nuclei were counterstained with 1:1000 4′,6-diamidino-2-phenylindole (DAPI) (Sigma-Aldrich) for 10 min at RT. After two washes with 1XPBS, and one wash with ddH_2O, cells were mounted with ProLong Gold Antifade reagent (Molecular Probes, Eugene).

Images were acquired with confocal microscope ZEISS LSM 880 using 63x/oil-immersion objective. Confocal images were taken on several planes (range: 3.75mm, slice thickness 0.54mm) with Z-stack function at ZEISS LSM 880 using 63x/oil-immersion.

For NE alterations, all shape abnormalities were counted: herniations, blebs, micronuclei, invaginations, and indentations. The analysis of circularity from random fields in 2D cells was based on DAPI staining and performed using Fiji particle analysis tool and StarDist plugin on 1024x1024 resolution tiff images. The circularity value is between 0-1 and calculated with following formula: NCI=4π×NA/(NP)^2 where NA represents nuclear area and NP nuclear perimeter.

7.13.2 Immunohistochemical tissue staining (IHC)

IHC staining was carried out on FFPE mouse tissue sections from primary tumour of control (n=4) and treated Balb/C mice (n=4). Four-micrometer thick tissue sections were deparaffinized, rehydrated and unmasked using Novocastra Epitope Retrieval Solutions at pH 6 or pH 9 (Leica Biosystems) in a thermostatic bath at 98°C for 30 min. The sections were then brought to RT and washed in PBS. After neutralization of

the endogenous peroxidase with 3% H_2O_2 and Fc blocking with 0.4% casein in PBS (Leica Biosystems), the sections were incubated overnight at 4°C with the following primary antibodies: anti-cGAS, anti-NCR1 and anti-CD8 (The list of primary antibodies employed is provided in Table 7).

IHC staining were developed using the IgG (H&L)-specific secondary antibodies and DAB (3,3′-Diaminobenzidine, Leica Biosystems) as substrate chromogen. IHC-stained slides were analyzed and imaged under a Zeiss Axioscope-A1 equipped with Axiocam 503 Color camera (Zeiss). Quantitative analyses were performed by calculating the average percentage of positive cells in five non-overlapping tumour area at medium-power magnification (x200) using the HALO image analysis software (v3.2.1851.229, Indica Labs) and the output was expressed as the “percentage of positive cells".

These experiments were performed by postdoctoral researcher Dr. V Cancila from C. Tripodo's Lab at the Tumour Immunology Unit, University of Palermo, Italy.

7.14 Correlative light-electron microscopy (CLEM) and electron tomography

Correlative light-electron microscopy (CLEM), electron microscopic examination, and electron tomography were performed as previously described (Beznoussenko & Mironov, 2015).

Embedding- DCIS cells transfected with a construct expressing GFP-cGAS were grown on MatTek glass bottom dishes (MatTek Corporation), fixed with 2.5% PFA and 2.5% glutaraldehyde (EMS) mixture in 0.1 M sodium cacodylate pH 7.4 for 2hr at RT, followed by 6 washes in 0.2 sodium cacodylate pH 7.2 at RT. Then cells were incubated in 1:1 mixture of 2% osmium tetra oxide (OsO_4) and 3% potassium ferrocyanide for 1hr at RT followed by 6 times rinsing in cacodylate buffer pH 6.9. Then samples were sequentially treated with 0.3% thiocarbohydrazide in 0.2 M cacodylate buffer for 10 min and 1% OsO_4 in 0.2 M cacodylate buffer pH 6.9 for 30 min. Samples were rinsed with 0.1 M sodium cacodylate buffer pH 6.9 until all traces of the yellow osmium fixative have been removed, washed in de-ionized water, treated with 1% uranyl acetate in water for 1hr and washed in water again (Beznoussenko & Mironov, 2015). Samples were subsequently dehydrated in ethanol and embedded in Epoxy resin at RT and polymerized for at least 72 hr in a 60 °C oven.

Sectioning- The cell of interest was selected during the analysis of the MatTek, optical sectioning and Z-stacking was performed using confocal microscope. During Z-stacking the distance between the bottom and the nucleus of the cell was estimated. Embedded samples were then sectioned with diamond knife (Diatome) using Leica EM UC7 ultra microtome (Leica Microsystems) and then cut the series of 200 nm and 70 nm sections. Sections were analyzed with a Tecnai20 High Voltage EM (FEI, now Thermo Fisher Scientific) operating at 200 kV.

Electron tomography- An ultramicrotome (Leica EM UC7; Leica Microsystems) was used to cut 200 nm serial semi-thick sections. Sections were collected on 1 % formvar films adhered to slot grids. Both sides of the grids were labelled with fiduciary 10 nm gold (PAG10, CMC, Utrecht). Tilt-series were collected from the samples from ±65° with 1° increments at 200 kV in Tecnai20 electron microscopes (FEI, now Thermo Fisher Scientific). Tilt series were acquired at a magnification of 7,800x, 9,600x, 11,500x, 14,500x, or 19,000x software supplied with the instrument. The nominal resolution in tomograms was 3 nm, based upon section thickness, the number of tilts, tilt increments, and tilt angle range. The IMOD package and its newest viewer, 3DMOD 4.0.11, were used to construct individual tomograms and for the assignment of the outer leaflet of organelle membrane contours, CLEM was performed as described (Beznoussenko et al., 2014).

These experiments were carried out by Dr. G. Beznoussenko at the IFOM Advanced Light Microscopy Core Facility and Electron Microscopy Cells & Tissues Core Facility.

7.15 RNA extraction and qRT-PCR

Total RNA was extracted from cells with TriFast II (EUROGOLD) following manufacturer's instructions. Complementary DNA (cDNA) was obtained with iScript™ Advanced cDNA Synthesis Kit (Biorad, cat. #172-5038). Quantitative real time PCR (qRT-PCR) was performed using iTaq Universal SYBR® Green Supermix (Biorad cat. #1725124) on a CFX96™ Real-Time PCR System (Biorad). Histone *H3* was used as reference gene in human cell lines while *Gapdh* was used for mouse cell lines. *18s* gene was used as a reference to validate the depletion of mitochondrial DNA in DCIS cells. For miRNA analysis, total RNA was extracted and retrotranscribed and amplified with miRCURY™ RT Kit (Qiagen cat. #339340) and miRCURY LNA™ SYBR Green PCR Kit (Qiagen cat. # 339346) respectively, following manufacturer's instructions and

data were analyzed on Biorad CFX96™ RT-PCR Software. *RNU5G* gene was used as a reference. For all experiments, n ≥ 3 independent experiments were performed, with at least two replicates each. Quantification was performed based on 2−ΔΔCt method using the above-mentioned housekeeping gene levels as normalizers. Oligonucleotides used for PCR are listed in Table 3.

7.16 In vivo Balb/C mice experiments

For the *in vivo* study, 6- to 8-week-old female syngeneic Balb/C immunocompetent mice were orthotopically injected into the mammary fat pad with 2.5x10^4 4T1 cells stably expressing miR-30d Decoy construct or control vector in PBS. Injections were performed under general anesthesia with 1-3% isoflurane (Merial Italia S.p.A, Italy). Tumour growth was monitored every 2 or 3 days by caliper measurements and the tumour volume was calculated using the formula: Tumour volume (mm^3) = $Dxd^2/2$ where “D” and “d” are the longest and the shortest diameter, respectively. At 25 days post injection mice were euthanized, primary tumours were extracted, and half was directly frozen in liquid nitrogen for molecular analysis, while the other half were washed in PBS, collected for fixation in 10% neutral buffered formalin for 24hr, then washed with water, processed and embedded in paraffin.

To evaluate immune checkpoint inhibition, mice were treated with five intraperitoneal (IP) injections of 200 μg anti-mouse PD-1 (Clone: 29F.1A12TM, BioXCell cat. # BE0273;) or isotype control (Clone: polyclonal Syrian hamster IgG, BioXCell cat. #BE0087) administered at two days interval starting on day 8, after tumour reached a volume of 25 mm^3. Treatment continued until the end of the experiment.

All mice were housed in ventilated cages, food and water were provided ad libitum throughout the study and weight measured at least twice per week. They were handled according to institutional guidelines, and experimental procedures approved by the Ethical Committee of International Center for Genetic Engineering and Biotechnology (ICGEB) review board, with full conformity with national (D. L. 26/2014 and subsequent implementing circulars) and international (EU Directive 2010/63/EU for animal experiments) laws and policies, and the experimental protocol (Authorization n. 347/2022-PR) was approved by the Italian Ministry of Health.

7.17 Omics data analyses and statistics

7.17.1 RNA-sequencing and data analysis

RNA-seq was performed on three biological replicates. MCF10.DCIS.com were transfected for 48hr with LNA-30d or non-targeting control LNA, and total RNA was extracted as described above (see section 7.15). Sample quality was checked using the Tape Station (Agilent RNA Screen Tape System), and expression of miR-30d target genes *KLHL20* and *SNX16*, and of *IFNA1*, *IFNB* and ISGs mRNAs was analyzed by qRT-PCR prior to sequencing. mRNA libraries were obtained by the Illumina TruSeq stranded total RNA and were sequenced using Illumina NovaSeq 6000 for 100 bp paired-end sequencing (average 56 M reads/sample) by Macrogen Europe sequencing service.

Read quality was verified using fast QC (version 0.11.9; http://www.bioinformatics.babraham.ac.uk/projects/fastqc/). Raw reads were trimmed for adapters, polyA read-through, and low-quality tails using Trim Galore (version 0.6.10; https://www.bioinformatics.babraham.ac.uk/projects/trim_galore/) and Cutadapt (version 3.5). Reads were subsequently aligned to the reference genome (hg38) and raw gene counts were obtained using STAR (version 2.7.10b) with default parameters. Gene counts were normalized to Z-scores subtracting the mean expression across samples and dividing it for the standard deviation of each single gene to obtain heatmaps in Fig. 7d, 22a, 24j and 26a. Differential gene expression analysis was performed using the DESeq function of the DESeq2 package (version 1.44.0). Over-representation analysis was performed using Gene Set Enrichment Analysis and gene sets of the Reactome and Hallmark collections from the Broad Institute Molecular Signatures Database (http://software.broadinstitute.org/gsea/msigdb). GSEA software (http://www.broadinstitute.org/gsea/index.jsp) was applied on expression data. Gene sets were considered significantly enriched at FDR < 5% when using Signal2Noise as a metric and 1,000 permutations of gene sets. All analyses were performed using R 4.4.0 and publicly available packages explicitly cited in the thesis. No custom functions were written for the analysis.

For identification of miR-30d putative targets involved in YAP regulation, the list of 3766 genes upregulated (p-value < 0.05) upon LNA-30d transfection in DCIS cells, as identified by RNA-seq, was intersected with 1576 predicted miR-30 target genes from

TargetScan v8 (http://www.targetscan.org/vert_71/4) and 979 genes from the YAP1 interactome (BioGRID). The intersections were performed using Venny (http://bioinfogp.cnb.csic.es/tools/venny/index.html).
These analyses were performed by Dr. L Triboli, former phD student in the lab.

7.17.2 Gene expression datasets (TCGA, METABRIC)

Raw gene expression counts and clinical information from the TCGA breast cancer dataset (TCGA-BRCA) were obtained from the Genomic Data Commons (GDC) Portal using the GDC Data Transfer Tool (version 2.0.0) (Heath et al., 2021). The METABRIC collection, comprising gene expression data and clinical annotations for 768 breast cancer samples, was downloaded from the European Genome-Phenome Archive (EGA, http://www.ebi.ac.uk/ega/) under accession number EGAD00010000210 (Curtis et al., 2012). Original Illumina probe identifiers have been mapped to Entrez gene IDs using the Bioconductor illuminaHumanv3.db annotation package for Illumina HT-12 v3 arrays obtaining log2 intensity values for a total of 19,761 genes. For both the TCGA and METABRIC datasets, raw signals (counts or intensities) were normalized, and Z-scores were calculated by subtracting the mean expression across samples and dividing by the standard deviation of each gene. These analyses were performed by Dr. L Triboli, former phD student in the lab.

7.17.3 Tumour classification based on signature scores

The "miR-30d activity" signature consists of both upregulated and downregulated genes (p-value < 0.05) identified from RNA-seq analysis of DCIS cells treated with LNA-30d compared to control LNA. We then calculated the correlation between the normalized expression of these genes and miR-30d expression in the TCGA dataset, applying the following filtering criteria: genes with a negative fold change after treatment were required to have a positive correlation with miR-30d expression, while genes with a positive fold change were required to have a negative correlation (Pearson’s correlation). Next, we further refined these gene lists by selecting the top 10% and bottom 10% percentiles based on their Pearson’s correlation scores (Table 4). Finally, we applied the Kolmogorov-Smirnov test based on the ECDF to compare these refined gene lists against a randomly selected set of genes (Fig. 34).

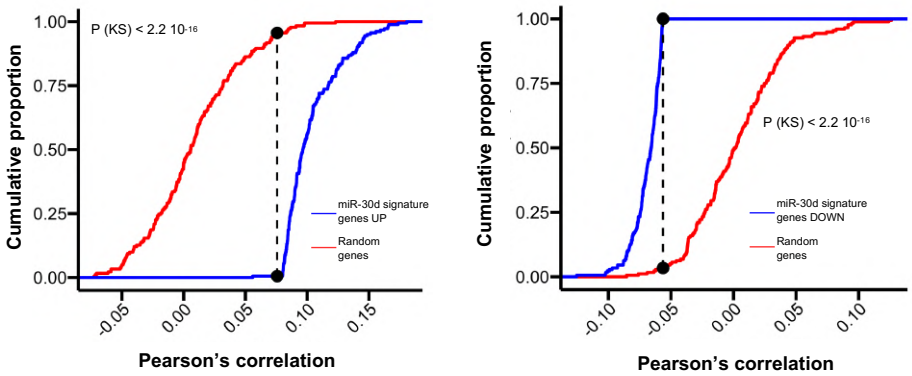

Figure 34. **Empirical Cumulative Distribution Function (ECDF) on miR-30d activity signature.**

Empirical Cumulative Distribution Function (ECDF) curves depicting correlation changes (Pearson's correlation) for miR-30d signature genes (blue) compared to randomly selected genes from TCGA dataset (red). Statistical significance of the difference between ECDFs is indicated (P-value from Kolmogorov-Smirnov (KS) test).

The "Activated_CD8_TCells", "MHCII", and "TILs" signatures were obtained from (Bagaev et al., 2021; López et al., 2024; Truntzer et al., 2019) respectively. The "IFNγ_Response" signature was retrieved from the MSigDB database.

The "Cyto-DNA Response" (Cyto-DR) signature was derived by combining the following gene sets: GOBP_INTERFERON_ALPHA_PRODUCTION, HALLMARK_INTERFERON_ALPHA_RESPONSE,GOBP_INTERFERON_BETA_PRODUCTION, and GOBP_TYPE_I_INTERFERON_PRODUCTION from MsigDB, along with 9 genes derived from (Frittoli et al., 2023) (Table 5). To calculate the signature scores, we used the R package SingScore (version 1.24.0) (Foroutan et al., 2018), applying it to both cases where gene sets contained upregulated and downregulated genes, as well as those with only upregulated genes. After having calculated the scores, we applied the Pearson correlation among all the signatures using the R function rcorr from the package Hmisc (v5.1.3).

7.18 Statistical analysis and reproducibility

All the experiments are representative of at least three independent replicates. Statistical analysis was performed using GraphPad Prism software. Details of the statistical tests are reported in figure legends. Graph bars represent single data point mean ± SD from at least n=3 biological replicates. The values of statistically significant p values are indicated in each figure and were obtained using: Two-tailed Student's unpaired parametric t-test with a 95% confidence threshold; One-way ANOVA (Fisher's LSD) ($\alpha < 0.05$); Two-tailed modified t-test adjusted for multiple testing using Benjamini-Hochberg method ($\alpha < 0.05$); Kolmogorov-Smirnov (KS) test.

8 APPENDIX

Table 1: List of oligonucleotides used for RNA Interference.

siRNA Name	Sequence	Manufacturer
STING	GCAUUACAACAACCUGCUA	Eurofins MWG
IRF3	GGGAAGAGUGGGAGUUCGA	Eurofins MWG
p65 (RELA)	GCCCUAUCCCUUUACGUCA	Eurofins MWG
DGKZ	GCCGCUUUCGGAAUAAGAUGU	Eurofins MWG
LMNB1	AACGCGCUUGGUAGAGGUGGA	Eurofins MWG
YAP	CUGGUCAGAGAUACUUCUU	Eurofins MWG
LATS2	AAAGGCGUAUGGCGAGUAG	Eurofins MWG
TREX1	CCAAGACCAUCUGCUGUCA	Eurofins MWG

Table 2: List of oligonucleotides used for cloning.

Target sequence	Sequence	Direction	Purpose
STING1	AATTACTAGTATGCCCCACTCCAGCCTG	Fw	to generate pTRIP-CMV-TagRFP-flag-STING1 from pTRIP-CMV-TagRFP-flag-cGAS
STING1	AATTCTCGAGTCAAGAGAAATCCGTGCGGAGA	Rv	to generate pTRIP-CMV-TagRFP-flag-STING1 from pTRIP-CMV-TagRFP-flag-cGAS
3'UTR-LAST2 external	AAATTTTCTAGACAGTGTGCTGATAATGTATTGTGCG	Fw	to mutagenize pGL3-spacer-3'UTR-*LATS2*
3'UTR-LAST2 external	AAATTTGGATCCGCTGTGGAATGTGTGTCAGTT	Rv	to mutagenize pGL3-spacer-3'UTR-*LATS2*
3'UTR-LAST2 internal	TCCTGTGTACTGCCCCCCATTTGTGTGAGTG	Fw	to mutagenize pGL3-spacer-3'UTR-*LATS2*
3'UTR-LAST2 internal	CACTCACACAAATGGGGGGCAGTACACAGGA	Rv	to mutagenize pGL3-spacer-3'UTR-*LATS2*
3'UTR-LATS2	CATCATCATATGCCGAGGGCTGTTTTGTTTTAAA	Fw	to clone 3'UTR-*LATS2* into pGL3-spacer vector
3'UTR-LATS2	CATCATACCGGTTGTGCCAGTAGAAGCTTTTCAA	Rv	to clone 3'UTR-*LATS2* into pGL3-spacer vector
miR-30d	CTCGAGCTTCCAGTCGGGGATGTTTACAAGAGAACTTAGAGAACTTCTTCCAGTCGGGGATGTTTACA	Fw	guide Fw to generate TWEEN 3' UTR EGFP-Decoy-30d

miR-30d	TCTAGATGTAAACATCCCCGACTGGAAGAAGTTCTCTAAGTTCTCTTGTAAACATCCCCGACTGGAAGC	Rv	guide Rv to generate TWEEN 3' UTR EGFP-Decoy-30d
p53 R175H	AGCACATGACGGAGGTTGTG		guide to generate KI DCIS for p53 R175H
p53 R175H	GCACCACCACACTATGTCGA	Fw	to amplify and sequence gDNA from DCIS KI p53 (R175H)
p53 R175H	CGCCAACTCTCTCTAGCTCG	Rv	to amplify gDNA from DCIS KI p53 (R175H)

Table 3: List of oligonucleotides used for qRT-PCR in the study.

Gene Target	Primer Sequence	Direction
Human *IFNA1*	5'-ACTCATACACCAGGTCACGC-3'	Fw
	3'-GCAGGGGTGAGAGTCTTTGAA-5'	Rv
Human *IFNB*	5'-AGTAGGCGACACTGTTCGTG-3'	Fw
	3'-GCCTCCCATTCAATTGCCAC-5'	Rv
Human *ISG15*	5'-GGTGGACAAATGCGACGAAC-3'	Fw
	3'-TCGAAGGTCAGCCAGAACAG-5'	Rv
Human *IFIT1*	5'-AAGCTTTCAAATCCCTTCCGC-3'	Fw
	3'-GCCTTGGCCCGTTCATAATT-5'	Rv
Human *IFI44*	5'-CCA CCG AGA TGT CAG AAA GAG-3'	Fw
	3'-TGGTACATGTGGCTTTGCTC-5'	Rv
Human *OAS1*	5'-GATTCTGCTGGCTGAAAGCAA-3'	Fw
	3'-CTGGGATCGTCGGTCTCATC-5'	Rv

Human *STING*	5’-CTTCACTTGGATGCTTGCC-3’	Fw
	3’-CCCGTAGCAGGTTGTTGTAATG-5’	Rv
Human *IRF3*	5’-GACCTTCCATCGTAGGCCG-3’	Fw
	3’-AATCCTCCTGCTGTGCATCC-5’	Rv
Human *p65 (RELA)*	5’-GGGGACTACGACCTGAATGC-3’	Fw
	3’-TTGGGGGCACGATTGTCAAA-5’	Rv
Human *LMNB1*	5’-CGCGTGCGTGTCTATGCTAA-3’	Fw
	3’-GAGGCTTCCAACTGGGCAAT-5’	Rv
Human *LMNB2*	5’-ATCAAGGCGCTGTACGAGTC-3’	Fw
	3’-TCTTGGCGCTCTTGTTGACC-5’	Rv
Human *LMNAC*	5’-ATCGCTTGGCGGTCTACATC-3’	Fw
	3’-TTGGTATTGCGCGCTTTCAG-5’	Rv
Human *LATS2*	5’-GCAGATTGTGCGGGTCATTA-3’	Fw
	3’-GGCATGAGCCCCTTTCCT-5’	Rv
Human *AMOTL2*	5’-AGTGAGCGACAAACAGCAGACG-3’	Fw
	3’-ATCTCTGCTCCCGTGTTTGGCA-5’	Rv
Human *WWP1*	5’-TGAACAGTGGCAATCTCAGCGG-3’	Fw
	3’-CTGGTGGCAAAGGTCCATAAGG-5’	Rv
Human *PTPN21*	5’-TGGCAGATGGTATGGGAACAGG-3’	Fw
	3’-CCATAGGTGACAGTGTTGTGCC-5’	Rv
Human *YAP*	5’-GCCGGAGCCCAAATCC-3’	Fw
	3’-GCAGAGAAGCTGGAGAGGAATG-5’	Rv
Human *DGKZ*	5’-AGCAGTACTGTGTAGCCAGGAT-3’	Fw
	3’-CACGGAAGGACGGCTTACAG-5’	Rv
Human *ND5*	5’-TTCAAACTAGACTACTTCTCCATAATATTCATC-3’	Fw
	3’-TTGGGTCTGAGTTTATATATCACAGTGA-5’	Rv
Human *18S*	5’-AGTCGGAGGTTCGAAGACGAT-3’	Fw
	3’-GCGGGTCATGGGAATAACG-5’	Rv
Human *H3*	5’-GTGAAGAAACCTCATCGTTACAGGCCTGGT-3’	Fw
	3’-CTGCAAAGCACCAATAGCTGCACTCTGGAA-5’	Rv
Mouse *Ifna1*	5’-GGATGTGACCTTCCTCAG ACTC-3’	Fw

	3’-ACCTTCTCCTGCGGGAATCCAA-5’	Rv
Mouse *Ifnb*	5’-CTGGCTTCCATCATGAACAA-3’	Fw
	3’-AGAGGGCTGTGGTGGAGAA-5’	Rv
Mouse *Isg15*	5’-AGCAATGGCCTGGGACCTAA3’-	Fw
	3’-CACGGACACCAGGAAATCGT-5’	Rv
Mouse *Gapdh*	5’-AAGGGCATCTTGGGCTACAC-3’	Fw
	3’-TGAAGTCGCAGGAGACAACC-5’	Rv
Mouse *Pd-l1*	5’-GCTCCAAAGGACTTGTACGTG-3’	Fw
	3’-TGATCTGAAGGGCAGCATTTC-5’	Rv

Table 4: miR-30d activity signature.

miR-30d_activity_DOWNREGULATED genes

"MUC1" "WFDC5" "OSM" "PSTPIP2" "WFDC12" "CYP51A1P2" "KLF8" "PDCD1LG2" "SPANXN3" "TLR6" "MORC4" "KDELR3" "ASPHD2" "NFAM1" "APOBEC3A" "APOBEC3G" "NANS" "DAPK1" "PRDM1" "PDLIM1" "ENTPD7" "NFKBIE" "DUSP18" "LCP1" "SAMD9L" "BIRC3" "WIPF2" "KIF13B" "ITGA5" "SMIM10L2B" "COSMOC" "GPX8" "PLEKHA8" "KLHDC7B" "FGD6" "LTBP1" "ADGRE5" "APOL6" "LINC02577" "APOL2" "PAX9" "TEX29" "ULBP1" "AQP9" "GLRX" "B4GALT1" "LINC02073" "CD180" "SLC7A7" "TMEM263" "AKR1B1" "DIAPH2" "STARD4" "PTENP1" "HMGN1P13" "SLC37A2" "PILRA" "IFITM4P" "ENTPD3" "RNF149" "SLC35C1" "HSPA5" "PELATON" "RNF180" "NUMB" "LAPTM5" "RBMS2P1" "FBLIM1" "PPIC" "C5AR1" "MANF" "GALNT5" "CDCP1" "ELL2" "RELB" "INHBA" "LGALS9C" "CD68" "TNFSF9" "TLCD2" "AFAP1-AS1" "PPP1R18" "NAT1" "IL4I1" "LDLR" "CXCL11" "GORASP2" "TIGAR" "CFB" "SPATS2L" "PRKCH" "ICAM1" "KCNS3" "SPTLC2" "FPR2" "ERP44" "SELPLG" "HOXA1" "ULBP2" "MAP3K9-DT" "FPR1" "LINC01968" "PDE4DIP" "RAP2B" "ARF4" "PCDHA4" "RNF217" "VANGL2" "EXT1" "NCEH1" "COPA" "CAST" "TFG" "LDAF1" "LINC02818" "MYD88" "MPZL1" "MMP3" "ATP2C1" "TUBB3" "CSGALNACT1" "PDIA3" "COP1" "CCNYL1" "SUCO" "IDH1" "PFKFB2" "LAMB3" "IL32" "GRIN2D" "ABL2" "GOLT1B" "SLFN5" "HLA-L" "MYO7A" "ZNF281" "PANX1" "CCL5" "EGOT" "KRAS" "GBP6" "IFIH1" "CD300C" "ANKFN1" "GJA5" "MIA3" "LPP" "FDPS" "KRT17" "COPG1" "SEC61A1" "ATP13A5" "C1orf116" "SH3BGRL3" "F11R" "NECTIN4" "DEDD" "SLC39A1" "TOR1AIP2" "MBOAT2" "CTSS" "GBP2" "SH2D2A" "KPRP" "OPN3" "PSME4" "LIMS1" "IKBKE" "RABGAP1L" "IVL" "TDRKH" "GBP5" "BLZF1" "NCF2" "SMG7" "LINC01133"

miR-30d_activity_UPREGULATED genes

"SNED1" "PAN3-AS1" "PCNT" "PABPC1L" "CBR1" "C21orf58" "UCKL1" "ZNF512B" "COX5BP6" "CLBA1" "FOXF2" "PRKAR1B" "MICALL2" "SERPINA5" "COL9A3" "HDAC10" "WDR90" "TELO2" "HSPA4L" "STUB1" "PFKM" "MCRIP2" "RTEL1-TNFRSF6B" "ARFRP1" "LINC00235" "DPH7" "LIME1" "SLC2A4RG" "UNKL" "NUDT16L1" "RHOT2" "CARS2" "CA8" "CHTF18" "NUP107" "EGFL7" "FEM1A" "MAMDC4" "DNLZ" "COQ7" "HOMER2" "GTPBP3" "RPL29P11" "TMEM129" "PAXIP1-DT" "CEBPD" "MIR25" "PPP1R35" "TMEM14B-DT" "ENHO" "TCEA1P2" "MACROD1" "TAS2R4" "MRPL13" "NUDT14" "ZNF837" "SDR39U1" "NELFA" "RHPN1" "USF2" "PRSS53" "JRK" "DDX51" "ST3GAL1-DT" "RHPN1-AS1" "YEATS4" "TEDC1" "TMEM121" "PHRF1" "C8orf33" "RAB28" "TAF6L" "PIGQ" "AARSD1" "ROGDI" "FBN2" "JPH1" "LTC4S" "LIPT2" "JMJD7-PLA2G4B" "FBXL6" "CPSF1" "CCDC61" "FAAP100" "ZNF76" "NUBP2" "PUF60" "EIF4A1" "GPAA1" "B4GALNT4" "ABCA2" "ANTKMT" "CCDC106" "CPNE7" "CDK10" "SNHG20" "D2HGDH" "TKFC" "SSBP4" "ARRDC1-AS1" "ISYNA1" "EML3" "GPS2" "DICER1-AS1" "SNHG10" "OXLD1" "TMEM128" "GSDMD" "MROH6" "NAPRT" "MRPL38" "TIGD5" "PYCR3" "BAIAP3" "RAD9A" "ZNF771" "DUT-AS1" "SCLY" "BRAT1" "SNRNP70" "HEXD" "TIMM13" "MAP2K7" "SPPL2B" "ZNF358" "SRRM2" "RGR" "FBXW9" "PPP1R16A" "MFSD3" "RECQL4" "ING5" "GPER1" "AMDHD2" "NBEAL2" "DUSP28" "TMEM80" "QTRT1" "PSMC3IP" "GNPTG" "SEMA6B" "DECR2" "DPY19L2P2" "EEF1D" "SNORD104" "MINCR" "NME3" "TNNI2" "DBIL5P" "CELSR2" "COPS9" "SERTAD4-AS1" "PRPF31" "GCDH" "HEBP1" "SYT8" "H19" "TMA7" "AFG3L1P" "DHX30" "ATRIP" "CIRBP" "CHDH" "MIR4733HG" "PLEKHJ1" "STK11" "GPX4" "KAT2A" "PRANCR" "POLRMT" "RNF126" "CCDC12"

Table 5: Cyto-DR signature.

“ANAPC4”	“IFNA2”	“IFNA21”	“IFNA5”	“IFNA6”	“IRF9”	“IKBKB”	
“STING1”	“IRF7”	“IFNA1”	“IL6”	“IFNB1”	“CHUK”	“DDX3X2”	“DHX36”
“DHX9”	“HAVCR2	“HSPD1”	“IFIH1”	“IL10”	“IRF3”	“IRF5”	“LILRA4”	“MAVS”
“MMP12”	“NLRC3”	“NMB”	“NMBR”	“NMI”	“PTPRS”	“RIGI”	“RIPK2”
“SETD2”	“STAT1”	“TBK1”	“TLR3”	“TLR4”	“TLR7”	“TLR8”	
“TLR9”	“TRIM65”	“ADAR”	“B2M”	“BATF2”	“BST2”	“C1S”	“CASP1”
“CASP8”	“CCRL2”	“CD47”	“CD74”	“CMPK2”	“CMTR1”	“CNP”	
“CSF1”	“CXCL10”	“CXCL11”	“DDX60”	“DHX58”	“EIF2AK2”	“ELF1”	“EPSTI1”
“GBP2”	“GBP4”	“GMPR”	“HELZ2”	“HERC6”	“HLA-C”	“IFI27”	
“IFI30”	“IFI35”	“IFI44”	“IFI44L”	“IFIT2”	“IFIT3”	“IFITM1”	“IFITM2”	“IFITM3”
“IL15”	“IL4R”	“IL7”	“IRF1”	“IRF2”	“ISG15”	“ISG20”	“LAMP3”	“LAP3”
“LGALS3BP”	“LPAR6”	“LY6E”	“MOV10”	“MVB12A”	“MX1”	“NCOA7”	“NUB1”
“OAS1”	“OASL”	“OGFR”	“PARP12”	“PARP14”	“PARP9”	“PLSCR1”	
“PNPT1”	“PROCR”	“PSMA3”	“PSMB8”	“PSMB9”	“PSME1”	“PSME2”	
“RNF31”	“RSAD2”	“RTP4”	“SAMD9”	“SAMD9L”	“SELL”	“SLC25A28”	“SP110”
“STAT2”	“TAP1”	“TDRD7”	“TENT5A”	“TMEM140”	“TRAFD1”	“TRIM14”	
“TRIM21”	“TRIM25”	“TRIM26”	“TRIM5”	“TXNIP”	“UBA7”	“UBE2L6”	
“USP18”	“WARS1”	“ARRDC4”	“CACTIN”	“FLOT1”	“HMGB2”		
“HSP90AA1”	“LILRB1”	“MIR26B”	“MORC3”	“NLRX1”	“OAS2”	“OAS3”	
“POLR3A”	“POLR3B”	“POLR3C”	“POLR3D”	“POLR3F”	“POLR3G	“PPM1B”	
“PTPN11”	“PYCARD”	“REL”	“RELB”	“RIOK3”	“RNF135”	“RNF216”	“SIRPA”
“TICAM1”	“TIRAP”	“TLR2”	“TOMM70”	“TRAF3”	“TRAIP”	“TRIM38”	
“TRIM56”	“YY1”	“ZBTB20”	“ACOD1”	“ATG12”	“ATG5”	“BANF1”	“CD14”
“CGAS”	“CUL3”	“CYLD”	“DDX56”	“DHX33”	“DTX4”	“G3BP1”	“GAPDH”
“GARIN5A”	“GBP7”	“GPATCH3”	“IKBKE”	“ILRUN”	“IRAK1”	“IRF8”	
“IRGM”	“ITCH”	“KAT8”	“KLHL22”	“KPNA2”	“MIR21”	“MYD88”	“NPLOC4”
“OTUD5”	“PLCG2”	“POLA1”	“PQBP1”	“PTPN22”	“RAB2B”	“RBX1”	
“RNF125”	“RNF26”	“SIGLEC1”	“SYK”	“TANK”	“TICAM2”	“TRAF3IP1”	
“TRAF3IP3”	“TRAF6”	“TREX1”	“TRIM15”	“TRIM27”	“TYROBP”	“UAP1”	
“UFD1”	“USP22”	“XAF1”	“XIAP”	“ZC3HAV1”	“ZCCHC3”		

Table 6: List of candidate genes related to Figure 24a,b.

" IDH1"	"PTPN13"	"PRRG1"	"AMOTL2"	"TEAD1"	"NFAT5"	"WWP1"	"TULP4"
"UBN2"	"CCDC120"	"TAB3"	"LATS2"	"BEAN1"	"WASL"	"RAPGEF2"	"CALD1" "
"WDR1"	"AMOTL1"	"AHNAK"	"KRAS"	"PTPN21"	"CD2AP"	"PKNOX2"	"HSPA5"
"HSPA2"							

Table 7: List of primary and secondary antibodies used in the study.

Primary Ab	Company/ Code	WB dilution	IF dilution	IHC dilution
Phospho S172-TBK1	CST-5483S	1:1000	1:50	
TBK1	CST-3504	1:1000		
Phospho S366-STING	CST-19781	1:1000		
STING (D2P2F)	CST-13647S	1:1000		
Phospho S127 YAP	CST-4911	1:1000		
YAP	Santa Cruz-101199	1:1000		
YAP1	abcam-52771		1:100	
LATS1	CST-3477	1:1000		
LATS2	abcam-243657	1:1000		
Lamin-B1	abcam-16048	1:1000	1:200	
Lamin-B2	abcam-151735	1:1000		
Lamin A/C	Santa Cruz-7292	1:1000	1:200	
p53 (DO-1)	Santa Cruz-126	1:1000		
cGAS	CST-15102		1:100	1:100
dsDNA	abcam-27156		1:10000	
γ-H2AX	Millipore-05-636		1:300	
53BP1	Santa Cruz-22760		1:100	
GM130	BD Biosciences-610822		1:200	
PDI	abcam-2792		1:100	

GFP	CST-2955		1:200	
RFP	Invitrogen-R10367		1:200	
CD8	CST-98941			1:400
NCR1	abcam-233558			1:100
BrdU	GE Healthcare-RPN202		1:2	
Hsp90	Santa Cruz-13119	1:5000		
Secondary Ab	**Company/ Code**	**WB dilution**	**IF dilution**	**IHC dilution**
goat anti-mouse Alexa Fluor 488	Life Technologies- A-11001		1:500	
goat anti-mouse Alexa Fluor 568	Life Technologies- A-11004		1:500	
donkey anti-mouse Alexa Fluor 594	Life Technologies- A-21203		1:500	
donkey anti-rabbit Alexa Fluor 488	Life Technologies- A-21206		1:500	
goat anti-rabbit Alexa Fluor 568	Life Technologies- A-11011		1:500	
goat anti-mouse IgG h+l HRP-conjugated	Bethyl A120-201P	1:2000		
goat anti-rabbit IgG h+l HRP-conjugated	Bethyl A90-516P	1:2000		

9 Acknowledgements

I extend my heartfelt gratitude to my supervisor **Prof. Giannino Del Sal**, for granting me the opportunity to pursue this research endeavor under his unwavering guidance. I believe his rigorous scientific approach and attention made me to become a much confident researcher for which I am extremely grateful. I am deeply grateful to my co-supervisor **Prof. Fiamma Mantovani**, for following me in every detail for the critical scientific discussions and corrections of the thesis. Thank you for the relentless support, encouragement, patience and all the advice throughout my research journey. Their positive attitude and enthusiasm motivated me to work harder and successfully execute my research work.

I express my sincere thanks to Dr. Serena Torrini and Dr. Alessandra Rustighi for the experimental advice that helped me better execute my thesis. I would like to thank Dr. Silvano Piazza and Dr. Luca Triboli for helping in performing with the bioinformatic analysis. I would like to express my gratitude to the entire Cancer Cell Signalling Group of ICGEB, both past and present, who have shared this journey with me, supported me both in the lab and outside, and have strongly contributed to making my life happier and more cheerful. I am thankful to all the collaborators, especially Dr. G. Beznoussenko for the CLEM analysis and Dr. V. Cancila for the IHC analysis, whose contributions were invaluable.

I am also grateful to the entire team of Arturo Falaschi PhD Fellowship, administrative, accounts, purchase, health, and technical staff members for their support during my entire stay at the University of Trieste and ICGEB, Italy.

I owe a lot to my parents Mr. Surjit Chatterjee and Mrs. Shanta Chatterjee, for their immense sacrifices, upbringing of me, and constant support at every stage of my personal and academic life, and longed to see this achievement come true. I am very much indebted to all my family members and friends, especially Dr. Chandan Kumar whose encouragement has been my greatest source of strength during these exciting years.

Last but not the least, I want to thank the Almighty God for blessing me to achieve my goal and to be successful in this part of my life's journey so far.

10 REFERENCES

Abate, M., Lombardi, A., Luce, A., Porru, M., Leonetti, C., Bocchetti, M., Campani, V., De Rosa, G., Graziano, S. F., Nele, V., Cardile, F., Marino, F. Z., Franco, R., Ronchi, A., Scrima, M., Sperlongano, R., Alfano, R., Misso, G., Amler, E., … Zappavigna, S. (2023). Fluorescent nanodiamonds as innovative delivery systems for MiR-34a replacement in breast cancer. *Molecular Therapy Nucleic Acids*, *33*, 127–141. https://doi.org/10.1016/j.omtn.2023.06.012

Ablasser, A., Goldeck, M., Cavlar, T., Deimling, T., Witte, G., Röhl, I., Hopfner, K. P., Ludwig, J., & Hornung, V. (2013). CGAS produces a 2′-5′-linked cyclic dinucleotide second messenger that activates STING. *Nature*, *498*(7454), 380–384. https://doi.org/10.1038/nature12306

Acuña-Pilarte, K., & Koh, M. Y. (2025). The HIF axes in cancer: angiogenesis, metabolism, and immune-modulation. In *Trends in Biochemical Sciences* (Vol. 50, Number 8, pp. 677–694). Elsevier Ltd. https://doi.org/10.1016/j.tibs.2025.06.005

Ahn, J., Xia, T., Konno, H., Konno, K., Ruiz, P., & Barber, G. N. (2014). Inflammation-driven carcinogenesis is mediated through STING. *Nature Communications*, *5*. https://doi.org/10.1038/ncomms6166

Alvarado-Ortiz, E., de la Cruz-López, K. G., Becerril-Rico, J., Sarabia-Sánchez, M. A., Ortiz-Sánchez, E., & García-Carrancá, A. (2021). Mutant p53 Gain-of-Function: Role in Cancer Development, Progression, and Therapeutic Approaches. In *Frontiers in Cell and Developmental Biology* (Vol. 8). Frontiers Media S.A. https://doi.org/10.3389/fcell.2020.607670

Amelio, I., Mancini, M., Petrova, V., Cairns, R. A., Vikhreva, P., Nicolai, S., Marini, A., Antonov, A. A., Le Quesne, J., Baena Acevedo, J. D., Dudek, K., Sozzi, G., Pastorino, U., Knight, R. A., Mak, T. W., & Melino, G. (2018). p53 mutants cooperate with HIF-1 in transcriptional regulation of extracellular matrix components to promote tumor progression. *Proceedings of the National Academy of Sciences of the United States of America*, *115*(46), E10869–E10878. https://doi.org/10.1073/pnas.1808314115

Anand, U., Dey, A., Chandel, A. K. S., Sanyal, R., Mishra, A., Pandey, D. K., De Falco, V., Upadhyay, A., Kandimalla, R., Chaudhary, A., Dhanjal, J. K., Dewanjee, S., Vallamkondu, J., & Pérez de la Lastra, J. M. (2023). Cancer chemotherapy and beyond: Current status, drug candidates, associated risks and progress in targeted therapeutics. In *Genes and Diseases* (Vol. 10, Number 4, pp. 1367–1401). KeAi Communications Co. https://doi.org/10.1016/j.gendis.2022.02.007

Arnaiz, E., & Harris, A. L. (2022). Role of Hypoxia in the Interferon Response. In *Frontiers in Immunology* (Vol. 13). Frontiers Media S.A. https://doi.org/10.3389/fimmu.2022.821816

Aylon, Y., Michael, D., Shmueli, A., Yabuta, N., Nojima, H., & Oren, M. (2006). A positive feedback loop between the p53 and Lats2 tumor suppressors prevents tetraploidization. *Genes and Development*, *20*(19), 2687–2700. https://doi.org/10.1101/gad.1447006

Baeriswyl, V., & Christofori, G. (2009). The angiogenic switch in carcinogenesis. In *Seminars in Cancer Biology* (Vol. 19, Number 5, pp. 329–337). https://doi.org/10.1016/j.semcancer.2009.05.003

Bagaev, A., Kotlov, N., Nomie, K., Svekolkin, V., Gafurov, A., Isaeva, O., Osokin, N., Kozlov, I., Frenkel, F., Gancharova, O., Almog, N., Tsiper, M., Ataullakhanov, R., & Fowler, N. (2021). Conserved pan-cancer microenvironment subtypes predict response to immunotherapy. *Cancer Cell*, *39*(6), 845-865.e7. https://doi.org/10.1016/j.ccell.2021.04.014

Bakhoum, S. F., Ngo, B., Laughney, A. M., Cavallo, J. A., Murphy, C. J., Ly, P., Shah, P., Sriram, R. K., Watkins, T. B. K., Taunk, N. K., Duran, M., Pauli, C., Shaw, C., Chadalavada, K., Rajasekhar, V. K., Genovese, G., Venkatesan, S., Birkbak, N. J., McGranahan, N., … Cantley, L. C. (2018). Chromosomal instability drives metastasis through a cytosolic DNA response. *Nature*, *553*(7689), 467–472. https://doi.org/10.1038/nature25432

Baliakas, P., & Soussi, T. (2025). The TP53 tumor suppressor gene: From molecular biology to clinical investigations. In *Journal of Internal Medicine* (Vol. 298, Number 2, pp. 78–96). John Wiley and Sons Inc. https://doi.org/10.1111/joim.20106

Bandopadhyay, S., & Patranabis, S. (2023). Mechanisms of HIF-driven immunosuppression in tumour microenvironment. In *Journal of the Egyptian National Cancer Institute* (Vol. 35, Number 1). Springer Science and Business Media Deutschland GmbH. https://doi.org/10.1186/s43046-023-00186-z

Beaver, J. A., Amiri-Kordestani, L., Charlab, R., Chen, W., Palmby, T., Tilley, A., Zirkelbach, J. F., Yu, J., Liu, Q., Zhao, L., Crich, J., Chen, X. H., Hughes, M., Bloomquist, E., Tang, S., Sridhara, R., Kluetz, P. G., Kim, G., Ibrahim, A., … Cortazar, P. (2015). FDA approval: Palbociclib for the treatment of postmenopausal patients with estrogen receptor-positive, HER2-negative metastatic breast cancer. *Clinical Cancer Research*, *21*(21), 4760–4766. https://doi.org/10.1158/1078-0432.CCR-15-1185

Beernaert, B., & Parkes, E. E. (2023). CGAS-STING signalling in cancer: Striking a balance with chromosomal instability. *Biochemical Society Transactions*, *51*(2), 539–555. https://doi.org/10.1042/BST20220838

Behbod, F., Kittrell, F. S., LaMarca, H., Edwards, D., Kerbawy, S., Heestand, J. C., Young, E., Mukhopadhyay, P., Yeh, H. W., Allred, D. C., Hu, M., Polyak, K., Rosen, J. M., & Medina, D. (2009). An intraductal human-in-mouse transplantation model mimics the subtypes of ductal carcinoma in situ. *Breast Cancer Research*, *11*(5). https://doi.org/10.1186/bcr2358

Bertolio, R., Napoletano, F., & Del Sal, G. (2023). Dynamic links between mechanical forces and metabolism shape the tumor milieu. In *Current Opinion in Cell Biology* (Vol. 84). Elsevier Ltd. https://doi.org/10.1016/j.ceb.2023.102218

Beznoussenko, G. V., & Mironov, A. A. (2015). Correlative video-light–electron microscopy of mobile organelles. *Methods in Molecular Biology*, *1270*. https://doi.org/10.1007/978-1-4939-2309-0_23

Beznoussenko, G. V., Parashuraman, S., Rizzo, R., Polishchuk, R., Martella, O., Giandomenico, D. Di, Fusella, A., Spaar, A., Sallese, M., Capestrano, M. G., Pavelka, M., Vos, M. R., Rikers, Y. G. M., Helms, V., Mironov, A. A., & Luini, A. (2014). Transport of

soluble proteins through the Golgi occurs by diffusion via continuities across cisternae. *ELife*, *2014*(3). https://doi.org/10.7554/eLife.02009

Biffi, G., & Tuveson, D. A. (2021). Diversity and biology of cancer associated fibroblasts. *Physiological Reviews*, *101*(1), 147–176. https://doi.org/10.1152/physrev.00048.2019

Bona, M. Di, & Bakhoum, S. F. (2024). Micronuclei and Cancer. In *Cancer Discovery* (Vol. 14, Number 2, pp. 214–216). American Association for Cancer Research Inc. https://doi.org/10.1158/2159-8290.CD-23-1073

Bonci, D., Coppola, V., Musumeci, M., Addario, A., Giuffrida, R., Memeo, L., D'Urso, L., Pagliuca, A., Biffoni, M., Labbaye, C., Bartucci, M., Muto, G., Peschle, C., & De Maria, R. (2008). The miR-15a-miR-16-1 cluster controls prostate cancer by targeting multiple oncogenic activities. *Nature Medicine*, *14*(11), 1271–1277. https://doi.org/10.1038/nm.1880

Bonjardim, C. A. (2005). Interferons (IFNs) are key cytokines in both innate and adaptive antiviral immune responses - And viruses counteract IFN action. In *Microbes and Infection* (Vol. 7, Number 3, pp. 569–578). Elsevier Masson SAS. https://doi.org/10.1016/j.micinf.2005.02.001

Bonnans, C., Chou, J., & Werb, Z. (2014). Remodelling the extracellular matrix in development and disease. In *Nature Reviews Molecular Cell Biology* (Vol. 15, Number 12, pp. 786–801). Nature Publishing Group. https://doi.org/10.1038/nrm3904

Braal, C. L., Jongbloed, E. M., Wilting, S. M., Mathijssen, R. H. J., Koolen, S. L. W., & Jager, A. (2021). Inhibiting CDK4/6 in Breast Cancer with Palbociclib, Ribociclib, and Abemaciclib: Similarities and Differences. In *Drugs* (Vol. 81, Number 3, pp. 317–331). Adis. https://doi.org/10.1007/s40265-020-01461-2

Camps, C., Saini, H. K., Mole, D. R., Choudhry, H., Reczko, M., Guerra-Assunção, J. A., Tian, Y. M., Buffa, F. M., Harris, A. L., Hatzigeorgiou, A. G., Enright, A. J., & Ragoussis, J. (2014). Integrated analysis of microRNA and mRNA expression and association with HIF binding reveals the complexity of microRNA expression regulation under hypoxia. *Molecular Cancer*, *13*(1). https://doi.org/10.1186/1476-4598-13-28

Cao, Y., Yi, Y., Han, C., & Shi, B. (2024). NF-κB signaling pathway in tumor microenvironment. In *Frontiers in Immunology* (Vol. 15). Frontiers Media SA. https://doi.org/10.3389/fimmu.2024.1476030

Capaci, V., Bascetta, L., Fantuz, M., Beznoussenko, G. V., Sommaggio, R., Cancila, V., Bisso, A., Campaner, E., Mironov, A. A., Wiśniewski, J. R., Ulloa Severino, L., Scaini, D., Bossi, F., Lees, J., Alon, N., Brunga, L., Malkin, D., Piazza, S., Collavin, L., … Del Sal, G. (2020). Mutant p53 induces Golgi tubulo-vesiculation driving a prometastatic secretome. *Nature Communications*, *11*(1). https://doi.org/10.1038/s41467-020-17596-5

Chang, H. A., Ou Yang, R. Z., Su, J. M., Nguyen, T. M. H., Sung, J. M., Tang, M. J., & Chiu, W. T. (2023). YAP nuclear translocation induced by HIF-1α prevents DNA damage under hypoxic conditions. *Cell Death Discovery*, *9*(1). https://doi.org/10.1038/s41420-023-01687-5

Chaplin, D. D. (2010). Overview of the immune response. *Journal of Allergy and Clinical Immunology*, *125*(2 SUPPL. 2). https://doi.org/10.1016/j.jaci.2009.12.980

Chattopadhyay, S., Marques, J. T., Yamashita, M., Peters, K. L., Smith, K., Desai, A., Williams, B. R. G., & Sen, G. C. (2010). Viral apoptosis is induced by IRF-3-mediated activation of Bax. *EMBO Journal*, *29*(10), 1762–1773. https://doi.org/10.1038/emboj.2010.50

Chen, Y., Gao, D. Y., & Huang, L. (2015). In vivo delivery of miRNAs for cancer therapy: Challenges and strategies. In *Advanced Drug Delivery Reviews* (Vol. 81, pp. 128–141). Elsevier B.V. https://doi.org/10.1016/j.addr.2014.05.009

Chi, H., Pepper, M., & Thomas, P. G. (2024). Principles and therapeutic applications of adaptive immunity. In *Cell* (Vol. 187, Number 9, pp. 2052–2078). Elsevier B.V. https://doi.org/10.1016/j.cell.2024.03.037

Chow, M. T., Möller, A., & Smyth, M. J. (2012). Inflammation and immune surveillance in cancer. In *Seminars in Cancer Biology* (Vol. 22, Number 1, pp. 23–32). https://doi.org/10.1016/j.semcancer.2011.12.004

Chowaniec, H., Ślubowska, A., Mroczek, M., Borowczyk, M., Braszka, M., Dworacki, G., Dobosz, P., & Wichtowski, M. (2024). New hopes for the breast cancer treatment: perspectives on the oncolytic virus therapy. In *Frontiers in Immunology* (Vol. 15). Frontiers Media SA. https://doi.org/10.3389/fimmu.2024.1375433

Civril, F., Deimling, T., De Oliveira Mann, C. C., Ablasser, A., Moldt, M., Witte, G., Hornung, V., & Hopfner, K. P. (2013). Structural mechanism of cytosolic DNA sensing by cGAS. *Nature*, *498*(7454), 332–337. https://doi.org/10.1038/nature12305

Colangelo, N. W., Gerber, N. K., Vatner, R. E., & Cooper, B. T. (2024). Harnessing the cGAS-STING pathway to potentiate radiation therapy: current approaches and future directions. In *Frontiers in Pharmacology* (Vol. 15). Frontiers Media SA. https://doi.org/10.3389/fphar.2024.1383000

Cole, K., Al-Kadhimi, Z., & Talmadge, J. E. (2023). Highlights into historical and current immune interventions for cancer. *International Immunopharmacology*, *117*. https://doi.org/10.1016/j.intimp.2023.109882

Cooks, T., Pateras, I. S., Jenkins, L. M., Patel, K. M., Robles, A. I., Morris, J., Forshew, T., Appella, E., Gorgoulis, V. G., & Harris, C. C. (2018). Mutant p53 cancers reprogram macrophages to tumor supporting macrophages via exosomal miR-1246. *Nature Communications*, *9*(1). https://doi.org/10.1038/s41467-018-03224-w

Courbot, O., & Elosegui-Artola, A. (2025). The role of extracellular matrix viscoelasticity in development and disease. *Npj Biological Physics and Mechanics*, *2*(1). https://doi.org/10.1038/s44341-025-00014-6

Croci, O., De Fazio, S., Biagioni, F., Donato, E., Caganova, M., Curti, L., Doni, M., Sberna, S., Aldeghi, D., Biancotto, C., Verrecchia, A., Olivero, D., Amati, B., & Campaner, S. (2017). Transcriptional integration of mitogenic and mechanical signals by Myc and YAP. *Genes and Development*, *31*(20), 2017–2022. https://doi.org/10.1101/gad.301184.117

Curtis, C., Shah, S. P., Chin, S. F., Turashvili, G., Rueda, O. M., Dunning, M. J., Speed, D., Lynch, A. G., Samarajiwa, S., Yuan, Y., Gräf, S., Ha, G., Haffari, G., Bashashati, A.,

Russell, R., McKinney, S., Aparicio, S., Brenton, J. D., Ellis, I., … Caldas, C. (2012). The genomic and transcriptomic architecture of 2,000 breast tumours reveals novel subgroups. *Nature*, *486*(7403), 346–352. https://doi.org/10.1038/nature10983

De Cola, A., Lamolinara, A., Lanuti, P., Rossi, C., Iezzi, M., Marchisio, M., Todaro, M., & De Laurenzi, V. (2018). MiR-205-5p inhibition by locked nucleic acids impairs metastatic potential of breast cancer cells. *Cell Death and Disease*, *9*(8). https://doi.org/10.1038/s41419-018-0854-9

de Oliveira Mann, C. C., Orzalli, M. H., King, D. S., Kagan, J. C., Lee, A. S. Y., & Kranzusch, P. J. (2019). Modular Architecture of the STING C-Terminal Tail Allows Interferon and NF-κB Signaling Adaptation. *Cell Reports*, *27*(4), 1165-1175.e5. https://doi.org/10.1016/j.celrep.2019.03.098

de Visser, K. E., & Joyce, J. A. (2023). The evolving tumor microenvironment: From cancer initiation to metastatic outgrowth. In *Cancer Cell* (Vol. 41, Number 3, pp. 374–403). Cell Press. https://doi.org/10.1016/j.ccell.2023.02.016

Di Agostino, S., Sorrentino, G., Ingallina, E., Valenti, F., Ferraiuolo, M., Bicciato, S., Piazza, S., Strano, S., Del Sal, G., & Blandino, G. (2016). YAP enhances the pro-proliferative transcriptional activity of mutant p53 proteins . *EMBO Reports*, *17*(2), 188–201. https://doi.org/10.15252/embr.201540488

Di Minin, G., Bellazzo, A., Dal Ferro, M., Chiaruttini, G., Nuzzo, S., Bicciato, S., Piazza, S., Rami, D., Bulla, R., Sommaggio, R., Rosato, A., DelSal, G., & Collavin, L. (2014). Mutant p53 Reprograms TNF Signaling in Cancer Cells through Interaction with the Tumor Suppressor DAB2IP. *Molecular Cell*, *56*(5), 617–629. https://doi.org/10.1016/j.molcel.2014.10.013

Diamantopoulos, M. A., Boti, M. A., Sarri, T., & Scorilas, A. (2025). Non-Coding RNAs in Health and Disease: From Biomarkers to Therapeutic Targets. *LabMed*, *2*(3), 17. https://doi.org/10.3390/labmed2030017

Diamantopoulos, M. A., Tsiakanikas, P., & Scorilas, A. (2018). Non-coding RNAs: the riddle of the transcriptome and their perspectives in cancer. *Annals of Translational Medicine*, *6*(12), 241–241. https://doi.org/10.21037/atm.2018.06.10

Diamond, M. S., Kinder, M., Matsushita, H., Mashayekhi, M., Dunn, G. P., Archambault, J. M., Lee, H., Arthur, C. D., White, J. M., Kalinke, U., Murphy, K. M., & Schreiber, R. D. (2011). Type I interferon is selectively required by dendritic cells for immune rejection of tumors. *Journal of Experimental Medicine*, *208*(10), 1989–2003. https://doi.org/10.1084/jem.20101158

Dobbs, N., Burnaevskiy, N., Chen, D., Gonugunta, V. K., Alto, N. M., & Yan, N. (2015). STING activation by translocation from the ER is associated with infection and autoinflammatory disease. *Cell Host and Microbe*, *18*(2), 157–168. https://doi.org/10.1016/j.chom.2015.07.001

Dong, Z. Y., Zhong, W. Z., Zhang, X. C., Su, J., Xie, Z., Liu, S. Y., Tu, H. Y., Chen, H. J., Sun, Y. L., Zhou, Q., Yang, J. J., Yang, X. N., Lin, J. X., Yan, H. H., Zhai, H. R., Yan, L. X., Liao, R. Q., Wu, S. P., & Wu, Y. L. (2017). Potential predictive value of TP53 and KRAS mutation status for response to PD-1 blockade immunotherapy in lung adenocarcinoma.

Clinical Cancer Research, *23*(12), 3012–3024. https://doi.org/10.1158/1078-0432.CCR-16-2554

Driscoll, J., Gondaliya, P., Zinn, D. A., Jain, R., Yan, I. K., Dong, H., & Patel, T. (2025). Using aptamers for targeted delivery of RNA therapies. In *Molecular Therapy* (Vol. 33, Number 4, pp. 1344–1367). Cell Press. https://doi.org/10.1016/j.ymthe.2025.02.047

Du, J. min, Qian, M. jia, Yuan, T., Chen, R. han, He, Q. jun, Yang, B., Ling, Q., & Zhu, H. (2022). cGAS and cancer therapy: a double-edged sword. In *Acta Pharmacologica Sinica* (Vol. 43, Number 9, pp. 2202–2211). Springer Nature. https://doi.org/10.1038/s41401-021-00839-6

Du, M., & Chen, Z. J. (2018). DNA-induced liquid phase condensation of cGAS activates innate immune signaling. *Science, 361*(6403), 704-709. https://www.science.org/doi/abs/10.1126/science.aat1022

Duong, E., Fessenden, T. B., Lutz, E., Dinter, T., Yim, L., Blatt, S., Bhutkar, A., Wittrup, K. D., & Spranger, S. (2022). Type I interferon activates MHC class I-dressed CD11b+ conventional dendritic cells to promote protective anti-tumor CD8+ T cell immunity. *Immunity*, *55*(2), 308-323.e9. https://doi.org/10.1016/j.immuni.2021.10.020

Dzobo, K., & Dandara, C. (2020). Architecture of Cancer-Associated Fibroblasts in Tumor Microenvironment: Mapping Their Origins, Heterogeneity, and Role in Cancer Therapy Resistance. In *OMICS A Journal of Integrative Biology* (Vol. 24, Number 6, pp. 314–339). Mary Ann Liebert Inc. https://doi.org/10.1089/omi.2020.0023

Fan, C., Zhu, W., Chen, Y., Zhu, W., & Ding, J. (2025). Cancer-Associated Fibroblasts: Origin, Classification, Tumorigenicity, and Targeting for Cancer Therapy. In *MedComm* (Vol. 6, Number 11). John Wiley and Sons Inc. https://doi.org/10.1002/mco2.70415

Fan, H., Liu, W., Zeng, Y., Zhou, Y., Gao, M., Yang, L., Liu, H., Shi, Y., Li, L., Ma, J., Ruan, J., Cao, R., Jin, X., Chen, J., Cheng, G., & Yang, H. (2023). DNA damage induced by CDK4 and CDK6 blockade triggers anti-tumor immune responses through cGAS-STING pathway. *Communications Biology*, *6*(1). https://doi.org/10.1038/s42003-023-05412-x

Feng, Z., Zhang, C., Wu, R., & Hu, W. (2011). Tumor suppressor p53 meets microRNAs. *Journal of Molecular Cell Biology*, *3*(1), 44–50. https://doi.org/10.1093/jmcb/mjq040

Fontemaggi, G., Dell'Orso, S., Trisciuoglio, D., Shay, T., Melucci, E., Fazi, F., Terrenato, I., Mottolese, M., Muti, P., Domany, E., Del Bufalo, D., Strano, S., & Blandino, G. (2009). The execution of the transcriptional axis mutant p53, E2F1 and ID4 promotes tumor neo-angiogenesis. *Nature Structural and Molecular Biology*, *16*(10), 1086–1093. https://doi.org/10.1038/nsmb.1669

Foroutan, M., Bhuva, D. D., Lyu, R., Horan, K., Cursons, J., & Davis, M. J. (2018). Single sample scoring of molecular phenotypes. *BMC Bioinformatics*, *19*(1). https://doi.org/10.1186/s12859-018-2435-4

Frantz, C., Stewart, K. M., & Weaver, V. M. (2010). The extracellular matrix at a glance. In *Journal of Cell Science* (Vol. 123, Number 24, pp. 4195–4200). https://doi.org/10.1242/jcs.023820

Freed-Pastor, W. A., & Prives, C. (2012). Mutant p53: One name, many proteins. *Genes and Development*, *26*(12), 1268–1286. https://doi.org/10.1101/gad.190678.112

Frittoli, E., Palamidessi, A., Iannelli, F., Zanardi, F., Villa, S., Barzaghi, L., Abdo, H., Cancila, V., Beznoussenko, G. V., Della Chiara, G., Pagani, M., Malinverno, C., Bhattacharya, D., Pisati, F., Yu, W., Galimberti, V., Bonizzi, G., Martini, E., Mironov, A. A., … Scita, G. (2023). Tissue fluidification promotes a cGAS–STING cytosolic DNA response in invasive breast cancer. *Nature Materials*, *22*(5), 644–655. https://doi.org/10.1038/s41563-022-01431-x

Fu, Z., Mowday, A. M., Smaill, J. B., Hermans, I. F., & Patterson, A. V. (2021). Tumour hypoxia-mediated immunosuppression: Mechanisms and therapeutic approaches to improve cancer immunotherapy. In *Cells* (Vol. 10, Number 5). MDPI. https://doi.org/10.3390/cells10051006

Gan, Y., Li, X., Han, S., Liang, Q., Ma, X., Rong, P., Wang, W., & Li, W. (2022). The cGAS/STING Pathway: A Novel Target for Cancer Therapy. In *Frontiers in Immunology* (Vol. 12). Frontiers Media S.A. https://doi.org/10.3389/fimmu.2021.795401

Gao, P., Ascano, M., Wu, Y., Barchet, W., Gaffney, B. L., Zillinger, T., Serganov, A. A., Liu, Y., Jones, R. A., Hartmann, G., Tuschl, T., & Patel, D. J. (2013). Cyclic [G(2′,5′)pA(3′,5′)p] is the metazoan second messenger produced by DNA-activated cyclic GMP-AMP synthase. *Cell*, *153*(5), 1094–1107. https://doi.org/10.1016/j.cell.2013.04.046

Gao, Y., Yi, J., Zhang, K., Bai, F., Feng, B., Wang, R., Chu, X., Chen, L., & Song, H. (2017). Downregulation of miR-31 stimulates expression of LATS2 via the hippo pathway and promotes epithelial-mesenchymal transition in esophageal squamous cell carcinoma. *Journal of Experimental and Clinical Cancer Research*, *36*(1). https://doi.org/10.1186/s13046-017-0622-1

Gareev, I., de Jesus Encarnacion Ramirez, M., Goncharov, E., Ivliev, D., Shumadalova, A., Ilyasova, T., & Wang, C. (2023). MiRNAs and lncRNAs in the regulation of innate immune signaling. In *Non-coding RNA Research* (Vol. 8, Number 4, pp. 534–541). KeAi Communications Co. https://doi.org/10.1016/j.ncrna.2023.07.002

Gaziel-Sovran, A., Segura, M. F., Di Micco, R., Collins, M. K., Hanniford, D., Vega-Saenz de Miera, E., Rakus, J. F., Dankert, J. F., Shang, S., Kerbel, R. S., Bhardwaj, N., Shao, Y., Darvishian, F., Zavadil, J., Erlebacher, A., Mahal, L. K., Osman, I., & Hernando, E. (2011). MiR-30b/30d Regulation of GalNAc Transferases Enhances Invasion and Immunosuppression during Metastasis. *Cancer Cell*, *20*(1), 104–118. https://doi.org/10.1016/j.ccr.2011.05.027

Gershoni, A., Hassin, O., Nataraj, N. B., Baruch, S., Avioz-Seligman, A., Pirona, A. C., Fellus-Alyagor, L., Meir Salame, T., Mukherjee, S., Mallel, G., Yarden, Y., Aylon, Y., & Oren, M. (2023). TAZ facilitates breast tumor growth by promoting an immune-suppressive tumor microenvironment. *Molecular Oncology*, *17*(12), 2675–2693. https://doi.org/10.1002/1878-0261.13525

Ghosh, M., Saha, S., Bettke, J., Nagar, R., Parrales, A., Iwakuma, T., van der Velden, A. W. M., & Martinez, L. A. (2021). Mutant p53 suppresses innate immune signaling to promote

tumorigenesis. *CancerCell*, *39*(4), 494-508.e5. https://doi.org/10.1016/j.ccell.2021.01.003

Ghosh, M., Saha, S., Li, J., Montrose, D. C., & Martinez, L. A. (2023). p53 engages the cGAS/STING cytosolic DNA sensing pathway for tumor suppression. *Molecular Cell*, *83*(2), 266-280.e6. https://doi.org/10.1016/j.molcel.2022.12.023

Gil Del Alcazar, C. R., Huh, S. J., Ekram, M. B., Trinh, A., Liu, L. L., Beca, F., Zi, X., Kwak, M., Bergholtz, H., Su, Y., Ding, L., Russnes, H. G., Richardson, A. L., Babski, K., Kim, E. M. H., McDonnell, C. H., Wagner, J., Rowberry, R., Freeman, G. J., … Polyak, K. (2017). Immune escape in breast cancer during in situ to invasive carcinoma transition. *Cancer Discovery*, *7*(10), 1098–1115. https://doi.org/10.1158/2159-8290.CD-17-0222

Han, H. S., Kim, M. J., Han, J. H., Yun, J., Kim, H. K., Yang, Y., Kim, K. B., & Park, S. M. (2020). Bile-derived circulating extracellular miR-30d-5p and miR-92a-3p as potential biomarkers for cholangiocarcinoma. *Hepatobiliary and Pancreatic Diseases International*, *19*(1), 41–50. https://doi.org/10.1016/j.hbpd.2019.10.009

Han, M., Wang, Y., Guo, G., Li, L., Dou, D., Ge, X., Lv, P., Wang, F., & Gu, Y. (2018). microRNA-30d mediated breast cancer invasion, migration, and EMT by targeting KLF11 and activating STAT3 pathway. *Journal of Cellular Biochemistry*, *119*(10), 8138–8145. https://doi.org/10.1002/jcb.26767

Hao, F. (2022). An overview of the crosstalk between YAP and cGAS-STING signaling in non-small cell lung cancer: it takes two to tango. In *Clinical and Translational Oncology* (Vol. 24, Number 9, pp. 1661–1672). Springer Science and Business Media Deutschland GmbH. https://doi.org/10.1007/s12094-022-02826-7

Harris, M. A., Savas, P., Virassamy, B., O'Malley, M. M. R., Kay, J., Mueller, S. N., Mackay, L. K., Salgado, R., & Loi, S. (2024). Towards targeting the breast cancer immune microenvironment. In *Nature Reviews Cancer* (Vol. 24, Number 8, pp. 554–577). Nature Research. https://doi.org/10.1038/s41568-024-00714-6

He, T. S., Dang, L., Zhang, J., Zhang, J., Wang, G., Wang, E., Xia, H., Zhou, W., Wu, S., & Liu, X. (2022). The Hippo signaling component LATS2 enhances innate immunity to inhibit HIV-1 infection through PQBP1-cGAS pathway. *Cell Death and Differentiation*, *29*(1), 192–205. https://doi.org/10.1038/s41418-021-00849-1

Heath, A. P., Ferretti, V., Agrawal, S., An, M., Angelakos, J. C., Arya, R., Bajari, R., Baqar, B., Barnowski, J. H. B., Burt, J., Catton, A., Chan, B. F., Chu, F., Cullion, K., Davidsen, T., Do, P. M., Dompierre, C., Ferguson, M. L., Fitzsimons, M. S., … Grossman, R. L. (2021). The NCI Genomic Data Commons. In *Nature Genetics* (Vol. 53, Number 3, pp. 257–262). Nature Research. https://doi.org/10.1038/s41588-021-00791-5

Hernández Borrero, L. J., & El-Deiry, W. S. (2021). Tumor suppressor p53: Biology, signaling pathways, and therapeutic targeting. In *Biochimica et Biophysica Acta - Reviews on Cancer* (Vol. 1876, Number 1). Elsevier B.V. https://doi.org/10.1016/j.bbcan.2021.188556

Hida, K., Maishi, N., Torii, C., & Hida, Y. (2016). Tumor angiogenesis—characteristics of tumor endothelial cells. In *International Journal of Clinical Oncology* (Vol. 21, Number 2, pp. 206–212). Springer Tokyo. https://doi.org/10.1007/s10147-016-0957-1

Hines, J. B., Kacew, A. J., & Sweis, R. F. (2023). The Development of STING Agonists and Emerging Results as a Cancer Immunotherapy. In *Current Oncology Reports* (Vol. 25, Number 3, pp. 189–199). Springer. https://doi.org/10.1007/s11912-023-01361-0

Hooglugt, A., van der Stoel, M. M., Boon, R. A., & Huveneers, S. (2021). Endothelial YAP/TAZ Signaling in Angiogenesis and Tumor Vasculature. In *Frontiers in Oncology* (Vol. 10). Frontiers Media S.A. https://doi.org/10.3389/fonc.2020.612802

Hopfner, K. P., & Hornung, V. (2020). Molecular mechanisms and cellular functions of cGAS–STING signalling. In *Nature Reviews Molecular Cell Biology* (Vol. 21, Number 9, pp. 501–521). Nature Research. https://doi.org/10.1038/s41580-020-0244-x

Hosea, R., Hillary, S., Naqvi, S., Wu, S., & Kasim, V. (2024). The two sides of chromosomal instability: drivers and brakes in cancer. In *Signal Transduction and Targeted Therapy* (Vol. 9, Number 1). Springer Nature. https://doi.org/10.1038/s41392-024-01767-7

Hou, Y., Liang, H., Rao, E., Zheng, W., Huang, X., Deng, L., Zhang, Y., Yu, X., Xu, M., Mauceri, H., Arina, A., Weichselbaum, R. R., & Fu, Y.-X. (2018). Non-canonical NF-κB Antagonizes STING Sensor-Mediated DNA Sensing in Radiotherapy HHS Public Access. *Immunity*, *49*(3), 490–503. https://doi.org/10.1016/j.immuni

Houthuijzen, J. M., de Bruijn, R., van der Burg, E., Drenth, A. P., Wientjens, E., Filipovic, T., Bullock, E., Brambillasca, C. S., Pulver, E. M., Nieuwland, M., de Rink, I., van Diepen, F., Klarenbeek, S., Kerkhoven, R., Brunton, V. G., Scheele, C. L. G. J., Boelens, M. C., & Jonkers, J. (2023). CD26-negative and CD26-positive tissue-resident fibroblasts contribute to functionally distinct CAF subpopulations in breast cancer. *Nature Communications*, *14*(1). https://doi.org/10.1038/s41467-023-35793-w

Hu, J., Sánchez-Rivera, F. J., Wang, Z., Johnson, G. N., Ho, Y. jui, Ganesh, K., Umeda, S., Gan, S., Mujal, A. M., Delconte, R. B., Hampton, J. P., Zhao, H., Kottapalli, S., de Stanchina, E., Iacobuzio-Donahue, C. A., Pe'er, D., Lowe, S. W., Sun, J. C., & Massagué, J. (2023). STING inhibits the reactivation of dormant metastasis in lung adenocarcinoma. *Nature*, *616*(7958), 806–813. https://doi.org/10.1038/s41586-023-05880-5

Hu, M., Yao, J., Carroll, D. K., Weremowicz, S., Chen, H., Carrasco, D., Richardson, A., Violette, S., Nikolskaya, T., Nikolsky, Y., Bauerlein, E. L., Hahn, W. C., Gelman, R. S., Allred, C., Bissell, M. J., Schnitt, S., & Polyak, K. (2008). Regulation of In Situ to Invasive Breast Carcinoma Transition. *Cancer Cell*, *13*(5), 394–406. https://doi.org/10.1016/j.ccr.2008.03.007

Huang, R., Kang, T., & Chen, S. (2024). The role of tumor-associated macrophages in tumor immune evasion. In *Journal of Cancer Research and Clinical Oncology* (Vol. 150, Number 5). Springer Science and Business Media Deutschland GmbH. https://doi.org/10.1007/s00432-024-05777-4

Hwang, D., Kim, M., Kim, S., Kwon, M. R., Kang, Y. S., Kim, D., Kang, H. C., & Lim, D. S. (2021). AMOTL2 mono-ubiquitination by WWP1 promotes contact inhibition by facilitating LATS activation. *Life Science Alliance*, *4*(10). https://doi.org/10.26508/LSA.202000953

Ingallina, E., Sorrentino, G., Bertolio, R., Lisek, K., Zannini, A., Azzolin, L., Severino, L. U., Scaini, D., Mano, M., Mantovani, F., Rosato, A., Bicciato, S., Piccolo, S., & Del Sal, G.

(2018). Mechanical cues control mutant p53 stability through a mevalonate-RhoA axis. *Nature Cell Biology*, *20*(1), 28–35. https://doi.org/10.1038/s41556-017-0009-8

Ishikawa, H., & Barber, G. N. (2008). STING is an endoplasmic reticulum adaptor that facilitates innate immune signalling. *Nature*, *455*(7213), 674–678. https://doi.org/10.1038/nature07317

Ishikawa, H., Ma, Z., & Barber, G. N. (2009). STING regulates intracellular DNA-mediated, type i interferon-dependent innate immunity. *Nature*, *461*(7265), 788–792. https://doi.org/10.1038/nature08476

Iurescia, S., Fioretti, D., & Rinaldi, M. (2018). Targeting cytosolic nucleic acid-sensing pathways for cancer immunotherapies. In *Frontiers in Immunology* (Vol. 9, Number APR). Frontiers Media S.A. https://doi.org/10.3389/fimmu.2018.00711

Jacob, H., Stanisavljevic, L., Storli, K. E., Hestetun, K. E., Dahl, O., & Myklebust, M. P. (2017). Identification of a sixteen-microRNA signature as prognostic biomarker for stage II and III colon cancer. *Oncotarget, 8(50), 87837.* https://www.oncotarget.com/article/21237/text/

Jagosky, M., & Tan, A. R. (2021). Combination of pertuzumab and trastuzumab in the treatment of her2-positive early breast cancer: A review of the emerging clinical data. In *Breast Cancer: Targets and Therapy* (Vol. 13, pp. 393–407). Dove Medical Press Ltd. https://doi.org/10.2147/BCTT.S176514

Jia, H., Chen, X., Zhang, L., & Chen, M. (2025). Cancer associated fibroblasts in cancer development and therapy. In *Journal of Hematology and Oncology* (Vol. 18, Number 1). BioMed Central Ltd. https://doi.org/10.1186/s13045-025-01688-0

Junnuthula, V., Kolimi, P., Nyavanandi, D., Sampathi, S., Vora, L. K., & Dyawanapelly, S. (2022). Polymeric Micelles for Breast Cancer Therapy: Recent Updates, Clinical Translation and Regulatory Considerations. In *Pharmaceutics* (Vol. 14, Number 9). MDPI. https://doi.org/10.3390/pharmaceutics14091860

Kalluri, R. (2016). The biology and function of fibroblasts in cancer. In *Nature Reviews Cancer* (Vol. 16, Number 9, pp. 582–598). Nature Publishing Group. https://doi.org/10.1038/nrc.2016.73

Kalukula, Y., Stephens, A. D., Lammerding, J., & Gabriele, S. (2022). Mechanics and functional consequences of nuclear deformations. In *Nature Reviews Molecular Cell Biology* (Vol. 23, Number 9, pp. 583–602). Nature Research. https://doi.org/10.1038/s41580-022-00480-z

Katoh, K. (2025). Integrin and Its Associated Proteins as a Mediator for Mechano-Signal Transduction. In *Biomolecules* (Vol. 15, Number 2). Multidisciplinary Digital Publishing Institute (MDPI). https://doi.org/10.3390/biom15020166

Katuwal, N. B., Park, N., Pandey, K., Kang, M. S., Hong, S. D., Ghosh, M., Kim, S. G., Cho, Y. Bin, Hur, J., Kim, S. K., & Moon, Y. W. (2023). Preclinical Platform Using a Triple-negative Breast Cancer Syngeneic Murine Model to Evaluate Immune Checkpoint Inhibitors. *Anticancer Research*, *43*(1), 85–95. https://doi.org/10.21873/anticanres.16137

Kau, P., Nagaraja, G. M., Zheng, H., Gizachew, D., Galukande, M., Krishnan, S., & Asea, A. (2012). A mouse model for triple-negative breast cancer tumor-initiating cells (TNBC-TICs) exhibits similar aggressive phenotype to the human disease. *BMC Cancer*, *12*. https://doi.org/10.1186/1471-2407-12-120

Khosravi, G. R., Mostafavi, S., Bastan, S., Ebrahimi, N., Gharibvand, R. S., & Eskandari, N. (2024). Immunologic tumor microenvironment modulators for turning cold tumors hot. In *Cancer Communications* (Vol. 44, Number 5, pp. 521–553). John Wiley and Sons Inc. https://doi.org/10.1002/cac2.12539

Kim, E. H., Lee, J., Kwak, G., Jang, H., Kim, H., Cho, H., Jang, Y., Choi, J., Chi, S. G., Kim, K., Kwon, I. C., Yang, Y., & Kim, S. H. (2022). PDL1-binding peptide/anti-miRNA21 conjugate as a therapeutic modality for PD-L1high tumors and TAMs. In *Journal of Controlled Release* (Vol. 345, pp. 62–74). Elsevier B.V. https://doi.org/10.1016/j.jconrel.2022.02.031

Kim, H. S., & Nam, J. S. (2025). The multifaceted role of YAP in the tumor microenvironment and its therapeutic implications in cancer. In *Experimental and Molecular Medicine* (Vol. 57, Number 10, pp. 2201–2213). Springer Nature. https://doi.org/10.1038/s12276-025-01551-9

Kim, M., Kim, T., Johnson, R. L., & Lim, D. S. (2015). Transcriptional co-repressor function of the hippo pathway transducers YAP and TAZ. *Cell Reports*, *11*(2), 270–282. https://doi.org/10.1016/j.celrep.2015.03.015

Knarr, M., Avelar, R. A., Sekhar, S. C., Kwiatkowski, L. J., Dziubinski, M. L., McAnulty, J., Skala, S., Avril, S., Drapkin, R., & DiFeo, A. (2020). miR-181a initiates and perpetuates oncogenic transformation through the regulation of innate immune signaling. *Nature Communications*, *11*(1). https://doi.org/10.1038/s41467-020-17030-w

Kumar, M., Lu, Z., Takwi, A. A. L., Chen, W., Callander, N. S., Ramos, K. S., Young, K. H., & Li, Y. (2011). Negative regulation of the tumor suppressor p53 gene by microRNAs. *Oncogene*, *30*(7), 843–853. https://doi.org/10.1038/onc.2010.457

Kuo, L. J. , & Y. L. X. (2008). γ-H2AX – A Novel Biomarker for DNA Double-strand Breaks. *In vivo, 22*(3), 305-309. https://iv.iiarjournals.org/content/invivo/22/3/305.full.pdf

Lammerding, J., Fong, L. G., Ji, J. Y., Reue, K., Stewart, C. L., Young, S. G., & Lee, R. T. (2006). Lamins a and C but not lamin B1 regulate nuclear mechanics. *Journal of Biological Chemistry*, *281*(35), 25768–25780. https://doi.org/10.1074/jbc.M513511200

Lan, X., Li, W., Zhao, K., Wang, J., Li, S., & Zhao, H. (2025). Revisiting the role of cancer-associated fibroblasts in tumor microenvironment. In *Frontiers in Immunology* (Vol. 16). Frontiers Media SA. https://doi.org/10.3389/fimmu.2025.1582532

Larrieu, D., Britton, S., Demir, M., Rodriguez, R., & Jackson, S. P. (2014). Chemical inhibition of NAT10 corrects defects of laminopathic cells. *Science*, *344*(6183), 527–532. https://doi.org/10.1126/science.1252651

Lasek, W. (2022). Cancer immunoediting hypothesis: history, clinical implications and controversies. In *Central European Journal of Immunology* (Vol. 47, Number 2, pp. 168–174). Termedia Publishing House Ltd. https://doi.org/10.5114/ceji.2022.117376

Lee, R. C., Feinbaum, R. L., & Ambrost, V. (1993). The C. elegans Heterochronic Gene lin-4 Encodes Small RNAs with Antisense Complementarity to &II-14. In *Cell* (Vol. 75). https://www.cell.com/action/showPdf?pii=0092-8674%2893%2990529-Y

Li, J., Hubisz, M. J., Earlie, E. M., Duran, M. A., Hong, C., Varela, A. A., Lettera, E., Deyell, M., Tavora, B., Havel, J. J., Phyu, S. M., Amin, A. D., Budre, K., Kamiya, E., Cavallo, J. A., Garris, C., Powell, S., Reis-Filho, J. S., Wen, H., … Bakhoum, S. F. (2023). Non-cell-autonomous cancer progression from chromosomal instability. *Nature*, *620*(7976), 1080–1088. https://doi.org/10.1038/s41586-023-06464-z

Li, J., Salvador, A. M., Li, G., Valkov, N., Ziegler, O., Yeri, A., Yang Xiao, C., Meechoovet, B., Alsop, E., Rodosthenous, R. S., Kundu, P., Huan, T., Levy, D., Tigges, J., Pico, A. R., Ghiran, I., Silverman, M. G., Meng, X., Kitchen, R., … Das, S. (2021). Mir-30d Regulates Cardiac Remodeling by Intracellular and Paracrine Signaling. *Circulation Research*, *128*(1), E1–E23. https://doi.org/10.1161/CIRCRESAHA.120.317244

Li, J., Zhang, Q., Jiang, D., Shao, J., Li, W., & Wang, C. (2022). CircRNAs in lung cancer- role and clinical application. *Cancer Letters*, *544*. https://doi.org/10.1016/j.canlet.2022.215810

Li, N., Kaur, S., Greshock, J., Lassus, H., Zhong, X., Wang, Y., Leminen, A., Shao, Z., Hu, X., Liang, S., Katsaros, D., Huang, Q., Bützow, R., Weber, B. L., Coukos, G., & Zhang, L. (2012). A combined array-based comparative genomic hybridization and functional library screening approach identifies mir-30d as an oncomir in cancer. *Cancer Research*, *72*(1), 154–164. https://doi.org/10.1158/0008-5472.CAN-11-2484

Li, N., Xie, C., & Lu, N. (2017). Crosstalk between Hippo signalling and miRNAs in tumour progression. In *FEBS Journal* (Vol. 284, Number 7, pp. 1045–1055). Blackwell Publishing Ltd. https://doi.org/10.1111/febs.13985

Li, X., Tran, K. M., Aziz, K. E., Sorokin, A. V., Chen, J., & Wang, W. (2016). Defining the protein-protein interaction network of the human protein tyrosine phosphatase family. *Molecular and Cellular Proteomics*, *15*(9), 3030–3044. https://doi.org/10.1074/mcp.M116.060277

Lim, J., Rodriguez, R., Williams, K., Silva, J., Gutierrez, A. G., Tyler, P., Baharom, F., Sun, T., Lin, E., Martin, S., Kayser, B. D., Johnston, R. J., Mellman, I., Delamarre, L., West, N. R., Müller, S., Qu, Y., & Heger, K. (2024). The Exonuclease TREX1 Constitutes an Innate Immune Checkpoint Limiting cGAS/STING-Mediated Antitumor Immunity. *Cancer Immunology Research*, *12*(6), 663–672. https://doi.org/10.1158/2326-6066.CIR-23-1078

Lin, S., & Gregory, R. I. (2015). MicroRNA biogenesis pathways in cancer. In *Nature Reviews Cancer* (Vol. 15, Number 6, pp. 321–333). Nature Publishing Group. https://doi.org/10.1038/nrc3932

Lin, Z. yuan, Chen, G., Zhang, Y. qiong, He, H. chan, Liang, Y. xiang, Ye, J. heng, Liang, Y. ke, Mo, R. jun, Lu, J. ming, Zhuo, Y. jia, Zheng, Y., Jiang, F. neng, Han, Z. dong, Wu, S. lin, Zhong, W. de, & Wu, C. L. (2017). MicroRNA-30d promotes angiogenesis and tumor growth via MYPT1/c-JUN/VEGFA pathway and predicts aggressive outcome in prostate cancer. *Molecular Cancer*, *16*(1). https://doi.org/10.1186/s12943-017-0615-x

Liu, L., Yu, J., Liu, Y., Xie, L., Hu, F., & Liu, H. (2025). Hypoxia-driven angiogenesis and metabolic reprogramming in vascular tumors. In *Frontiers in Cell and Developmental Biology* (Vol. 13). Frontiers Media SA. https://doi.org/10.3389/fcell.2025.1572909

Lohard, S., Bourgeois, N., Maillet, L., Gautier, F., Fétiveau, A., Lasla, H., Nguyen, F., Vuillier, C., Dumont, A., Moreau-Aubry, A., Frapin, M., David, L., Loussouarn, D., Kerdraon, O., Campone, M., Jézéquel, P., Juin, P. P., & Barillé-Nion, S. (2020). STING-dependent paracriny shapes apoptotic priming of breast tumors in response to anti-mitotic treatment. *Nature Communications*, *11*(1). https://doi.org/10.1038/s41467-019-13689-y

López, L., Morosi, L. G., La Terza, F., Bourdely, P., Rospo, G., Amadio, R., Piperno, G. M., Russo, V., Volponi, C., Vodret, S., Joshi, S., Giannese, F., Lazarevic, D., Germano, G., Stoitzner, P., Bardelli, A., Dalod, M., Pace, L., Caronni, N., … Benvenuti, F. (2024). Dendritic cell-targeted therapy expands CD8 T cell responses to bona-fide neoantigens in lung tumors. *Nature Communications*, *15*(1). https://doi.org/10.1038/s41467-024-46685-y

Lowry, M. C., & O'Driscoll, L. (2018). Can hi-jacking hypoxia inhibit extracellular vesicles in cancer? In *Drug Discovery Today* (Vol. 23, Number 6, pp. 1267–1273). Elsevier Ltd. https://doi.org/10.1016/j.drudis.2018.03.006

Lozano, G., Prives, C., & Sabapathy, K. (2025). Mutant p53 Gain of Function: Why Many See It, Why Some Do Not. *Cancer Discovery*, *15*(6), 1099–1103. https://doi.org/10.1158/2159-8290.CD-24-1638

Lujambio, A., Akkari, L., Simon, J., Grace, D., Tschaharganeh, D. F., Bolden, J. E., Zhao, Z., Thapar, V., Joyce, J. A., Krizhanovsky, V., & Lowe, S. W. (2013). Non-cell-autonomous tumor suppression by p53. *Cell, 153*(2), 449-460. https://pmc.ncbi.nlm.nih.gov/articles/PMC3702034/

Luo, J., Xiang, X., Gong, G., & Jiang, L. (2025). Cancer-associated fibroblast-mediated immune evasion: molecular mechanisms of stromal-immune crosstalk in the tumor microenvironment. In *Frontiers in Immunology* (Vol. 16). Frontiers Media SA. https://doi.org/10.3389/fimmu.2025.1617662

Luo, J., Zou, H., Guo, Y., Tong, T., Chen, Y., Xiao, Y., Pan, Y., & Li, P. (2023). The oncogenic roles and clinical implications of YAP/TAZ in breast cancer. In *British Journal of Cancer* (Vol. 128, Number 9, pp. 1611–1624). Springer Nature. https://doi.org/10.1038/s41416-023-02182-5

Luo, Z., Tian, M., Yang, G., Tan, Q., Chen, Y., Li, G., Zhang, Q., Li, Y., Wan, P., & Wu, J. (2022). Hypoxia signaling in human health and diseases: implications and prospects for therapeutics. In *Signal Transduction and Targeted Therapy* (Vol. 7, Number 1). Springer Nature. https://doi.org/10.1038/s41392-022-01080-1

Ma, S., McGuire, M. H., Mangala, L. S., Lee, S., Stur, E., Hu, W., Bayraktar, E., Villar-Prados, A., Ivan, C., Wu, S. Y., Yokoi, A., Dasari, S. K., Jennings, N. B., Liu, J., Lopez-Berestein, G., Ram, P., & Sood, A. K. (2021). Gain-of-function p53 protein transferred via small extracellular vesicles promotes conversion of fibroblasts to a cancer-associated phenotype. *Cell Reports*, *34*(6). https://doi.org/10.1016/j.celrep.2021.108726

Mahat, D. B., Kumra, H., Castro, S. A., Metcalf, E., Nguyen, K., Morisue, R., Ho, W. W., Chen, I., Sullivan, B., Yim, L. H., Singh, A., Fu, J., Waterton, S. K., Cheng, Y. C., Moiso, E., Chauhan, V. P., Silva, H. M., Spranger, S., Jain, R. K., & Sharp, P. A. (2025). Mutant p53 exploits enhancers to elevate immunosuppressive chemokine expression and impair immune checkpoint inhibitors in pancreatic cancer. *Immunity*, *58*(7), 1688-1705.e9. https://doi.org/10.1016/j.immuni.2025.06.005

Maiato, H., & Silva, S. (2023). Double-checking chromosome segregation. In *Journal of Cell Biology* (Vol. 222, Number 5). Rockefeller University Press. https://doi.org/10.1083/jcb.202301106

Mantovani, F., Collavin, L., & Del Sal, G. (2019). Mutant p53 as a guardian of the cancer cell. In *Cell Death and Differentiation* (Vol. 26, Number 2, pp. 199–212). Nature Publishing Group. https://doi.org/10.1038/s41418-018-0246-9

Mao, L., Liu, S., Hu, L., Jia, L., Wang, H., Guo, M., Chen, C., Liu, Y., & Xu, L. (2018). MiR-30 Family: A Promising Regulator in Development and Disease. In *BioMed Research International* (Vol. 2018). Hindawi Limited. https://doi.org/10.1155/2018/9623412

Marcus, A., Mao, A. J., Lensink-Vasan, M., Wang, L. A., Vance, R. E., & Raulet, D. H. (2018). Tumor-Derived cGAMP Triggers a STING-Mediated Interferon Response in Non-tumor Cells to Activate the NK Cell Response. *Immunity*, *49*(4), 754-763.e4. https://doi.org/10.1016/j.immuni.2018.09.016

Martino, M. T. Di, Tagliaferri, P., & Tassone, P. (2025). MicroRNA in cancer therapy: breakthroughs and challenges in early clinical applications. In *Journal of Experimental and Clinical Cancer Research* (Vol. 44, Number 1). BioMed Central Ltd. https://doi.org/10.1186/s13046-025-03391-x

Matuszewska, K., Pereira, M., Petrik, D., Lawler, J., & Petrik, J. (2021). Normalizing tumor vasculature to reduce hypoxia, enhance perfusion, and optimize therapy uptake. In *Cancers* (Vol. 13, Number 17). MDPI. https://doi.org/10.3390/cancers13174444

Mc Neil, V., & Lee, S. W. (2025). Advancing Cancer Treatment: A Review of Immune Checkpoint Inhibitors and Combination Strategies. In *Cancers* (Vol. 17, Number 9). Multidisciplinary Digital Publishing Institute (MDPI). https://doi.org/10.3390/cancers17091408

McGettrick, A. F., & O'Neill, L. A. J. (2020). The Role of HIF in Immunity and Inflammation. In *Cell Metabolism* (Vol. 32, Number 4, pp. 524–536). Cell Press. https://doi.org/10.1016/j.cmet.2020.08.002

Melman, Y. F., Shah, R., Danielson, K., Xiao, J., Simonson, B., Barth, A., Chakir, K., Lewis, G. D., Lavender, Z., Truong, Q. A., Kleber, A., Das, R., Rosenzweig, A., Wang, Y., Kass, D. A., Singh, J. P., & Das, S. (2015). Circulating microRNA-30d is associated with response to cardiac resynchronization therapy in heart failure and regulates cardiomyocyte apoptosis: A translational pilot study. In *Circulation* (Vol. 131, Number 25, pp. 2202–2216). Lippincott Williams and Wilkins. https://doi.org/10.1161/CIRCULATIONAHA.114.013220

Miao, H., Fang, Y., Pan, C., Yang, H., Wang, Z., Qi, Y., Wu, Y., Zhang, Y., Liu, F., Huang, H., Tang, Y., Wu, D., & Li, N. (2025). Transforming the landscape of cancer treatment with

seven promising novel therapies: evolution and future perspectives. In *Medicine Plus* (Vol. 2, Number 2). KeAi Publishing Communications Ltd. https://doi.org/10.1016/j.medp.2025.100087

Miller, F., Santner, S., Tait, L., & Dawson, P. (2000). MCF10DCIS.com Xenograft Model of Human Comedo Ductal Carcinoma In Situ*. Journal of the National Cancer Institute, 92*(14), 1185a-1186*.* https://academic.oup.com/jnci/article/92/14/1185a/2905877

Miller, K. N., Victorelli, S. G., Salmonowicz, H., Dasgupta, N., Liu, T., Passos, J. F., & Adams, P. D. (2021). Cytoplasmic DNA: sources, sensing, and role in aging and disease. *Cell*, *184*(22), 5506–5526. https://doi.org/10.1016/j.cell.2021.09.034

Min, H. Y., & Lee, H. Y. (2022). Molecular targeted therapy for anticancer treatment. In *Experimental and Molecular Medicine* (Vol. 54, Number 10, pp. 1670–1694). Springer Nature. https://doi.org/10.1038/s12276-022-00864-3

Monjazeb, A. M., Wang, Z., Vick, L. V., Dunai, C., Minnar, C., Khuat, L. T., & Murphy, W. J. (2021). Mouse preclinical cancer immunotherapy modeling involving anti-pd-1 therapies reveals the need to use mouse reagents to mirror clinical paradigms. *Cancers*, *13*(4), 1–13. https://doi.org/10.3390/cancers13040729

Montagner, M., Enzo, E., Forcato, M., Zanconato, F., Parenti, A., Rampazzo, E., Basso, G., Leo, G., Rosato, A., Bicciato, S., Cordenonsi, M., & Piccolo, S. (2012). SHARP1 suppresses breast cancer metastasis by promoting degradation of hypoxia-inducible factors. *Nature*, *487*(7407), 380–384. https://doi.org/10.1038/nature11207

Morrissey, R. L., Thompson, A. M., & Lozano, G. (2022). Is loss of p53 a driver of ductal carcinoma in situ progression? In *British Journal of Cancer* (Vol. 127, Number 10, pp. 1744–1754). Springer Nature. https://doi.org/10.1038/s41416-022-01885-5

Moya, I. M., & Halder, G. (2019). Hippo–YAP/TAZ signalling in organ regeneration and regenerative medicine. In *Nature Reviews Molecular Cell Biology* (Vol. 20, Number 4, pp. 211–226). Nature Publishing Group. https://doi.org/10.1038/s41580-018-0086-y

Mukai, K., Konno, H., Akiba, T., Uemura, T., Waguri, S., Kobayashi, T., Barber, G. N., Arai, H., & Taguchi, T. (2016). Activation of STING requires palmitoylation at the Golgi. *Nature Communications*, *7*. https://doi.org/10.1038/ncomms11932

Müller, S., Wedler, A., Breuer, J., Glaß, M., Bley, N., Lederer, M., Haase, J., Misiak, C., Fuchs, T., Ottmann, A., Schmachtel, T., Shalamova, L., Ewe, A., Aigner, A., Rossbach, O., & Hüttelmaier, S. (2020). Synthetic circular miR-21 RNA decoys enhance tumor suppressor expression and impair tumor growth in mice. *NAR Cancer*, *2*(3). https://doi.org/10.1093/narcan/zcaa014

Nader, G. P. de F., Agüera-Gonzalez, S., Routet, F., Gratia, M., Maurin, M., Cancila, V., Cadart, C., Palamidessi, A., Ramos, R. N., San Roman, M., Gentili, M., Yamada, A., Williart, A., Lodillinsky, C., Lagoutte, E., Villard, C., Viovy, J. L., Tripodo, C., Galon, J., … Piel, M. (2021). Compromised nuclear envelope integrity drives TREX1-dependent DNA damage and tumor cell invasion. *Cell*, *184*(20), 5230-5246.e22. https://doi.org/10.1016/j.cell.2021.08.035

Nandwani, A., Rathore, S., & Datta, M. (2021). LncRNAs in cancer: Regulatory and therapeutic implications. In *Cancer Letters* (Vol. 501, pp. 162–171). Elsevier Ireland Ltd. https://doi.org/10.1016/j.canlet.2020.11.048

Obidiro, O., Battogtokh, G., & Akala, E. O. (2023). Triple Negative Breast Cancer Treatment Options and Limitations: Future Outlook. In *Pharmaceutics* (Vol. 15, Number 7). Multidisciplinary Digital Publishing Institute (MDPI). https://doi.org/10.3390/pharmaceutics15071796

Panciera, T., Azzolin, L., Cordenonsi, M., & Piccolo, S. (2017). Mechanobiology of YAP and TAZ in physiology and disease. *Nature Reviews Molecular Cell Biology*, *18*(12), 758–770. https://doi.org/10.1038/nrm.2017.87

Pantelidou, C., Sonzogni, O., Taveira, M. D. O., Mehta, A. K., Kothari, A., Wang, D., Visal, T., Li, M. K., Pinto, J., Castrillon, J. A., Cheney, E. M., Bouwman, P., Jonkers, J., Rottenberg, S., Guerriero, J. L., Wulf, G. M., & Shapiro, G. I. (2019). Parp inhibitor efficacy depends on CD8+ T-cell recruitment via intratumoral sting pathway activation in brca-deficient models of triple-negative breast cancer. *Cancer Discovery*, *9*(6), 722–737. https://doi.org/10.1158/2159-8290.CD-18-1218

Park, A. Y., Kim, J. H., Lee, S., Kim, H. S., Kim, H. K., Lee, H. B., & Han, W. (2025). Impact of PD-L1 upregulation on immune checkpoint inhibitor efficacy in triple-negative breast cancer using a 4T1 murine model. *International Journal of Oncology*, *67*(1). https://doi.org/10.3892/ijo.2025.5760

Petrosyan, A., Holzapfel, M. S., Muirhead, D. E., & Cheng, P. W. (2014). Restoration of compact golgi morphology in advanced prostate cancer enhances susceptibility to galectin-1-induced apoptosis by modifying mucin O-glycan synthesis. *Molecular Cancer Research*, *12*(12), 1704–1716. https://doi.org/10.1158/1541-7786.MCR-14-0291-T

Petrova, V., Annicchiarico-Petruzzelli, M., Melino, G., & Amelio, I. (2018). The hypoxic tumour microenvironment. In *Oncogenesis* (Vol. 7, Number 1). Nature Publishing Group. https://doi.org/10.1038/s41389-017-0011-9

Piccolo, S., Panciera, T., Contessotto, P., & Cordenonsi, M. (2023). YAP/TAZ as master regulators in cancer: modulation, function and therapeutic approaches. In *Nature Cancer* (Vol. 4, Number 1, pp. 9–26). Nature Research. https://doi.org/10.1038/s43018-022-00473-z

Piha-Paul, S. A., Tseng, C., Leung, C. H., Yuan, Y., Karp, D. D., Subbiah, V., Hong, D., Fu, S., Naing, A., Rodon, J., Javle, M., Ajani, J. A., Raghav, K. P., Somaiah, N., Mills, G. B., Tsimberidou, A. M., Zheng, X., Chen, K., & Meric-Bernstam, F. (2024). Phase II study of talazoparib in advanced cancers with BRCA1/2, DNA repair, and PTEN alterations. *Npj Precision Oncology*, *8*(1). https://doi.org/10.1038/s41698-024-00634-6

Prakash, J., & Shaked, Y. (2024). The Interplay between Extracellular Matrix Remodeling and Cancer Therapeutics. In *Cancer Discovery* (Vol. 14, Number 8, pp. 1375–1388). American Association for Cancer Research Inc. https://doi.org/10.1158/2159-8290.CD-24-0002

Pusztai, L., Yau, C., Wolf, D. M., Han, H. S., Du, L., Wallace, A. M., String-Reasor, E., Boughey, J. C., Chien, A. J., Elias, A. D., Beckwith, H., Nanda, R., Albain, K. S., Clark, A. S.,

Kemmer, K., Kalinsky, K., Isaacs, C., Thomas, A., Shatsky, R., … Esserman, L. J. (2021). Durvalumab with olaparib and paclitaxel for high-risk HER2-negative stage II/III breast cancer: Results from the adaptively randomized I-SPY2 trial. *Cancer Cell*, *39*(7), 989-998.e5. https://doi.org/10.1016/j.ccell.2021.05.009

Qian, J., & Liu, Y. (2025). Recent advances in adoptive cell therapy for cancer immunotherapy. In *Frontiers in Immunology* (Vol. 16). Frontiers Media SA. https://doi.org/10.3389/fimmu.2025.1665488

Qin, Z., Liu, H., Sheng, Q., Dan, J., Wu, X., Li, H., Wang, L., Zhang, S., Yuan, C., Yuan, H., Wang, H., Zhou, R., Luo, Y., & Xie, X. (2023). Mutant p53 leads to low-grade IFN-I-induced inflammation and impairs cGAS–STING signalling in mice. *European Journal of Immunology*, *53*(9). https://doi.org/10.1002/eji.202250211

Qu, S., Xu, R., Yi, G., Li, Z., Zhang, H., Qi, S., & Huang, G. (2024). Patient-derived organoids in human cancer: a platform for fundamental research and precision medicine. In *Molecular Biomedicine* (Vol. 5, Number 1). Springer. https://doi.org/10.1186/s43556-023-00165-9

Quail, D. F., & Joyce, J. A. (2013). Microenvironmental regulation of tumor progression and metastasis. In *Nature Medicine* (Vol. 19, Number 11, pp. 1423–1437). https://doi.org/10.1038/nm.3394

Quirico, L., Rizzolio, S., Bertone, S., Cirillo, P. D. R., Savino, A., Vitale, N., Catuogno, S., Esposito, C. L., Stadler, M. B., Defilippi, P., de Franciscis, V., Orso, F., & Taverna, D. (2025). The chimeric aptamer axl-miR-214sponge inhibits breast cancer and melanoma dissemination. *Molecular Therapy*, *33*(11), 5804–5816. https://doi.org/10.1016/j.ymthe.2025.07.039

Racacho, K. J., Shiau, Y. P., Villa, R., Mahri, S., Tang, M., Lin, T. Y., & Li, Y. (2025). The tumor immune microenvironment: implications for cancer immunotherapy, treatment strategies, and monitoring approaches. In *Frontiers in Immunology* (Vol. 16). Frontiers Media SA. https://doi.org/10.3389/fimmu.2025.1621812

Radisky, E. S. (2024). Extracellular proteolysis in cancer: Proteases, substrates, and mechanisms in tumor progression and metastasis. In *Journal of Biological Chemistry* (Vol. 300, Number 6). American Society for Biochemistry and Molecular Biology Inc. https://doi.org/10.1016/j.jbc.2024.107347

Ramos-Casals, M., Brahmer, J. R., Callahan, M. K., Flores-Chávez, A., Keegan, N., Khamashta, M. A., Lambotte, O., Mariette, X., Prat, A., & Suárez-Almazor, M. E. (2020). Immune-related adverse events of checkpoint inhibitors. In *Nature Reviews Disease Primers* (Vol. 6, Number 1). Nature Research. https://doi.org/10.1038/s41572-020-0160-6

Ranoa, D. R. E., Widau, R. C., Mallon, S., Parekh, A. D., Nicolae, C. M., Huang, X., Bolt, M. J., Arina, A., Parry, R., Kron, S. J., Moldovan, G. L., Khodarev, N. N., & Weichselbaum, R. R. (2019). STING promotes homeostasis via regulation of cell proliferation and chromosomal stability. *Cancer Research*, *79*(7), 1465–1479. https://doi.org/10.1158/0008-5472.CAN-18-1972

Rao, X., Di Leva, G., Li, M., Fang, F., Devlin, C., Hartman-Frey, C., Burow, M. E., Ivan, M., Croce, C. M., & Nephew, K. P. (2011). MicroRNA-221/222 confers breast cancer fulvestrant resistance by regulating multiple signaling pathways. *Oncogene*, *30*(9), 1082–1097. https://doi.org/10.1038/onc.2010.487

Ren, L., Guo, D., Wan, X., & Qu, R. (2022). EYA2 upregulates miR-93 to promote tumorigenesis of breast cancer by targeting and inhibiting the STING signaling pathway. *Carcinogenesis*, *43*(12), 1121–1130. https://doi.org/10.1093/carcin/bgab001

Ren, X., Lin, S., Guan, F., & Kang, H. (2024). Glycosylation Targeting: A Paradigm Shift in Cancer Immunotherapy. In *International Journal of Biological Sciences* (Vol. 20, Number 7, pp. 2607–2621). Ivyspring International Publisher. https://doi.org/10.7150/ijbs.93806

Ribatti, D. (2024). Aberrant tumor vasculature. Facts and pitfalls. In *Frontiers in Pharmacology* (Vol. 15). Frontiers Media SA. https://doi.org/10.3389/fphar.2024.1384721

Risom, T., Glass, D. R., Averbukh, I., Liu, C. C., Baranski, A., Kagel, A., McCaffrey, E. F., Greenwald, N. F., Rivero-Gutiérrez, B., Strand, S. H., Varma, S., Kong, A., Keren, L., Srivastava, S., Zhu, C., Khair, Z., Veis, D. J., Deschryver, K., Vennam, S., … Angelo, M. (2022). Transition to invasive breast cancer is associated with progressive changes in the structure and composition of tumor stroma. *Cell*, *185*(2), 299-310.e18. https://doi.org/10.1016/j.cell.2021.12.023

Rogers, T. J., Christenson, J. L., Greene, L. I., O'Neill, K. I., Williams, M. M., Gordon, M. A., Nemkov, T., D'Alessandro, A., Degala, G. D., Shin, J., Tan, A. C., Cittelly, D. M., Lambert, J. R., & Richer, J. K. (2019). Reversal of Triple-Negative Breast Cancer EMT by miR-200c Decreases Tryptophan Catabolism and a Program of Immunosuppression. *Molecular Cancer Research*, *17*(1), 30–41. https://doi.org/10.1158/1541-7786.MCR-18-0246

Ruiz-Iglesias, A., Guilbaud, E., Galluzzi, L., & Mañes, S. (2025). Context-dependent impact of type I interferon signaling in cancer. In *Molecular Cancer* (Vol. 24, Number 1). BioMed Central Ltd. https://doi.org/10.1186/s12943-025-02495-4

Sáenz, J. B., Sun, W. J., Chang, J. W., Li, J., Bursulaya, B., Gray, N. S., & Haslam, D. B. (2009). Golgicide A reveals essential roles for GBF1 in Golgi assembly and function. *Nature Chemical Biology*, *5*(3), 157–165. https://doi.org/10.1038/nchembio.144

Sahai, E., Astsaturov, I., Cukierman, E., DeNardo, D. G., Egeblad, M., Evans, R. M., Fearon, D., Greten, F. R., Hingorani, S. R., Hunter, T., Hynes, R. O., Jain, R. K., Janowitz, T., Jorgensen, C., Kimmelman, A. C., Kolonin, M. G., Maki, R. G., Powers, R. S., Puré, E., … Werb, Z. (2020). A framework for advancing our understanding of cancer-associated fibroblasts. In *Nature Reviews Cancer* (Vol. 20, Number 3, pp. 174–186). Nature Research. https://doi.org/10.1038/s41568-019-0238-1

Samson, N., & Ablasser, A. (2022). The cGAS–STING pathway and cancer. In *Nature Cancer* (Vol. 3, Number 12, pp. 1452–1463). Nature Research. https://doi.org/10.1038/s43018-022-00468-w

Shakya, R., Tarulli, G. A., Sheng, L., Lokman, N. A., Ricciardelli, C., Pishas, K. I., Selinger, C. I., Kohonen-Corish, M. R. J., Cooper, W. A., Turner, A. G., Neilsen, P. M., & Callen, D. F.

(2017). Mutant p53 upregulates alpha-1 antitrypsin expression and promotes invasion in lung cancer. *Oncogene*, *36*(31), 4469–4480. https://doi.org/10.1038/onc.2017.66

Shang, G., Zhang, C., Chen, Z. J., Bai, X. chen, & Zhang, X. (2019). Cryo-EM structures of STING reveal its mechanism of activation by cyclic GMP–AMP. *Nature*, *567*(7748), 389–393. https://doi.org/10.1038/s41586-019-0998-5

Shen, M., Jiang, X., Peng, Q., Oyang, L., Ren, Z., Wang, J., Peng, M., Zhou, Y., Deng, X., & Liao, Q. (2025). The cGAS–STING pathway in cancer immunity: mechanisms, challenges, and therapeutic implications. In *Journal of Hematology and Oncology* (Vol. 18, Number 1). BioMed Central Ltd. https://doi.org/10.1186/s13045-025-01691-5

Shiravand, Y., Khodadadi, F., Kashani, S. M. A., Hosseini-Fard, S. R., Hosseini, S., Sadeghirad, H., Ladwa, R., O'byrne, K., & Kulasinghe, A. (2022). Immune Checkpoint Inhibitors in Cancer Therapy. In *Current Oncology* (Vol. 29, Number 5, pp. 3044–3060). MDPI. https://doi.org/10.3390/curroncol29050247

Silva-Cazares, M. B., Saavedra-Leos, M. Z., Jordan-Alejandre, E., Nunez-Olvera, S. I., Compean-Martinez, I., & Lopez-Camarillo, C. (2020). Lipid-based nanoparticles for the therapeutic delivery of non-coding RNAs in breast cancer (Review). In *Oncology Reports* (Vol. 44, Number 6, pp. 2353–2363). Spandidos Publications. https://doi.org/10.3892/or.2020.7791

Sladitschek-Martens, H. L., Guarnieri, A., Brumana, G., Zanconato, F., Battilana, G., Xiccato, R. L., Panciera, T., Forcato, M., Bicciato, S., Guzzardo, V., Fassan, M., Ulliana, L., Gandin, A., Tripodo, C., Foiani, M., Brusatin, G., Cordenonsi, M., & Piccolo, S. (2022). YAP/TAZ activity in stromal cells prevents ageing by controlling cGAS–STING. *Nature*, *607*(7920), 790–798. https://doi.org/10.1038/s41586-022-04924-6

Sood, A. (2025). The cGAS-STING axis: a comprehensive review from immune defense to disease pathogenesis. In *Immunologic Research* (Vol. 73, Number 1). Springer. https://doi.org/10.1007/s12026-025-09648-z

Stowers, R. S. , & C. O. (2019). Matrix stiffness induces a tumorigenic phenotype in mammary epithelium through changes in chromatin accessibility. *Nature biomedical engineering, 3*(12), 1009-1019. https://www.nature.com/articles/s41551-019-0420-5

Stracker, T. H. (2024). Regulation of p53 by the mitotic surveillance/stopwatch pathway: implications in neurodevelopment and cancer. In *Frontiers in Cell and Developmental Biology* (Vol. 12). Frontiers Media SA. https://doi.org/10.3389/fcell.2024.1451274

Su, N., Lian, W., Zhang, B., Tian, Y., Li, L., Chen, Y., Zhi, X., Zeng, T., Wu, Q., Chen, L., Zhou, D., Wang, H. R., Cheng, S. C., Li, L., & Deng, X. (2025). Inhibiting NEDD4 in triple-negative breast cancer cells reprograms tumor immune microenvironment via the β-TrCP/YAP/ECM axis. *Cell Reports Medicine*, *6*(10). https://doi.org/10.1016/j.xcrm.2025.102420

Sullivan, K. D., Galbraith, M. D., Andrysik, Z., & Espinosa, J. M. (2018). Mechanisms of transcriptional regulation by p53. In *Cell Death and Differentiation* (Vol. 25, Number 1, pp. 133–143). Nature Publishing Group. https://doi.org/10.1038/cdd.2017.174

Sun, F., Liu, Z., Yang, Z., Liu, S., & Guan, W. (2019). The emerging role of STING-dependent signaling on cell death. In *Immunologic Research* (Vol. 67, Numbers 2–3, pp. 290–296). Humana Press Inc. https://doi.org/10.1007/s12026-019-09073-z

Sun, L., Wu, J., Du, F., Chen, X., & Chen, Z. J. (2013). Cyclic GMP-AMP synthase is a cytosolic DNA sensor that activates the type I interferon pathway. *Science*, *339*(6121), 786–791. https://doi.org/10.1126/science.1232458

Suresh, R. , & M. D. M. (2013). Pattern recognition receptors in innate immunity, host defense, and immunopathology. *Advances in physiology education, 37*(4), 284-291. https://journals.physiology.org/doi/full/10.1152/advan.00058.2013

Takasugi, M., Yoshida, Y., Hara, E., & Ohtani, N. (2023). The role of cellular senescence and SASP in tumour microenvironment. In *FEBS Journal* (Vol. 290, Number 5, pp. 1348–1361). John Wiley and Sons Inc. https://doi.org/10.1111/febs.16381

Tanaka, Y., & Chen, Z. J. (2012). STING specifies IRF3 phosphorylation by TBK1 in the cytosolic DNA signaling pathway. *Science Signaling*, *5*(214). https://doi.org/10.1126/scisignal.2002521

Tao, Y., Yang, Y., Zhou, R., & Gong, T. (2020). Golgi Apparatus: An Emerging Platform for Innate Immunity. In *Trends in Cell Biology* (Vol. 30, Number 6, pp. 467–477). Elsevier Ltd. https://doi.org/10.1016/j.tcb.2020.02.008

Thoresen, D., Wang, W., Galls, D., Guo, R., Xu, L., & Pyle, A. M. (2021). The molecular mechanism of RIG-I activation and signaling. In *Immunological Reviews* (Vol. 304, Number 1, pp. 154–168). John Wiley and Sons Inc. https://doi.org/10.1111/imr.13022

Truntzer, C., Isambert, N., Arnould, L., Ladoire, S., & Ghiringhelli, F. (2019). Prognostic value of transcriptomic determination of tumour-infiltrating lymphocytes in localised breast cancer. *European Journal of Cancer*, *120*, 97–106. https://doi.org/10.1016/j.ejca.2019.07.020

Tsuchida, T., Zou, J., Saitoh, T., Kumar, H., Abe, T., Matsuura, Y., Kawai, T., & Akira, S. (2010). The ubiquitin ligase TRIM56 regulates innate immune responses to intracellular double-stranded DNA. *Immunity*, *33*(5), 765–776. https://doi.org/10.1016/j.immuni.2010.10.013

Uhlorn, B. L., Gamez, E. R., Li, S., & Campos, S. K. (2020). Attenuation of cGAS/STING activity during mitosis. *Life Science Alliance*, *3*(9). https://doi.org/10.26508/lsa.201900636

Uppala, R., Sarkar, M. K., Young, K. Z., Ma, F., Vemulapalli, P., Wasikowski, R., Plazyo, O., Swindell, W. R., Maverakis, E., Gharaee-Kermani, M., Billi, A. C., Tsoi, L. C., Kahlenberg, J. M., & Gudjonsson, J. E. (2024). HERC6 regulates STING activity in a sex-biased manner through modulation of LATS2/VGLL3 Hippo signaling. *IScience*, *27*(2). https://doi.org/10.1016/j.isci.2024.108986

Vergnes, L., Terfy, P., Bergo, M. O., Young, S. G., & Reue, K. (2004). Lamin B1 is required for mouse development and nuclear integrity. *Proceedings of the National Academy of Sciences, 101*(28), 10428-10433. https://www.pnas.org/doi/full/10.1073/pnas.0401424101

Vesely, M. D., & Schreiber, R. D. (2013). Cancer immunoediting: Antigens, mechanisms, and implications to cancer immunotherapy. *Annals of the New York Academy of Sciences*, *1284*(1), 1–5. https://doi.org/10.1111/nyas.12105

Vilella, F., Moreno-Moya, J. M., Balaguer, N., Grasso, A., Herrero, M., Martínez, S., Marcilla, A., & Simón, C. (2015). Hsa-miR-30d, secreted by the human endometrium, is taken up by the pre-implantation embryo and might modify its transcriptome. *Development (Cambridge)*, *142*(18), 3210–3221. https://doi.org/10.1242/dev.124289

Vojdani, A., Koksoy, S., Vojdani, E., Engelman, M., Benzvi, C., & Lerner, A. (2024). Natural Killer Cells and Cytotoxic T Cells: Complementary Partners against Microorganisms and Cancer. In *Microorganisms* (Vol. 12, Number 1). Multidisciplinary Digital Publishing Institute (MDPI). https://doi.org/10.3390/microorganisms12010230

Volpini, L., Monaco, F., Santarelli, L., Neuzil, J., & Tomasetti, M. (2023). Advances in RNA cancer therapeutics: New insight into exosomes as miRNA delivery. In *Aspects of Molecular Medicine* (Vol. 1). Elsevier B.V. https://doi.org/10.1016/j.amolm.2023.100005

Waldman, A. D., Fritz, J. M., & Lenardo, M. J. (2020). A guide to cancer immunotherapy: from T cell basic science to clinical practice. In *Nature Reviews Immunology* (Vol. 20, Number 11, pp. 651–668). Nature Research. https://doi.org/10.1038/s41577-020-0306-5

Walerych, D., Lisek, K., Sommaggio, R., Piazza, S., Ciani, Y., Dalla, E., Rajkowska, K., Gaweda-Walerych, K., Ingallina, E., Tonelli, C., Morelli, M. J., Amato, A., Eterno, V., Zambelli, A., Rosato, A., Amati, B., Winiewski, J. R., & Del Sal, G. (2016). Proteasome machinery is instrumental in a common gain-of-function program of the p53 missense mutants in cancer. *Nature Cell Biology*, *18*(8), 897–909. https://doi.org/10.1038/ncb3380

Wang, B., Yu, W., Jiang, H., Meng, X., Tang, D., & Liu, D. (2024). Clinical applications of STING agonists in cancer immunotherapy: current progress and future prospects. In *Frontiers in Immunology* (Vol. 15). Frontiers Media SA. https://doi.org/10.3389/fimmu.2024.1485546

Wang, G., Lu, X., Dey, P., Deng, P., Wu, C. C., Jiang, S., Fang, Z., Zhao, K., Konaparthi, R., Hua, S., Zhang, J., Li-Ni-Ngtapia, E. M., Kapoor, A., Wu, C. J., Patel, N. B., Guo, Z., Ramamoorthy, V., Tieu, T. N., Heffernan, T., … Depinho, R. A. (2016). Targeting YAP-dependent MDSC infiltration impairs tumor progression. *Cancer Discovery*, *6*(1), 80–95. https://doi.org/10.1158/2159-8290.CD-15-0224

Wang, H., & Petrini, J. H. J. (2025). Innate immune sensing and signaling: Co-opted for genome surveillance? Implications for tumorigenesis. *DNA Repair*, *153*. https://doi.org/10.1016/j.dnarep.2025.103890

Wang, R., Lan, C., Benlagha, K., Camara, N. O. S., Miller, H., Kubo, M., Heegaard, S., Lee, P., Yang, L., Forsman, H., Li, X., Zhai, Z., & Liu, C. (2024). The interaction of innate immune and adaptive immune system. In *MedComm* (Vol. 5, Number 10). John Wiley and Sons Inc. https://doi.org/10.1002/mco2.714

Wang, T., Gilkes, D. M., Takano, N., Xiang, L., Luo, W., Bishop, C. J., Chaturvedi, P., Green, J. J., & Semenza, G. L. (2014). Hypoxia-inducible factors and RAB22A mediate formation of microvesicles that stimulate breast cancer invasion and metastasis. *Proceedings of the National Academy of Sciences of the United States of America*, *111*(31). https://doi.org/10.1073/pnas.1410041111

Wang, T. H., Chen, C. C., Leu, Y. L., Lee, Y. S., Lian, J. H., Hsieh, H. L., & Chen, C. Y. (2021). Palbociclib induces DNA damage and inhibits DNA repair to induce cellular senescence and apoptosis in oral squamous cell carcinoma. *Journal of the Formosan Medical Association*, *120*(9), 1695–1705. https://doi.org/10.1016/j.jfma.2020.12.009

Wang, X., Zhou, Y., Wang, Y., Yang, J., Li, Z., Liu, F., Wang, A., Gao, Z., Wu, C., & Yin, H. (2025). Overcoming cancer treatment resistance: Unraveling the role of cancer-associated fibroblasts. In *Journal of the National Cancer Center* (Vol. 5, Number 3, pp. 237–251). Chinese National Cancer Center. https://doi.org/10.1016/j.jncc.2025.03.002

Wang, Y., Li, S., Hu, M., Yang, Y., McCabe, E., Zhang, L., Withrow, A. M., Ting, J. P. Y., & Liu, R. (2024). Universal STING mimic boosts antitumour immunity via preferential activation of tumour control signalling pathways. *Nature Nanotechnology*, *19*(6), 856–866. https://doi.org/10.1038/s41565-024-01624-2

Wei, S. C., Duffy, C. R., & Allison, J. P. (2018). Fundamental mechanisms of immune checkpoint blockade therapy. In *Cancer Discovery* (Vol. 8, Number 9, pp. 1069–1086). American Association for Cancer Research Inc. https://doi.org/10.1158/2159-8290.CD-18-0367

Weis, S. M., & Cheresh, D. A. (2011). Tumor angiogenesis: Molecular pathways and therapeutic targets. In *Nature Medicine* (Vol. 17, Number 11, pp. 1359–1370). https://doi.org/10.1038/nm.2537

White, M. J., McArthur, K., Metcalf, D., Lane, R. M., Cambier, J. C., Herold, M. J., Van Delft, M. F., Bedoui, S., Lessene, G., Ritchie, M. E., Huang, D. C. S., & Kile, B. T. (2014). Apoptotic caspases suppress mtDNA-induced STING-mediated type i IFN production. *Cell*, *159*(7), 1549–1562. https://doi.org/10.1016/j.cell.2014.11.036

Won, J. K., & Bakhoum, S. F. (2020). The cytosolic DNA-sensing cGAS–sting pathway in cancer. In *Cancer Discovery* (Vol. 10, Number 1, pp. 26–39). American Association for Cancer Research Inc. https://doi.org/10.1158/2159-8290.CD-19-0761

Wu, M. Z., Cheng, W. C., Chen, S. F., Nieh, S., O'Connor, C., Liu, C. L., Tsai, W. W., Wu, C. J., Martin, L., Lin, Y. S., Wu, K. J., Lu, L. F., & Izpisua Belmonte, J. C. (2017). MiR-25/93 mediates hypoxia-induced immunosuppression by repressing cGAS. *Nature Cell Biology*, *19*(10), 1286–1296. https://doi.org/10.1038/ncb3615

Xie, R., Wu, S. N., Gao, C. C., Yang, X. Z., Wang, H. G., Zhang, J. L., Yan, W., & Ma, T. H. (2017). MicroRNA-30d inhibits the migration and invasion of human esophageal squamous cell carcinoma cells via the post-transcriptional regulation of enhancer of zeste homolog 2. *Oncology Reports*, *37*(3), 1682–1690. https://doi.org/10.3892/or.2017.5405

Xu, B., Maimaitijiang, A., Nuerbiyamu, D., Su, Z., & Li, W. (2025). The Multifaceted Role of p53 in Cancer Molecular Biology: Insights for Precision Diagnosis and Therapeutic Breakthroughs. In *Biomolecules* (Vol. 15, Number 8). Multidisciplinary Digital Publishing Institute (MDPI). https://doi.org/10.3390/biom15081088

Xu, H., Chen, X., Lu, Y., Sun, N., Weisgerber, K. E., Xu, M., & Bai, R. Y. (2025). Neutrophil Dynamics in Response to Cancer Therapies. In *Cancers* (Vol. 17, Number 15). Multidisciplinary Digital Publishing Institute (MDPI). https://doi.org/10.3390/cancers17152593

Xu, X., Zong, K., Wang, X., Dou, D., Lv, P., Zhang, Z., & Li, H. (2021). miR-30d suppresses proliferation and invasiveness of pancreatic cancer by targeting the SOX4/PI3K-AKT axis and predicts poor outcome. *Cell Death and Disease*, *12*(4). https://doi.org/10.1038/s41419-021-03576-0

Xue, W., Zender, L., Miething, C., Dickins, R. A., Hernando, E., Krizhanovsky, V., Cordon-Cardo, C., & Lowe, S. W. (2007). Senescence and tumour clearance is triggered by p53 restoration in murine liver carcinomas. *Nature*, *445*(7128), 656–660. https://doi.org/10.1038/nature05529

Yan, W., & Chen, X. (2009). Identification of GRO1 as a critical determinant for mutant p53 gain of function. *Journal of Biological Chemistry*, *284*(18), 12178–12187. https://doi.org/10.1074/jbc.M900994200

Yan, Y., Tan, X., Song, B., Yi, M., Chu, Q., & Wu, K. (2025). Breaking barriers: The cGAS-STING pathway as a novel frontier in cancer immunotherapy. In *Cancer Communications* (Vol. 45, Number 11, pp. 1513–1546). John Wiley and Sons Inc. https://doi.org/10.1002/cac2.70067

Yang, H., Yang, J., Zheng, X., Chen, T., Zhang, R., Chen, R., Cao, T., Zeng, F., & Liu, Q. (2024). The Hippo Pathway in Breast Cancer: The Extracellular Matrix and Hypoxia. In *International Journal of Molecular Sciences* (Vol. 25, Number 23). Multidisciplinary Digital Publishing Institute (MDPI). https://doi.org/10.3390/ijms252312868

Yao, J., Liang, L., Huang, S., Ding, J., Tan, N., Zhao, Y., Yan, M., Ge, C., Zhang, Z., Chen, T., Wan, D., Yao, M., Li, J., Gu, J., & He, X. (2010). Microrna-30d promotes tumor invasion and metastasis by targeting galphai2 in hepatocellular carcinoma. *Hepatology*, *51*(3), 846–856. https://doi.org/10.1002/hep.23443

Yu, F. X., Zhao, B., & Guan, K. L. (2015). Hippo Pathway in Organ Size Control, Tissue Homeostasis, and Cancer. In *Cell* (Vol. 163, Number 4, pp. 811–828). Cell Press. https://doi.org/10.1016/j.cell.2015.10.044

Yum, S. , L. M. , F. Y. , & C. Z. J. (2021). TBK1 recruitment to STING activates both IRF3 and NF-κB that mediate immune defense against tumors and viral infections. *Proceedings of the National Academy of Sciences. 118*(14), 2100225118. https://doi.org/10.1073/pnas.2100225118/-/DCSupplemental

Zabeti Touchaei, A., & Vahidi, S. (2024). MicroRNAs as regulators of immune checkpoints in cancer immunotherapy: targeting PD-1/PD-L1 and CTLA-4 pathways. In *Cancer Cell International* (Vol. 24, Number 1). BioMed Central Ltd. https://doi.org/10.1186/s12935-024-03293-6

Zanconato, F., Battilana, G., Forcato, M., Filippi, L., Azzolin, L., Manfrin, A., Quaranta, E., Di Biagio, D., Sigismondo, G., Guzzardo, V., Lejeune, P., Haendler, B., Krijgsveld, J., Fassan, M., Bicciato, S., Cordenonsi, M., & Piccolo, S. (2018). Transcriptional addiction in cancer cells is mediated by YAP/TAZ through BRD4. *Nature Medicine*, *24*(10), 1599–1610. https://doi.org/10.1038/s41591-018-0158-8

Zanconato, F., Cordenonsi, M., & Piccolo, S. (2016). YAP/TAZ at the Roots of Cancer. In *Cancer Cell* (Vol. 29, Number 6, pp. 783–803). Cell Press. https://doi.org/10.1016/j.ccell.2016.05.005

Zanconato, F., Forcato, M., Battilana, G., Azzolin, L., Quaranta, E., Bodega, B., Rosato, A., Bicciato, S., Cordenonsi, M., & Piccolo, S. (2015). Genome-wide association between YAP/TAZ/TEAD and AP-1 at enhancers drives oncogenic growth. *Nature Cell Biology*, *17*(9), 1218–1227. https://doi.org/10.1038/ncb3216

Zhang, C., Shang, G., Gui, X., Zhang, X., Bai, X. chen, & Chen, Z. J. (2019). Structural basis of STING binding with and phosphorylation by TBK1. *Nature*, *567*(7748), 394–398. https://doi.org/10.1038/s41586-019-1000-2

Zhang, H., Liu, C. Y., Zha, Z. Y., Zhao, B., Yao, J., Zhao, S., Xiong, Y., Lei, Q. Y., & Guan, K. L. (2009). TEAD transcription factors mediate the function of TAZ in cell growth and epithelial-mesenchymal transition. *Journal of Biological Chemistry*, *284*(20), 13355–13362. https://doi.org/10.1074/jbc.M900843200

Zhang, J., Hu, M. M., Wang, Y. Y., & Shu, H. B. (2012). TRIM32 protein modulates type I interferon induction and cellular antiviral response by targeting MITA/STING protein for K63-linked ubiquitination. *Journal of Biological Chemistry*, *287*(34), 28646–28655. https://doi.org/10.1074/jbc.M112.362608

Zhang, J., Wu, H., Ren, X., Chen, Z., Ye, S., Chen, S., Fang, J., Wu, Q., & Zhao, T. (2025). Hippo/YAP signaling's multifaceted crosstalk in cancer. In *Frontiers in Cell and Developmental Biology* (Vol. 13). Frontiers Media SA. https://doi.org/10.3389/fcell.2025.1595362

Zhang, L. , R. S. , S. Y. , H. Y. , W. C. , W. X. , & L. Y. (2024). miR-30d-5p inhibits proliferation, invasion and migration of breast cancer cells by targeting SERPINE1 and promoting fatty acid β-oxidation. *Aging (Albany NY), 16*(7), 5856. https://pmc.ncbi.nlm.nih.gov/articles/PMC11042962/

Zhang, M., Liu, C., Tu, J., Tang, M., Ashrafizadeh, M., Nabavi, N., Sethi, G., Zhao, P., & Liu, S. (2025). Advances in cancer immunotherapy: historical perspectives, current developments, and future directions. In *Molecular Cancer* (Vol. 24, Number 1). BioMed Central Ltd. https://doi.org/10.1186/s12943-025-02305-x

Zhang, M., & Zhang, B. (2025). Extracellular matrix stiffness: mechanisms in tumor progression and therapeutic potential in cancer. In *Experimental Hematology and Oncology* (Vol. 14, Number 1). BioMed Central Ltd. https://doi.org/10.1186/s40164-025-00647-2

Zhang, Q., Meng, F., Chen, S., Plouffe, S. W., Wu, S., Liu, S., Li, X., Zhou, R., Wang, J., Zhao, B., Liu, J., Qin, J., Zou, J., Feng, X. H., Guan, K. L., & Xu, P. (2017). Hippo signalling governs cytosolic nucleic acid sensing through YAP/TAZ-mediated TBK1 blockade. *Nature Cell Biology*, *19*(4), 362–374. https://doi.org/10.1038/ncb3496

Zhang, R., Xu, J., Zhao, J., & Bai, J. (2017). Mir-30d suppresses cell proliferation of colon cancer cells by inhibiting cell autophagy and promoting cell apoptosis. *Tumor Biology*, *39*(6). https://doi.org/10.1177/1010428317703984

Zhang, S., Regan, K., Najera, J., Grinstaff, M. W., Datta, M., & Nia, H. T. (2023). The peritumor microenvironment: physics and immunity. In *Trends in Cancer* (Vol. 9, Number 8, pp. 609–623). Cell Press. https://doi.org/10.1016/j.trecan.2023.04.004

Zhang, Z. D., & Zhong, B. (2022). Regulation and function of the cGAS-MITA/STING axis in health and disease. In *Cell Insight* (Vol. 1, Number 1). Elsevier B.V. https://doi.org/10.1016/j.cellin.2021.100001

Zhang, Z., Huang, Y., Li, J., Su, F., Kuo, J. C. T., Hu, Y., Zhao, X., & Lee, R. J. (2023). Antitumor Activity of Anti-miR-21 Delivered through Lipid Nanoparticles. *Advanced Healthcare Materials*, *12*(6). https://doi.org/10.1002/adhm.202202412

Zhang, Z., Samsa, W. E., De, Y., Zhang, F., Reizes, O., Almasan, A., & Gong, Z. (2023). HDGFRP3 interaction with 53BP1 promotes DNA double-strand break repair. *Nucleic Acids Research*, *51*(5), 2238–2256. https://doi.org/10.1093/nar/gkad073

Zhang, Z., & Zhang, C. (2025). Regulation of cGAS–STING signalling and its diversity of cellular outcomes. In *Nature Reviews Immunology* (Vol. 25, Number 6, pp. 425–444). Nature Research. https://doi.org/10.1038/s41577-024-01112-7

Zhao, B., Li, L., Lu, Q., Wang, L. H., Liu, C. Y., Lei, Q., & Guan, K. L. (2011). Angiomotin is a novel Hippo pathway component that inhibits YAP oncoprotein. *Genes and Development*, *25*(1), 51–63. https://doi.org/10.1101/gad.2000111

Zhao, B., Wei, X., Li, W., Udan, R. S., Yang, Q., Kim, J., Xie, J., Ikenoue, T., Yu, J., Li, L., Zheng, P., Ye, K., Chinnaiyan, A., Halder, G., Lai, Z. C., & Guan, K. L. (2007). Inactivation of YAP oncoprotein by the Hippo pathway is involved in cell contact inhibition and tissue growth control. *Genes and Development*, *21*(21), 2747–2761. https://doi.org/10.1101/gad.1602907

Zheng, M., Hou, L., Ma, Y., Zhou, L., Wang, F., Cheng, B., Wang, W., Lu, B., Liu, P., Lu, W., & Lu, Y. (2019). Exosomal let-7d-3p and miR-30d-5p as diagnostic biomarkers for non-invasive screening of cervical cancer and its precursors. *Molecular Cancer*, *18*(1). https://doi.org/10.1186/s12943-019-0999-x

Zhou, M., Liu, L., Wang, J., & Liu, W. (2022). The role of long noncoding RNAs in therapeutic resistance in cervical cancer. In *Frontiers in Cell and Developmental Biology* (Vol. 10). Frontiers Media S.A. https://doi.org/10.3389/fcell.2022.1060909

Zhu, K., Wang, J., Zhu, J., Jiang, J., Shou, J., & Chen, X. (1999). p53 induces TAP1 and enhances the transport of MHC class I peptides. *Oncogene, 18*(54), 7740-7747. https://www.nature.com/articles/1203235

Zielińska, M. K., Ciążyńska, M., Sulejczak, D., Rutkowski, P., & Czarnecka, A. M. (2025). Mechanisms of Resistance to Anti-PD-1 Immunotherapy in Melanoma and Strategies to Overcome It. In *Biomolecules* (Vol. 15, Number 2). Multidisciplinary Digital Publishing Institute (MDPI). https://doi.org/10.3390/biom15020269